

Berichte

zur Polar-
und Meeresforschung

679
2014

Reports
on Polar and Marine Research



The Expedition of the Research Vessel "Polarstern"
to the Antarctic in 2013 (ANT-XXIX/6)

Edited by
Peter Lemke
with contributions of the participants



Alfred-Wegener-Institut
Helmholtz-Zentrum für Polar-
und Meeresforschung
D-27570 BREMERHAVEN
Bundesrepublik Deutschland

ISSN 1866-3192

Hinweis

Die Berichte zur Polar- und Meeresforschung werden vom Alfred-Wegener-Institut Helmholtz-Zentrum für Polar- und Meeresforschung in Bremerhaven* in unregelmäßiger Abfolge herausgegeben.

Sie enthalten Beschreibungen und Ergebnisse der vom Institut (AWI) oder mit seiner Unterstützung durchgeführten Forschungsarbeiten in den Polargebieten und in den Meeren.

Es werden veröffentlicht:

- Expeditionsberichte
(inkl. Stationslisten und Routenkarten)
- Expeditions- und Forschungsergebnisse
(inkl. Dissertationen)
- wissenschaftliche Berichte der
Forschungsstationen des AWI
- Berichte wissenschaftlicher Tagungen

Die Beiträge geben nicht notwendigerweise die Auffassung des Instituts wieder.

Notice

The Reports on Polar and Marine Research are issued by the Alfred-Wegener-Institut Helmholtz-Zentrum für Polar- und Meeresforschung in Bremerhaven*, Federal Republic of Germany. They are published in irregular intervals.

They contain descriptions and results of investigations in polar regions and in the seas either conducted by the Institute (AWI) or with its support.

The following items are published:

- expedition reports
(incl. station lists and route maps)
- expedition and research results
(incl. Ph.D. theses)
- scientific reports of research stations
operated by the AWI
- reports on scientific meetings

The papers contained in the Reports do not necessarily reflect the opinion of the Institute.

The „Berichte zur Polar- und Meeresforschung“
continue the former „Berichte zur Polarforschung“

* Anschrift / Address

Alfred-Wegener-Institut
Helmholtz-Zentrum für Polar-
und Meeresforschung
D-27570 Bremerhaven
Germany
www.awi.de

Editor:
Dr. Horst Bornemann

Assistant editor:
Birgit Chiaventone

Die "Berichte zur Polar- und Meeresforschung" (ISSN 1866-3192) werden ab 2008 als Open-Access-Publikation herausgegeben (URL: <http://epic.awi.de>).

Since 2008 the "Reports on Polar and Marine Research" (ISSN 1866-3192) are available as open-access publications (URL: <http://epic.awi.de>)

The Expedition of the Research Vessel "Polarstern" to the Antarctic in 2013 (ANT-XXIX/6)

**Edited by
Peter Lemke
with contributions of the participants**

Please cite or link this publication using the identifiers
hdl:10013/epic.44124 or <http://hdl.handle.net/10013/epic.44124> and
doi:10.2312/BzPM_0679_2014 or http://doi.org/10.2312/BzPM_0679_2014

ISSN 1866-3192

ANT-XXIX/6

8 June 2013 - 12 August 2013

Cape Town – Punta Arenas

**Chief Scientist
Peter Lemke**

**Coordinator
Rainer Knust**

Contents

1.	Zusammenfassung und Fahrtverlauf	2
	Summary and Itinerary	3
2.	Weather Conditions	5
3.	Meteorology	9
4.	Atmospheric Chemistry	16
4.1	Detection of halogen oxides	20
4.2	<i>In-situ</i> and local measurements of halogen oxides IO and BrO by "Mode-Locked Cavity Enhanced Absorption Spectroscopy"	22
4.3	Sea salt aerosols and blowing snow	22
4.4	Volatile halogenated organic compounds	24
4.5	Mercury	26
5.	Sea Ice Physics	29
5.1	Airborne sea ice surveys	29
5.2	Ground-based Electromagnetics GEM-2	32
5.3	Sea-ice thickness, snow depth and freeboard from manual drilling	40
5.4	Visual observation of sea-ice conditions from the ship's bridge	42
5.5	Light transmission through sea ice and snow	43
5.6	Snow pit measurements	55
5.7	Snow topography	61
5.8	Autonomous buoys	69
6.	Sea Ice Biogeochemistry	75
7.	Oceanography	109
7.1	Modification of water masses	109
8.	Overwintering Strategies of Antarctic Copepods: Physiological Mechanisms and Buoyancy Regulation by Ammonium	126
9.	Acoustic Ecology of Antarctic Minke Whales	130
	APPENDICES	
A.1	Teilnehmende Institute / Participating Institutions	135
A.2	Fahrtteilnehmer / Cruise Participants	138
A.3	Schiffsbesatzung / Ship's Crew	140
A.4	Stationsliste / Station List PS81	142

1. ZUSAMMENFASSUNG UND FAHRTVERLAUF

Peter Lemke

AWI

Polarstern ist am 8. Juni 2013 abends in Kapstadt (Südafrika) ausgelaufen. Das Ziel der Expedition war die Durchführung eines interdisziplinären Forschungsprogramms in Atmosphäre, Meereis, Ozean und Ökosystem im antarktischen Winter, um die physikalischen und biogeochemischen Eigenschaften und Prozesse während der Meereiswachstumsphase besser zu verstehen. Es war die erste antarktische Winterexpedition seit 2006, und der geplante Kurs wurde das erste Mal seit 1992 wieder im antarktischen Winter gefahren (Abb. 1.1). Zwei wesentliche Fragen bestimmten das Forschungsprogramm. Warum nimmt die Ausbreitung des antarktischen Meereises leicht zu, während die Meereisbedeckung in der Arktis stetig zurückgeht? Welche Mechanismen lassen das Ökosystem des Südpolarmeeres nach dem langen, kalten und dunklen Winter wieder erwachen?

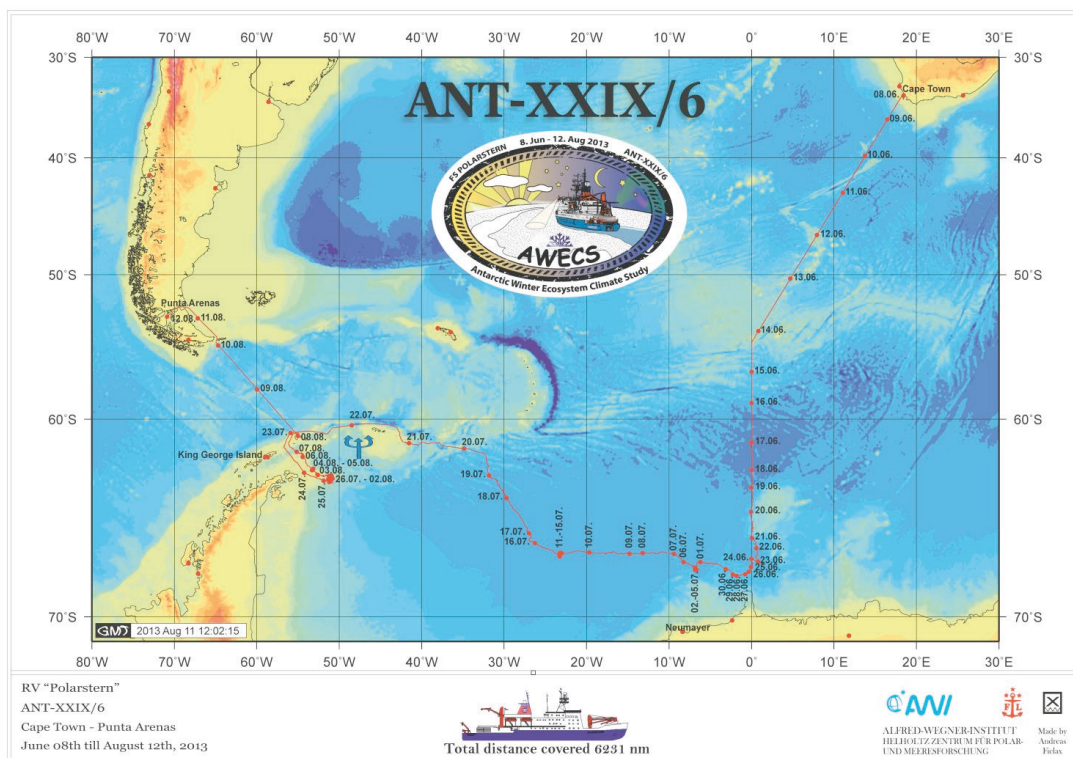


Abb. 1.1: Polarstern-Fahrtroute während ANT-XXIX/6

Fig. 1.1: Cruise track of RV Polarstern during ANT-XXIX/6

Um diese Fragen wenigstens teilweise zu beantworten wurde zunächst ein ozeanographisches und biologisches Messprogramm von 55°S bis zum Kontinent entlang des Greenwich Meridians durchgeführt, welches im Wesentlichen aus den typischen hydrographischen Profilen, wie z.B. von Temperatur und Salzgehalt, bestand und die Produktion von Tiefen- und Bodenwasser im Winter genauer beleuchten sollte. Parallel dazu wurden das Multinetz und das Bongonetz eingesetzt, um die Überwinterungsstrategie der Copepoden (Ruderfußkrebse) zu untersuchen. Innerhalb des Packeises kamen verschiedene Untersuchungen zur Physik und Biogeochemie des Meereises und zur Struktur der atmosphärischen Grenzschicht dazu. Während der ganzen Expedition fanden zudem Untersuchungen

zu verschiedenen Aspekten der Chemie der Atmosphäre und zur akustischen Ökologie statt.

Wegen der dichten Eisverhältnisse konnten die letzten Stationen am Kontinent nicht mehr erreicht werden, so dass der Querschnitt durch das Weddellmeer hin zur Antarktischen Halbinsel bei 68°16'S beginnen musste.

Bei der Hälfte dieses Schnittes wurde das Forschungsprogramm im zentralen Weddellmeer am 17. Juli wegen eines medizinischen Notfalls und der deswegen notwendigen Fahrt nach King George Island für 7 Tage unterbrochen. Nach erfolgreicher Übergabe der Patientin an das medizinische Personal der chilenischen Luftwaffe, die den Flug nach Punta Arenas durchführte, wurde das Forschungsprogramm am Kontinentalhang östlich der Antarktischen Halbinsel auf der geplanten Route aber in umgekehrter Richtung erfolgreich weitergeführt.

Insgesamt wurden 19 Multinetz- und 3 Bongo-Netz-Stationen und 35 CTD/Kranzwasserschöpfer-Einsätze durchgeführt. Das Herzstück der Expedition waren die Eisstationen, bei denen alle Disziplinen beteiligt waren. Zwei Langzeitstationen dauerten 4 Tage, und eine war nach 3 Tagen beendet. Dazu kamen noch 5 Stationen zu jeweils 10 Stunden, und zusätzlich fanden 10 kurze Eisstationen von einigen Stunden Dauer statt.

Das Besondere an dieser Expedition war, dass nach zwei Dekaden Pause sowohl das Klima- als auch das Ökosystem im Mittwinter auf zwei hydrographischen Schnitten durch das Weddellmeer genauer untersucht werden konnten. Die Ergebnisse sind in allen Fällen einzigartig und in einigen Beispielen auch überraschend.

Am 12.8.2013 lief *Polarstern* vormittags in Punta Arenas ein. An der Expedition ANT-XXIX/6 nahmen 49 Wissenschaftler und Techniker (inklusive zwei Hub-schrauberpiloten) aus 13 Ländern teil. Die hervorragende Unterstützung von 44 Besatzungsmitgliedern stellte sicher, dass das Forschungsprogramm mit großem Erfolg durchgeführt werden konnte.

SUMMARY AND ITINERARY

Polarstern left port in Cape Town (South Africa) on the evening of 8 June 2013. The aim of the cruise was to carry out an interdisciplinary research programme on atmosphere, sea ice, ocean and ecosystem during winter to obtain an understanding of physical and biogeochemical properties and processes during the sea ice growth season. This was the first Antarctic winter expedition since 2006, and on the planned cruise track it was the first since 1992 (Fig. 1.1). Two main goals determined the research programme. Why is the Antarctic sea ice expanding slightly, whereas the Arctic sea ice is retreating strongly? Which processes are responsible for the revival of the ecosystem after the cold and dark winter?

To answer these questions an oceanographic and biological programme was performed on the Greenwich Meridian from 55°S to the continent, which consisted of typical hydrographic profiles, such as temperature and salinity, to investigate the production of deep and bottom water in winter. In parallel, multinet and bongo net casts have been undertaken to study the overwintering strategies of copepods.

In the sea ice covered area, various investigations concerning the physics and biogeochemistry of sea ice and the atmospheric boundary layer were performed. During the entire expedition measurements concerning atmospheric chemistry and acoustic ecology have been undertaken.

Because of the heavy ice conditions, some stations close to the Antarctic coast could not be reached. Therefore, the North-South section had to be terminated at 68°16'S.

From here, the crossing of the Weddell Gyre towards the tip of the Antarctic Peninsula started. Near the midpoint of this section in the Central Weddell Sea the expedition had to be interrupted on 17 July for 7 days because of a medical emergency. After the successful transfer of the patient to the medical staff of the Chilean Air Force on King George Island, who flew the patient to Punta Arenas, the expedition continued its investigations on the east slope off the tip of the Antarctic Peninsula.

In total, 19 multinet, 3 bongo net and 35 CTD stations have been successfully performed during the expedition. The core of the investigations was formed by the ice stations, in which all disciplines participated. During the cruise two long ice stations lasted four days each and one station took three days. In addition, five ten-hour stations and ten shorter sea ice stations were undertaken.

An important and special feature of this expedition was the repeated dual crossing of the Weddell Gyre in winter (north to south and south-east to north-west) after two decades, during which the climate and ecosystem has been investigated in detail. The results obtained were all unique and some were surprising.

On 12 August 2013 *Polarstern* reached port in Punta Arenas. Forty-nine scientists and technicians, including two helicopter pilots from thirteen countries participated in the expedition. They were excellently supported by 44 crew members, who guaranteed the big success of the cruise.

2. WEATHER CONDITIONS

Harald Rentsch DWD

The first hours of the expedition were dominated by cold air in upper levels of the atmosphere within a cold front, and together with warmer air on the surface we got often rain showers. The airstream came with 5 to 6 wind forces from south-east. The sea rose up to 4 m already after we had left Cape Town. One day later, during the 9th June, wind turned north-westward and braised up to 7 Beaufort (Bft), wave heights were reduced in average to 3.5 m.

Connected with the passage of Subtropic- and Sub Antarctic front, which occurred between the 10th and 12th June, it became colder, clearly seen on the decreasing SST (sea-surface temperatures) of the Southern Atlantic.

Until the 13th June fronts and depressions brought some rain and drizzle. After that time south of 50° S along Greenwich meridian we got a mix of rain and snow, the alternating winds reached nearly 6 Bft, and the sea did not exceed 3 m.

On 15th June a last significant front passage caused wind force 8 and the wave field rose up to 4.5 m. Before we got the first ice contact nearby 61°30' S, it was mostly pan-cake ice; we measured an air temperature of around -17°C and noticed a nearly calmed sea, in spite of fresh winds up to 6 Bft.

At the same day wind direction changed to south-east, later south-west and dry air came from Antarctic towards the ship; a very cold wintry period began.

Between June 19th and 21st ("Midwinter") a dry southerly wind flow around 6 Bft, often clear sky conditions and daylight for 3 hours, enabled some helicopter flights for ice thickness measurements. In this clear air without clouds the temperatures lowered to around -28°C, and wind chill temperatures fell below -50°C.

Already one day later fog and low clouds dominated the weather nearby the ship, warmer air was pushed from northerly wind directions towards our ships track. During our expedition towards south the ice became thicker and multi-layered, afterwards open waters were seldom seen. Thus, the first ice station was established.

On 23rd June, Sunday, fronts, which came from Weddell Sea, brought first heavy snow and mitigation to us; by north-easterly winds of around 5 Bft we calculated only wind chill temperatures of -35°C. One day later in connection with the passing of a depression north of our working area stronger easterly winds up to 8 wind forces were measured.

From 24th to 26th June some polar depressions influenced the expedition track by a snowstorm and blowing snow, and sea-ice was pressed together more and more,

caused by north-easterly winds of 8 to 9 Bft. On 27th June in the afternoon the highest one minute-mean value of wind speed was measured during this expedition: 56 kt (Bft 11; see also Fig. 2.2).

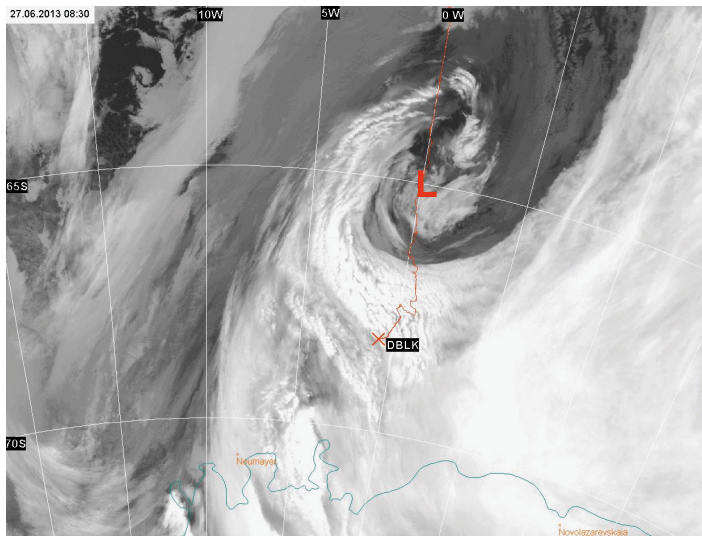


Fig. 2.1: IR-satellite picture NOAA 16 for 27.06.2013, 15:00 UTC. The position of the vessel Polarstern is marked by X.

After the wind turned towards south-east, later south, there was some more space between the ice floes, which made it easier for *Polarstern* to master passing. On 28th June the ship's expedition proceeded towards west through the pack-ice. On 29th June a dry wind flow from Antarctica provided us good meteorological conditions for flights for that one day. The following day we had to deal with fronts again, moderate north-easterly winds and light snowfall, and it became a little bit warmer.

The first two days of the month of July frontal influences dominated, that means south-westerly winds up to 6 Bft caused overcast skies, drifting snow and temperatures around -20°C . The next five days until 7th July were influenced by air masses from Antarctica, weak southerly winds built up a strong temperature inversion near surface. So, night temperatures fell nearby -28°C , and together with winds around 5 Bft the wind chill temperature exceeded -50°C for a while. During this period high low cloud coverage associated with moderate to poor conditions for horizon and contrast frequently prevented helicopter operations over the sea-ice. On 6th and 7th July colder and dryer air masses from Antarctica brought scattered and broken clouds in upper layers, this fact and a long period of sunlight enabled some long distance flights of the helicopters to place buoys on the ice in Weddell Sea.

During the period 8th to 14th July the weather in the boundary layer was caused by cooling and wetting effects of the sea-ice and by many leads. At mostly calmed, but often changing winds we got a strong temperature inversion and thus low stratus clouds were built up. Besides, some passages of weak fronts brought often light snow and drifting snow, consequently horizon and contrast getting insufficient for helicopter flights. As the wind came from northerly directions we had a warming of air and temperatures raised up to -6°C , otherwise airflow from southerly latitudes produced temperatures nearby -20°C within some hours (see also Fig. 2.4).

On 15th July another depression and its fronts brought snow and blowing snow together with northerly winds up to 8 wind forces and temperatures near surface of around -1°C. Some more similar weather sequences followed on 18th and 21st of July to provide us with high wind speed and huge temperature differences of nearly 20 degrees during a 24 hours time interval.

Based on a serious disease of a participant of this expedition we changed our course on 17th July to reach a rescue flight from Eduardo Frei (62° 12' S, 58° 57' 51" W, King Georg Island, Chile) to Punta Arenas. On 23rd July in open waters and with nearly 4 m waves we came in flight range to King George Island to make a long range helicopter flight of around 100 nm to the aerodrome. Although the weather window was only five hours it had been possible to carry out the flight under good flight conditions, just in time before fog and very low clouds encountered the area.

Between the 18th and 19th, and on 22nd of July some similar weather developments with the passage of fronts and high wind speeds happened, and also big temperature differences of more than 20°C during one day were measured several times. On 20th July was the coldest day during this expedition. A south-easterly air flow came directly from Antarctic, producing temperatures of minus 31.2°C in a height of 29 m above sea level (ASL). Induced by influence of very dry air masses we had excellent flight conditions in meteorological terms and very good contrast during daylight. The following two days, returning back to the compact ice, low pressure systems with some fronts and snowfall, but also low clouds, dominated the weather in the vicinity of the ship. From 25th July on, a period with south-westerly winds up to 8 wind forces (gusts up to 51 kts), strong blowing snow were registered and the dry airflow from the Antarctic continent pushed the temperatures often below -23°C (see Fig. 2.4). Compact sea ice coverage by ice thickness of nearly 2.5-3 m stopped our movements towards southeast for some hours.

On 28th July probably little changes of wind speed and direction, as well as changes in tides, affected the course of our expedition towards 63.4°S 50.5°W (mooring position) against a north-easterly ice drift. Between July 28 and 30, a strong temperature inversion caused overcast conditions nearby 63°S 51°W. At nearly soft south-westerly-, later fresh south-easterly winds and temperatures up to -28.8°C helicopters couldn't work properly most of the time because of bad contrast and horizon. One of the best flight conditions during the expedition we had from July 31 to August 2, during our last 4-day ice station. A ridge of high pressure provided us in connection with nearly calm winds and dryer air very good flight weather conditions. This allowed us to successfully complete some scientific helicopter flights.

On 8th August we reached Elephant Island and the sea ice edge. Because of frontal influences and foggy conditions there was no sight of the island. The following transit through Drake Passage was affected by waves up to 6 m and a strong westerly wind of force 7 to 9. Wet and windy weather dominated on 12th August in the morning when *Polarstern* reached its final destination, the port of Punta Arenas.

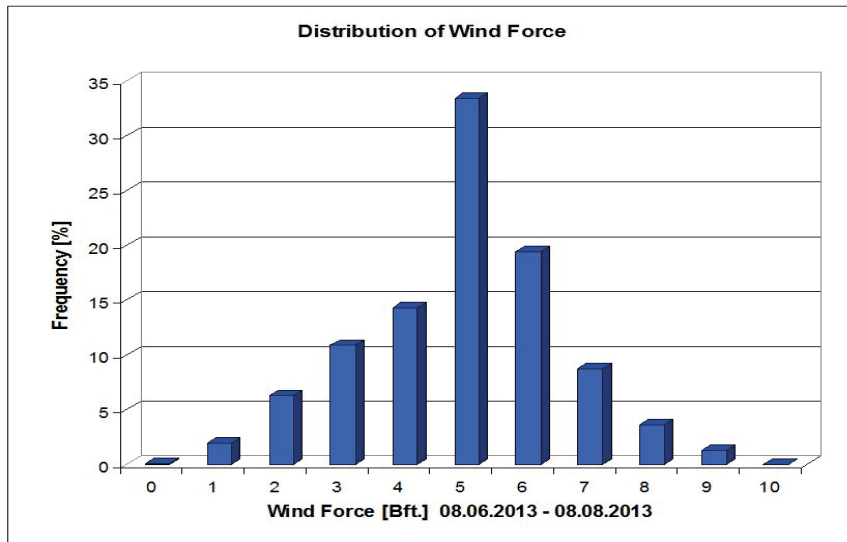


Fig. 2.2:
Distribution of
wind force during
ANT-XXIX/6

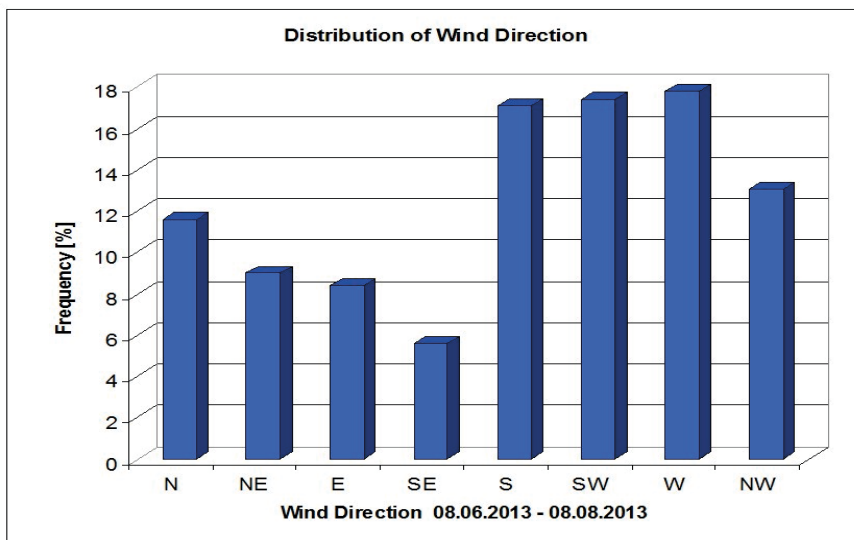


Fig. 2.3:
Distribution of
wind direction
during ANT-
XXIX/6

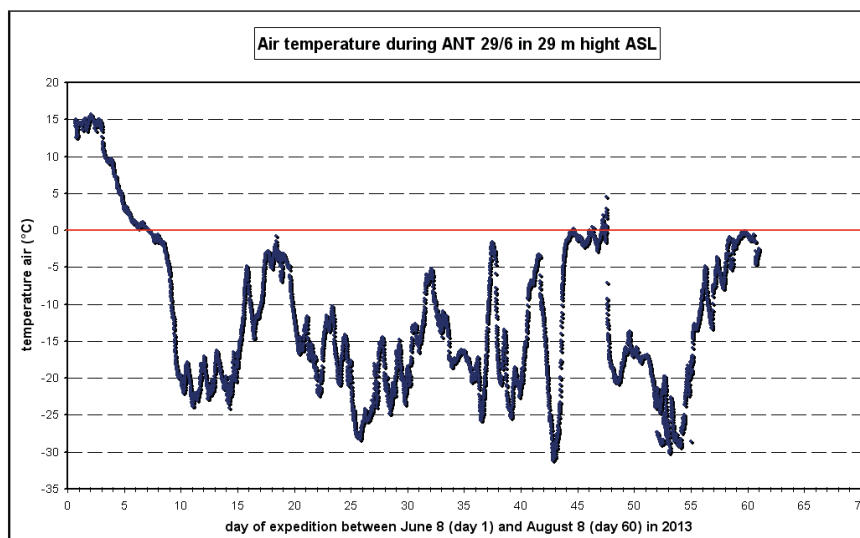


Fig. 2.4: Air
temperature
during ANT-
XXIX/6

3. METEOROLOGY

Priit Tisler¹, Marius Jonassen¹, Barbara Altstädter², Andreas Scholtz², Christof Lüpkes³ (not on board), Timo Vihma¹ (not on board), Astrid Lampert² (not on board)

¹FMI
²TU-BS
³AWI

Objectives

This project aims at filling the gap of knowledge about the structure of the atmospheric boundary layer (ABL) over the sea ice covered Weddell Sea during winter. Observations were carried out to obtain a better understanding of the interaction between atmosphere, sea ice and ocean.

The project includes both an observational part during the cruise and the following data analysis. It consists of joint work by groups from the Finnish Meteorological Institute in Helsinki (FMI), from the Technische Universität Braunschweig (TU-BS), and from the Alfred-Wegener-Institut Helmholtz-Zentrum für Polar- und Meeresforschung (AWI). Observations of wind, temperature, and humidity have been carried out by several unmanned aerial systems (UAS). The core of the project is based on the operation of an unmanned aircraft SUMO (Small Unmanned Meteorological Observer) and a small quadrocopter (both run by FMI), and the unmanned aircraft M²AV (Meteorological Mini Aerial Vehicle) by TU-BS. The data from these airborne instruments are supplemented by the routine meteorological observations at *Polarstern*, by *Polarstern* soundings, and by meteorological observations from a mast on the sea ice, installed by FMI group during stations.

The M²AV aircraft enables highly resolved measurements of the wind components and temperature so that turbulent fluxes can be derived by application of the eddy covariance method. Based on the profiles of mean and turbulent quantities, which have been obtained by all UAVs together, the structure of the atmospheric boundary layer will be characterized along the cruise track in different ice morphology regimes, where so far only very limited data is available for this time of year.

Work at sea

Work at sea was restricted to the operation of the different UAVs during ice stations because take-off and landing was not possible from *Polarstern*. Altogether we had 8 ice-stations with different length, but weather conditions were not always favourable for flying. The factors limiting operation on ice were strong wind (over 10m/s), poor visibility due to low foggy clouds and ice formation on the UAVs' wings and propeller blades. Finding suitable landing and take-off stripe, particularly for M²AV, was also very difficult due to rough sea ice. Note that the take-off of M²AV requires a winch system that was fixed to the ice. In this sense the quadrocopter has an obvious advantage compared to SUMO and M²AV, as it does not need large flat areas for landing and take-off.



Fig. 3.1: Priit (right) and Marius (left) launching SUMO for a mission (photo taken by Mario Hoppmann)



Fig. 3.2: Priit landing the quadcopter (photo taken by Mario Hoppmann)

SUMO (Fig. 3.1) was operated during 5 ice-stations. The typical flight pattern for SUMO consists of vertical profiles with a maximum altitude between 1.0 km and 1.7 km. When lower profiles were considered, two profiles were made during one flight.

The quadcopter (Fig. 3.2) was operated during 3 ice-stations. It has a rather slow ascending and descending rate and was used in order to get more precise measurements of temperature and humidity from the lowest 100m layer of the atmosphere. No serious technical problems were observed during operating both the SUMO and quadcopter.

The weather mast was deployed on ice during 7 ice-stations. The temperature was measured at 0.1 m, 0.5 m and at 2 m height. Wind speed and wind direction were measured at 2 m height. The measurements were obtained by using Aanderaa and MSR145 sensors/datalogging systems.

In addition to UAV flights and mast measurements FMI group deployed and left in ice two ice mass balance buoys.

A summary of FMI group UAV flights and mast measurements is given in Table 3.1.

Tab. 3.1: Summary of SUMO and quadcopter (QC) flights by the FMI group. Maximum altitudes of profiles per flight are given along with the measurement period of the weather mast during the ice-stations.

ICE-STATION		UAV flights					WEATHER MAST (measurement period)
		SUMO	QC	DATE	TIME (UTC)	HEIGHT	
1	S66.45 E000.10	x		21.6.2013	19:14 - 19:43	1 km + 1km	15:58(21.06) - 22:07(21.06)
		x		21.6.2013	20:01 - 20:35	1 km + 1km	
		x		21.6.2013	21:16 - 21:50	1 km + 1km	
2	S67.45 E000.02			24.6.2013	-	-	09:04(24.06) - 16:49(24.06)
3	S67.95 W006.70	x		3.7.2013	13:18 - 13:38	1.1 km	10:57(03.07) - 14:12(04.07)
		x		3.7.2013	13:57 - 14:14	1.1 km	
		x		3.7.2013	15:55 - 16:15	1.1 km	
		x		3.7.2013	16:49 - 17:19	1.1 km + 1.1 km	
		x		3.7.2013	19:46 - 20:16	1.1 km + 1.1 km	
		x		3.7.2013	20:42 - 21:13	1.1 km + 1.1 km	
4	S67.19 W013.20		x	8.7.2013	17:08 - 17:10	30 m	-
			x	8.7.2013	17:54 - 17:57	50 m	
			x	8.7.2013	18:04 - 18:07	50 m	
			x	8.7.2013	20:09 - 20:14	100 m	
			x	8.7.2013	20:36 - 20:40	100 m	
			x	8.7.2013	20:45 - 20:50	100 m	

ICE-STATION	UAV flights					WEATHER MAST (measurement period)	
	SUMO	QC	DATE	TIME (UTC)	HEIGHT		
5	S67.18 W023.20	x		11.7.2013	14:20 - 14:43	1.1 km + 500m	11:17(11.07) - 10:03(15.07)
		x		11.7.2013	18:35 - 19:09	1.1 km + 1.1 km	
		x	x	11.7.2013	19:55 - 20:00	100 m	
		x		11.7.2013	20:08 - 20:40	1.1 km + 1.1 km	
		x	x	11.7.2013	21:03 - 21:08	100 m	
		x		11.7.2013	21:19 - 21:50	1.1 km + 1.1 km	
		x	x	11.7.2013	22:19 - 22:23	100 m	
		x		11.7.2013	22:37 - 23:05	1.1 km + 1.1 km	
		x	x	11.7.2013	23:17 - 23:22	100 m	
		x		11.7.2013	23:36 - 00:03	1.1 km + 1.1 km	
		x		13.7.2013	12:51 - 13:30	1.1 km + 1.1 km	
		x	x	13.7.2013	13:53 - 13:57	100 m	
		x		13.7.2013	14:48 - 15:18	1.1 km + 1.1 km	
		x	x	13.7.2013	15:29 - 15:33	100 m	
		x		13.7.2013	15:47 - 16:17	1.1 km + 1.1 km	
		x	x	13.7.2013	16:29 - 16:33	100 m	
		x		13.7.2013	16:42 - 17:13	1.1 km + 1.1 km	
		x	x	13.7.2013	17:30 - 17:34	100 m	
		x		13.7.2013	17:43 - 18:14	1.1 km + 1.1 km	
		x	x	13.7.2013	18:23 - 18:27	100 m	
		x		13.7.2013	18:40 - 19:10	1.1 km + 1.1 km	
		x	x	13.7.2013	19:18 - 19:23	100 m	
		x		13.7.2013	19:29 - 20:01	1.1 km + 1.1 km	
		x	x	13.7.2013	20:16 - 20:20	100 m	
x		13.7.2013	20:31 - 20:58	1.1 km + 1.1 km			
x		14.7.2013	14:00 - 14:33	1.1 km + 1.1 km			
x	x	14.7.2013	14:43 - 14:48	100 m			
x		14.7.2013	14:57 - 15:29	1.1 km + 1.1 km			
x	x	14.7.2013	15:40 - 15:46	100 m			
x		14.7.2013	15:49 - 16:21	1.1 km + 1.1 km			
x	x	14.7.2013	16:38 - 16:44	100 m			
x		14.7.2013	16:50 - 17:21	1.1 km + 1.1 km			
x	x	14.7.2013	17:37 - 17:44	100 m			
x		14.7.2013	17:50 - 18:06	1.1 km			
6	S63.40 W051.20			26.7.2013	-	-	13:29(26.07) - 22:50(26.07)
7	S63.40 W051.15	x		29.7.2013	16:50 - 17:07	1.5 km	15:34(29.07) - 16:37(02.08)
		x	x	29.7.2013	17:30 - 17:35	100m	
		x		29.7.2013	17:45 - 18:09	1.6 km	
		x	x	29.7.2013	18:29 - 18:34	100m	
		x		29.7.2013	18:44 - 19:05	1.6 km	
		x	x	29.7.2013	19:16 - 19:21	100m	
		x		29.7.2013	19:30 - 19:52	1.6 km	
		x		31.7.2013	12:49 - 13:09	1.6 km	
		x		31.7.2013	13:27 - 13:50	1.6 km	
		x		31.7.2013	15:33 - 15:58	1.7 km	
		x		31.7.2013	16:33 - 16:57	1.7 km	
		x		31.7.2013	17:56 - 18:19	1.7 km	
		x		31.7.2013	18:37 - 19:01	1.7 km	
		x		31.7.2013	19:26 - 19:50	1.7 km	
		x		31.7.2013	20:12 - 20:35	1.7 km	
		x		31.7.2013	20:56 - 21:02	421 m	
		x		31.7.2013	21:17 - 21:41	1.7 km	
		x		2.8.2013	12:21 - 12:45	1.7 km	
x		2.8.2013	13:00 - 13:10	750 m			
x		2.8.2013	13:25 - 13:46	1.7 km			
8	S62.94 W053.35	x		4.8.2013	19:45 - 20:05	1.5 km	15:30(04.08) - 22:20(04.08)
		x		4.8.2013	20:20 - 20:39	1.5 km	
		x		4.8.2013	20:48 - 21:07	1.5 km	
		x		4.8.2013	21:18 - 21:37	1.5 km	
		x		4.8.2013	21:44 - 22:02	1.5 km	

The TU-BS group performed 11 flights with M²AV during the cruise in order to get meteorological parameters with particular interest in turbulent fluxes (Fig. 3.3). During the first flight complications concerning the propulsion system have been observed due to (a) very low temperature and (b) a too long preparation time before the take-off. After changing the preparation procedure the problems were solved. The following flights were successfully performed so the altitude was increased up to 1,500 m during vertical profiling and the flight time duration was extended to about 1h. Vertical profiles were flown automatically in a rectangle with an edge length of about 1,000 m (Fig. 3.4). The rectangular flight pattern was used for calibrating wind components. At the beginning and at the end of flights, manually flown vertical profiles complete the data set. For measuring turbulent fluxes horizontal flights larger than 3 km are necessary. Those flights were flown perpendicular over leads in various heights whereby the racetrack began in a distance of 3 km to the lead and ended about 1 km behind it. The nearby leads had an average width of 400 m. Different altitudes of the horizontal flight patterns had been chosen to investigate the impact of warm open water on the ABL vertical structure.



Fig. 3.3: The unmanned aircraft M²AV above the Antarctic sea ice during the cruise ANT-XXIX/6 (photo taken by Mario Hoppmann).

M²AV Flight Nr.5 13.07.2013 11:51-12:38 UTC

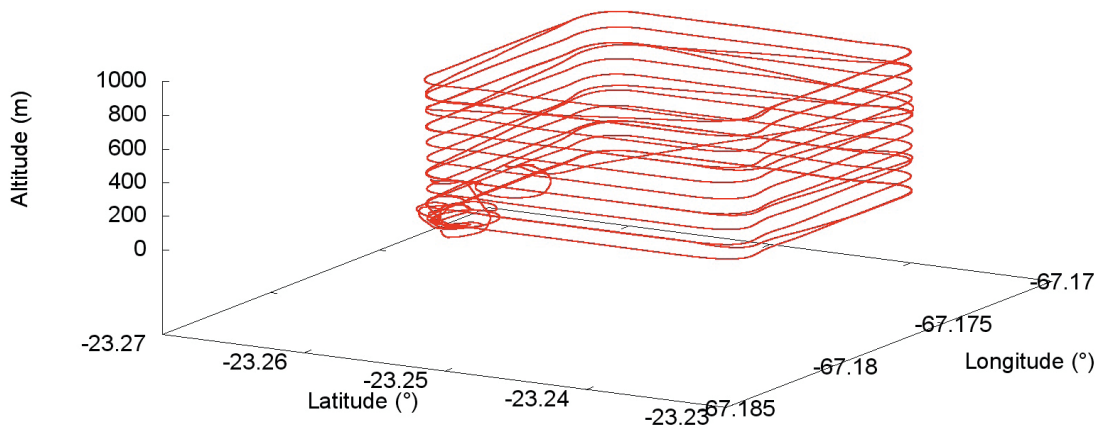


Fig. 3.4: Vertical flight pattern flown by the M²AV in a 3D-graphic. The rectangular shape is needed for calibrating wind components.

First data evaluations were performed directly after each flight to assure valuable information of the measurement. A summary of the flights performed by TU-BS during the cruise is given in Table 3.2.

Tab. 3.2: M²AV flights during the ANT-XXIX/6 cruise. Vertical profiles deliver information about the structure of the atmospheric boundary layer. Horizontal flight patterns (racetracks with more than 3 km distance) were flown over leads and in various heights to measure turbulent fluxes.

Date	Time (UTC)	Flight duration (min)	Mission profile	Altitude (m)
03.07.2013	16:07	5	Vertical	200
11.07.2013	17:18	30	Vertical	100-500
11.07.2013	23:32	38	Vertical	100-800
12.07.2013	15:11	23	Racetrack	100-200
13.07.2013	11:51	47	Vertical	100-1000
13.07.2013	15:59	54	Vertical	100-1500
29.07.2013	16:53	37	Vertical	100-400
31.07.2013	11:11	60	Vertical	100-1000
02.08.2013	02:08	38	Lead, racetrack	50, 100
02.08.2013	13:04	44	Lead, racetrack	25, 50, 75
02.08.2013	19:04	42	Lead, racetrack	15, 50, 150

Preliminary (expected) results

During this cruise a unique and high-quality dataset about vertical structure of the ABL over the Antarctic sea ice covered Weddell Sea during winter was obtained. This dataset increases our knowledge about the Antarctic climate system. In addition it can be used to validate operational weather prediction systems, and to improve boundary layer parameterizations for models of different scales from the micro-scale to the scale of climate models. The data set allows us also to compare measurements from different UAVs with data obtained from radiosoundings of the *Polarstern*. An example of preprocessed and quality-checked data is given in Fig. 3.5.

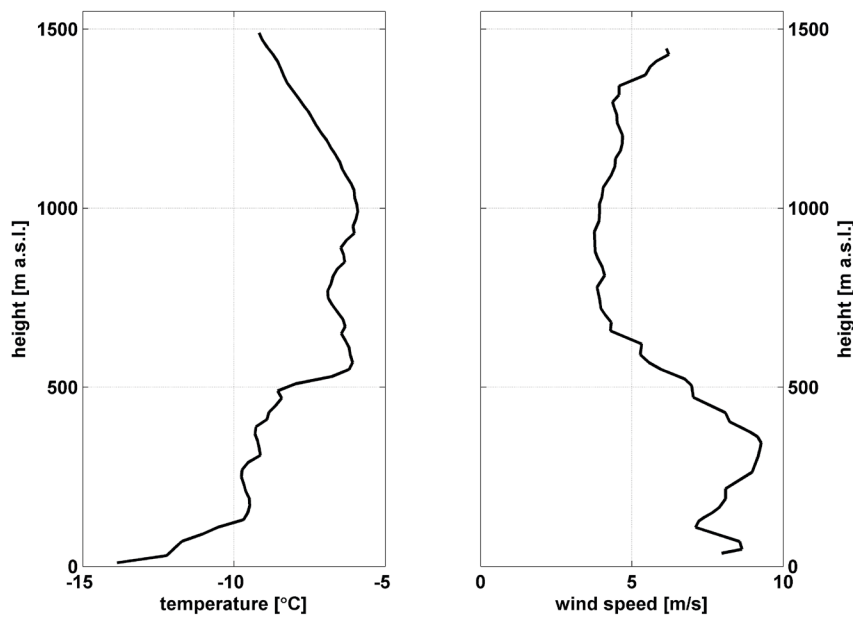


Fig. 3.5: Temperature and wind speed profile, measured by SUMO at 20:15UTC, 04.08.2013 (S62.94, W053.42)

Data management

All data obtained during this *Polarstern* expedition will be stored by the FMI and TU-BS groups for post-processing. Access to data will be possible on request when processing and corrections have been finalized, and results are published in a peer-reviewed journal.

4. ATMOSPHERIC CHEMISTRY

Katarina Abrahamsson¹, Martin Ahnoff¹,
Joelle Buxmann² Markus Frey³, Anna
Granfors¹, Katarina Gårdfeldt⁴, Hans
Werner Jacobi⁵ (not on board), David
Jones³, Bruno Jourdain⁵, Guillaume
Méjean⁶, Michelle Nerentorp⁴.

¹GU

²UHD

³BAS

⁴Chalmers

⁵LGGE

⁶LIPhy

Objectives

In the last decades more focus has been given to snow and ice chemistry in the polar regions. The original motivation was the observation of polar ozone depletion events by brominated species e.g. the reactive halogen species (RHS) BrO, Br and HOBr (Simpson et al., 2007). Later, it was found that RHS containing Cl or I, play an important role in the chemistry of the troposphere as well. The formation of reactive halogens changes the oxidizing capacity of the atmosphere by destruction of ozone and affects the partitioning of hydroxyl radicals (HO_x) and nitrogen oxides (NO_x).

Additionally, ozone depletion episodes could be associated with events of mercury depletion through oxidation by halogen radicals followed by deposition of oxidized products (Steffen et al., 2008). For the upper troposphere-lower stratosphere region, it has been suggested that halogens could destroy ozone, through the formation of halogen radicals, which is affected by ice heterogeneous chemistry. Also, many short-lived organo-halogen gases initially degrade in this region, delivering reactive halogens to the atmosphere.

Moreover, iodine takes part in new particle formation and chlorine radicals reduce the lifetime of the potent greenhouse gas methane. Therefore RHS may influence the polar (and potentially global) climate system.

There are still a number of open questions concerning the substrates of halogen activation as well as active halogen sources. First-year sea ice has been pointed out as a tentative important source due to the high salinities found within the brine formed at the surfaces (e.g. Wagner et al., 2007). Snow on sea ice can become saline being in contact with flooded sea ice and is blown into the surface near atmosphere during strong winds providing a potential source of polar sea salt aerosol and reactive bromine. However, the physical processes involved and their impact on snow, aerosol and air chemistry are still poorly understood. Research in this area has mainly concentrated round the inorganic sources of active halogens. However, a number of biologically produced volatile halogenated organic compounds (halocarbons) are associated with ice covered regions, and the question remains if the organo-iodine species and some of the organo-bromides may be of importance. Therefore efforts should be made to determine the balance between biotic and abiotic production of bromine and iodine in snow covered regions.

A stable boundary layer seems to be favourable for the build-up of a 'bromine explosion' event (auto catalytic, heterogeneous releases of reactive bromine). However, recent findings have suggested the high wind speed events inducing blowing snow may trigger ozone depletion events. There is still a lack of measurement data, which could allow us to understand if the processes that control bromine explosions are driven more dynamically than chemically. Consequently, measurement of the sea salt produced and the chemical composition of particles lifted during blowing snow event could perhaps answer this question.

One aim of the atmospheric chemistry group has been to investigate the role of sea ice and snow in the formation of reactive halogenated compounds and production of sea salt aerosol in the atmosphere. In addition, establishing a relationship between sea salt aerosol production above sea ice and its deposition on the Antarctic continent is key to using the sea salt ice core record as a proxy for past sea ice extent. More specifically, the six groups involved, have studied the interplay between halogens, ozone and mercury, as well as the sea salt burden in the Weddell Sea. The cruise offered the possibility to study these processes during the dark period of the year, which is seldom performed, as well as, during the onset of spring.

Work at sea

The chemical composition of the different components of the ocean and cryosphere like snow, sea ice, frost flowers, and sea water was determined to study the role of these different compartments on the release of sea salt aerosols and reactive halogen and mercury compounds to the atmosphere. The atmospheric measurements included continuous measurements of specific species relevant to the formation of reactive halogen species, such as halogen oxides and volatile halogenated organic compounds, gaseous elemental, oxidized, organic and particulate fractions of mercury, and ozone. Furthermore, particle size and concentration of snow and aerosols along with basic meteorology were monitored continuously at various levels above the sea ice. In addition, salinity and major ion chemistry of aerosol and snow are measured and will allow to assess the role of blowing snow for the production of sea salt aerosol. A summary of the measurements is given in Table 4.1.

Tab. 4.1: Summary of the measurements carried out during ANT-XXIX/6

Atmospheric sampling

Parameter	Technique	Resolution	Dates	Involved staff
Ozone	UV abs	1 min	11-06-2013 to 12-08-2013	B. Jourdain
Acidic gases (HCl, HBr, HNO ₃ , SO ₂)	Na ₂ CO ₃ coated denuder tubes	Weakly samplings	20-06-2013 to 06-08-2013	B. Jourdain
Particle number distribution (0.03 – 10µm)	Electrical Low Pressure Impactor	1 min	21-06-2013 to 20-07-2013	B. Jourdain

Parameter	Technique	Resolution	Dates	Involved staff
Size segregated aerosol chemical composition	Electrical Low Pressure Impactor	Weakly samplings	21-06-2013 to 20-07-2013	B. Jourdain
Particulate NO ₃ ⁻ N and O isotopic composition	High Volume sampler	Weakly samplings	14-06-2013 to 12-08-2013	B. Jourdain
Halocarbons*	Gas chromatography	1,5 h	13-06-2013 to 21-07-2013	K. Abrahamsson, A. Granfors, M. Ahnoff
Aerosol concentration & size distribution (0.3 - 10µm)	Compact Light-Weight Aerosol Spectrometer	1 Hz	13-06-2013 to 08-08-2013	M. Frey, D. Jones
Aerosol chemical composition (major ions & some halogens)	Filter samples	4-24 h	13-06-2013 to 08-08-2013	M. Frey, D. Jones
Snow particle concentration & size distribution (50 - 500µm)	Optical snow particle counter	1 Hz	13-06-2013 to 08-08-2013	M. Frey, D. Jones
Atmospheric turbulence	Sonic Anemometer	25 Hz	During ice stations 13-06-2013 to 08-08-2013	M. Frey, D. Jones
Temperature & RH	AWS	1 s	During ice stations 13-06-2013 to 08-08-2013	M. Frey, D. Jones
BrO, IO, NO ₂ , O ₃ , H ₂ O, OClO, O ₄ , HCHO	Ship based MAX-DOAS	3 min	08-06-2013 to 12-08-2013	J.Buxmann
BrO, IO, NO ₂ , O ₃ , H ₂ O, OClO, O ₄ , HCHO	Air borne MAX DOAS	1 s	During Helicopter flights**	J.Buxmann
IO, NO ₂ , OClO	Cavity enhanced DOAS	30 s	During ice stations 13-06-2013 to 08-08-2013	J.Buxmann
Ozone	UV abs.	1 min	11-06-2013 to 12-08-2013	J.Buxmann
Aerosol Optical Depth	hand held sunphotometer	15 min during sunshine	01-08-2013	J.Buxmann
Mercury speciation Hg ⁰ (g), Hg(II)(g), Hg(II)(particulate phase)	Tekran 1135 CVAFS	5 min	11-06-2013 to 12-08-2013	K. Gardfeldt M. Nerentorp
IO or BrO	Mode-Locked Cavity Enhanced Absorption Spectroscopy	1 min 2 min	12-07-2013 to 04-08-2013	G. Méjean

Sea-ice / snow sampling

Parameter	Technique	Resolution	Dates	Involved staff
Snow chemical composition	Surface and -20 cm sampling	Daily during ice station	21-06-2013 to 05-08-2013	B. Jourdain
Snow, halocarbons*	Gas chromatography	Daily during ice stations, 10 cm	21-06-2013 to 02-08-2013	K. Abrahamsson, A. Granfors, M. Ahnoff
Sea ice, halocarbons*	Gas chromatography	Daily during ice stations, 5-10 cm	21-06-2013 to 02-08-2013	K. Abrahamsson, A. Granfors, M. Ahnoff
Snow chemical composition & salinity	Ion chromatography, conductivitymeter	Daily during ice stations, total snow column	13-06-2013 to 08-08-2013	M. Frey, D. Jones
Snow, mercury species Dissolved Hg ⁰ Hg-total Methyl-Hg ⁺	Purge and trap CVAFS Derivatisation Gas chromatography	Daily during ice stations, 10 cm	21-06-2013 to 02-08-2013	K. Gardfeldt M. Nerentorp
Sea ice, mercury species Dissolved Hg ⁰ Hg-total Methyl-Hg ⁺	Purge and trap CVAFS Derivatisation Gas chromatography	Dissolved Hg ⁰ Daily during ice stations, 5-10 cm. Hg-total Methyl-Hg ⁺ Selected samples	21-06-2013 to 02-08-2013	K. Gardfeldt M. Nerentorp

Sea-water sampling

Parameter	Technique	Resolution	Dates	Involved staff
Surface water, halocarbons*	Gas chromatography	1.5 h	13-06-2013 to 21-07-2013	K. Abrahamsson, A. Granfors, M. Ahnoff
Water column, halocarbons	Gas chromatography	CTD stations	15-06-2013 to 1-08-2013	K. Abrahamsson, A. Granfors, M. Ahnoff
Water column, Dissolved Hg ⁰ Hg-total Methyl-Hg ⁺	Purge and trap CVAFS Derivatisation Gas chromatography	CTD stations	15-06-2013 to 4-08-2013	K. Gardfeldt M. Nerentorp

*Halocarbons: CH₃I, CH₃CH₂I, CH₃CHICH₃, CH₃CH₂CH₂I, CH₃CHICH₂CH₃, CH₃CH₂CH₂CH₂I, CH₂ClI, CH₂BrI, CH₂I₂, CH₂Br₂, CH₂BrCl, CHBrCl₂, CHBr₂Cl, CHBr₃, CH₃CCl₃, CCl₄, CHCl=CCl₂, CCl₂=CCl₂

**Helicopter flights with MAX-DOAS measurements were performed on the following days: 16-06-2013, 17-06-2013, 18-06-2013, 19-06-2013, 20-06-2013, 21-06-2013, 07-07-2013, 30-07-2013, 31-07-2013, 01-08-2013, 04-08-2013, 05-08-2013, 06-08-2013

Preliminary (expected) results

Ozone and the other relevant atmospheric compounds were recorded during the entire cruise. A first well marked ozone depletion event was observed during night time the 16th July, as the ship was South of 67°S. Five major ones and a few less pronounced ones were measured later until the sea-ice zone was left on the 8th August.

The preliminary examination of the global data set obtained for the period from 11th to 23rd July, as the ship was going North from 67°15 to 60°20S is quite exciting and promising. The main observations are summarised below:

- As we were travelling north, the global radiation increased. In the meantime, a decreasing tendency had been clearly observed for the volatile halogenated organic compounds levels, suggesting an enhanced active photochemistry. Production of halogenated active species is expected from this photochemical activity.
- Five ozone depletion events were recorded during that period. Large elemental gaseous mercury depletion events were systematically recorded at the same time, whereas a large increase of particulate mercury and, to a lesser extent of oxidised mercury species, was observed. Also, organo iodine levels decreased during those events, suggesting a more pronounced production of active iodide compounds, whereas organo bromine compounds seemed to slightly increase. During two cases when the depletion occurred during daytime, high tropospheric BrO levels were also measured by the DOAS device. Moreover, an increase in the total particulate number measured both by the Compact Light-Weight Aerosol Spectrometer and the electrical low pressure impactor was quite systematically observed during these events, suggesting that heterogeneous processes also have to be considered. Finally, blowing snow events are suggested to initiate the ozone and mercury depletion events since several of these were preceded by periods with strong winds above the threshold of snow particle uplift from the surface.
- Enhanced number of particles is observed during blowing snow events.

4.1 Detection of halogen oxides

4.1.1 Iodine monoxide measurements

Although satellite measurements, as well as MAX-DOAS measurements indicate high levels of IO in Antarctica (Frieß et al. 2010), surprisingly low IO concentrations, with IO being below the detection limit (< 0.5 ppt) of the active DOAS instruments were found in the data evaluated so far. This confirms the findings of two measurement campaigns conducted at the German Research Station Neumayer (70°S, 8°W) in austral summer 2011 and the New Zealand Station Scott Base (177°E, 78°S) in spring/summer 2013 (Frieß et al., 2013). Putting the results for detection of IO of the whole cruise from the active and passive instruments together, this will help to solve the question to what extent IO is of importance for the chemistry of the Antarctic MBL. Additionally a comparison for situations where IO has been detected and where it stayed below the detection limit, might give a hint about the differences in Antarctic and Arctic as well.

4.1.2 Remote sensing of BrO by MAX-DOAS

From the spectral analysis of the MAX-DOAS measurements the so called slant column density (SCD) is retrieved. The SCD is the integrated trace gas concentration along the light path through the atmosphere. As a reference spectrum zenith measurements are used, which also contain atmospheric absorption structures of the atmospheric trace gases. Thus the result of the DOAS analysis represents the difference of the SCDs of the measured zenith spectrum taken as reference and the evaluated spectrum (which is typically at a different elevation angle, but could be an earlier/later zenith spectrum as well). In the following differential slant column densities ($dSCD = SCD_{meas} - SCD_{ref}$) will be shown. Extensive radiative transfer modelling after the cruise will give detailed knowledge about the actual light path and concentrations/mixing ratios can be retrieved.

Both MAX-DOAS instruments indicate elevated differential slant column densities during large periods of the cruise under different sea ice and snow conditions. To what extent the different conditions and how the air masses were transported, influence the strength of a bromine explosion event will be addressed by further evaluation using wind trajectories and satellite observations as well. Additionally different conditions observed during the flights and the cruise will be compared.

The diurnal variation of BrO observed by the ship based MAX-DOAS over the sea ice is frequently characterised by a maximum in the morning and evening, and a local minimum around noon.

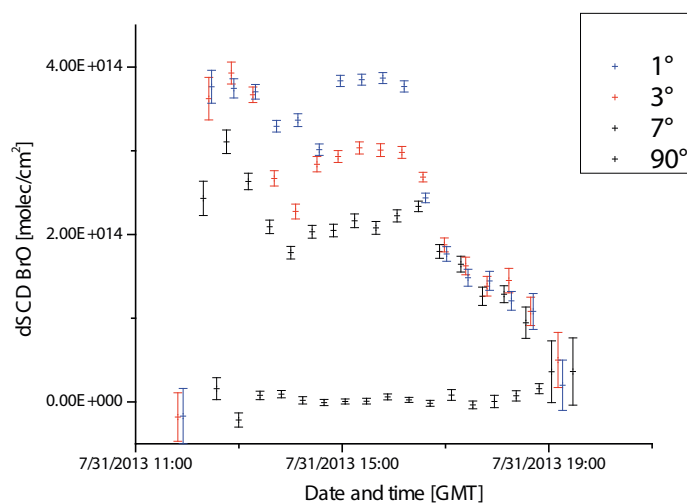


Fig. 4.1: Diurnal shape of $dSCD$ BrO in molec/cm^2 showing a double peak with maxima after sunrise and before sunset

Similar double peaks have been reported e.g. during springtime in the Amundsen Gulf (Pöhler et al. 2012). Model studies by von Glasow et al. (2002) suggest that the differences in the photolysis spectra of O_3 and Br_2 cause this diurnal variation. Br_2 is more rapidly photolysed to form Br radicals and through ozone destruction BrO, and thus the main source of BrO in polar regions. The main sink in the absence of NO_2 is reaction of BrO with HO_2 to form HOBr. HO_2 is a product of O_3 photolysis and subsequent reactions, which starts later in the day due to absorption at longer wavelengths.

4.3 Sea salt aerosols and blowing snow

In summary the information about the vertical and special distribution of the detected BrO, will help to answer what role the sea ice plays in the generation of sea salt aerosols and reactive halogens. In particular the collaboration with the sea ice physics group might be a big step forward. Ozone and mercury depletion events were detected together with high BrO values. Consequences on atmospheric chemistry will be discussed after further evaluation. If Organohalogen measured during the cruise can be a sufficient source of the detected halogen oxides will be addressed later, as well as influences of blowing snow events.

4.2 *In-situ* and local measurements of halogen oxides IO and BrO by “Mode-Locked Cavity Enhanced Absorption Spectroscopy”

MOCAMAR project financed by the ANR gave birth to the first field instrument, based on the technique ML-CEAS (Mode-Locked Cavity-Enhanced Absorption Spectroscopy) dedicated to IO, BrO, NO₂ and CH₂O, and able to measure their natural concentrations which are extremely low (sub ppbv) and highly variable in time and space. These species are measured selectively and accurately with rms noise levels corresponding to 20 ppqv (in 5 min), 1 pptv (in 1 min), 5 pptv (5 min) 100 pptv (1 min), respectively. The instrument was deployed successfully at the Dumont D’Urville French station on the east coast of Antarctica .

Following this success, we have been contacted by Hans-Werner Jacobi from LGGE to participate in this field campaign onboard the *Polarstern*. Our objective was to measure IO and BrO for a better understanding of the role that the sea ice plays in sea salt aerosol generation and the consequences for atmospheric chemistry of halogen oxides. These measurements are very challenging on board a ship since the instrument relies on ML-CEAS technique where the cavity Free Spectral Range is adjusted to be twice the laser repetition rate thanks to a motorized translation stage while piezo-electric tube transducers allow for fast modulation of cavity modes across a global resonance with the laser comb teeth. To avoid any noise, it is necessary to control the cavity length with sub-micrometer accuracy.

In spite of the modifications of the system to absorb the vibrations of the ship, the limit of detection of the instrument has been reduced due to the vibrations of the engine. Nevertheless, the limit of detection of IO was quite good with a value of 0.04 pptv, corresponding to the rms noise level. The situation was more delicate for the measurement of BrO, since the limit of detection was only of 5 pptv which corresponds already to a very high level of BrO in the atmosphere. Neither BrO nor IO had been measured during this field campaign even during depletion events of ozone and mercury which occurred at the end of July. These measurements confirm that there is no emission of IO during winter in Antarctica or the emission is at such a low level that there is no impact in the atmospheric budget. The poor limit of detection of BrO does not permit any conclusion.

4.3 Sea salt aerosols and blowing snow

At most parts of the Earth, sea salt aerosol (SSA) derives from sea spray and bubble bursting at the open ocean surface. It plays (as the major component of marine aerosol) several important roles. It is a significant direct contributor to the radiative balance; it can act as a cloud condensation nucleus; it contributes surface area for heterogeneous chemical reactions; and finally it takes part in some of

these reactions, for example between salt and atmospheric acids, and in reactions leading to the production of activated halogen compounds.

In Antarctica evidence from year-round sampling of aerosols and ice core analysis points to a winter source of sea salt aerosol located in the sea ice region. However, in order to quantify the relationship between sea salts measured in ice cores and past sea ice extent a number of processes still need to be investigated. In particular, no observations exist on how saline snow gets lifted into the air and contributes to the production of sea salt aerosol and reactive bromine.

It was recently suggested that sublimation of saline blowing snow, formed from mobilisation of snow on sea ice, was the most important source of SSA in the polar regions (Yang et al., 2008). This would provide a clear mechanism for lofting aerosol into the atmosphere, and the brine wicked up into snowpack (providing salinity) should be fractionated. It was estimated that aerosol production from salty blowing snow could be an order of magnitude greater than that from a similar area of open ocean (Yang et al., 2008). This is therefore a highly plausible mechanism for SSA and reactive Br production. With current parameterisation (Yang et al., 2008), it partly reproduces observed polar BrO columns (Yang et al., 2010).

The ANT-XXIX/6 cruise with the *Polarstern* into the Weddell Sea during winter provided the opportunity to test the blowing snow hypothesis. A number of measurements were done continuously from the level of the ship's crows nest (29 m) and on the sea ice during ice stations (Table 4.1). These included observations of snow particle and aerosol concentrations along with their size distribution. In addition aerosol filter samples (4-24h resolution) and samples of surface and blowing snow were collected for salinity measurements performed on board and later analysis of chemical composition including major ions, bromine and iodine (Table 4.1). The snow lying on the sea ice was sampled during ice stations at 2-cm depth resolution. Furthermore, temperature and relative humidity profiles as well as friction velocity were measured during ice stations to calculate the respective fluxes of moisture, aerosol and snow particles.

Preliminary results show that the surface and blowing snow have very low salinities of <0.1 psu, whereas frostflowers are typically at >60 psu. This is likely due to the fact that average snow depth on the sampled ice floes was significantly higher than reported previously, possibly due to above average precipitation. However, significant aerosol production in the size range of sea salt (1-10 μm) was observed during and after blowing snow events. Wind speeds necessary to cause uplift of snowparticles ranged around 10 m/s (Fig. 4.2). On occasion rocket traps were employed to determine the horizontal snow mass flux yielding several kilograms per m^2 and minute. This suggests that even though snow salinity is low, the large mass flux still can provide significant sea salt aerosol loading to the lower atmosphere. To a first order the atmospheric impact of the blowing snow source is seen by ozone and mercury depletion events some of which immediately follow a blowing snow event. Further analysis including chemical composition of aerosols and snow samples will allow to further quantify the full sequence of processes, from salt uptake of snow at the surface to the production of sea salt aerosol above the blowing snow layer.

4.4 Volatile halogenated organic compounds

Naturally produced halocarbons are a group of compounds consisting of one to three carbon atoms with one to three halogen atoms (Table 4.1). They are considered to be short-lived in the troposphere, since they have atmospheric lifetimes shorter than 6 months. Still, there is evidence that brominated very short-lived substances may contribute about 5 pptv to total stratospheric inorganic bromine (Law and Sturges, 2007).

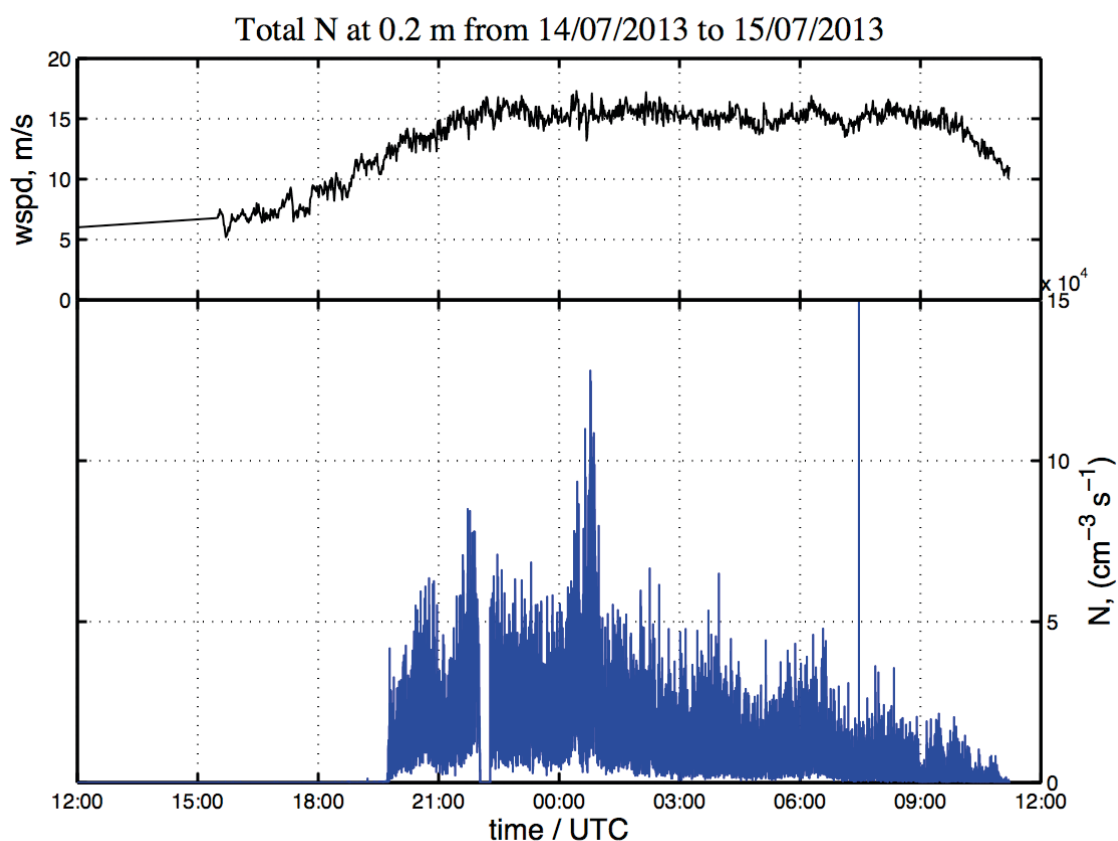


Fig. 4.2: Total snow particle flux N at 0.2 m above the sea ice during Jul 14-15 (bottom panel) along with wind speed (top panel)

Halocarbons are formed through the reaction of HOCl, HOBr and HOI with the dissolved organic matter by the haloform reaction. These species can be formed by marine organisms or by chemical reactions. In the haloform reaction the above mentioned halocarbons, except iodomethane, is produced. Of the brominated compounds, CHBr_3 is the main contributor of organo-bromine (Quack and Wallace, 2003). For the iodinated ones, CH_2I_2 contributes to the largest extent to organo-iodine, however, it is seldom at concentrations above detection limits in open oceans (Carpenter et al., 2007) or in sea ice (Granfors et al., 2013). The above mentioned mechanism cannot be applied for the formation of methyl halides. Instead, it has been suggested that they are produced through another enzymatic pathway, i.e. methyl chloride transferase (Wuosmaa and Hager, 1990). Alternatively, beta-dimethyl-sulphoniopropionate (DMSP) could react with halide ions forming CH_3X (White, 1982).

The release of bromine from snow and sea ice surfaces has mainly been attributed to the reaction of HOBr with bromide at acidic conditions to form Br₂. Little attention has been given to the role of halocarbons in the formation of reactive halogen species in the atmosphere during bromine explosion events. These compounds are emitted from the different compartments of the cryosphere to the atmosphere, where they are photolysed to BrO and IO which are involved in the degradation of ozone.

In order to elucidate the importance of brominated and iodinated halocarbons in atmospheric halogen chemistry during polar winter, the distribution of these compounds were measured in sea ice, snow, surface water and air. For spatial and temporal resolution see Table 4.1.

Also, studies of the distribution of halocarbons in the water column were performed with special emphasis on the release of halocarbons from sediment.

4.4.1 Sea ice and snow as sources of halocarbons

In total 12 ice stations were sampled with respect to sea ice, snow, brine and under ice water.

Sea ice cores (63), as well as snow were collected and analysed for their content of halocarbons. At the majority of the stations, brine from different depths could be sampled. In addition at four occasions frost flowers were collected.

High concentrations, nM range, of brominated and iodinated halocarbons were found in the upper part of the sea ice. This is approximately a 100 times higher than what has been found in summer Antarctic sea ice (Granfors et al., 2013). These extremely high levels were reflected both in brine, frost flowers and at the snow-ice interface. The fact that the cruise commenced during the dark period enabled us to detect and quantify the iodinated compound CH₂I₂, an important precursor of IO, which is highly susceptible to photolysis.

At the end of the cruise we encountered multi-year ice which differed significantly in its halocarbon distribution, with the highest concentrations found in the lower most part.

CH₃I, with its different formation mechanism, had maximum concentrations in the center of the ice, with a strong relation to DMS (see sea ice biogeochemistry section).

The snow was sampled in 10 cm sections, and there was in most cases a gradient with decreasing concentration towards the surface. This indicates that there could be a flux of halocarbons from the sea ice, through the snow, to the atmosphere.

4.4.2 Continuous measurements in air and surface waters

Continuous measurements of halocarbons in air and surface sea water were performed from the start of the expedition until 22nd July, when the instrument broke down. Our preliminary findings suggest that the sea ice is in fact a source of halogens to the atmosphere, since the air concentrations found in ice covered areas were substantially higher than what was found over the open ocean. Also, the sea water concentrations did not vary to any larger extent, and were highly under-saturated with respect to the air.

4.5 Mercury

4.4.3 Distribution of halocarbons in the water column

The CTD/rosette was sampled along two transects, in total 33 stations. The distribution of halocarbons showed, in general, the highest concentrations in the upper water column due to the production of halocarbons by micro algae. The concentrations increased at the bottom which confirms earlier findings that sediments could act as local sources of halocarbons.

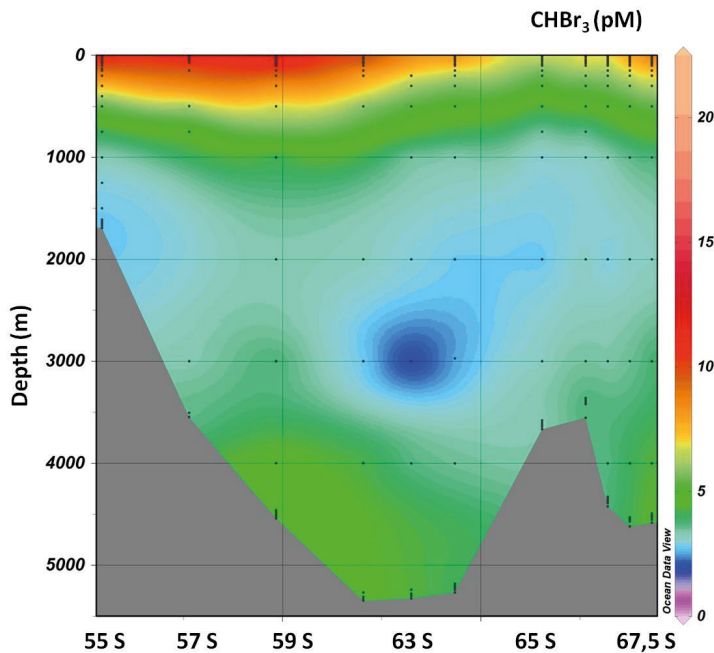


Fig. 4.3: The distribution of bromoform (CHBr₃) along E 0 from S55 to S67.5

4.5 Mercury

At several occasions atmospheric mercury depletion events (AMDE) were monitored during the expedition cruise track. After these events, elevated concentrations of mercury were found in the surface snow lawyer, probably as a consequence of AMDE and subsequent deposition of fractions of oxidized mercury. The evasion and deposition of elemental mercury from snow surface and air were studied at a few occasions during the expedition using gradient measurement. At those occasions the flux were near zero, therefore we assume that deposited mercury after AMDE will not be re-emitted to the atmosphere in its elemental form, but rather trapped in the snow pack. From these findings we assume that we have a net deposition of mercury species which are accumulated in snow and ice during polar winter.

Dissolved gaseous mercury (DGM) in surface sea water was found to be supersaturated to several hundred percent as measured 8 m below the ice cap. The concentrations of DGM under the sea ice were also found to be higher than during measurements conducted during a summer campaign 2010/11 in the Amundsen Sea. This was also confirmed by discrete samples from the CTD water system during both summer and winter campaigns. The reason for this is probably that the winter ice is a more efficient cap than summer ice.

The concentrations of elemental mercury in ice cores, on the other hand, was found to be at a lower level compared to summer ice, and also less variable due to diurnal cycling, during polar night compared to summer measurements 2010/11.

Data management

Quality-controlled data of the continuous atmospheric and sea water measurements will be available in public data bases (e.g. Pangaea) in the form of time series with maximum available temporal resolution after publication in peer-reviewed literature. Similarly, published results regarding the analysis of snow, sea ice and sea water will also be made available.

References

- Carpenter LJ, Wevill DJ, Palmer CJ, Michels J (2007) Depth profiles of volatile iodine and bromine-containing halocarbons in coastal Antarctic waters. *Marine Chemistry*, 103, 227-236.
- Frieß U, Deutschmann T, Gilfedder BS, Weller R, Platt U (2010), Iodine monoxide in the Antarctic snowpack, *Atmos. Chem. Phys.*, 10, 2439–2456.
- Friess U, Zielcke J, Pöhler D, Hay T, Kreher K, Platt U (2013), Iodine Monoxide in the Antarctic Marine Boundary Layer: Recent Discoveries, Vol. 15, EGU General Assembly 8643.
- Granfors A, Karlsson A, Mattsson E, Smith Jr WO, Abrahamsson K (2013) Contribution of sea ice in the Southern Ocean to the cycling of volatile halogenated organic compounds. *Geophysical Research Letters*, in press.
- Grilli R, Méjean G, Abd Alrahman C, Ventrillard I, Kassi S, Romanini D (2012a) Cavity-enhanced Multiplexed Comb Spectroscopy down to the Photon Shot Noise. *Physical Review A* 85 051804.
- Grilli R, Méjean G, Kassi S, Ventrillard I, Abd-Alrahman C, Fasci E, Romanini D (2011) Trace Measurement of BrO at the ppt Level by a Transportable Mode-locked Frequency-doubled Cavity-enhanced Spectrometer. *Applied Physics B* 107 (1): 205–212.
- Grilli R, Legrand M, Kukui A, Méjean G, Preunkert S, Romanini D (2013) First Investigations of IO, BrO, and NO₂ Summer Atmospheric Levels at a Coastal East Antarctic Site Using Mode-locked Cavity Enhanced Absorption Spectroscopy. *Geophysical Research Letters* 40: 1–6.
- Grilli R, Méjean G, Kassi S, Ventrillard I, Abd-Alrahman C, Romanini D (2012) Frequency Comb Based Spectrometer for in Situ and Real Time Measurements of IO, BrO, NO₂, and H₂CO at Pptv and Ppqv Levels. *Environmental Science & Technology* 46 (19) 10704–10.
- Méjean G, Grilli R, Abd-Alrahman C, Ventrillard I, Kassi S, Romanini D (2012) A Transportable Spectrometer for in Situ and Local Measurements of Iodine Monoxide at Mixing Ratios in the 10-14 Range. *Applied Physics Letters* 100 (25): 251110.
- Pöhler D, Vogel L, Friess U, Platt U (2010) Observation of halogen species in the Amundsen Gulf, Arctic, by active long-path differential optical absorption spectroscopy, *P. Natl. Acad. Sci. USA*, 107, 6582–6587.
- Quack B, Wallace DWR (2003) Air-sea flux of bromoform: Controls, rates and implications. *Global Biogeochemical Cycles*, 17, 1023.
- Simpson WR, Von Glasow R, Riedel K, Anderson P, Ariya P, Bottenheim J, Burrows J,

4.5 Mercury

- Carpenter LJ, Frieß U, Goodsite ME, Heard D, Hutterli M, Jacobi HW, Kaleschke L, Neff B, Plane J, Platt U, Richter A, Roscoe H, Sander R, Shepson P, Sodeau J, Steffen A, Wagner T, Wolff E (2007) Halogens and their role in polar boundary-layer ozone depletion, *Atmospheric Chemistry and Physics*, 7, 4375-4418.
- Steffen A, Douglas T, Amyot M, Ariya P, Aspmo K, Berg T, Bottenheim J, Brooks S, Cobbett F, Dastoor A, Dommergue A, Ebinghaus R, Ferrari C, Gardfeldt K, Goodsite M E, Lean D, Poulain A J, Scherz C, Skov H, Sommar, J Temme C (2008) A synthesis of atmospheric mercury depletion event chemistry in the atmosphere and snow, *Atmospheric Chemistry and Physics*, 8, 1445-1482.
- von Glasow R, Sander R, Bott A, Crutzen P J (2002) Modeling halogen chemistry in the marine boundary layer – 1. Cloud-free MBL, *J. Geophys. Res. Atmos.*, 107, 4341.
- Wagner T, Ibrahim O, Sinreich R, Frieß U, von Glasow R, Platt U (2007) Enhanced tropospheric BrO over Antarctic sea ice in mid winter observed by MAX-DOAS on board the research vessel Polarstern, *Atmospheric Chemistry and Physics*, 7, 3129-3142.
- White RH (1982) Analysis of dimethyl sulfonium compounds in marine algae, *Journal of Marine Research*, 40, 529-536.
- Wuosmaa AM, Hager LP (1990) Methyl chloride transferase: A carbocation route for biosynthesis of halometabolites, *Science*, 249, 160-162.
- Yang X, Pyle J A, Cox R A (2008) Sea salt aerosol production and bromine release: Role of snow on sea ice "Geophys. Res. Lett." 35, doi:10.1029/2008GL034536.
- Yang X, Pyle J A, Cox R A, Theys N, Van Roozendaal, M (2010) Snow-sourced bromine and its implications for polar tropospheric ozone, *Atmos. Chem. Phys.*, 10, 7763–7773, doi:10.5194/acp-10-7763-2010.

5. SEA ICE PHYSICS

Sandra Schwegmann¹, Stefan Hendricks¹, Priska Hunkeler¹, Mario Hoppmann¹, Stephan Paul², Stefanie Arndt¹, Katherine Leonard^{3,4}, Nander Wever³, Seth White⁴, Marcel Nicolaus¹ (not on board), Ted Maksym⁵ (not on board), Petra Heil⁶ (not on board), Jenny Hutchings⁷ (not on board), Ignatius Rigor⁸ (not on board)

¹AWI

²University of Trier

³WSL Institute for Snow and Avalanche Research SLF

⁴University of Colorado

⁵Woods Hole Oceanographic Institute

⁶University of Tasmania

⁷University of Alaska

⁸University of Washington

5.1 Airborne sea ice surveys

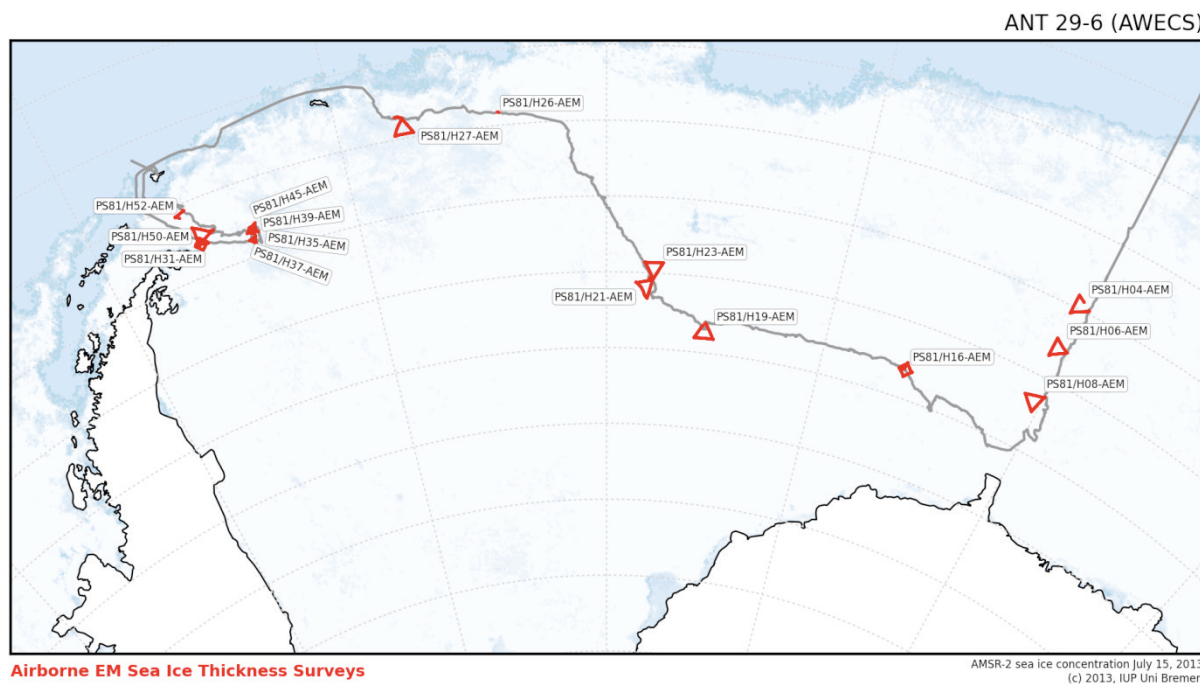


Fig. 5.1.1: Map of airborne electromagnetic induction sounding (AEM) surveys of sea-ice thickness during ANT-XXIX/6

Objectives

The mid-winter sea-ice thickness in the Weddell Sea is poorly covered by observational data. Data exist from upward-looking sonars and few *Polarstern* cruises. Satellite data of sea-ice thickness is currently limited to the ICESat period, however programs exist to evaluate sea-ice thickness retrievals from CryoSat-2 and thin ice thickness by SMOS.

5.1 Airborne sea ice surveys

One scope of airborne surveys during ANT-XXIX/6 is therefore to obtain validation data for satellite retrieval algorithms of Antarctic winter sea-ice thickness. On the other hand, sea-ice thickness data are required to be collected on regional scale with higher spatial resolution than achievable from satellites in order to analyse thermodynamic and dynamic processes, which govern the recently observed increasing trend in Antarctic sea-ice extent.

Work at sea

We used airborne electromagnetic (AEM) induction sounding to measure sea-ice thickness by helicopter surveys. The instrumentation consists of a 4 m long sensor (EM-Bird) which is towed on a 20 m long cable at an altitude between 10 and 15 m above the sea-ice surface. The EM-method utilizes the difference of electrical conductivity between sea ice and sea water to estimate the thickness of sea ice including the snow layer, if present. The system was equipped with an aerial nadir camera (Canon EOS 5D Mk II) and an Inertial Navigation System. The nadir aerial imagery visually documents sea ice conditions and enables the classification of sea-ice surface properties. The internal timestamp of the camera was synchronized with the GPS timestamp of the AEM sensor to use sensor attitude and altitude information to create a geo-reference for each image.

Preliminary results

The survey work amounted to 16 science flights with more than 2,000 km of profile data. In addition to the short periods of daylight, flight operations were significantly hampered by weather conditions with low clouds and low contrast in the first half of the cruise. Therefore, flights over predominantly first-year sea ice are spaced by several days and scattered along the cruise track (see Fig. 5.1.1 and Table 5.1.1). In the second part of the cruise, after the deviation, weather conditions lead to better flying conditions with several surveys over thicker multi-year sea ice. After processing, the sea-ice thickness data will be available as point data with an average spacing of 3 to 4 meters and a footprint of approximately 40 m.

The availability of aerial images depends on light conditions during the flight and the used sensor systems. In total 1,770 images were shot from sea-ice surfaces including aerial mapping of the ice stations. Depending on altitude, the images cover an area from below to several hundreds of meters.

Data management

The sea-ice thickness data will be released following final processing after the cruise in the PANGAEA Data Publisher for Earth & Environmental Science and international databases like the Sea Ice Thickness Climate Data Record (Sea Ice CDR). The large dataset of the aerial images will be archived at the AWI long-term data storage system.

Table 5.1.1: List of airborne sea-ice thickness surveys during *Polarstern* cruise ANT-XXIX/6 (AWECS)

Event	Latitude	Longitude	Label	Device	Date	Comment 1	Comment 2
PS81/H04	-63.65912	-0.66581	PS81/H04-AEM	Airborne EM (EM-Bird)	6/19/2013	Length 145.4 km	ID: 20130619_01
PS81/H06	-64.91750	-0.70349	PS81/H06-AEM	Airborne EM (EM-Bird)	6/20/2013	Length 167.5 km	ID: 20130620_01
PS81/H08	-66.44231	-0.45240	PS81/H08-AEM	Airborne EM (EM-Bird)	6/21/2013	Length 180.9 km	ID: 20130621_01
PS81/H16	-67.05111	-9.22244	PS81/H16-AEM	Airborne EM (EM-Bird)	7/07/2013	Length 181.7 km	ID: 20130707_01
PS81/H19	-67.21140	-23.24552	PS81/H19-AEM	Airborne EM (EM-Bird)	7/13/2013	Length 165.0 km	ID: 20130713_01
PS81/H21	-66.18520	-27.41541	PS81/H21-AEM	Airborne EM (EM-Bird)	7/17/2013	Length 173.8 km	ID: 20130717_01
PS81/H23	-65.71409	-26.95300	PS81/H23-AEM	Airborne EM (EM-Bird)	7/17/2013	Length 190.5 km	ID: 20130717_02
PS81/H26	-61.65030	-36.02103	PS81/H26-AEM	Airborne EM (EM-Bird)	7/20/2013	Length 6.7 km	ID: 20130720_00
PS81/H27	-61.40819	-41.34452	PS81/H27-AEM	Airborne EM (EM-Bird)	7/21/2013	Length 199.0 km	ID: 20130721_01
PS81/H31	-63.01030	-54.18309	PS81/H31-AEM	Airborne EM (EM-Bird)	7/24/2013	Length 133.9 km	ID: 20130724_01
PS81/H35	-63.45939	-51.10852	PS81/H35-AEM	Airborne EM (EM-Bird)	7/30/2013	Length 15.3 km	ID: 20130730_01
PS81/H37	-63.38253	-51.24973	PS81/H37-AEM	Airborne EM (EM-Bird)	7/31/2013	Length 87.1 km	ID: 20130731_01
PS81/H39	-63.21228	-51.27125	PS81/H39-AEM	Airborne EM (EM-Bird)	7/31/2013	Length 67.5 km	ID: 20130731_02
PS81/H45	-63.14899	-51.06527	PS81/H45-AEM	Airborne EM (EM-Bird)	8/2/2013	Length 109.8 km	ID: 20130802_01
PS81/H50	-62.69193	-53.98401	PS81/H50-AEM	Airborne EM (EM-Bird)	8/4/2013	Length 192.1 km	ID: 20130804_01
PS81/H52	-61.46840	-54.89668	PS81/H52-AEM	Airborne EM (EM-Bird)	8/6/2013	Length 211.0 km	ID: 20130806_01

5.2 Ground-based Electromagnetics GEM-2

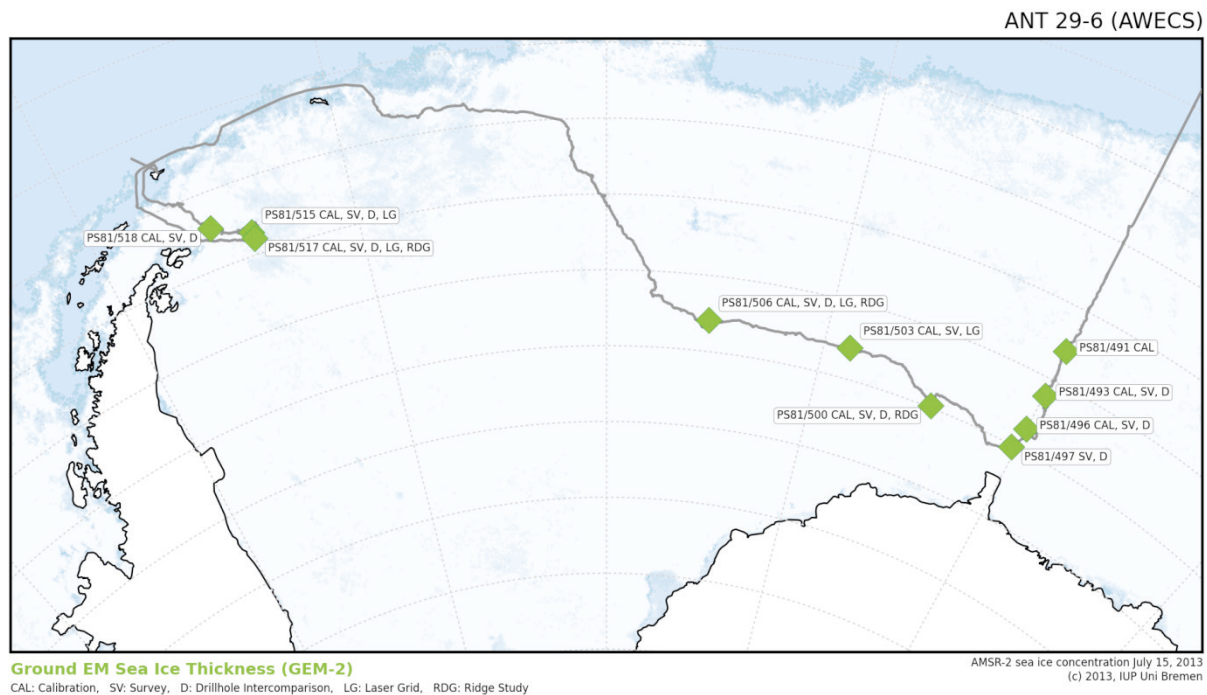


Fig. 5.2.1: GEM-2 measurement sites during ANT-XXIX/6

Objectives

Characterization of the state of the sea-ice cover is of great importance for the evaluation of the polar climate system. Sea-ice thickness datasets are sparse and rarely combine high-resolution thickness information and high spatial coverage. Furthermore, instrument design and processing techniques are usually based on a simple 1D representation of the sea-ice layer and the sea-ice cover is interpreted as level ice. This mostly affects thickness measurements of sea-ice pressure ridges, whose thicknesses may be underestimated by as much as 50 percent.

For further development of EM sea-ice thickness retrieval and high-resolution thickness information, we used a multi-frequency device (GEM-2) during this expedition. Our main goal is to resolve complex and small-scale sea-ice thickness and conductivity structures with different sounding depths. In addition, snow depths and sea-ice thicknesses were measured to obtain the sea-ice thickness distributions on individual floes. The GEM-2 data will also be compared to the EM-Bird data in order to estimate the influence of the different footprints of these instruments. Furthermore, the GEM-2 data will be compared to winter Weddell Sea sea-ice thickness time series, especially to 1989/1992.

Work at sea

We used the ground-based electromagnetic device GEM-2 to measure sea-ice plus snow thickness (Fig. 5.2.1). The measurement principle is similar to that of the EM-Bird already described above. The instrumentation consists of two coils with a separation of 1.67 m. The device was either operated directly on the snow surface or mounted in a modified plastic sled and pulled over the snow surface. The instrument was calibrated several times on different sea-ice thicknesses with

the help of a wooden ladder. During GEM-2 thickness surveys, we simultaneously operated a Magnaprobe (see Chapter 5.7) in order to obtain the snow-depth distribution along the survey track.

Preliminary results

In order to further development the EM sea-ice thickness retrieval method, GEM-2 data were acquired on 4 deformed sea-ice structures along 50 meter transects. In addition, 561 bore holes were drilled to measure freeboard, snow and sea-ice thickness and validate the GEM-2 data ("ridge survey", "ridge drilling" in Tab 5.2.1). During 9 ice stations we measured the sea-ice thickness and snow-depth distribution on ice floes ("Survey" in Tab 5.2.1). At the laser scanning sites, we simultaneously recorded EM-based sea-ice thickness distributions and Magnaprobe-based snow-depth distributions. In order to compare the GEM-2 data to sea-ice thickness time series of 1989/1992, the transects of the manual drilling (Chapter 5.3) were measured in higher spatial resolution with the GEM-2 ("Drillhole intercomparison" in Tab 5.2.1.).

Data management

The final processed datasets will be released in the PANGAEA Data Publisher for Earth & Environmental Science.

5.2 Ground-based Electromagnetics GEM-2

Tab. 5.2.1: List of ground-based EM sea ice-thickness measurements and validation drillings. Comment 1 describes the measurements and comment 2 is the internal GEM-2 file number.

Event	Latitude	Longitude	Label	Device	Date	Comment 1	Comment 2
PS81/491-1	-65.17661570	-0.05180290	PS81/491_CAL1	GEM2	6/20/2013	Calibration, Setup 1	108
PS81/491-1	-65.17662167	-0.05178483	PS81/491_CAL2	GEM2	6/20/2013	Calibration, Setup 3	109
PS81/491-1	-65.17482657	-0.05301236	PS81/491_CAL3	GEM2	6/20/2013	Calibration, Setup 6	110
PS81/491-1	-65.17348984	-0.05386784	PS81/491_CAL4	GEM2	6/20/2013	Calibration, Setup 6, testing influence of person	111
PS81/493-2	-66.45823021	0.10033125	PS81/493_CAL1	GEM2	6/21/2013	Calibration, Setup 6	112
PS81/493-2	-66.45694167	0.10089647	PS81/493_CAL2	GEM2	6/21/2013	Calibration, Setup 3	113
PS81/493-2	-66.45463433	0.10207365	PS81/493_CAL3	GEM2	6/21/2013	Calibration, Setup 1	115
PS81/493-2	-66.43999079	0.12403921	PS81/493_SV1	GEM2	6/21/2013	Survey	116
PS81/493-2	-66.43982565	0.12782232	PS81/493_SV2	GEM2	6/21/2013	Drillhole intercomparison	117
PS81/493-2	-66.43908833	0.12755739	PS81/493_SV3	GEM2	6/21/2013	Survey	118
PS81/496-1	-67.45380603	0.00495461	PS81/496_CAL1	GEM2	6/24/2013	Calibration, Setup 1, abort	119
PS81/496-1	-67.45963833	-0.01034108	PS81/496_CAL2	GEM2	6/24/2013	Calibration, Setup 1, drift	120
PS81/496-1	-67.46130167	-0.01436998	PS81/496_CAL3	GEM2	6/24/2013	Calibration, Setup 2, drift	121
PS81/496-1	-67.46297142	-0.01830475	PS81/496_CAL4	GEM2	6/24/2013	Calibration, Setup 3, drift	122
PS81/496-1	-67.46505833	-0.02296036	PS81/496_CAL5	GEM2	6/24/2013	Calibration, Setup 4, drift	123

Event	Latitude	Longitude	Label	Device	Date	Comment 1	Comment 2
PS81/496-1	-67.46719930	-0.02772640	PS81/496_CAL6	GEM2	6/24/2013	Calibration, Setup 6, drift	124
PS81/496-1	-67.46930097	-0.03265333	PS81/496_CAL7	GEM2	6/24/2013	Calibration, Setup 1, drift	125
PS81/496-1	-67.4758034	-0.04976667	PS81/496_SV1	GEM2	6/24/2013	Drillhole intercomparison, GPS from Magnaprobe	126
PS81/496-1	-67.4811834	-0.06009667	PS81/496_SV2	GEM2	6/24/2013	Survey, GPS from Magnaprobe	127
PS81/496-1	-67.48186167	-0.06117492	PS81/496_SV3	GEM2	6/24/2013	Survey	128
PS81/497-1	-68.05011860	-0.33536500	PS81/497_SV1	GEM2	6/26/2013	Survey	129
PS81/497-1	-68.05225027	-0.33548253	PS81/497_SV2	GEM2	6/26/2013	Survey	130
PS81/497-1	-68.05462298	-0.33587833	PS81/497_SV3	GEM2	6/26/2013	Survey	131
PS81/497-1	-68.05470855	-0.33591689	PS81/497_SV4	GEM2	6/26/2013	Survey	132
PS81/497-1	-68.05481189	-0.33544261	PS81/497_SV5	GEM2	6/26/2013	Drillhole intercomparison	133
PS81/497-1	-68.05587833	-0.33408382	PS81/497_SV6	GEM2	6/26/2013	Drillhole intercomparison	134
PS81/497-1	-68.05723867	-0.33571833	PS81/497_SV7	GEM2	6/26/2013	Survey	135
PS81/500-5	-67.95075833	-6.66155094	PS81/500_CAL1	GEM2	7/3/2013	Calibration, Setup 1	146
PS81/500-5	-67.95404167	-6.66112425	PS81/500_RDG1	GEM2	7/3/2013	Ridge study	136
PS81/500-5	-67.95341000	-6.66179439	PS81/500_RDG2	GEM2	7/3/2013	Ridge study	138
PS81/500-5	-67.95325816	-6.66195557	PS81/500_RDG3	GEM2	7/3/2013	Ridge study	139
PS81/500-5	-67.95311000	-6.66213462	PS81/500_RDG4	GEM2	7/3/2013	Ridge study	140
PS81/500-5	-67.95305323	-6.66294656	PS81/500_RDG5	GEM2	7/3/2013	Ridge study	141
PS81/500-5	-67.95280333	-6.66250799	PS81/500_RDG6	GEM2	7/3/2013	Ridge study	142

5.2 Ground-based Electromagnetics GEM-2

Event	Latitude	Longitude	Label	Device	Date	Comment 1	Comment 2
PS81/500-5	-67.95281392	-6.65887461	PS81/500_SV1	GEM2	7/3/2013	Drillhole intercomparison	143
PS81/500-5	-67.95316770	-6.65774500	PS81/500_SV2	GEM2	7/3/2013	Drillhole intercomparison	144
PS81/500-5	-67.92564573	-6.72766740	PS81/500_RDG7	GEM2	7/4/2013	Ridge study	147
PS81/500-5	-67.92564573	-6.72766740	PS81/500_RDG_ AUGER1	AUGER	7/4/2013	Ridge drilling	
PS81/500-5	-67.84215744	-6.90023267	PS81/500_SV3	GEM2	7/5/2013	Survey	148
PS81/500-5	-67.84160667	-6.90606044	PS81/500_SV4	GEM2	7/5/2013	Survey	149
PS81/500-5	-67.84075100	-6.91454900	PS81/500_SV5	GEM2	7/5/2013	Survey	150
PS81/500-5	-67.84064833	-6.91676892	PS81/500_SV6	GEM2	7/5/2013	Survey	151
PS81/500-5	-67.83951269	-6.92600180	PS81/500_SV7	GEM2	7/5/2013	Survey	152
PS81/503-2	-67.18947000	-13.21598089	PS81/503_CAL1	GEM2	7/8/2013	Calibration, Setup 1, Ferrit	153
PS81/503-2	-67.18957265	-13.21663304	PS81/503_CAL2	GEM2	7/8/2013	Calibration, Setup 1	155
PS81/503-2	-67.18967500	-13.21733122	PS81/503_CAL3	GEM2	7/8/2013	Calibration, Setup 1, Ferrit	156
PS81/503-2	-67.19193572	-13.24001617	PS81/503_LG1	GEM2	7/8/2013	Laser grid	160
PS81/503-2	-67.19180408	-13.22433719	PS81/503_SV1	GEM2	7/8/2013	Survey	157
PS81/503-2	-67.19046473	-13.22993958	PS81/503_SV2	GEM2	7/8/2013	Survey	158
PS81/503-2	-67.19223090	-13.22695270	PS81/503_SV2	GEM2	7/8/2013	Survey	159
PS81/506-1	-67.18243667	-23.00191149	PS81/506_RDG1	GEM2	7/11/2013	Ridge study	164
PS81/506-1	-67.18256833	-23.00031060	PS81/506_RDG2	GEM2	7/11/2013	Ridge study	165
PS81/506-1	-67.18256833	-23.00031060	PS81/506_RDG_ AUGER1	AUGER	7/11/2013	Ridge drilling	
PS81/506-1	-67.19838436	-23.08272631	PS81/506_RDG3	GEM2	7/12/2013	Ridge study	002

Event	Latitude	Longitude	Label	Device	Date	Comment 1	Comment 2
PS81/506-1	-67.19762333	-23.09375803	PS81/506_RDG4	GEM2	7/12/2013	Ridge study	003
PS81/506-1	-67.19859583	-23.09359833	PS81/506_RDG5	GEM2	7/12/2013	Ridge study	004
PS81/506-1	-67.18257667	-23.25780500	PS81/506_RDG6	GEM2	7/13/2013	Ridge study	005
PS81/506-1	-67.18241833	-23.25897935	PS81/506_RDG7	GEM2	7/13/2013	Ridge study	006
PS81/506-1	-67.18241833	-23.25897935	PS81/506_RDG_ AUGER2	AUGER	7/13/2013	Ridge drilling	
PS81/506-1	-67.19800090	-23.22848437	PS81/506_LG1	GEM2	7/14/2013	Laser grid	178
PS81/506-1	-67.20157189	-23.23261950	PS81/506_LG2	GEM2	7/14/2013	Laser grid	179
PS81/506-1	-67.17367833	-23.20662600	PS81/506_SV1	GEM2	7/14/2013	Survey	173
PS81/506-1	-67.17353439	-23.20866728	PS81/506_SV2	GEM2	7/14/2013	Drillhole intercomparison	174
PS81/506-1	-67.17430167	-23.20893833	PS81/506_SV3	GEM2	7/14/2013	Drillhole intercomparison	175
PS81/506-1	-67.17361092	-23.21010649	PS81/506_SV4	GEM2	7/14/2013	Survey	176
PS81/506-1	-67.17422232	-23.20630965	PS81/506_SV5	GEM2	7/14/2013	Survey	177
PS81/506-1	-67.17203333	-23.20704667	PS81/506_ ZERO1	GEM2	7/14/2013	Zero, Setup 1	007
PS81/506-1	-67.17208554	-23.20700000	PS81/506_ ZERO2	GEM2	7/14/2013	Zero, Setup 1	008
PS81/506-1	-67.17211833	-23.20707966	PS81/506_ ZERO3	GEM2	7/14/2013	Zero, Setup 1	166
PS81/506-1	-67.17214742	-23.20715592	PS81/506_ ZERO4	GEM2	7/14/2013	Zero, Setup 2	167
PS81/506-1	-67.17219167	-23.20715199	PS81/506_ ZERO5	GEM2	7/14/2013	Zero, Setup 3	168
PS81/506-1	-67.17220730	-23.20715540	PS81/506_ ZERO6	GEM2	7/14/2013	Zero, Setup 4	169

5.2 Ground-based Electromagnetics GEM-2

Event	Latitude	Longitude	Label	Device	Date	Comment 1	Comment 2
PS81/506-1	-67.17223434	-23.20718833	PS81/506_ ZERO7	GEM2	7/14/2013	Zero, Setup 5	170
PS81/506-1	-67.17225833	-23.20719116	PS81/506_ ZERO8	GEM2	7/14/2013	Zero, Setup 6	171
PS81/506-1	-67.17227768	-23.20726333	PS81/506_ ZERO9	GEM2	7/14/2013	Zero, Setup 1	172
PS81/506-1	-67.34996833	-23.28459604	PS81/501_CAL1	GEM2	7/15/2013	Calibration, Setup 1	181
PS81/515-1	-63.41594732	-51.26489362	PS81/515_CAL1	GEM2	7/26/2013	Calibration, Setup 1	182
PS81/515-1	-63.39406572	-51.18608861	PS81/515_LG1	GEM2	7/26/2013	Laser grid	186
PS81/515-1	-63.40225667	-51.21979363	PS81/515_SV1	GEM2	7/26/2013	Survey	183
PS81/515-1	-63.40172070	-51.21505308	PS81/515_SV2	GEM2	7/26/2013	Drillhole intercomparison	184
PS81/515-1	-63.40045067	-51.21248566	PS81/515_SV3	GEM2	7/26/2013	Survey	185
PS81/517-2	-63.58755924	-51.20353682	PS81/517_SV1	GEM2	7/29/2013	Survey	187
PS81/517-2	-63.58557000	-51.20054565	PS81/517_SV2	GEM2	7/29/2013	Survey	188
PS81/517-2	-63.58361714	-51.20060047	PS81/517_SV3	GEM2	7/29/2013	Survey	189
PS81/517-2	-63.58375167	-51.20019333	PS81/517_SV4	GEM2	7/29/2013	Survey	190
PS81/517-2	-63.50719500	-51.11332758	PS81/517_RDG1	GEM2	7/30/2013	Ridge study	191
PS81/517-2	-63.50429399	-51.11317236	PS81/517_RDG2	GEM2	7/30/2013	Ridge study	192
PS81/517-2	-63.50429399	-51.11317236	PS81/517_RDG_ AUGER1	AUGER	7/30/2013	Ridge drilling	
PS81/517-2	-63.28437833	-51.25435833	PS81/517_CAL1	GEM2	8/1/2013	Calibration, abort	193
PS81/517-2	-63.28408647	-51.25464333	PS81/517_CAL2	GEM2	8/1/2013	Calibration, Setup 1	194
PS81/517-2	-63.28163333	-51.25687833	PS81/517_CAL3	GEM2	8/1/2013	Calibration, Setup 1	195
PS81/517-2	-63.27845077	-51.25971167	PS81/517_CAL4	GEM2	8/1/2013	Calibration, Setup 1	196

Event	Latitude	Longitude	Label	Device	Date	Comment 1	Comment 2
PS81/517-2	-63.26748260	-51.26499113	PS81/517_SV5	GEM2	8/1/2013	Drillhole intercomparison	197
PS81/517-2	-63.26678061	-51.26459500	PS81/517_SV6	GEM2	8/1/2013	Drillhole intercomparison	198
PS81/517-2	-63.26882900	-51.26678600	PS81/517_LG1	GEM2	8/1/2013	Laser grid	199
PS81/517-2	-63.26389945	-51.26432887	PS81/517_LG2	GEM2	8/2/2013	Laser grid	200
PS81/518-3	-62.94399440	-53.42393879	PS81/518_CAL1	GEM2	8/5/2013	Calibration, Setup 1	205
PS81/518-3	-62.92999500	-53.38136070	PS81/518_SV1	GEM2	8/5/2013	Drillhole intercomparison	201
PS81/518-3	-62.93014667	-53.39874264	PS81/518_SV2	GEM2	8/5/2013	Drillhole intercomparison	202
PS81/518-3	-62.93056432	-53.40426092	PS81/518_SV3	GEM2	8/5/2013	Survey	203
PS81/518-3	-62.93193500	-53.40540328	PS81/518_SV4	GEM2	8/5/2013	Survey	204

5.3 Sea-ice thickness, snow depth and freeboard from manual drilling

Objectives

Sea-ice thickness is one of the most important parameters in sea-ice research but also one of the less frequently observed ones so far. Satellite data of Antarctic sea-ice thickness is currently limited to the ICESat period and electromagnetic measurements have only been obtained sporadically. Besides those few data, only very basic measurements (mainly drillings) are available for the investigation of changes in the sea-ice thickness distribution over the last decades. To compare the basic measurements with the advanced technologies that are available today, one has to account for the differences in the measurement techniques. Therefore, the basic manual drillings were performed during ANT-XXIX/6 in addition to the advanced technologies of GEM-2 and EM-Bird flights. Those measurements will help to create a validation chain from small-scale to large-scale measurement and will help to combine previous with new data sets.

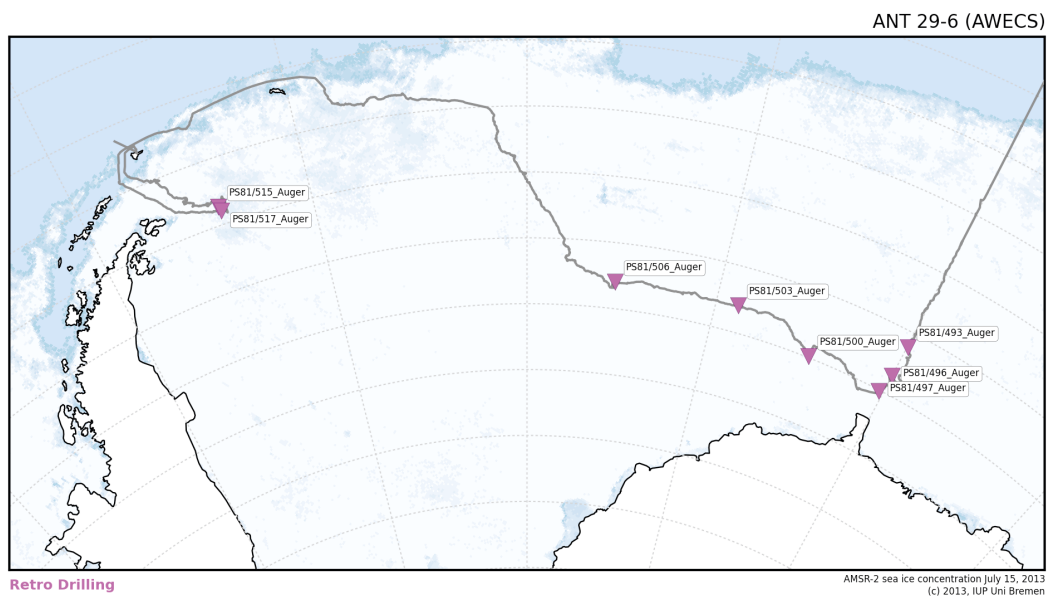


Fig. 5.3.1: Drilling sites during ANT-XXIX/6. Background: Sea-ice concentration from July 15, 2013

Work at sea

Sea-ice thickness, freeboard and snow depth were measured every 5 m along two crossing lines of 100 m at 8 stations. At one other station, 9 bore holes were drilled at random sampling sites. Care was taken to choose sampling sites which were as representative of the surrounding sea ice as possible. Further comparisons of these sampling sites with EM-based sea-ice thickness distribution of the entire floe will help to identify the actual representativeness of such chosen spots on the one hand and the comparability between both methods on the other hand.

Preliminary results

All sampling sites of manual drillings during the expedition are shown in Fig. 5.3.1. In total, 296 holes were drilled during 9 stations, and sea-ice thicknesses, snow depths and freeboard were measured (see Table 5.3.1). Seven of those stations were located on first-year sea-ice floes and 2 stations were located on second-year sea-ice floes. The average sea-ice thicknesses and snow depths at all 9 stations were calculated as 0.86 m and 0.27 m, respectively. Freeboard varied between -0.26 m and 0.3 m.

Tab. 5.3.1: List of all drilling sites during ANT-XXIX/6 with given PANGAEA-label, date, and lat/lon position.

Event	Latitude	Longitude	Label	Device	Date	Comment 1	Comment 2
PS81/493-2	-66.4642	0.0955	PS81/493_D_Auger1	Auger	06/21/2013	ice thickness, snow depth, freeboard	41 bore holes, 5 m distances, along two lines
PS81/496-1	-67.4467	0.0302	PS81/496_D_Auger1	Auger	06/24/2013	ice thickness, snow depth, freeboard	41 bore holes, 5 m distances, along two lines
PS81/497-1	-68.0395	-0.3370	PS81/497_D_Auger1	Auger	06/26/2013	ice thickness, snow depth, freeboard	41 bore holes, 5 m distances, along two lines
PS81/500-5	-67.9668	-6.6555	PS81/500_D_Auger1	Auger	07/03/2013	ice thickness, snow depth, freeboard	41 bore holes, 5 m distances, along two lines
PS81/503-2	-67.1868	-13.2248	PS81/503_D_Auger1	Auger	07/08/2013	ice thickness, snow depth, freeboard	41 bore holes, 5 m distances, along two lines
PS81/506-1	-67.1975	-23.0557	PS81/506_D_Auger1	Auger	07/11/2013	ice thickness, snow depth, freeboard	41 bore holes, 5 m distances, along two lines
PS81/515-1	-63.4610	-51.3213	PS81/515_D_Auger1	Auger	07/26/2013	ice thickness, snow depth, freeboard	9 bore holes, random distances, randomly placed
PS81/517-2	-63.6027	-51.2152	PS81/517_D_Auger1	Auger	07/29/2013	ice thickness, snow depth, freeboard	41 bore holes, 5 m distances, along two lines

5.4 Visual observation of sea-ice conditions from the ship's bridge

A comparison of sea-ice thickness retrievals by the GEM-2 and the manual drillings yields a good agreement between the datasets; the distribution look very similar and differences in modal and mean values are low.

The sea-ice thickness, snow depth and freeboard distribution will be used for the comparison with data from previous winter cruises, performed in 1989, 1992 and 2006. They are expected to show the variability of those parameters during the mentioned winter periods. Combined with other data sources they may also indicate the tendency of sea-ice thickness and snow depth over the past three decades.

Data management

Data from the drilling sites will be delivered to PANGAEA Data Publisher for Earth & Environmental Science within one year after the cruise.

5.4 Visual observation of sea-ice conditions from the ship's bridge

Objectives

Over the last three decades, ship-based visual observations of the state of the sea ice and its snow cover have been performed over all seasons and serve the best-available observational data set of Antarctic sea ice. The recordings follow the Antarctic Sea Ice Processes and Climate (ASPeCt) protocol and include information on sea-ice concentration, sea-ice thickness and snow depth as well as sea-ice type, surface topography and floe size. Those data are combined with information about meteorological conditions like air temperature, wind speed and cloud coverage. This protocol is a useful method to obtain a broad range of characterization and documentation of different sea-ice states and specific features during the cruise.

Work at sea

Every full hour during day and sporadically during night, depending on observers working shifts, the sea-ice observation was carried out by 22 people. A notebook was installed on the bridge, where the observations directly could be typed in. The observations follow the ASPeCt protocol (Worby, 1999), with the standard software being provided on a notebook on the ship's bridge. For every observation, pictures were taken in three different directions.

Date, time and position of the observation were obtained from the DSHIP system, along with standard meteorological data (current sea temperature, air temperature, true wind speed, true wind direction, visibility). The characterisation of the ice conditions were then estimated by taking the average between observation to port side, ahead and to starboard side. Ice thicknesses of tilted floes were estimated by observing a stick attached to the ships starboard side.

Preliminary results

We performed hourly sea-ice observations as soon as we passed the sea-ice edge on 17 June 2013 at 61.233°S at the Greenwich Meridian. The ship left the sea-ice zone on 08 August 2013 at 60.433°S and 56.033°W. Over the 53 days, 461 individual observations were recorded. Sea-ice observations were skipped when the ship was stopped, for example at CTD and ice stations or when trapped in

heavy sea ice. The mean sea-ice concentration was calculated as 88 %, from which 87.65 % were covered by snow.

Data management

The visual sea-ice observations will be post-processed after the cruise and will be published together with the taken pictures to PANGAEA Data Publisher for Earth & Environmental Science within 3 months after the cruise.

5.5 Light transmission through sea ice and snow

Objectives

The amount and the seasonal timing of energy fluxes into sea ice and its snow cover are of critical importance for biological processes and biogeochemical fluxes at the sea-ice underside and the upper ocean. Studies of light regimes under sea ice are sparse in the Antarctic, particularly in winter. Therefore, most biological studies and numerical models are based on rough estimates from few observations.

During ANT-XXIX/6, the sea-ice physics group operated several spectral radiometers above and below the sea ice to contribute to a better understanding of the light regimes under Antarctic sea ice in winter.

Work at sea

At the time of highest sun elevation during an ice station, we measured incident and transmitted irradiance/radiance at representative sampling sites, mostly near the general coring site of the biogeochemistry group. The instrument setup comprised a total of three RAMSES sensors, one upward-looking reference sensor, and two transmittance sensors mounted on a custom-made L-Arm.

The radiometers were operated on a generator-powered IPS Box, and simultaneous spectra were manually recorded by the software MSDA_XE installed on a Panasonic Toughbook.

During instrument set-up, we tried to leave the sampling site as undisturbed as possible. We used two different sensors on the L-Arm, one measuring incident irradiance by integrating over the entire half-sphere, and one radiance sensor with a 7° angular characteristic. During a manually triggered measurement, incident and transmitted irradiance/radiance were recorded simultaneously. We repeated each measurement at least three times, and then rotated the L-Arm approximately 45° (90°, 135°) to cover small-scale spatial variabilities. During most ice stations, favourable diffuse light conditions prevailed. Nevertheless, care was taken to face the sensor towards the sun and to avoid shadowing of the sampling site.

Near the end of the expedition, when more light was available, an under-ice camera was used to monitor the under-ice sensor to check for misalignments.

After a cycle of measurements with both under-ice sensors, snow depth was recorded above the sensor positions. To investigate the influence of the snow cover on the under-ice light regime at our sampling sites, we removed the snow as careful as possible in a circle about 2-3 m in diameter directly above the sensor positions and repeated all measurements in the same way.

5.5 Light transmission through sea ice and snow

All spectra recorded under the sea ice were normalized to incoming irradiance measured simultaneously by the reference sensor at the surface.

By normalizing the transmittance measurements with snow to the transmittance measurements without snow, we obtain the influence of the snow cover alone on under-ice light regimes.

In addition to the under-ice light measurements described above, one irradiance sensor was operated on the third level of *Polarstern's* crow's nest during the entire cruise. A spectrum was recorded every 10 minutes. Unfortunately, the IPS interface box had to be removed during ice stations to power the field sensors, which causes some gaps in the dataset. Furthermore, the sensor was observed to be covered by ice for periods of the cruise, mainly in mid-July, causing possible underestimates of irradiance.

After the optical measurements, five sea-ice cores were drilled directly above the sensor positions. A sea-ice temperature profile with a spacing of 5 cm was obtained in the field using a regular handheld thermometer, while the other four cores were transported directly to the freezer lab for further processing. The salinity/density core was quickly cut into 5 cm segments, weighted and then melted at room temperature. Brine drainage was not observed during the transport. After melting, salinity was determined by a calibrated WTW salinometer. Brine volume and brine salinity were calculated using the formulas given by Petrich & Eicken (2010). Thin sections of all cores were prepared with the help of a Leica microtome, and photographed between crossed polarizers.

The fourth core was melted at +4°C and a sub-sample of >500 ml was filtered through a 25 mm Whatman GF/F glass fibre filter. Afterwards, Chl-a and Phaeophytin were determined using the fluorometric method.

Finally, one core was archived and will be transported to Bremerhaven in November.

Preliminary results

Optical measurements were performed at 16 different sampling sites, with sea-ice thicknesses ranging from 34 cm (Pancakes) to 160 cm. Snow depths ranged from 0 to 46 cm. A set of five sea-ice cores were taken directly at the optics sampling site during 9 ice stations. Textures of sea-ice cores at 7 stations are illustrated in Fig. 5.5.1. During other ice stations, optics measurements were performed in the vicinity of the main coring site of the biogeochemistry group, taking advantage of their coring program. The main factors influencing light transmission through sea ice and snow will be derived by comparison of the optical data with sea-ice core properties, snow pit data and chl-a values. Sea-ice thickness and snow depth distributions, obtained by GEM-2 transects, EM Bird flights, and Magnaprobe surveys, will allow for an upscaling of the spot measurements. The data will also be valuable in interpreting the medium scale optical measurements on ANT-XXIX/7, where the same sensors will be mounted on a ROV and an under-ice trawler (SUIT).

In addition, more than 6,000 spectra of incoming irradiance were recorded on 54 days by the sensor mounted on *Polarstern's* crow's nest. Broadband irradiances are shown in Fig. 5.5.2. These data will allow for a temporal extrapolation of the data obtained during the short-timescale light-transmission measurements.

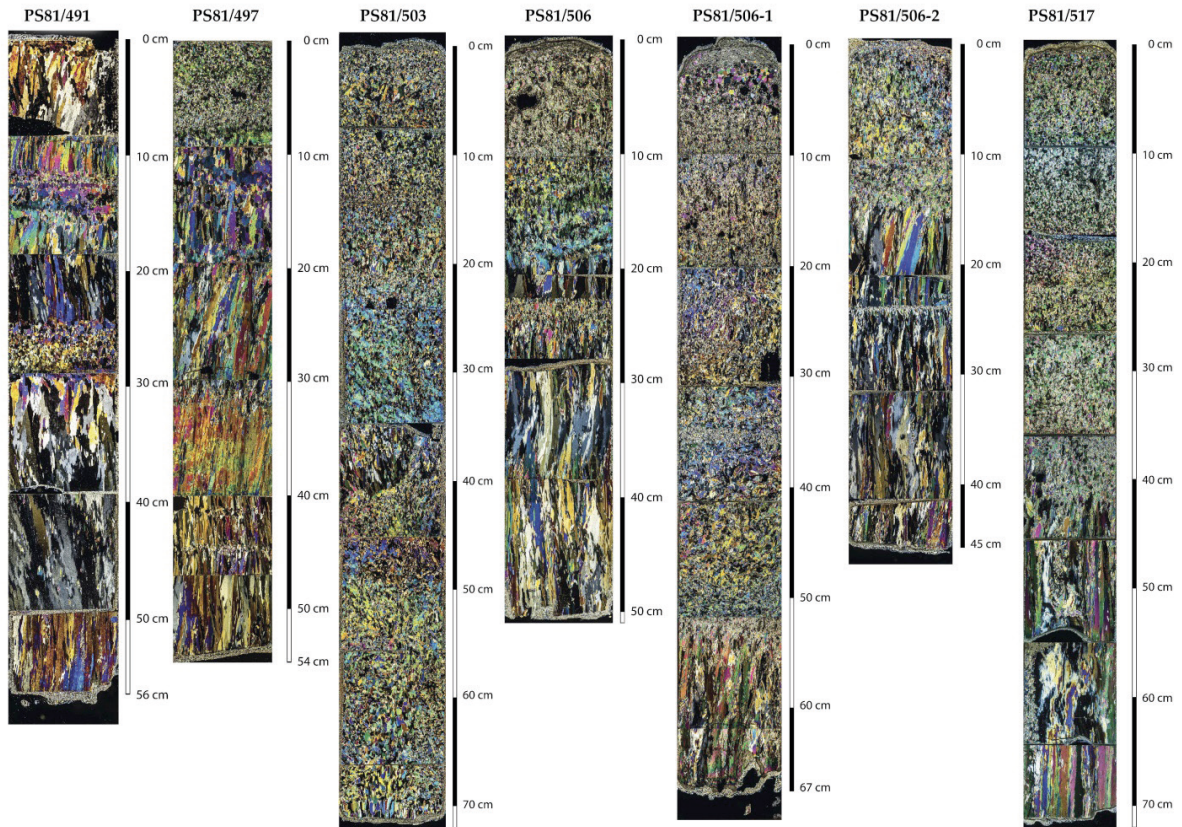


Fig. 5.5.1: Texture from sea-ice cores taken directly at optics sites

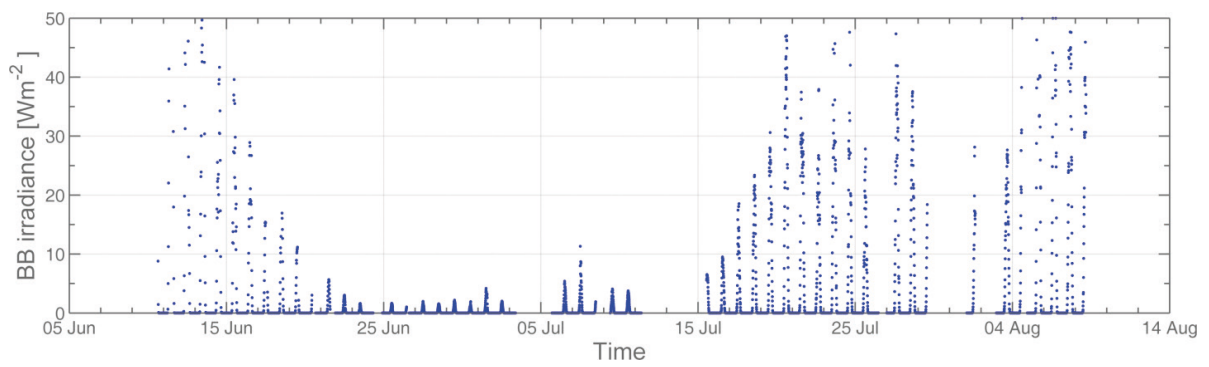


Fig. 5.5.2: Broadband irradiance as measured on the crow's nest

See Tab. 5.5.1 for a list of sea ice cores, and Tab. 5.5.2 for a list of optical data obtained during ANT-XXIX/6.

5.5 Light transmission through sea ice and snow

Tab. 5.5.1: List of sea-ice cores obtained during ANT-XXIX/6 (AWECS)

Event	Lat.	Long.	Label	Device	Date	Comment 1
PS81/491-1	-65.1766	-0.0518	PS81/491_CORE_SAL	Sea-Ice Corer	6/20/2013	Core length [m]: 0,56
PS81/491-1	-65.1766	-0.0518	PS81/491_CORE_DEN	Sea-Ice Corer	6/20/2013	Core length [m]: 0,56
PS81/491-1	-65.1766	-0.0518	PS81/491_CORE_TEMP	Sea-Ice Corer	6/20/2013	Core length [m]: 0,57
PS81/491-1	-65.1766	-0.0518	PS81/491_CORE_TEX	Sea-Ice Corer	6/20/2013	Core length [m]: 0,57
PS81/491-1	-65.1766	-0.0518	PS81/491_CORE_ARC	Sea-Ice Corer	6/20/2013	Core length [m]: 0,57
PS81/497-1	-68.0501	-0.3354	PS81/497_CORE_SAL	Sea-Ice Corer	6/26/2013	Core length [m]: 0,6
PS81/497-1	-68.0501	-0.3354	PS81/497_CORE_DEN	Sea-Ice Corer	6/26/2013	Core length [m]: 0,6
PS81/497-1	-68.0501	-0.3354	PS81/497_CORE_TEMP	Sea-Ice Corer	6/26/2013	Core length [m]: 0,6
PS81/497-1	-68.0501	-0.3354	PS81/497_CORE_TEX	Sea-Ice Corer	6/26/2013	Core length [m]: 0,54
PS81/497-1	-68.0501	-0.3354	PS81/497_CORE_ARC	Sea-Ice Corer	6/26/2013	Core length [m]: 0,54
PS81/500-5	-67.9508	-6.6616	PS81/500_CORE_SAL	Sea-Ice Corer	7/03/2013	Core length [m]: 0,73
PS81/500-5	-67.9508	-6.6616	PS81/500_CORE_DEN	Sea-Ice Corer	7/03/2013	Core length [m]: 0,73
PS81/500-5	-67.9508	-6.6616	PS81/500_CORE_TEMP	Sea-Ice Corer	7/03/2013	Core length [m]: 0,98
PS81/500-5	-67.9508	-6.6616	PS81/500_CORE_TEX	Sea-Ice Corer	7/03/2013	Core length [m]: 0,57
PS81/500-5	-67.9508	-6.6616	PS81/500_CORE_ARC	Sea-Ice Corer	7/03/2013	Core length [m]: 0,57
PS81/503-2	-67.1895	-13.2160	PS81/503_CORE_SAL	Sea-Ice Corer	7/08/2013	Core length [m]: 0,66
PS81/503-2	-67.1895	-13.2160	PS81/503_CORE_DEN	Sea-Ice Corer	7/08/2013	Core length [m]: 0,66
PS81/503-2	-67.1895	-13.2160	PS81/503_CORE_TEMP	Sea-Ice Corer	7/08/2013	Core length [m]: 0,66
PS81/503-2	-67.1895	-13.2160	PS81/503_CORE_TEX	Sea-Ice Corer	7/08/2013	Core length [m]: 0,69
PS81/503-2	-67.1895	-13.2160	PS81/503_CORE_ARC	Sea-Ice Corer	7/08/2013	Core length [m]: 0,67
PS81/503-2	-67.1895	-13.2160	PS81/503_CORE_CHL	Sea-Ice Corer	7/08/2013	Core length [m]: 0,67
PS81/506-1	-67.1824	-23.0019	PS81/506_CORE_SAL-1	Sea-Ice Corer	7/11/2013	Core length [m]: 0,46

5. Sea Ice Physics

Event	Lat.	Long.	Label	Device	Date	Comment 1
PS81/491-1	-65.1766	-0.0518	PS81/491_CORE_SAL	Sea-Ice Corer	6/20/2013	Core length [m]: 0,56
PS81/506-1	-67.1824	-23.0019	PS81/506_CORE_DEN-1	Sea-Ice Corer	7/11/2013	Core length [m]: 0,46
PS81/506-1	-67.1824	-23.0019	PS81/506_CORE_TEMP-1	Sea-Ice Corer	7/11/2013	Core length [m]: 0,43
PS81/506-1	-67.1824	-23.0019	PS81/506_CORE_TEX-1	Sea-Ice Corer	7/11/2013	Core length [m]: 0,49
PS81/506-1	-67.1824	-23.0019	PS81/506_CORE_ARC-1	Sea-Ice Corer	7/11/2013	Core length [m]: 0,46
PS81/506-1	-67.1824	-23.0019	PS81/506_CORE_CHL-1	Sea-Ice Corer	7/11/2013	Core length [m]: 0,46
PS81/506-1	-67.1824	-23.0019	PS81/506_CORE_SAL-2	Sea-Ice Corer	7/12/2013	Core length [m]: 0,66
PS81/506-1	-67.1824	-23.0019	PS81/506_CORE_DEN-2	Sea-Ice Corer	7/12/2013	Core length [m]: 0,66
PS81/506-1	-67.1824	-23.0019	PS81/506_CORE_TEMP-2	Sea-Ice Corer	7/12/2013	Core length [m]: 0,63
PS81/506-1	-67.1824	-23.0019	PS81/506_CORE_TEX-2	Sea-Ice Corer	7/12/2013	Core length [m]: 0,66
PS81/506-1	-67.1824	-23.0019	PS81/506_CORE_ARC-2	Sea-Ice Corer	7/12/2013	Core length [m]: 0,66
PS81/506-1	-67.1824	-23.0019	PS81/506_CORE_CHL-2	Sea-Ice Corer	7/12/2013	Core length [m]: 0,66
PS81/506-1	-67.1824	-23.0019	PS81/506_CORE_SAL-2	Sea-Ice Corer	7/14/2013	Core length [m]: 0,44
PS81/506-1	-67.1824	-23.0019	PS81/506_CORE_DEN-3	Sea-Ice Corer	7/14/2013	Core length [m]: 0,44
PS81/506-1	-67.1824	-23.0019	PS81/506_CORE_TEMP-3	Sea-Ice Corer	7/14/2013	Core length [m]: 0,43
PS81/506-1	-67.1824	-23.0019	PS81/506_CORE_TEX-3	Sea-Ice Corer	7/14/2013	Core length [m]: 0,44
PS81/506-1	-67.1824	-23.0019	PS81/506_CORE_ARC-3	Sea-Ice Corer	7/14/2013	Core length [m]: 0,44
PS81/506-1	-67.1824	-23.0019	PS81/506_CORE_CHL-3	Sea-Ice Corer	7/14/2013	Core length [m]: 0,44
PS81/517-2	-63.5876	-51.2035	PS81/517_CORE_SAL-1	Sea-Ice Corer	7/29/2013	Core length [m]: 0,71
PS81/517-2	-63.5876	-51.2035	PS81/517_CORE_DEN-1	Sea-Ice Corer	7/29/2013	Core length [m]: 0,71
PS81/517-2	-63.5876	-51.2035	PS81/517_CORE_TEMP-1	Sea-Ice Corer	7/29/2013	Core length [m]: 0,74
PS81/517-2	-63.5876	-51.2035	PS81/517_CORE_TEX-1	Sea-Ice Corer	7/29/2013	Core length [m]: 0,73
PS81/517-2	-63.5876	-51.2035	PS81/517_CORE_ARC-1	Sea-Ice Corer	7/29/2013	Core length [m]: 0,73

5.5 Light transmission through sea ice and snow

Event	Lat.	Long.	Label	Device	Date	Comment 1
PS81/491-1	-65.1766	-0.0518	PS81/491_CORE_SAL	Sea-Ice Corer	6/20/2013	Core length [m]: 0,56
PS81/517-2	-63.5876	-51.2035	PS81/517_CORE_CHL-1	Sea-Ice Corer	7/29/2013	Core length [m]: 0,73
PS81/517-2	-63.5876	-51.2035	PS81/517_CORE_SAL-2	Sea-Ice Corer	7/30/2013	Core length [m]: 1,50
PS81/517-2	-63.5876	-51.2035	PS81/517_CORE_DEN-2	Sea-Ice Corer	7/30/2013	Core length [m]: 1,50
PS81/517-2	-63.5876	-51.2035	PS81/517_CORE_TEMP-2	Sea-Ice Corer	7/30/2013	Core length [m]: 1,48
PS81/517-2	-63.5876	-51.2035	PS81/517_CORE_TEX-2	Sea-Ice Corer	7/30/2013	Core length [m]: 1,50
PS81/517-2	-63.5876	-51.2035	PS81/517_CORE_ARC-2	Sea-Ice Corer	7/30/2013	Core length [m]: 1,50
PS81/517-2	-63.5876	-51.2035	PS81/517_CORE_CHL-2	Sea-Ice Corer	7/30/2013	Core length [m]: 1,50

Data management

Data from the drilling sites will be delivered to PANGAEA Data Publisher for Earth & Environmental Science.

Tab. 5.5.2: List of optical data obtained during ANT-XXIX/6 (AWECS)

Event	Lat	Long	Label	Device	Date	Comment 1	Comment 2	Comment 3	FileNames
PS81/488-2	-67.9588	0.0027	PS81/488_OPT-01	L-Arm/RAMSES	6/18/2013	Irradiance under sea ice		Sampling Site 1	20130618_Larm_Irrad_Site1_[1-2]
PS81/488-2	-67.9588	0.0027	PS81/488_OPT-02	L-Arm/RAMSES	6/18/2013	Radiance under sea ice		Sampling Site 1	20130618_Larm_Rad_Site1_[1-2]
PS81/488-2	-67.9588	0.0027	PS81/488_OPT-03	L-Arm/RAMSES	6/18/2013	Irradiance under sea ice	Pancakes, SI: 34 cm; SD: 0 cm	Sampling Site 2	20130618_Larm_Irrad_Site2_[1-2]
PS81/488-2	-67.9588	0.0027	PS81/488_OPT-04	L-Arm/RAMSES	6/18/2013	Radiance under sea ice	Pancakes, SI: 34 cm; SD: 0 cm	Sampling Site 2	20130618_Larm_Rad_Site2_[1-2]
PS81/489-2	-63.9030	-0.0302	PS81/489_OPT-01	L-Arm/RAMSES	6/19/2013	Irradiance under sea ice	Pancakes, SI: 48 cm; SD: 10 cm, FB: 0 cm		20130619_Larm_Irrad_[1-2]
PS81/489-2	-63.9030	-0.0302	PS81/489_OPT-02	L-Arm/RAMSES	6/19/2013	Radiance under sea ice	Pancakes, SI: 48 cm; SD: 10 cm, FB: 0 cm		20130619_Larm_Rad_[1-2]
PS81/491-1	-65.1766	-0.0518	PS81/491_OPT-01	L-Arm/RAMSES	6/20/2013	Irradiance under sea ice	SI: 57 cm	Frostflowers on bare sea-ice surface	20130620_Larm_Irrad_[1-4]
PS81/491-1	-65.1766	-0.0518	PS81/491_OPT-02	L-Arm/RAMSES	6/20/2013	Radiance under sea ice	SI: 57 cm	Frostflowers on bare sea-ice surface	20130620_Larm_Rad_[1-4]
PS81/496-1	-65.1766	-0.0518	PS81/496_OPT-01	L-Arm/RAMSES	6/24/2013	Irradiance under sea ice with snow	SI: 90 cm; SD: 18 cm; FB: 9cm	10m from main Coringsite	20130624_Larm_Irrad_[1-2]

5.5 Light transmission through sea ice and snow

Event	Lat	Long	Label	Device	Date	Comment 1	Comment 2	Comment 3	Filenames
PS81/496-1	-65.1766	-0.0518	PS81/496_OPT-02	L-Arm/RAMSES	6/24/2013	Radiance under sea ice with snow	SI: 90 cm; SD: 18 cm; FB: 9cm	10m from main Coringsite	20130624_Larm_Rad_[1-2]
PS81/496-1	-65.1766	-0.0518	PS81/496_OPT-03	L-Arm/RAMSES	6/24/2013	Irradiance under sea ice without snow	SI: 90 cm; SD: 18 cm; FB: 9cm	10m from main Coringsite	20130624_Larm_Irrad_[1-2]_nosnow
PS81/496-1	-65.1766	-0.0518	PS81/496_OPT-04	L-Arm/RAMSES	6/24/2013	Radiance under sea ice without snow	SI: 90 cm; SD: 18 cm; FB: 9cm	10m from main Coringsite	20130624_Larm_Rad_1_nosnow
PS81/497-1	-68.0501	-0.3354	PS81/497-OPT-01	L-Arm/RAMSES	6/26/2013	Irradiance under sea ice with snow	SI: 61 cm; SD:		20130626_Larm_Irrad_[1-3]
PS81/497-1	-68.0501	-0.3354	PS81/497-OPT-02	L-Arm/RAMSES	6/26/2013	Radiance under sea ice with snow	SI: 61 cm; SD:		20130626_Larm_Rad_[1-3]
PS81/497-1	-68.0501	-0.3354	PS81/497-OPT-03	L-Arm/RAMSES	6/26/2013	Irradiance under sea ice without snow	SI: 61 cm; SD:		20130626_Larm_Irrad_[1-2]_nosnow
PS81/497-1	-68.0501	-0.3354	PS81/497-OPT-04	L-Arm/RAMSES	6/26/2013	Radiance under sea ice without snow	SI: 61 cm; SD:		20130626_Larm_Rad_[1-2]_nosnow
PS81/500-5	-67.9507	-6.6616	PS81/500-OPT-01	L-Arm/RAMSES	7/03/2013	Irradiance under sea ice with snow	SI: 98 cm; SD:34 cm		20130703_Larm_Irrad_[1-3]
PS81/500-5	-67.9507	-6.6616	PS81/500-OPT-02	L-Arm/RAMSES	7/03/2013	Radiance under sea ice with snow	SI: 98 cm; SD:34 cm		20130703_Larm_Rad_[1-3]

5. Sea Ice Physics

Event	Lat	Long	Label	Device	Date	Comment 1	Comment 2	Comment 3	FileNames
PS81/500-5	-67.9507	-6.6616	PS81/500-OPT-03	L-Arm/RAMSES	7/03/2013	Irradiance under sea ice without snow	SI: 98 cm; SD:34 cm		20130703_Larm_Irrad_[1-2]_nosnow
PS81/500-5	-67.9507	-6.6616	PS81/500-OPT-04	L-Arm/RAMSES	7/03/2013	Radiance under sea ice without snow	SI: 98 cm; SD:34 cm		20130703_Larm_Rad_[1-2]_nosnow
PS81/500-5	-67.9507	-6.6616	PS81/500-OPT-05	RAMSES	7/03/2013	Irradiance spectrum of shiplight			20130703_Shiplight_Irrad
PS81/500-5	-67.9507	-6.6616	PS81/500-OPT-06	RAMSES	7/03/2013	Radiance spectrum of shiplight			20130703_Shiplight_Rad
PS81/503-2	-67.1895	-13.2160	PS81/503-OPT-01	L-Arm/RAMSES	7/08/2013	Irradiance under sea ice with snow	SI: 66 cm; SD: 15 cm	Sampling Site 1	20130708_Larm_Irrad_[1-3]
PS81/503-2	-67.1895	-13.2160	PS81/503-OPT-02	L-Arm/RAMSES	7/08/2013	Radiance under sea ice with snow	SI: 66 cm; SD: 15 cm	Sampling Site 1	20130708_Larm_Rad_[1-4]
PS81/503-2	-67.1895	-13.2160	PS81/503-OPT-03	L-Arm/RAMSES	7/08/2013	Irradiance under sea ice without snow	SI: 66 cm; SD: 15 cm	Sampling Site 1	20130708_Larm_Irrad_[1-3]_nosnow
PS81/503-2	-67.1895	-13.2160	PS81/503-OPT-04	L-Arm/RAMSES	7/08/2013	Radiance under sea ice without snow	SI: 66 cm; SD: 15 cm	Sampling Site 1	20130708_Larm_Rad_[1-4]_nosnow
PS81/503-2	-67.1895	-13.2160	PS81/503-OPT-05	L-Arm/RAMSES	7/08/2013	Irradiance under sea ice with snow	SI: 60 cm; SD: 21 cm; FB: 1 cm	Sampling Site 2 (5 m from main Coringsite)	20130708_Larm_Site2_Irrad_[1-2]

5.5 Light transmission through sea ice and snow

Event	Lat	Long	Label	Device	Date	Comment 1	Comment 2	Comment 3	Filenames
PS81/503-2	-67.1895	-13.2160	PS81/503-OPT-07	L-Arm/RAMSES	7/08/2013	Irradiance under sea ice without snow	SI: 60 cm; SD: 21 cm; FB: 1 cm	Sampling Site 2 (5 m from main Coringsite)	20130708_Larm_Site2_Irrad_1_nosnow
PS81/506-1	-67.1824	-23.0019	PS81/506-OPT-01	L-Arm/RAMSES	7/11/2013	Irradiance under sea ice with snow	SI: 43 cm; SD: 12 cm; FB: 3 cm	Sampling Site 1 (10m from main Coringsite)	20130711_Larm_Irrad_[1-7]
PS81/506-1	-67.1824	-23.0019	PS81/506-OPT-02	L-Arm/RAMSES	7/11/2013	Radiance under sea ice with snow	SI: 43 cm; SD: 12 cm; FB: 3 cm	Sampling Site 1 (10m from main Coringsite)	20130711_Larm_Rad_[1-3]
PS81/506-1	-67.1824	-23.0019	PS81/506-OPT-03	L-Arm/RAMSES	7/11/2013	Irradiance under sea ice without snow	SI: 43 cm; SD: 12 cm; FB: 3 cm	Sampling Site 1 (10m from main Coringsite)	20130711_Larm_Irrad_[1-3]_nosnow
PS81/506-1	-67.1824	-23.0019	PS81/506-OPT-04	L-Arm/RAMSES	7/11/2013	Radiance under sea ice without snow	SI: 43 cm; SD: 12 cm; FB: 3 cm	Sampling Site 1 (10m from main Coringsite)	20130711_Larm_Rad_[1-3]_nosnow
PS81/506-1	-67.1824	-23.0019	PS81/506-OPT-05	L-Arm/RAMSES	7/12/2013	Irradiance under sea ice with snow	SI: 63 cm; SD: 12 cm; FB: 6 cm	Sampling Site 2	20130712_Larm_Irrad_[1-3]
PS81/506-1	-67.1824	-23.0019	PS81/506-OPT-06	L-Arm/RAMSES	7/12/2013	Radiance under sea ice with snow	SI: 63 cm; SD: 12 cm; FB: 6 cm	Sampling Site 2	20130712_Larm_Rad_[1-3]
PS81/506-1	-67.1824	-23.0019	PS81/506-OPT-07	L-Arm/RAMSES	7/12/2013	Irradiance under sea ice without snow	SI: 63 cm; SD: 12 cm; FB: 6 cm	Sampling Site 2	20130712_Larm_Irrad_1_nosnow
PS81/506-1	-67.1824	-23.0019	PS81/506-OPT-08	L-Arm/RAMSES	7/12/2013	Radiance under sea ice without snow	SI: 63 cm; SD: 12 cm; FB: 6 cm	Sampling Site 2	20130712_Larm_Rad_1_nosnow

5. Sea Ice Physics

Event	Lat	Long	Label	Device	Date	Comment 1	Comment 2	Comment 3	FileNames
PS81/506-1	-67.1824	-23.0019	PS81/506-OPT-09	L-Arm/RAMSES	7/14/2013	Irradiance under sea ice with snow	SI: 44 cm; SD: 20 cm;	Sampling Site 3	20130714_Larm_Irrad_[1-3]
PS81/506-1	-67.1824	-23.0019	PS81/506-OPT-10	L-Arm/RAMSES	7/14/2013	Radiance under sea ice with snow	SI: 44 cm; SD: 20 cm;	Sampling Site 3	20130714_Larm_Rad_[1-3]
PS81/506-1	-67.1824	-23.0019	PS81/506-OPT-11	L-Arm/RAMSES	7/14/2013	Irradiance under sea ice without snow	SI: 44 cm; SD: 20 cm;	Sampling Site 3	20130714_Larm_Irrad_[1-3]_nosnow
PS81/506-1	-67.1824	-23.0019	PS81/506-OPT-12	L-Arm/RAMSES	7/14/2013	Radiance under sea ice without snow	SI: 44 cm; SD: 20 cm;	Sampling Site 3	20130714_Larm_Rad_[1-3]_nosnow
PS81/517-2	-63.5876	-51.2035	PS81/517-OPT-01	L-Arm/RAMSES	7/29/2013	Irradiance under sea ice with snow	SI: 74 cm; SD: 28 cm;	Sampling Site 1	20130729_Larm_Irrad_[1-3]
PS81/517-2	-63.5876	-51.2035	PS81/517-OPT-02	L-Arm/RAMSES	7/29/2013	Radiance under sea ice with snow	SI: 74 cm; SD: 28 cm;	Sampling Site 1	20130729_Larm_Rad_[1-3]
PS81/517-2	-63.5876	-51.2035	PS81/517-OPT-03	L-Arm/RAMSES	7/29/2013	Irradiance under sea ice without snow	SI: 74 cm; SD: 28 cm;	Sampling Site 1	20130729_Larm_Irrad_[1-3]_nosnow
PS81/517-2	-63.5876	-51.2035	PS81/517-OPT-04	L-Arm/RAMSES	7/29/2013	Radiance under sea ice without snow	SI: 74 cm; SD: 28 cm;	Sampling Site 1	20130729_Larm_Rad_[1-3]_nosnow
PS81/517-2	-63.5876	-51.2035	PS81/517-OPT-05	L-Arm/RAMSES	7/30/2013	Irradiance under sea ice with snow	SI: 143 cm; SD: 37 cm; FB: -5 cm	Sampling Site 2 (Retro Drilling Site)	20130730_Larm_Irrad_[1-3]

5.5 Light transmission through sea ice and snow

Event	Lat	Long	Label	Device	Date	Comment 1	Comment 2	Comment 3	Filenames
PS81/517-2	-63.5876	-51.2035	PS81/517-OPT-06	L-Arm/RAMSES	7/30/2013	Radiance under sea ice with snow	SI: 143 cm; SD: 37 cm; FB: -5 cm	Sampling Site 2 (Retro Drilling Site)	20130730_Larm_Rad_[1-3]
PS81/517-2	-63.5876	-51.2035	PS81/517-OPT-07	L-Arm/RAMSES	7/30/2013	Irradiance under sea ice without snow	SI: 143 cm; SD: 37 cm; FB: -5 cm	Sampling Site 2 (Retro Drilling Site)	20130730_Larm_Irrad_1_nosnow
PS81/517-2	-63.5876	-51.2035	PS81/517-OPT-08	L-Arm/RAMSES	7/30/2013	Radiance under sea ice without snow	SI: 143 cm; SD: 37 cm; FB: -5 cm	Sampling Site 2 (Retro Drilling Site)	20130730_Larm_Rad_1_nosnow
PS81/517-2	-63.5876	-51.2035	PS81/517-OPT-09	L-Arm/RAMSES	8/01/2013	Irradiance under sea ice with snow	SI: 114 cm; SD: 46 cm; FB: 0 cm	Sampling Site 3 (15m from main Coringsite)	20130801_Larm_Irrad_[1-4]
PS81/517-2	-63.5876	-51.2035	PS81/517-OPT-10	L-Arm/RAMSES	8/01/2013	Radiance under sea ice with snow	SI: 114 cm; SD: 46 cm; FB: 0 cm	Sampling Site 3 (15m from main Coringsite)	20130801_Larm_Rrad_[1-2]
PS81/517-2	-63.5876	-51.2035	PS81/517-OPT-11	L-Arm/RAMSES	8/01/2013	Irradiance under sea ice with snow	SI: 160 cm; SD: 33 cm; FB: 1 cm	Sampling Site 4 (5 m from main Coringsite)	20130801_Larm_Irrad_Site2
PS81/517-2	-63.5876	-51.2035	PS81/517-OPT-12	L-Arm/RAMSES	8/01/2013	Radiance under sea ice with snow	SI: 160 cm; SD: 33 cm; FB: 1 cm	Sampling Site 4 (5 m from main Coringsite)	20130801_Larm_Rad_Site2
PS81/517-2	-63.5876	-51.2035	PS81/517-OPT-13	L-Arm/RAMSES	8/01/2013	Irradiance under sea ice without snow	SI: 160 cm; SD: 33 cm; FB: 1 cm	Sampling Site 4 (5 m from main Coringsite)	20130801_Larm_Rad_Site2_nosnow
PS81/517-2	-63.5876	-51.2035	PS81/517-OPT-14	L-Arm/RAMSES	8/01/2013	Radiance under sea ice without snow	SI: 160 cm; SD: 33 cm; FB: 1 cm	Sampling Site 4 (5 m from main Coringsite)	20130801_Larm_Rad_Site2_nosnow

5.6 Snow pit measurements

Objectives

Snow stratigraphy and physical snow properties are highly variable even on small horizontal scales. Hence, mapping the spatial and temporal differences in density, temperature, salinity and liquid water content with depth as well as the snow pack stratigraphy are of high relevance. This data is primarily intended to be used as ground truth data for the interpretation of radar backscatter satellite imagery. To achieve a maximum spatial coverage and variability of different snow packs during the cruise, measurements were taken on different sea-ice floes (FYI/MYI) during the short and long ice stations as well as by helicopter-based floe hopping (Fig. 5.6.1).

Work at sea

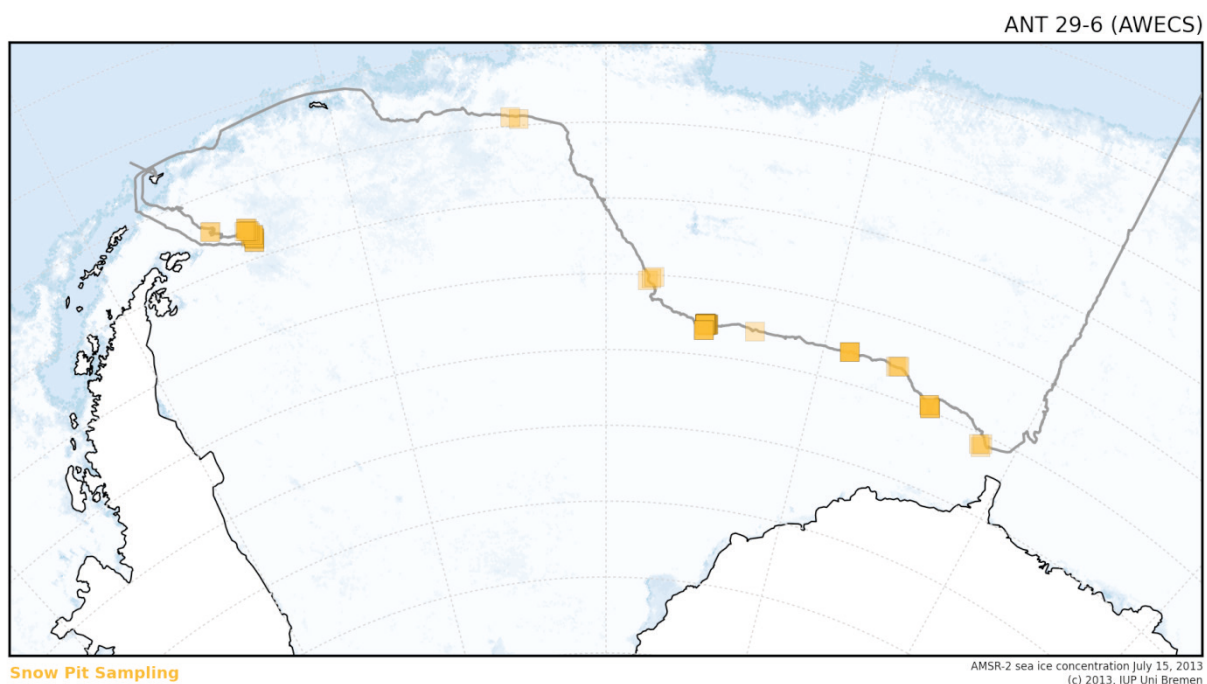


Fig. 5.6.1: Locations of snow pits sampled during the ANT-XXIX/6

The physical snow parameters as well as the snow stratigraphy, e.g. grain size distribution, snow crystal typography, snow hardness, liquid water content, temperature and density profiles, were obtained from snow pits. These covered the main core site of the biogeochemistry group, the BAS site, the laser scanning grid as well as all optic/light measurement sites to add information about the snow pack to those measurements. In addition to that, maximum spatial coverage of representative areas on the floes was tried to be achieved. Every snow pit comprised temperature, salinity, and density profiles as well as liquid water content profiles in addition to the estimation of snow stratigraphic parameters such as snow hardness, grain size and crystal type for each layer in the snow pack.

5.6 Snow pit measurements

Tab. 5.6.1: List of all snow pits during the cruise with given label, date, lat/lon position and reference to other measurements

Event	Latitude	Longitude	Label	Device	Date	Comment 1	Comment 2
PS81/493-2	NA	NA	PS81/493_SP-01	Snow pit	6/21/2013	Snow pit 1	Snow pit
PS81/493-2	NA	NA	PS81/493_SP-02	Snow pit	6/21/2013	Snow pit 2	Snow pit
PS81/493-2	NA	NA	PS81/493_SP-03	Snow pit	6/21/2013	Snow pit 3	Snow pit coring site
PS81/496-1	NA	NA	PS81/496_SP-01	Snow pit	6/24/2013	Snow pit 1	Snow pit Retro Drilling
PS81/496-1	NA	NA	PS81/496_SP-02	Snow pit	6/24/2013	Snow pit 2	Snow pit Retro Drilling
PS81/496-1	NA	NA	PS81/496_SP-03	Snow pit	6/24/2013	Snow pit 3	Snow pit Retro Drilling
PS81/496-1	NA	NA	PS81/496_SP-04	Snow pit	6/24/2013	Snow pit 4	Snow pit Retro Drilling
PS81/496-1	NA	NA	PS81/496_SP-05	Snow pit	6/24/2013	Snow pit 5	Snow pit coring site
PS81/497-1	NA	NA	PS81/497_SP-01	Snow pit	6/26/2013	Snow pit 1	Snow pit optics
PS81/H11	-68.325	-2.395	PS81/H11_SP-01	Snow pit	6/29/2013	Snow pit 1 Helicopter	Snow pit Helicopter
PS81/H11	-68.2667	-2.6	PS81/H11_SP-02	Snow pit	6/29/2013	Snow pit 2 Helicopter	Snow pit Helicopter
PS81/H11	-68.2333	-2.3667	PS81/H11_SP-03	Snow pit	6/29/2013	Snow pit 3 Helicopter	Snow pit Helicopter
PS81/500-5	-67.9231	-6.7422	PS81/500_SP-01	Snow pit	7/3/2013	Snow pit 1	Snow pit coring site
PS81/500-5	-67.8468	-6.8854	PS81/500_SP-02	Snow pit	7/4/2013	Snow pit 2	Snow pit Retro Drilling
PS81/500-5	-67.8473	-6.8865	PS81/500_SP-03	Snow pit	7/4/2013	Snow pit 3	Snow pit Retro Drilling
PS81/500-5	-67.921	-6.7364	PS81/500_SP-04	Snow pit	7/4/2013	Snow pit 4	Snow pit
PS81/500-5	-67.9209	-6.7379	PS81/500_SP-05	Snow pit	7/4/2013	Snow pit 5	Snow pit Retro Drilling
PS81/500-5	-67.9199	-6.7563	PS81/500_SP-06	Snow pit	7/4/2013	Snow pit 6	Snow pit Ridge study
PS81/500-5	-67.8455	-6.8923	PS81/500_SP-07	Snow pit	7/5/2013	Snow pit 7	Snow pit Retro Drilling
PS81/H17	-67.201	-9.9423	PS81/H17_SP-01	Snow pit	7/7/2013	Snow pit 1 Helicopter	Snow pit Helicopter

Event	Latitude	Longitude	Label	Device	Date	Comment 1	Comment 2
PS81/H17	-67.1746	-9.8018	PS81/H17_SP-02	Snow pit	7/7/2013	Snow pit 2 Helicopter	Snow pit Helicopter
PS81/H17	-67.1749	-9.703	PS81/H17_SP-03	Snow pit	7/7/2013	Snow pit 3 Helicopter	Snow pit Helicopter
PS81/503-2	-67.188	-13.2197	PS81/503_SP-01	Snow pit	7/8/2013	Snow pit 1	Snow pit optics
PS81/503-2	-67.1872	-13.2147	PS81/503_SP-02	Snow pit	7/8/2013	Snow pit 2	Snow pit coring site
PS81/503-2	-67.1883	-13.2209	PS81/503_SP-03	Snow pit	7/8/2013	Snow pit 3	Snow pit BAS site
PS81/503-2	-67.1895	-13.2232	PS81/503_SP-04	Snow pit	7/8/2013	Snow pit 4	Snow pit
PS81/503-2	-67.1915	-13.2235	PS81/503_SP-05	Snow pit	7/8/2013	Snow pit 5	Snow pit
PS81/H18	-67.2042	-19.8094	PS81/H18_SP-01	Snow pit	7/10/2013	Snow pit 1 Helicopter	Snow pit Helicopter
PS81/506-1	-67.1864	-23.037	PS81/506_SP-01	Snow pit	7/11/2013	Snow pit 1	Snow pit optics
PS81/506-1	-67.182	-23.0075	PS81/506_SP-02	Snow pit	7/11/2013	Snow pit 2	Snow pit coring site
PS81/506-1	-67.1821	-23.0064	PS81/506_SP-03	Snow pit	7/11/2013	Snow pit 3	BAS site
PS81/506-1	-67.1985	-23.0437	PS81/506_SP-04	Snow pit	7/12/2013	Snow pit 4	Snow pit Retro Drilling
PS81/506-1	-67.1994	-23.0647	PS81/506_SP-05	Snow pit	7/12/2013	Snow pit 5	Snow pit Retro Drilling
PS81/506-1	-67.1987	-23.0981	PS81/506_SP-06	Snow pit	7/12/2013	Snow pit 6	Snow pit Retro Drilling
PS81/506-1	-67.1986	-23.106	PS81/506_SP-07	Snow pit	7/12/2013	Snow pit 7	Snow pit Retro Drilling
PS81/506-1	-67.1805	-23.2556	PS81/506_SP-08	Snow pit	7/13/2013	Snow pit 8	Snow pit
PS81/506-1	-67.1802	-23.2576	PS81/506_SP-09	Snow pit	7/13/2013	Snow pit 9	Snow pit
PS81/506-1	-67.1798	-23.2594	PS81/506_SP-10	Snow pit	7/13/2013	Snow pit 10	Snow pit
PS81/506-1	-67.1795	-23.2602	PS81/506_SP-11	Snow pit	7/13/2013	Snow pit 11	Snow pit
PS81/H20	-67.2326	-23.2207	PS81/H20_SP-01	Snow pit	7/13/2013	Snow pit 1 Helicopter	Snow pit Helicopter

5.6 Snow pit measurements

Event	Latitude	Longitude	Label	Device	Date	Comment 1	Comment 2
PS81/H20	-67.2019	-23.1536	PS81/H20_SP-02	Snow pit	7/13/2013	Snow pit 2 Helicopter	Snow pit Helicopter
PS81/H20	-67.1653	-23.1256	PS81/H20_SP-03	Snow pit	7/13/2013	Snow pit 3 Helicopter	Snow pit Helicopter
PS81/506-1	-67.1775	-23.2581	PS81/506_SP-12	Snow pit	7/13/2013	Snow pit 12	Snow pit Ridge study
PS81/506-1	-67.171	-23.2064	PS81/506_SP-13	Snow pit	7/14/2013	Snow pit 13	Snow pit
PS81/506-1	-67.1712	-23.2068	PS81/506_SP-14	Snow pit	7/14/2013	Snow pit 14	Snow pit
PS81/506-1	-67.1713	-23.2069	PS81/506_SP-15	Snow pit	7/14/2013	Snow pit 15	Snow pit optics
PS81/506-1	-67.1715	-23.2069	PS81/506_SP-16	Snow pit	7/14/2013	Snow pit 16	Snow pit
PS81/506-1	-67.1722	-23.2063	PS81/506_SP-17	Snow pit	7/14/2013	Snow pit 17	Snow pit
PS81/506-1	-67.1733	-23.2056	PS81/506_SP-18	Snow pit	7/14/2013	Snow pit 18	Snow pit
PS81/506-1	-67.1732	-23.2056	PS81/506_SP-19	Snow pit	7/14/2013	Snow pit 19	Snow pit
PS81/506-1	-67.1746	-23.2055	PS81/506_SP-20	Snow pit	7/14/2013	Snow pit 20	Snow pit
PS81/506-1	-67.1754	-23.2056	PS81/506_SP-21	Snow pit	7/14/2013	Snow pit 21	Snow pit
PS81/506-1	-67.1769	-23.206	PS81/506_SP-22	Snow pit	7/14/2013	Snow pit 22	Snow pit
PS81/506-1	-67.2013	-23.232	PS81/506_SP-23	Snow pit	7/14/2013	Snow pit 23	Snow pit laser scanning
PS81/506-1	-67.2034	-23.2344	PS81/506_SP-24	Snow pit	7/14/2013	Snow pit 24	Snow pit laser scanning
PS81/506-1	-67.3446	-23.2927	PS81/506_SP-25	Snow pit	7/15/2013	Snow pit 25	Snow pit Retro Drilling
PS81/506-1	-67.3472	-23.2863	PS81/506_SP-26	Snow pit	7/15/2013	Snow pit 26	Snow pit
PS81/506-1	-67.3483	-23.2799	PS81/506_SP-27	Snow pit	7/15/2013	Snow pit 27	Snow pit coring site
PS81/506-1	-67.3498	-23.2765	PS81/506_SP-28	Snow pit	7/15/2013	Snow pit 28	Snow pit coring site
PS81/H22	-66.1492	-27.2735	PS81/H22_SP-01	Snow pit	7/17/2013	Snow pit 1 Helicopter	Snow pit Helicopter
PS81/H22	-66.0929	-27.0328	PS81/H22_SP-02	Snow pit	7/17/2013	Snow pit 2 Helicopter	Snow pit Helicopter

Event	Latitude	Longitude	Label	Device	Date	Comment 1	Comment 2
PS81/H22	-66.0514	-26.8528	PS81/H22_SP-03	Snow pit	7/17/2013	Snow pit 3 Helicopter	Snow pit Helicopter
PS81/H24	-61.831	-34.8708	PS81/H24_SP-01	Snow pit	7/20/2013	Snow pit 1 Helicopter	Snow pit Helicopter
PS81/H24	-61.7636	-35.3329	PS81/H24_SP-02	Snow pit	7/20/2013	Snow pit 2 Helicopter	Snow pit Helicopter
PS81/515-1	-63.4413	-51.2962	PS81/515_SP-01	Snow pit	7/26/2013	Snow pit 1	Snow pit optics
PS81/515-1	-63.4125	-51.2518	PS81/515_SP-02	Snow pit	7/26/2013	Snow pit 2	Snow pit coring site
PS81/515-1	-63.3978	-51.1961	PS81/515_SP-03	Snow pit	7/26/2013	Snow pit 3	Snow pit laser scanning
PS81/517-2	-63.5883	-51.205	PS81/517_SP-01	Snow pit	7/29/2013	Snow pit 1	Snow pit optics
PS81/517-2	-63.5719	-51.1754	PS81/517_SP-02	Snow pit	7/29/2013	Snow pit 2	Snow pit
PS81/517-2	-63.5717	-51.1767	PS81/517_SP-03	Snow pit	7/29/2013	Snow pit 3	Snow pit BAS site
PS81/517-2	-63.505	-51.1144	PS81/517_SP-04	Snow pit	7/30/2013	Snow pit 4	Snow pit Retro Drilling
PS81/517-2	-63.4965	-51.1153	PS81/517_SP-05	Snow pit	7/30/2013	Snow pit 5	Snow pit Retro Drilling
PS81/517-2	-63.4774	-51.1159	PS81/517_SP-06	Snow pit	7/30/2013	Snow pit 6	Snow pit coring site
PS81/517-2	-63.4594	-51.1006	PS81/517_SP-07	Snow pit	7/30/2013	Snow pit 7	Snow pit
PS81/517-2	-63.3911	-51.1053	PS81/517_SP-08	Snow pit	7/31/2013	Snow pit 8	Snow pit Ridge study
PS81/517-2	-63.388	-51.1189	PS81/517_SP-09	Snow pit	7/31/2013	Snow pit 9	Snow pit
PS81/517-2	-63.3929	-51.1311	PS81/517_SP-10	Snow pit	7/31/2013	Snow pit 10	Snow pit Retro Drilling
PS81/517-2	-63.3098	-51.2305	PS81/517_SP-11	Snow pit	8/1/2013	Snow pit 11	Snow pit
PS81/H41	-63.1812	-51.3179	PS81/H41_SP-01	Snow pit	8/1/2013	Snow pit 1 Helicopter	Snow pit Helicopter
PS81/H41	-63.1632	-51.3955	PS81/H41_SP-02	Snow pit	8/1/2013	Snow pit 2 Helicopter	Snow pit Helicopter

5.6 Snow pit measurements

Event	Latitude	Longitude	Label	Device	Date	Comment 1	Comment 2
PS81/H41	-63.1874	-51.3824	PS81/H41_SP-03	Snow pit	8/1/2013	Snow pit 3 Helicopter	Snow pit Helicopter
PS81/517-2	-63.2641	-51.2635	PS81/517_SP-12	Snow pit	8/2/2013	Snow pit 12	Snow pit laser scanning
PS81/H47	-63.2525	-51.322	PS81/H47_SP-01	Snow pit	8/2/2013	Snow pit 1 Helicopter	Snow pit Helicopter
PS81/H47	-63.2487	-51.432	PS81/H47_SP-02	Snow pit	8/2/2013	Snow pit 2 Helicopter	Snow pit Helicopter
PS81/H47	-63.2366	-51.5203	PS81/H47_SP-03	Snow pit	8/2/2013	Snow pit 3 Helicopter	Snow pit Helicopter
PS81/518-3	-62.9307	-53.3597	PS81/518_SP-01	Snow pit	8/4/2013	Snow pit 1	Snow pit
PS81/518-3	-62.9339	-53.4145	PS81/518_SP-02	Snow pit	8/4/2013	Snow pit 2	Snow pit

Preliminary (expected) results

A total number of 87 snow pits were sampled (see Table 5.6.1) with an average depth of 29.5 ± 19 cm. From this total amount, 21 snow pits were obtained during helicopter flight missions. 23 out of 87 snow pits were conducted on MYI floes in contrast to FYI floes. Due to unexpected delays in the cruise track or other uncertainties/problems, satellite image coverage could only be achieved for four different ice stations. This data, combined with the data from a previous campaign, is expected to increase our understanding of which snow properties influence the X-band radar backscatter and thereby create possibilities to extract large scale snow information (e.g. internal structure of the snowpack or snow thickness) from remote sensing data. Besides that, the acquired snow pit data is expected to contribute to the results of several other working groups of our cruise.

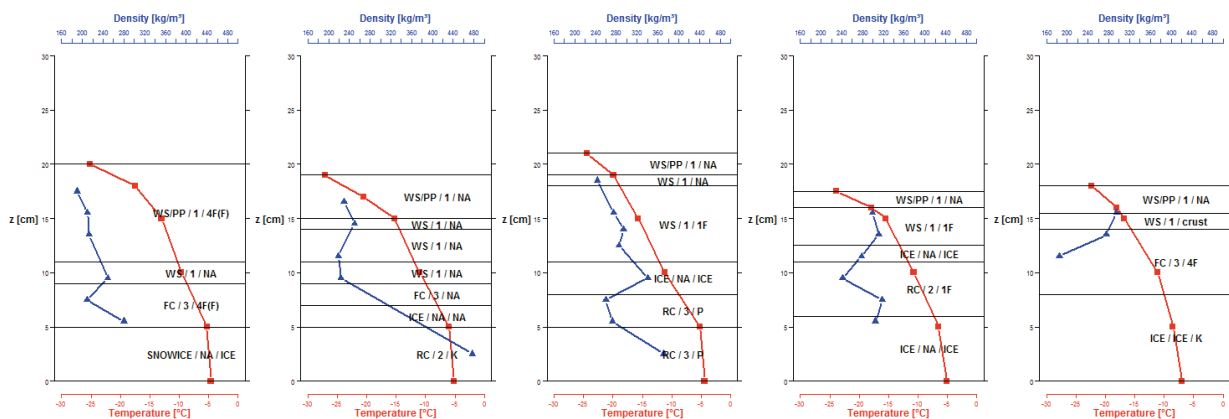


Fig. 5.6.2: Extract from a 10 m snow pit transect conducted at ice station PS81/506. The red line indicates temperature in °C, the blue line shows density and the horizontal black lines indicate the different layer interfaces.

Fig. 5.6.2 shows an example of the acquired data. It presents an extract of 5 pits of 2 m spacing from a 10 m transect. The site for this transect was chosen visually for its homogenous surface appearance. However, the internal structure of each snow pack differs quite significantly and is an excellent example for the small scale horizontal differences in the snowpack.

Data management

Data will be delivered to PANGAEA Data Publisher for Earth & Environmental Science within two years after the cruise.

5.7 Snow topography

Objectives

In order to better understand the effect of blowing snow on the snow (re)distribution, measurements of snow surface topography and microstructure were combined with blowing snow measurements and wind speed profiles. Furthermore, the study of surface roughness upwind of the measurement site and its effect on the wind speed profile is important in many exchange processes between the snow pack and the atmosphere.

5.7 Snow topography

Work at sea

The work at the sea ice consisted of a detailed study of a 50 x 50 m (long ice station) or 25 x 25 m (short ice station) study area, respectively.

We deployed a blowing snow mast with snow particle counters at 4 heights and wind speed at 4 heights, wind direction at 1 height and temperature/relative humidity at 2 heights. In case of blowing snow, measurements were extended by Formvar experiments in rocket traps to determine blowing snow size distribution.

Then, terrestrial laser scanners were used to determine surface topography of the study site, providing surface topography at a resolution of 10 - 50 cm.

After the scan, we performed Magnaprobe / GPS survey of the study site, to determine snow height distribution with 1- 2 m resolution and a GEM-2 survey to determine ice thickness at the study site (see Chapter 5.2).

In addition, precision GPS surveys of the laser scanner targets were performed in order to allow spatial referencing and the combination of laser scans.

For the quantification of the spatial variability of the internal snow cover microstructure, snow micro penetrometer measurements at transects in the study site was also performed.

At three ice stations, ice mass balance buoys, snow depth buoys and/or automatic weather stations were deployed to monitor the further development of the study site and the floe (see Chapter 5.8).

In the end of each station, GPS survey of each science group's study areas on the ice floe were conducted in order to create a station map.

Short description of ice stations

The ice stations with a useful dataset are described here. Other stations were used for testing equipment and measurement procedures only.

1) PS81/503 (10 hrs): The measurement site was approximately 25 x 25 m, consisting of slightly rough snow surface, with structures (dunes/ridges) up to 30 cm. The inhomogeneities are quite homogenous distributed. The study site was covered by three scan positions with the FARO laser scanner. The blowing snow mast was deployed for approximately 6 hours, and the study site was surveyed with the magnaprobe and GEM-2 instruments afterwards.

2) PS81/506 (4 days): The measurement site was approximately 50 x 50 m, located in a ridged area. Flat parts inside the study area are surrounded by ridges up to 60 cm. Larger ridges, up to 1.5 m were away outside the study site. The ice thickness at the study site was very variable, with 30 cm thick parts, up to 80 cm. The site was covered by 2 scans with the Riegl LPM-321 and 2 additional FARO scans. The FARO scans will be used to compare data quality between both scanners. Furthermore, 1 FARO scan filled up a gap not covered by the two Riegl scan positions. The second FARO scan was performed very close to the blowing snow mast, in order to get a better roughness length information upwind of the blowing snow mast. The blowing snow mast was deployed for a little over 3.5 days. The site was surveyed with the magnaprobe and GEM-2 instruments afterwards, although due to increasing winds and the onset of blowing snow, the magnaprobe may show discrepancies to the laser scanner results.

3) PS81/515 (10 hrs): This station was characterized by strong winds and important snow drift. The floe was small, and very ridged. The vessel was beset in the sea ice, so the ice station was downwind of the ship. We moved our study site to the bow of the ship, and had a more or less clean upwind fetch over a somewhat flat area. The scanning site is about 25 x 25 m and surrounded by 1-2 m high ridges. Due to presence of blowing snow, only 1 FARO scan was performed, close to the blowing snow mast to provide some information about upwind roughness. The scan quality is relatively low, due to the presence of blowing snow, and increasing winds during the day prevented further scans.

The blowing snow mast was deployed for about 8 hours. Unfortunately, the snow upwind of the mast got disturbed by skidoo and foot traffic from another group, which makes interpretation of data from early in the station difficult. However later in the station, the amount of blowing snow was high enough that we believe the unwanted disturbance is negligible. The rocket traps were used together with Formvar to get blowing snow particle size distributions at three levels. Unfortunately, the upper level was measured later in time, with even stronger snow drift than the lowest two levels. The site was surveyed with the magnaprobe and GEM-2 instruments at the end of the station. Massive snow drift had already occurred and may cause some discrepancies between the laser scan earlier in the day. Furthermore, the snow depth was regularly over 1.2 m, which exceeded the measurement limit of the magnaprobe.

4) PS81/517 (4.5 days): This station was characterized by flat areas, with clearly identifiable ridges. The study site was chosen to contain such a ridge, with flat parts at both sides. The ridges were up to 1.5 m high. The site was 50 x 50 m, and was covered by 3 scan positions with the Riegl LPM-321 laser scanner. An additional scan was performed with the FARO between the blowing snow mast and the AWS, to get information of the terrain around and upwind of these stations. After magnaprobing and GEM-2 surveying the study site, two transects with the Snow Micro Penetrometer (SMP) were measured. The first transect (spacing about 40 cm) is about 2 - 3 m downwind of the ridge, the second transect (spacing about 70 cm) is almost perpendicular to the first transect, starting at the blowing snow mast. Finally, a snow pit was dug in the scanned area. There was a slight blowing snow event at the end of the station, but the amounts were too small to be of importance for the comparison of magnaprobe and laser scan. See Table 5.7.1 for a list of snow topography and roughness measurements.

Preliminary results

To spatially reference and combine TLS and magnaprobe/GPS measurements, differential GPS is used. However analysis of the GPS signals is not straightforward due to floe drifting and rotation. A data processing strategy has been developed, but the GPS data has not yet been processed. Therefore, no preliminary results for TLS or magnaprobe surveys can be presented.

5.7 Snow topography

Tab. 5.7.1: List of snow topography and roughness measurements

Event	Latitude	Longitude	Label	Device	Date	Comment 1	Comment 2
PS81/493-2	-66.43266667	0.1453333333	PS81/493-2_GPS_ BASE_ICE2	Survey GPS	06/21/2013	GPS base station	
PS81/493-2	-66.43266667	0.1453333333	PS81/493-2_GPS_ BASE_ICE3	Survey GPS	06/21/2013	GPS base station	
PS81/493-2	-66.43266667	0.1453333333	PS81/493-2_GPS_ ROVER_ICE1	Survey GPS	06/21/2013	GPS rover, for station map, TLS targets, and TLS magnaprobe	
PS81/493-2	-66.43266667	0.1453333333	PS81/493-2_ MAGNA_TLS	Magnaprobe	06/21/2013	Magnaprobe of Faro scan area	
PS81/496-1	-67.446	0.0325	PS81/496-1_GPS_ BASE_ICE2	Survey GPS	06/24/2013	GPS base station	
PS81/496-1	-67.446	0.0325	PS81/496-1_GPS_ BASE_ICE3	Survey GPS	06/24/2013	GPS base station	
PS81/496-1	-67.446	0.0325	PS81/496-1_GPS_ ROVER_ICE1	Survey GPS	06/24/2013	GPS rover, for station map	
PS81/496-1	-67.446	0.0325	PS81/496-1_ MAGNA_GEM	Magnaprobe	06/24/2013	Magnaprobe with GEM survey	
PS81/497-1	-68.0395	-0.337	PS81/497-1_ MAGNA_GEM	Magnaprobe	06/26/2013	Magnaprobe with GEM survey	
PS81/500-5	-67.91983333	-6.739166667	PS81/500-5_BS	Blowing snow mast	07/04/2013	Blowing snow mast, near TLS area	

Event	Latitude	Longitude	Label	Device	Date	Comment 1	Comment 2
PS81/500-5	-67.91983333	-6.739166667	PS81/500-5_GPS_ BASE_ICE2	Survey GPS	07/04/2013	GPS base station	
PS81/500-5	-67.91983333	-6.739166667	PS81/500-5_GPS_ BASE_ICE3	Survey GPS	07/04/2013	GPS base station	
PS81/500-5	-67.91983333	-6.739166667	PS81/500-5_ MAGNA_GEM	Magnaprobe	07/05/2013	Magnaprobe with GEM survey	
PS81/503-2	-67.19783333	-13.24766667	PS81/503-2_BS	Blowing snow mast	07/08/2013	Blowing snow mast, near TLS area	
PS81/503-2	-67.19783333	-13.24766667	PS81/503-2_GPS_ BASE_ICE2	Survey GPS	07/08/2013	GPS base station	
PS81/503-2	-67.19783333	-13.24766667	PS81/503-2_GPS_ BASE_ICE3	Survey GPS	07/08/2013	GPS base station	
PS81/503-2	-67.19783333	-13.24766667	PS81/503-2_GPS_ ROVER_ICE1	Survey GPS	07/08/2013	GPS rover, for station map, TLS targets, and TLS magnaprobe	
PS81/503-2	-67.19783333	-13.24766667	PS81/503-2_TLS_ FARO_SP1	TLS_FARO	07/08/2013	ScanPosition 1	faro_scan_071
PS81/503-2	-67.19783333	-13.24766667	PS81/503-2_TLS_ FARO_SP2	TLS_FARO	07/08/2013	ScanPosition 2	faro_scan_073
PS81/503-2	-67.19783333	-13.24766667	PS81/503-2_TLS_ FARO_SP3	TLS_FARO	07/08/2013	ScanPosition 3	faro_scan_074
PS81/503-2	-67.19783333	-13.24766667	PS81/503-2_ MAGNA_TLS	Magnaprobe	07/08/2013	Magnaprobe of Faro scan area	
PS81/503-2	-67.19783333	-13.24766667	PS81/503-2_ MAGNA_GEM	Magnaprobe	07/08/2013	Magnaprobe with GEM survey	
PS81/506-1	-67.3555	-23.26783333	PS81/506-1_BS	Blowing snow mast	07/11/2013	Blowing snow mast, near TLS area	

5.7 Snow topography

Event	Latitude	Longitude	Label	Device	Date	Comment 1	Comment 2
PS81/506-1	-67.3555	-23.26783333	PS81/506-1_GPS_ BASE_ICE2	Survey GPS	07/11/2013	GPS base station	
PS81/506-1	-67.3555	-23.26783333	PS81/506-1_GPS_ BASE_ICE3	Survey GPS	07/11/2013	GPS base station	
PS81/506-1	-67.3555	-23.26783333	PS81/506-1_GPS_ ROVER_ICE1	Survey GPS	07/12/2013	GPS rover, for station map, TLS targets, and TLS magnaprobe	
PS81/506-1	-67.3555	-23.26783333	PS81/506-1_TLS_ RIEGL_SP1	TLS_RIEGL_LPM- 321	07/12/2013	ScanPosition 1	
PS81/506-1	-67.3555	-23.26783333	PS81/506-1_TLS_ RIEGL_SP2	TLS_RIEGL_LPM- 321	07/13/2013	ScanPosition 2	
PS81/506-1	-67.3555	-23.26783333	PS81/506-1_TLS_ FARO_SP3	TLS_FARO	07/14/2013	ScanPosition 3	faro_scan_075
PS81/506-1	-67.3555	-23.26783333	PS81/506-1_TLS_ FARO_SP4	TLS_FARO	07/14/2013	ScanPosition 4	faro_scan_076
PS81/506-1	-67.3555	-23.26783333	PS81/506-1_ MAGNA_TLS	Magnaprobe	07/14/2013	Magnaprobe of Reigl / Faro scan area	
PS81/506-1	-67.3555	-23.26783333	PS81/506-1_ MAGNA_GEM	Magnaprobe	07/14/2013	Magnaprobe with GEM survey	
PS81/506-1	-67.3555	-23.26783333	PS81/506-1_ FORMVAR	Formvar/ Rockettraps	07/15/2013	Collection of snowflakes using rocket trap and formvar	
PS81/515-1	-63.36866667	-51.1365	PS81/515-1_BS	Blowing snow mast	07/26/2013	Blowing snow mast, near TLS area	
PS81/515-1	-63.36866667	-51.1365	PS81/515-1_GPS_ BASE_ICE2	Survey GPS	07/26/2013	GPS base station	

Event	Latitude	Longitude	Label	Device	Date	Comment 1	Comment 2
PS81/515-1	-63.36866667	-51.1365	PS81/515-1_GPS_ BASE_ICE3	Survey GPS	07/26/2013	GPS base station	
PS81/515-1	-63.36866667	-51.1365	PS81/515-1_GPS_ ROVER_ICE1	Survey GPS	07/26/2013	GPS rover, for station map, TLS targets, and TLS magnaprobe	
PS81/515-1	-63.36866667	-51.1365	PS81/515-1_TLS_ FARO_SP1	TLS_FARO	07/26/2013	Scanposition 1	faro_scan_077
PS81/515-1	-63.36866667	-51.1365	PS81/515-1_ FORMVAR	Formvar/ Rockettraps	07/26/2013	Collection of snowflakes using rocket trap and formvar	
PS81/515-1	-63.36866667	-51.1365	PS81/515-1_ MAGNA_TLS	Magnaprobe	07/26/2013	Magnaprobe of Faro scan area	
PS81/515-1	-63.36866667	-51.1365	PS81/515-1_ MAGNA_GEM	Magnaprobe	07/26/2013	Magnaprobe with GEM survey	
PS81/517-2	-63.25783333	-51.223	PS81/517-2_BS	Blowing snow mast	07/29/2013	Blowing snow mast, near TLS area	
PS81/517-2	-63.25783333	-51.223	PS81/517-2_GPS_ BASE_ICE2	Survey GPS	07/29/2013	GPS base station	
PS81/517-2	-63.25783333	-51.223	PS81/517-2_GPS_ BASE_ICE3	Survey GPS	07/29/2013	GPS base station	
PS81/517-2	-63.25783333	-51.223	PS81/517-2_GPS_ ROVER_ICE1	Survey GPS	07/31/2013	GPS rover, for station map, TLS targets, and TLS magnaprobe	
PS81/517-2	-63.25783333	-51.223	PS81/517-2_TLS_ RIEGL_SP1	TLS_RIEGL_LPM- 321	07/29/2013	Scanposition 1	
PS81/517-2	-63.25783333	-51.223	PS81/517-2_TLS_ RIEGL_SP2	TLS_RIEGL_LPM- 321	07/29/2013	Scanposition 2	

5.6 Snow pit measurements

Event	Latitude	Longitude	Label	Device	Date	Comment 1	Comment 2
PS81/517-2	-63.25783333	-51.223	PS81/517-2_TLS_RIEGL_SP3	TLS_RIEGL_LPM-321	07/30/2013	Scanposition 3	
PS81/517-2	-63.25783333	-51.223	PS81/517-2_IMB_FARO	TLS_FARO	07/31/2013	FARO Laserscan at site of IMB and snow depth buoy	
PS81/517-2	-63.25783333	-51.223	PS81/517-2_SNOWPIT_SMP	SnowMicroPen	07/31/2013	At snowpits	No 93-119
PS81/517-2	-63.25783333	-51.223	PS81/517-2_TLS_FARO_SP4	TLS_FARO	08/01/2013	Scanposition 4	
PS81/517-2	-63.25783333	-51.223	PS81/517-2_IMB_SMP	SnowMicroPen	08/01/2013	At IMB site	No 120-124
PS81/517-2	-63.25783333	-51.223	PS81/517-2_SDBUOY_SMP	SnowMicroPen	08/01/2013	At snow depth buoy site	No 126-128
PS81/517-2	-63.25783333	-51.223	PS81/517-2_TLS_SMP	SnowMicroPen	08/02/2013	Transect TLS site	No 152-270
PS81/517-2	-63.25783333	-51.223	PS81/517-2_TLS_SMP	SnowMicroPen	08/02/2013	Transect TLS site + snowpit TLS site	No 129-152
PS81/517-2	-63.25783333	-51.223	PS81/517-2_MAGNA_TLS	Magnaprobe	07/29/2013	Magnaprobe of Reigl / Faro scan area	
PS81/517-2	-63.25783333	-51.223	PS81/517-2_MAGNA_GEM	Magnaprobe	08/01/2013	Magnaprobe with GEM survey	
PS81/518-3	-62.87666667	-53.2355	PS81/518-3_FLOE_SMP	SnowMicroPen	08/04/2013	Snowpits and at retrodrilling grid	No 271-306
PS81/518-3	-62.87666667	-53.2355	PS81/517-2_MAGNA_GEM	Magnaprobe	08/04/2013	Magnaprobe with GEM survey	

5.8 Autonomous buoys

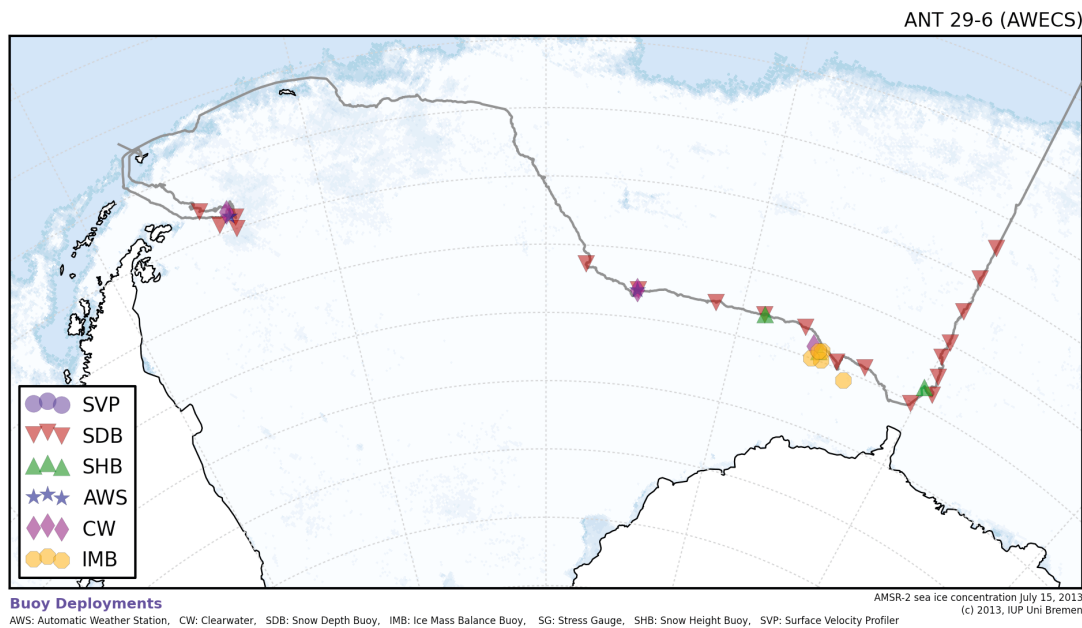


Fig. 5.8.1: Buoy deployments during ANT-XXIX/6. Background: sea-ice concentration from July 15, 2013

Objectives

The investigation of physical sea-ice and snow parameters like sea ice thickness, snow depth and sea-ice drift is possible also beyond the cruise by deploying autonomous buoys. Those buoys record the afore mentioned parameters mostly along with the meteorological variables like air temperature and sea level pressure and yield valuable information about the evolution of the investigated sea-ice floe and the surrounding area. The objective for ANT-XXIX/6 was to deploy

- 30 Surface Velocity Profiler (SVP) buoys along the ship's course to monitor large-scale, long-term ice motion throughout the Weddell Sea,
- a "deformation array", consisting of 10 marker buoys and 2 stress gauge buoys in a specific geometry on a ~ 100 km scale, to monitor sea ice motion and strain through the Weddell Gyre,
- 4 newly developed snow depth buoys in combination with ice mass balance buoys (IMB)
- Three sets of automatic weather stations, IMBs and snow height buoys.

Work at sea

- SVP buoys. A total of 19 SVP buoys were deployed (Fig. 5.8.1, Tab. 5.8.1), 12 using the ship's mummy chair, 5 during ice stations, and 2 by helicopter. Prior to deployment, all buoys were tested, with two malfunctioning buoys found. Therefore, 9 buoys remain, and are stored onboard *Polarstern* for deployment on cruise ANT-XXIX/9.
- Deformation Array. Due to difficult sea ice conditions and flight limitations, it was not possible to deploy the deformation array at the target location, or in the intended 12-buoy geometry. Instead, a smaller array consisting of 5 buoys (4 marker buoys + 1 stress gauge buoy) was deployed at the farthest south location possible during the cruise, with the array centered around

5.8 Autonomous buoys

67.7°S, 8.4°W. One additional marker buoy was deployed at 68.3°S, 5.9°W, on a previous flight which was shortened due to weather. The one remaining stress gauge buoy will be returned to Tasmania, while the remaining 5 marker buoys are stored onboard *Polarstern* for deployment on cruise ANT-XXIX/9.

- Snow depth buoys. In total 3 snow depth buoys were deployed during the cruise, one together with an AWI IMB, another one together with an IMB of the FMI. The buoys were tested prior to deployment, which has been on ice stations for two of them. The set consisting of the snow depth buoy and AWI's IMB was deployed by helicopter, located in the center of the deformation array.
- Buoy sets. At three ice stations, ice mass balance buoys, snow height buoys and/or automatic weather stations were deployed to continue monitoring of the study site and the floe.

Preliminary results

As of this writing, 15 SVP buoys are still reporting. For the deformation array, it was not possible to access buoy data from the ship, therefore it is not known how many buoys are still reporting. However, since two AWI buoys were deployed within the array, it is assumed that the deformation array has followed the approximate path of the AWI buoys, which did not enter the Weddell Gyre, but instead are slowly drifting north. Fig. 5.8.2 shows the pass of the three deployed AWI snow depth buoys, from which the middle one lies within the mentioned buoy array.

For AWS, IMB, and snow height buoys, data delivery to *Polarstern* was accomplished using Iridium SBD and ship email. Data retrieval to the USA is also ongoing, however measurement time series have not yet been generated.

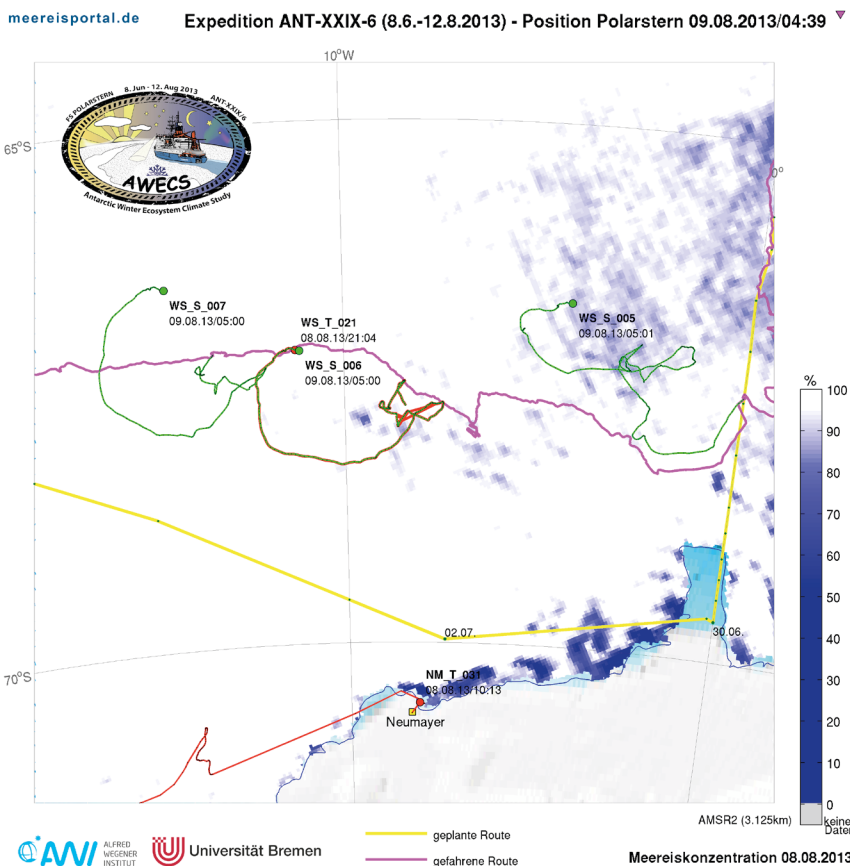


Fig. 5.8.2: Drift track of snow depth buoys (green) and an ice mass balance buoy (red, next to the snow depth buoy) deployed during ANT-XXIX/6

Tab. 5.8.1: List and initial positions of all deployed buoys during ANT-XXIX/6

Event	Latitude	Longitude	Label	Device	Date	Comment 1	Comment 2
SVP BUOYS							
PS81/488-2	-62.9083	-0.01	PS81/488-2_SVP	SVP	06/18/2013	Drift velocity	Surface Temperature
PS81/489-2	-63.9083	-0.0433	PS81/489-2_SVP	SVP	06/19/2013	Drift velocity	Surface Temperature
PS81/491-1	-64.9717	0	PS81/491-1_SVP	SVP	06/20/2013	Drift velocity	Surface Temperature
PS81/491-2	-65.9567	0.185	PS81/491-2_SVP	SVP	06/21/2013	Drift velocity	Surface Temperature
PS81/493-2	-66.435	0.135	PS81/493-2_SVP	SVP	06/21/2013	Drift velocity	Surface Temperature
PS81/494-1	-66.9983	0.5883	PS81/494-1_SVP	SVP	06/22/2013	Drift velocity	Surface Temperature
PS81/495-3	-67.5383	0.83	PS81/495-3_SVP	SVP	06/23/2013	Drift velocity	Surface Temperature
PS81/497-1	-68.0483	-0.3367	PS81/497-1_SVP	SVP	06/26/2013	Drift velocity	Surface Temperature
PS81/499-2	-67.685	-4.7167	PS81/499-2_SVP	SVP	07/01/2013	Drift velocity	Surface Temperature
PS81/500-5	-67.8467	-6.885	PS81/500-5_SVP	SVP	07/05/2013	Drift velocity	Surface Temperature
PS81/502-4	-67.2	-10.0217	PS81/502-4_SVP	SVP	07/07/2013	Drift velocity	Surface Temperature
PS81/503-2	-67.1983	-13.2483	PS81/503-2_SVP	SVP	07/08/2013	Drift velocity	Surface Temperature

5.8 Autonomous buoys

Event	Latitude	Longitude	Label	Device	Date	Comment 1	Comment 2
PS81/504-3	-67.19	-17.04	PS81/504-3_SVP	SVP	07/08/2013	Drift velocity	Surface Temperature
PS81/506-1	-67.185	-22.995	PS81/506-1_SVP	SVP	07/11/2013	Drift velocity	Surface Temperature
PS81/507-4	-66.55	-27.0333	PS81/507-4_SVP	SVP	07/17/2013	Drift velocity	Surface Temperature
PS81/516-4	-63.6817	-50.8567	PS81/516-4_SVP	SVP	07/29/2013	Drift velocity	Surface Temperature
PS81/H38-1	-64.0067	-51.0233	PS81/H38-1_SVP	SVP	07/31/2013	Drift velocity	Surface Temperature
PS81/H38-2	-63.75	-52.0133	PS81/H38-2_SVP	SVP	07/31/2013	Drift velocity	Surface Temperature
PS81/518-2	-63.1767	-52.95	PS81/518-2_SVP	SVP	08/03/2013	Drift velocity	Surface Temperature
DEFORMATION ARRAY BUOYS							
PS81/500-5	-68.2683	-5.8683	PS81/500-5_CWB	CLEARWATER	07/03/2013	Drift velocity	partly air pressure, air and surface temperature
PS81/H14-1	-67.7	-8.2233	PS81/H14-1_CWB	CLEARWATER	07/06/2013	Drift velocity	partly air pressure, air and surface temperature
PS81/H14-2	-67.96	-8.0667	PS81/H14-2_CWB	CLEARWATER	07/06/2013	Drift velocity	partly air pressure, air and surface temperature
PS81/H14-3	-67.9983	-8.845	PS81/H14-3_CWB	CLEARWATER	07/06/2013	Drift velocity	partly air pressure, air and surface temperature
PS81/H14-4	-67.7317	-8.4717	PS81/H14-4_CWB	STRESS GAUGE	07/06/2013	Drift velocity	partly air pressure, air and surface temperature

Event	Latitude	Longitude	Label	Device	Date	Comment 1	Comment 2
PS81/H14-5	-67.645	-8.96	PS81/H14-5_CWB	CLEARWATER	07/06/2013	Drift velocity	partly air pressure, air and surface temperature
Others							
PS81/506-1	-67.198	-23.0563	PS81/506-1_AWS	AWS	07/14/2013	Automatic weather station buoy	
PS81/506-1	-67.198	-23.0563	PS81/506-1_IMB	IMB	07/14/2013	Ice mass balance buoy	
PS81/506-1	-67.198	-23.0563	PS81/506-1_SHB	SNOW HEIGHT BUOY	07/14/2013	Snow height buoy	
PS81/515-1	-63.461	-51.3123	PS81/515-1_AWS	AWS	07/26/2013	Automatic weather station buoy	
PS81/517-2	-63.6027	-51.2152	PS81/517-2_AWS	AWS	08/01/2013	Automatic weather station buoy	
PS81/517-2	-63.6027	-51.2152	PS81/517-2_IMB	IMB	08/01/2013	Ice mass balance buoy	
PS81/517-2	-63.6027	-51.2152	PS81/517-2_SHB	SNOW HEIGHT BUOY	08/01/2013	Snow height buoy	
PS81/496-1	-67.4467	0.0302	PS81/496_Buoy-Snow	Buoy, Snow Depth	06/24/2013	Snow Depth buoy with 4 sensors	averages snow depth [m]: 0.27
PS81/H15-1	-67.7388	-8.4664	PS81/H15_Buoy-Snow	Buoy, Snow Depth	07/06/2013	Snow Depth buoy with 4 sensors	averages snow depth [m]: 0.38
PS81/H15-1	-67.7388	-8.4664	PS81/H15_Buoy-IMB	Buoy, IMB	07/06/2013	Ice mass balance buoy	ice thickness [m]: 0.795
PS81/503-2	-67.1566	-13.2248	PS81/503_Buoy-Snow	Buoy, Snow Depth	07/08/2013	Snow Depth buoy with 4 sensors	averages snow depth [m]: 0.13

Data management

All data from autonomous drift buoys will be available through different project home pages. Buoy positions and atmospheric parameters will also be accessible through the website of the International Program for Antarctic buoys within two years after data collection. Furthermore, we are currently integrating buoy data into the AWI-based sea-ice portal www.meereisportal.de.

References

- Worby A P (1999) Observing operating in the Antarctic sea ice: A practical guide for conducting sea ice observations from vessels operating in the Antarctic pack ice.
- Petrich C, Eicken E (2010) Growth, Structure and Properties of Sea Ice. *Sea Ice*, Wiley-Blackwell, 23-77.

6. SEA ICE BIOGEOCHEMISTRY

Bruno Delille ¹	¹ ULg
Jeroen de Jong ²	² ULB
Julie Janssens ³	³ IMAS, UTas
Gerhard Dieckmann ⁴	⁴ AWI
Nikolaus Gussone ⁵	⁵ UM
Annemari Luhtanen ⁶	⁶ UH
Daiki Nomura ⁷	⁷ HU
Janne-Markus Rintala ⁶	
Jean-Louis Tison ²	
Christiane Uhlig ⁴	

Objectives

Main objectives

The main objective of the sea ice Biogeochemistry group is to contribute to the understanding of how the Antarctic sea ice physical environment affects the seasonal and regional dynamics of biogeochemical cycles. In the last 15 years, this has been mainly investigated in Spring and Summer around Antarctica, but reliable annual budgets require observation data and understanding of driving processes from the Winter too, hence this contribution to the AWECS cruise.

The research team is highly multi-disciplinary, with contribution from glaciologists, chemical oceanographers, biologists and sea ice modellers. The work program is to measure the variability of sea ice and snow properties on small-regional scales using a multiple platform approach that includes ice coring surveys and instrument deployment on sea ice in an attempt to integrate it into a coherent model for winter sea ice biogeochemical dynamics in the whole of the Weddell Sea. The data collected will be available for the validation and calibration of process studies on sea ice biogeochemistry and the improved parameterization of sea ice processes in climate and ecosystem models. The physical measurements will support a suite of biogeochemical and ecological process studies that focus on the major physical and biogeochemical drivers controlling e.g. gas exchange and nutrients recycling in the sea ice zone. This work also entails the investigation of functional relationships between the physical and biogeochemical properties of sea ice and sea ice microbes ranging from viruses to protozoans.

Specific objectives

Trace metal and their isotopes in the sea ice environment

The main objective is here to identify and quantify processes that control the distribution of key trace elements and isotopes in the sea ice environment, and their sensitivity to changing environmental conditions, in order to elucidate sources

of micronutrients, contaminant dispersal and ocean tracers. To this end we will measure the concentrations of trace metals Fe, Mn, Al, Co, Cu, Ni, Zn, Pb, Cd, Mo and Ba as well the isotopic compositions of Fe and Zn, in snow, sea ice, brine and seawater. Of particular interest is the opportunity during expedition ANT-XXIX/6 AWECS to study the spatial distribution and temporal evolution of trace metals in sea ice during the period of formation of the sea ice.

The availability of Fe and other bio-essential metals such as Mn, Co, Cu and Zn are regulatory factors for primary productivity and the associated uptake of carbon over large areas of the ocean. These metals thus play an important role in the carbon cycle, and changes in its supply to the surface ocean may have had a significant effect on atmospheric carbon dioxide concentrations over glacial–interglacial cycles (e.g. Martin, 1990).

The large abundance of ice algae dwelling in sea ice, in combination with the large-scale distribution of sea ice and the strong seasonal changes in coverage of the Southern Ocean, pose questions about the availability of trace metals in sea ice, the influence of sea ice on the oceanic biogeochemical cycle of trace metals and the role of sea ice in the carbon cycle. It was established in recent years that Fe was not a limiting factor in sea ice, in an otherwise well-recognized HNLC environment! Indeed, the first measurements of iron in Antarctic sea ice (Löscher et al., 1997) highlighted enhanced levels of iron by a factor of 10-100 as compared to water column data (10-100 nM vs. <1nM). A later, much more elaborate study of Fe distributions in East-Antarctic sea-ice during late austral winter/early spring 2003 confirmed this (Lannuzel et al., 2007). Budget calculations suggested also that the source of iron in sea ice must predominantly be from below by vertical advection and turbulent mixing. The observed accumulation of iron in sea ice may be later pulse-released during spring melt. Melting sea ice could thus not only play a role in seeding ice edge blooms, but could also provide the micronutrients such as Fe, Mn, Co, Cu and Zn. During a time series ice station in the Weddell Sea (ISPOL) in late austral spring/early summer 2004, it was observed that iron concentrations in the ice decreased by a factor of 10 in 4 weeks time due to advancing sea ice melting (Lannuzel et al., 2008), and a significant flux of iron to the surface waters was deduced from this. As to which process could be responsible for the accumulation of iron in sea ice, it is thought that the phytoplankton being scavenged during sea ice formation act as efficient active scavengers of trace metals itself, and it continues entraining trace metals from the underlying seawater while associated with the sea ice (Lannuzel et al., 2008). High concentrations of organic matter as transparent exopolymeric particles in the sea ice make the sea ice internal habitat resemble a bio-gel (Becquevort et al., 2009), which could play a role in the passive chelative scavenging of trace metals in sea ice and could also increase their bioavailability (Hassler et al., 2011).

Recent own results from ice cores from ISPOL, McMurdo Sound and the Arctic Ocean confirm for other trace metals what we have seen for Fe, notably an enrichment by one to two orders of magnitude or even higher.

During ANT-XXIX/6 samples were taken to study the evolution in the distribution and behavior of trace metals and Fe/Zn isotopic compositions in snow, sea-ice and the water column during winter in the Weddell Sea. Full water column profiles were sampled by CTD-Rosette on a transect from the inner continental shelf of the Antarctic Peninsula to the abyssal Weddell Sea. This transect will provide insights in lateral transport of trace metals off the continental shelf. The importance of the

Antarctic Peninsula continental shelf as natural Fe fertilizer was recently shown (e.g. de Jong et al., 2012 and references therein). Our goal is now to establish the potential of the Antarctic Peninsula shelf to enrich the Southern Ocean with other bioactive metals and to show by flux calculations what the consequences are for the trace metal inventory of sea ice. By measuring Fe/Zn isotopic compositions we hope to shed some light on biological processes in the sea ice environment e.g. autotrophy versus heterotrophy, sorption/desorption to marine particles or a-biologic processes such as physical-chemically driven dissolution/precipitation processes.

Incorporation of Particulate organic matter, microorganisms and iron in young sea ice

Another more specific focus has been placed on improving our theoretical understanding of the processes that govern how dissolved and particulate organic matter, micro-organisms and iron are incorporated into newly forming sea ice. The accumulation pathways will be investigated using a combination of numerical modeling (improving and extension of an existing model to the incorporation of biological particles, organic matter and iron), laboratory experiments and field-studies. The main targets are:

- Compare the segregation coefficient of particles based on their size and speciation with special emphasis on the effect of surface-stickiness
- Compare the accumulation rate of dissolved and particulate organic matter in different types of ice (frazil, snow ice and columnar)
- Develop a numerical model to quantify the fluxes of both organic matter and iron into newly forming sea ice

Sea ice paleo proxies

Finally, the research also focuses on the impact of sea ice biogeochemical processes on paleoceanographic reconstructions such as the sea ice paleo-extension or SST reconstructions. The isotopic signature of sea ice nutrients ($\delta^{29}\text{Si}$ and $\delta^{15}\text{N}$) will be analyzed in order to a) tackle the proportion of recycled vs. new production in the brine network and b) evidence specific fractionation in the sea ice environment that might be considered as a tracer of paleo-sea ice extent if it is significantly different from the signature of surface open waters.

Neogloboquadrina pachyderma (sin.) is the dominant planktonic foraminifer in high latitudes. Their tests, which are composed of calcium carbonate, are one of the most important archives for geochemical proxies in polar regions. In particular, SST reconstructions are based on $\delta^{18}\text{O}$ and Mg/Ca ratios. However, *N. pachyderma* is not only present in the water column, but also in channels within the sea ice, filled with brine (Spindler and Dieckmann, 1986; Dieckmann et al., 1991). As the brine properties significantly differ from seawater in respect to salinity, ionic strength and oxygen isotope composition, calcification of foraminifer tests within such brines could potentially bias paleoceanographic reconstructions based on *N. pachyderma*. Therefore, we aim to find evidence, indicating if *N. pachyderma* is able to form new calcite tests while trapped in the sea ice brines, and if possible, characterize the geochemical signature of these newly formed tests.

Work at sea

Our activities at sea articulated around five major work settings: a) Short lasting Mummy chair sampling b) 10 hours ice stations, c) 4 days ice stations d) occasional helicopter-borne ice core sampling and e) experimental runs "in situ" or "on board" (incubations with various objectives and the study of sequential incorporation of organic and inorganic impurities in young sea ice). As a whole **12** major ice stations were visited, resulting in the sampling of ice cores, snow samples, brine samples and water samples. These were partly treated "on site" or on the ship and partly preserved or kept frozen/stored for later measurements in the home laboratories.

Mummy Chair sampling

On the in-bound transect south, three stations (PS81/486, 488 and 489) were sampled from the mummy chair for collection of pan cake ice, snow and under-ice sea water, the latter with a Pristine PVDF water sampler borrowed from NIOZ-Textel.

10 hours ice stations

As underlined in the objectives, the aim of the consortium is to gather, at each ice station, a suite of physical and biogeochemical parameters that would enable us to decipher the biogeochemical dynamics of the sea ice and the controls on its exchanges across the atmosphere-ice-ocean interfaces. These target parameters are summarized in Table 6.1. They were typically collected, whenever possible, in air, snow, slush, ice and water down to 30 m, as schematically shown in Fig. 6.1.

Each Ice Station has been organized following a pattern similar to the one shown in Fig. 6.2, in specific conditions allowing to keep the site clean and suitable for trace metal studies.

Table 6.1: Target parameters for the sea ice stations

TOPIC	MEASUREMENTS
Physics and Inorganic Chemistry	Temperature Bulk Salinity Water Stable isotopes Fabrics
Gases	N ₂ , O ₂ , Ar, CH ₄ , N ₂ O CO ₂ (incl. air fluxes) DMS, DMSP, DMSO, VOC Gas ¹³ C and ² H isotopes Total gas content
Biology	Chl-a Microbial Foodweb: Targeted enumeration of algae, bacteria, viruses Primary and Bacterial production
Biogeochemistry	Nutrients EPS POC DOC $\delta^{13}\text{C}$, $\delta^{30}\text{Si}$, $\delta^{15}\text{N}$
Trace Metals	Fe, Zn, Mn, Cu, Cd, Ni, Mo, Co, Ba, Al, Pb

Carbonate System

DIC

Total Alkalinity (TA)

pH

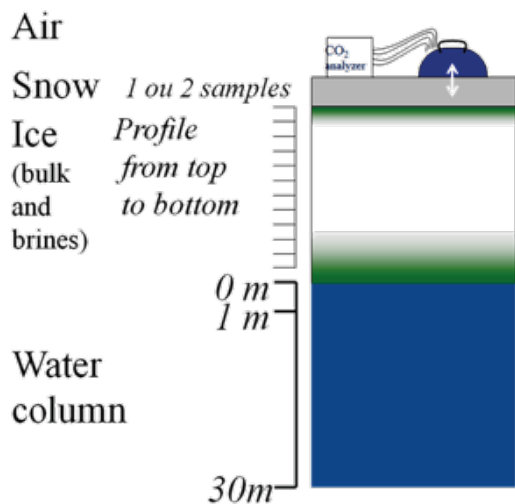
CaCO₃ crystals (Ikaïte) derived from either optical count and size ranking or TA anomaly

Fig. 6.1: Schematic of the various media sampled at each ice station

First, and in accordance with plans from the other AWECS teams, an adequate floe is chosen, and the ship anchored to it so that the trace metal clean biogeochemical sampling site is upwind of the ship (hopefully during the entire running of the ice station) and at a reasonable distance from it (300 m to 500 m). A 10 m by 10 m area is then flagged, in which access will only be permitted to operators wearing clean suits and plastic bags on their shoes to prevent contamination (Lannuzel et al. 2006). Power is provided by a 5 kVA generator placed 50 meters, away from the restricted area and downwind of it. Along the same line lies a table for ice core treatment, ice core storage boxes and the various

cargo boxes for transport. First, 5 operators get dressed with Tyvek clean room garments on top of their polar clothes and plastic bags on their shoes. Snow samples are then taken by one of the operators in the central part of the restricted area. Then, a first core is taken along the lower border of the restricted area. A temperature profile ($\pm 0.1^\circ\text{C}$) is immediately performed at a 5 cm resolution along the core by inserting a temperature probe in 4 mm diameter holes drilled along the sides and towards the inner part of the core. The core is then stored wrapped in -30°C cooling bags within the core storage box, to prevent brine drainage. It will be cut for salinity measurements (5 cm resolution) later on the ship.

A second "twin core" is collected for "in situ" salinity cutting (same resolution) and stored in containers to provide a thorough comparison of the two techniques. A sheltering tent is then deployed on top of the two holes that will be used to perform the water sampling at various depths with the help of a non-contaminating peristaltic pump, ensuring limited freezing in the sampling tubes.

In the meantime, another team starts the drilling of the "brine sackholes", incomplete holes drilled at two selected depths, supposed to collect internal brines in the course of time. The two depths are selected (based on the temperature profile) so that the shallower one collects brine from the upper impermeable layer (brine volume $<5\%$), and the deeper one from the lower permeable layer. Care is taken not to drill the latter sackholes too deep, to avoid seeping of sea water upward. In order to be able to collect enough brines for the suite of measurements to be performed, 6 sackholes of each depth range are drilled in close vicinity. They are immediately covered with foam corks, to prevent contamination from e.g. blowing

snow or other sources. Brine are left to slowly drain for typically a few hours. A second tent is eventually used to protect the operators during the collection of the brines, which is either performed with the help of a syringe or with the peristaltic pump, when the volumes are sufficient. Brines are also circulated in the Sea Ice Equilibrating System (SIES) (dedicated brine hole) which measures the “*in-situ*” $p\text{CO}_2$ of the brine using a method derived from underway $p\text{CO}_2$ measurements.

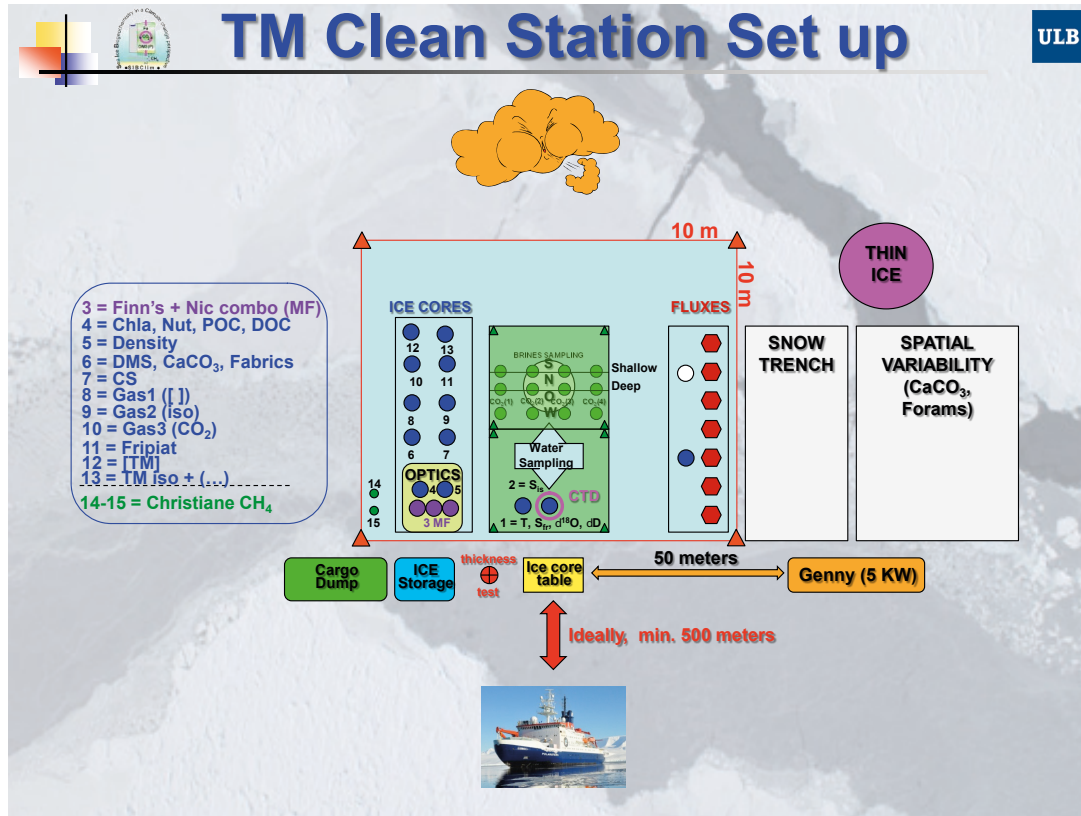


Fig. 6.2: Example, of setting for a 10 hours Ice Station. See text for details

As soon as the snow has been sampled, a third team starts the set up of a series of flux chambers (8 for CO_2 and 1 for VOC) alongside the restricted area (Fig. 6.3). For inter-calibration experiments, 2 kinds of CO_2 chamber systems are used: 1) semi-automated CO_2 chambers originally developed at Hokkaido University for soil CO_2 flux measurements (Nomura et al., in revision) and 2) long-term chambers (Li-8100, LI-COR Biosciences, USA) (Fischer, 2013). Different types of surfaces (on snow, on ice, on slush) are typically investigated, together with ancillary measurements, as discussed in the preliminary results section.

Finally, a series of 13 supplementary cores are collected in close vicinity to each other (no more than 20 cm apart), in order to collect the material for all the other measurements targeted in Table 6.1, and provide the material for some of the experiments to be performed on board (see details below). All coring was performed using a 14 cm diameter electro-polished stainless steel corer or a titanium corer, that have both been tested against contamination for the various trace metals investigated. Sea ice cores for trace metal determination (1x concentrations, 1x isotopes) were collected using the all-titanium ice corer (Lichtert Industries,

Brussels, Belgium) and immediately packed in acid cleaned plastic bags and stored at -25 °C for processing at ULB.

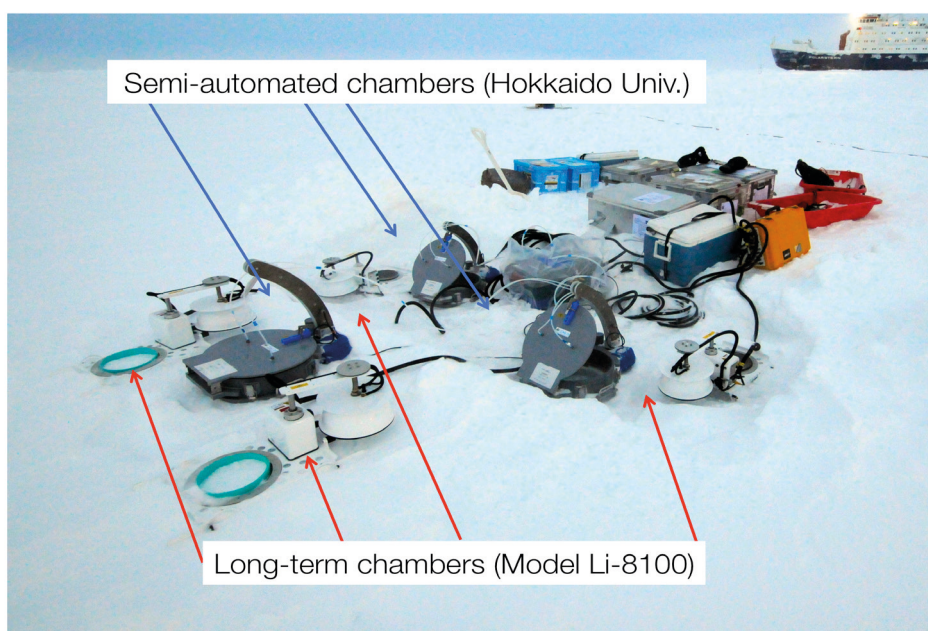


Fig. 6.3: Picture showing the semi-automated CO₂ chambers (Hokkaido Univ.) and long-term chambers (Model Li-8100) at St. 496 on 24 June 2013

If available, thin ice is also collected at the surface of reachable leads, to compare to the results of experiments on incorporation of organic and inorganic compounds in young sea ice (see details below).

Our sampling strategy also included the collection of samples of snow, brines and ice cores for the atmospheric chemistry group, in order to optimize data integration within the AWECS cruise.

To complete our investigation, close collaboration with the sea ice physics group ensured the processing of under-ice optic measurements and detailed snow-pit analyses at each ice station location.

4 Days ice stations

The work at a 4 days ice station mainly differs by the fact that two 10 hours ice stations are repeated at three days interval. The aim here, is to eventually detect sustained biogeochemical activity, in a season where it is not intuitively expected. For that purpose, two areas of 10 m x 10 m are initially delimited on arrival on the floe, and the procedure described above reproduced in the second area, the day before we leave the floe. The extra time on site is also used to develop

complementary activities such as studies on spatial variability of occurrence of ikaite crystals and foraminifers (see below), or, closely spaced (6 hours) time series on young sea ice "in-situ" growth in drill holes, and associated incorporation of organic and inorganic compounds (see below). Also, visually brown ice has been selected for documenting biodiversity.

In situ growth experiments

During the two 4-days ice station (506 and 517) two time series on ice growth were carried out *in-situ* under trace metal clean conditions. First a flat area close to the main biogeochemistry site and upwind from the ship and other activities on the ice was chosen. Upon removing the snow four rows of seven holes each were drilled using an electropolished stainless steel corer (14 cm internal diameter). Holes were meticulously cleaned with an acid-cleaned ice scoop to remove the ice in and around the holes, just prior to T0. Ice was allowed to grow in each hole. For every time step, 7 holes were sub-sampled to assess the different parameters described above as well as other trace metals in cooperation with J. de Jong (ULB) (see elsewhere in this cruise report). At T1 (6hours) the newly formed ice was sampled using a Ti coated saw. T2 was sampled after 12 hours, T3 after 24 and T4 after 48 hours all using the electro-polished stainless steel corer and/or a similar all-Ti corer. Seawater was collected from the main biogeochemistry site.

Frost flowers and newly formed ice sampling

At stations 486, 488 and 489 pancake ice has been sampled. The ice and the surface seawater have been collected from the mummy chair deployed on the ice surface while respecting trace metal clean conditions. Parallel to that, two frost flower samples were taken at stations 488 and 500, from the mummy chair and directly from the ice edge, respectively. During stations 496 and 500, thin grey ice was sampled from the ice edge.

Hydrocasts

Water column samples on a transect across the continental shelf of the Antarctic Peninsula into deep waters, were collected from a regular 24 General Oceanics Niskin bottle epoxy-coated rosette equipped with a Seabird CTD sensor package with oxygen sensor, fluorimeter and transmissiometer. It has been demonstrated that reliable trace metal concentrations can be obtained with Niskins (Measures and Vink, 2001). CTD Niskins were sub-sampled at the rosette by filling 500 mL Nalgene polyethylene bottles. Sample filtrations were immediately carried out, with 125 mL sub-samples for dissolved trace metals (DMe, filtered) being collected, and acidified to pH = 1.9 (1 mL acid per liter of sample) with Seastar ultrapure 14M nitric acid (HNO₃). Filters were collected in polypropylene cryovials and stored at -25°C.

Along the same transect, water samples were taken to study the evolution of the carbonate system, the dissolved gases (VOC, CH₄) and other biogeochemical properties such as nutrients and oxygen isotopic ratio, in conjunction with the Chl-a concentration.

Treatments on board

Main ice stations

Directly on return from the Ice Station, water, brine, snow and ice core samples were treated for analyses on-board or fixed and/or stored for further treatment in

the home laboratories. While water and brine samples were immediately measured (or treated) for Salinity, Chl_a, POC/DOC, EPS, Nutrients, pH, DIC, TA, $\delta^{13}\text{C}_{\text{CH}_4}$, $\delta\text{D}_{\text{CH}_4}$, δD and $\delta^{18}\text{O}_{\text{water}}$, CH_4 , pCO_2 , DMS, DMSP and VOC, some of the ice cores were sliced at the appropriate resolution (5 cm, 10 cm or 5 pieces per core with top and bottom part always at 15 cm, depending on the variable measured) in the cold reefer laboratory. These were measured for the same variables, once melted in the dark at room temperature or +4°C, depending on the variables concerned. Later on, thin sections were made all along the DMSP ice core to document the ice textures.

VOC flux measurements

For VOC flux measurements, the stainless steel chamber was installed over snow and sea ice/shush after removing the snow. At St. 517, we examined the flux measurement over the frost flower (Fig. 6.4). Experiments lasted for 30 min. Every 10 min during an experiment, 1 L of air in the chamber was collected using a 50 mL glass syringe with a three-way valve and then transferred to a 5 L gas tight bag (GL Science Inc., Japan). Air samples were quickly transported in a dark container to a laboratory onboard. For VOC measurements, 1 L of air in 3 L gas tight bag were trapped by the Tenax TA (GL Science Inc., Japan) in the 1/8 inch stainless pipe at the low temperature (-100 °C). After the cruise, VOC concentrations will be measured in Hokkaido University, Japan. Based on the time rate of change in the VOC concentration in the air within the metal chamber, VOC flux will be calculated.

Trace metals

Upon return to the ship, snow, brine and seawater samples were further processed inside a class 100 clean air cabinet. Snow was melted at room temperature. Snow melt water, brine and seawater samples were filtered across 0.2 mm pore size 47 mm diameter polycarbonate membrane filters in a polycarbonate filtration apparatus (Sartorius) with teflon O-rings under gentle vacuum (<0.5 bar). Filters were collected in polypropylene cryovials and stored at -25°C. Of each sample, 125 mL sub-samples for total dissolvable trace metals (TD-Me, unfiltered) and dissolved trace metals (DMe, filtered) were collected, and acidified to pH = 1.9 (1 mL acid per liter of sample) with Seastar ultrapure 14M nitric acid (HNO_3).

Additional snow and brine samples and sea-ice cores for Fe/Zn isotopic composition determination were taken as described above. A 1 m depth seawater sample was taken in a 10L Nalgene polyethylene carboy. This sample was filtered on-board across a 0.2 mm pore size 142 mm diameter polycarbonate membrane filter in a polycarbonate filtration apparatus (GeoTech) using the portable peristaltic pump. The filtrate was acidified to pH 1.9 and the filter stored at -25°C.

Further analytical treatment at home will involve:

Trace metal concentrations. TD-Me and DMe concentrations will be measured by isotope dilution inductively coupled mass spectrometry using an Agilent 7700x quadropole ICP-MS. Samples will be analyzed using a multi-element isotope dilution technique with pre-concentration on the Nobias PA1 Chelate resin (Sohrin et al., 2010). Particulate metals on filters will be acid digested in a nitric acid/hydrogen peroxide digestion and measured by the same multi-element isotope dilution technique without further pre-concentration.

Fe and Zn isotopic ratio measurement. Using a Nu Plasma multi-collector ICP-MS, Fe and Zn isotopic compositions will be analyzed of the dissolved and particulate

phases of snow, brine and sea-ice after following a purification of the sample by ion exchange chromatography involving the BioRad AG-MP1 anion exchange resin (de Jong et al., 2007). Pre-concentration of the dissolved phase uses magnesium hydroxide coprecipitation or lanthanum hydroxide coprecipitation for large volumes.



Fig. 6.4: Picture showing the metal chamber for VOC flux measurements over the frost flower at St. 517, 31 July 2013

Newly formed ice

In addition to the classic physical parameters such as salinity, temperature and ice texture, each sample has been processed to assess the concentration of DOC, POC/PON, macro-nutrients (Si(OH)_4 , PO_4^{3-} , NO_3+NO_2), ammonia (NH_3) + ammonium (NH_4^+), exopolysaccharides (EPS), particulate iron (PFe), dissolved iron (DFe), total dissolvable iron (TDFe, including the iron associated with lithogenic materials), organic ligands (CLECSV) and Chl *a*. Melted ice and underlying seawater will also be used for analysis of algal species and microbes counting. During fieldwork, seawater samples were brought back to the ship as soon as possible for the different filtrations. Ice was allowed to melt in the dark at room temperature and was filtered before as quickly as possible upon melting.

Foraminifera in sea ice

Ice cores for investigations on foraminifer abundance and distribution were taken at 9 stations (PS 81/488, 489, 497, 500, 503, 506, 515, 517 and 1 snow pit helicopter-site). The cores were cut into segments, melted at 4°C and filtered. The filters containing the foraminifers were stored in ethanol for further investigations at home.

At three stations (PS81/497, 503, 506) living *N. pachyderma* were collected for culture experiments. Ice cores were transferred to a -2 °C cool lab immediately after drilling. The ice cores were melted at -2°C in filtered seawater to prevent extreme freshening of the medium. Calcein was added as staining agent to the medium, to identify chambers grown under culture conditions. Foraminifers were exposed to different salinities and fed with ice algae.

Taxonomy, primary production, bacteria and viruses

Melting and Handling: The collected sea-ice material was put into open end PE-plastic pipe-bag (Mercamer Oy, Finland) that was sealed immediately after the sampling and kept covered from light until they were transported to the laboratory containers onboard *Polarstern* with set temperature of +4°C. where the obtained two ice cores were cut into similar sections using a Fiskars branch saw. Two similar sections were then crushed and pooled to gain large enough sample that would ensure that gained information would originate the same sample. After carefully homogenisation of the crushed ice of representing the layer it was divided into melting units and enclosed in 1L plastic containers. The samples used for bacterial production and bacterial dna analysis were let to melt without any addition at +4°C. In order to avoid organism losses due to cell lysis caused by rapid changes in salinity during melting (Garrison and Buck 1986, Kottmeier and Sullivan 1988), a graduated cylinder was used to measure the amount of 0,2 µm filtered sea water (FSW) (Sartorius Sartoban Sterile capsule 300) that was added to the crushed ice used for chlorophyll-a, microscopic and Photosynthetic-irradiance response analysis (PI).

All the samples were kept away from light and at +4°C during the melting. The melted samples were thoroughly mixed before volumes of the samples was measured with a graduated cylinder in order to be able to resolve the exact volume of sea ice put in each bucket. After which a dilution factor was calculated and it was used to correct the gained results for sea ice samples melted with additions of FSW. Subsamples were collected into 100-ml brown glass bottles and preserved with acid lugol solution, formaldehyde and glutaraldehyde (1.25 % final concentration) and stored in dark at +4°C.

800-1,000 ml of live material was concentrated using a 10 µm net of each section. Concentrated live material was examined with inverted light microscope (Leica DMIL) equipped with 12,5x oculars, 10x, 20x 40x objectives. After the life microscopy a drop of Lugol was added to the 2,5 ml sample in the microscope cuvette to stop the cell movement and a digital camera (Leica DC300F) was used for documentation of the encountered taxa. These live microscopic results cannot be interpreted as quantitative nor even semi-quantitative, thus they were called "algal observations" gave valuable information about the similarity of the ice sampled in different locations and whether the biota was the same throughout the ice column at different depths.

Thomas et al (1997) was used for identification.

Primary production: The photosynthetic efficiency (a), maximum photosynthetic capacity (P_{max}), photoinhibition (b) and light saturation index ($E_k = P_{max}/a$) of the sympagic communities were obtained from photosynthesis-irradiance response ($P-E$) curves measured as $^{14}C-CO_3$ incorporation at different light levels (Platt et al. 1980). Sample volumes of 3 ml with added $NaH^{14}CO_3$ (50 µl, final concentration of 0.33 a µCi ml⁻¹; International Agency for C14, DHI) were incubated for 2-3 h

under irradiance ranging from 0 to 4000 $\mu\text{E m}^{-2} \text{s}^{-1}$. The incubators were cooled by circulating ice-cold water with a peristaltic pump. The incubation was stopped by adding 100 μl of formaldehyde (final concentration 1.23 %). After which the samples were acidified with 1 N HCl for 48 h to remove the unincorporated $\text{NaH}^{14}\text{CO}_3$. Insta-Gel Plus (PerkinElmer) scintillation cocktail was added to the acidified samples and the activity was measured with a Perkin Elmer Tri-Carb 2900TR liquid scintillation analyser onboard *Polarstern*. The DIC concentration in sea ice was calculated from values given in Rysgaard et al. (2011), but they will be replaced later with real values measured by D Nomura after the cruise.

Bacterial production: Bacterial production was measured using ^3H -thymidine incorporation technique (Fuhrman and Azam 1980, 1982) from all separate layers. Each ice-core layer was crushed with electrical Ice O´Matic ice-cube crusher and a measured amount (approximately 7,5 g) of crushed ice was weighted into scintillation vials using an electrical scale. Addition of 2 ml of filtered seawater (0,2 μm) was done to ensure even distribution of labelled substrate. All the work was done in a cold room at +4° C. Incubations of bacterial activity were started immediately after sample collection. Duplicate or triplicate samples and formaldehyde killed adsorption control were incubated with [methyl- ^3H] thymidine (10 nM final concentration; Perkin-Elmer, Waltham, MA, USA) in an ice water bath inside culturing cabinet at -1,2°C for 18 hours. The incubations were terminated with the addition of formaldehyde and the samples were stored refrigerated until further processing. The samples were extracted with cold trichloroacetic acid (TCA, 5 % final concentration) and filtered onto 0,2 μm mixed cellulose ester filters (Advantec MSF, Inc., Pleasanton, CA, USA) under ice-cold conditions. The incorporated radioactivity was measured with Perkin-Elmer Tri-Carb 2900TR scintillation counter (Perkin-Elmer, Waltham, MA, USA) using InstaGel Plus (Perkin-Elmer, Waltham, MA, USA) scintillation cocktail as solvent.

Ice preparation for other samples: Ice from each separate ice layer was crushed and quickly melted by shaking in a hot water bath avoiding the warming of the samples. Melted sample water was stored at +4 °C.

Samples for cell counts and virus-like particle counts: Subsample of 20 ml of the melted ice was fixed with glutaraldehyde (1,25 % final concentration) for bacterial microscopic cell counts in glass scintillation vials. Samples were stored at +4 °C. Duplicate subsamples of 1,500 μm were fixed with paraformaldehyde (1 % final concentration), flash-frozen in a liquid nitrogen and stored at -80 °C for bacteria cell counts and virus-like particle counts with flow cytometry. Samples will be measured later.

DNA community analyses: For bacterial DNA analysis bacteria was collected from 500 ml of melted ice samples to 0,2 μm mixed cellulose ester membrane filters (Schleicher and Schuell, Bioscience GmbH, Dassel, Germany) and stored at -80° C. Analysis of the bacterial community will be processed later.

Bacteria and virus isolation: Melted ice was plated (100 μl) to ZoBell, concentrated ZoBell and MGM growth medias for bacteria isolation from all separate layers of ice cores from stations 500, 506 and 515. Plates were incubated inside a plastic box at +4 °C until bacterial colonies were formed. Colonies were stored in ZoBell agar in cryovials at +4 °C and most of them were also cultured in liquid ZoBell media at +4 °C and stored with 15 % glycerol at -80 °C. Ice core from station 515 was processed with uttermost care to avoid contamination. After sampling all surface layers of the ice core were removed with sterilized saw. Ice was melted in

sterilized buckets without crushing and all separate 12 layers were plaited. Melted samples were also taken from all layers and stored with 15 % glycerol at -80 °C. All bacterial strains will be purified later.

For later virus isolation samples were taken from stations 500 and 515. All different layers from melted ice sample from a station were pooled. All bacteria was removed by filtering (0,22 µm Millipore Durapore Membrane PVDF filter, EMD Millipore Corporation, Billerica, USA) from 500 ml of the sample. After that sample was concentrated (50:1) using Amicon Ultra-15 concentration units (MWCO 100,000 Da; Merck Millipore, Billerica, USA) by centrifugation (Beckman GS-6R, 3700 rpm, 5 min, +4 °C). Virus fractions were stored with 15 % glycerol at -80 °C.

Experimental runs on board

Cold-finger experiments

In parallel to the field experiments, coldfinger experiments have been conducted in order to compare the field data and those obtained in the lab. The coldfinger is an apparatus fully made of titanium and consists of a tube connected to a circulating water bath that kept anti-freeze (ethanol 90 %) at the desired temperature. The coldfinger is immersed straight in a polycarbonate bottle filled with seawater. The assembly is put on a magnetic stirrer and ice is allowed to grow for 8 hours at -15 °C. At the end of each experiment, the ice is removed from the coldfinger and allowed to melt at ambient temperature in the dark.

Sea ice and leftovers from the seawater samples were then processed to assess the volume, salinity, and the concentration of POC/PON, DOC, EPS, macro-nutrients (Si(OH)_4 , PO_4^{2-} , NO_3^- , NO_2^- , $\text{NH}_3^+\text{NH}_4^+$) in both ice and remaining seawater and ice fabrics. To keep the set up clean and free of outside contamination, these experiments were conducted inside a plastic bubble.

The experimental set-up was aimed at studying the fabric of the ice under three different freezing temperatures (-10, -15 and -20 °C), followed by three sets of triplicates that were carried out with initial solutions containing different concentrations of EPS: deep water containing low level of EPS (K. Meiners, personal communication), surface seawater and surface seawater enriched with xanthan gum.

Incubation experiments on DMSP conversion to DMS and possibly methane

The climate relevant gases methane and dimethylsulfide (DMS) can be found in high concentrations in polar sea ice in the Arctic and Antarctic, respectively, and are released from the ice to the atmosphere (Zhou et al., 2011, Trevena and Jones, 2006). Whereas methane is a potent greenhouse gas, DMS is thought to have a cooling effect on the atmosphere, since it can contribute to cloud formation. The production of methane and DMS is possibly linked via microbiological conversion pathways for dimethylsulfoniopropionate (DMSP - Kiene and Linn, 2000; Moran et al., 2008, Damm et al., 2010). It is thus of interest to investigate, under which conditions the sea ice derived DMSP is transformed to the cooling gas DMS or to the greenhouse gas methane. So far, high methane concentrations in sea ice have only been reported from the Arctic. The objective of incubation experiments on the AWACS cruise was to investigate methane and DMS production in Antarctic sea ice in winter, when abiotic conditions might favor methane production.

To gain a better understanding on the microbial processes involved in DMSP

conversion to DMS and possibly methane, incubation experiments were performed on board. On four different ice stations (Table 6.2) sea ice cores were collected approximately 10 m from the main coring site of the Biogeochemistry group. The ice cores were immediately transported to the onboard laboratory and crushed to small pieces inside a plastic bag using a hammer. Crushed ice from sufficient cores was pooled, mixed and distributed to experimental bottles. The crushed ice was submersed in a defined volume of sterile filtered seawater that had been sampled earlier with Niskin bottles mounted on a CTD rosette. The experimental bottles were incubated for up to two weeks at slightly subzero temperatures and different illumination patterns. The following treatments were applied each in triplicates in various combinations: dark, illuminated, addition of DMSP, nitrate, phosphate. Experimental bottles were kept closed and gas tight during the course of the experiment. Gas and liquid samples for all parameters shown in Table 6.3 were taken with syringes through a septum in the lid of the bottles, except for the final sampling when the bottle was opened for the liquid sampling. Methane from the headspace as well as DMS and DMSP from the liquid phase were measured directly on board using a gas chromatograph equipped with a pulsed flame photometric detector (PFPD).

Table 6.2: Sea ice sampled for microbial incubation experiments

Station	Core length	Ice type	comment	Experiment
PS81/486	12 cm	Pancake ice	Small pancakes sampled from mummy chair	1
PS81/488	38 cm	Pancake ice	No coloration visible	2
PS81/500	72 cm	1 st year ice	Biomass colored area approx. 20cm from bottom	3
Heli20130720	30 cm	1 st year ice	No coloration visible	4

Samples for the other parameters were fixed and stored at the desired temperatures for later analysis in the home laboratory. Samples for molecular biology were collected onto 0.2µm Sterivex filtration cartridges, with pre-filtration through 5.0 µm Polydisc filters.

For comparison to methane concentrations in the sea ice, sections of sea ice cores were melted in gas tight containers and the methane concentration of the headspace was determined via gas chromatography.

Table 6.3: Parameters that were or will be measured on board or in the home laboratory. Except for methane all parameters were determined from the liquid phase.

On board	Home laboratory
Methane (headspace)	DMSO
DMS and DMSP	Total counts (bacteria)
Nutrients (Silicate, Nitrate, Nitrite, Phosphate, Ammonium) (during ANT-XXIX/7)	Bacterial diversity (Fluorescence-in-situ-hybridisation, 16S sequencing, denaturing gradient gel electrophoresis)

DMSP conversion genes (Metagenome sequencing, qPCR)
 Living samples (liquid, agar plates)

Ikaite precipitation experiments

In order to clarify the time dependence on the ikaite precipitation during the sea-ice formation, we have carried out tank experiments in a low-temperature room in Polarstern. 800 ml of natural seawater collected from under-way water pumping systems was put in the 1,000 mL plastic bottle. We prepared four bottles, and experiments were carried out at four different kinds of conditions (Table 6.4). After each experiment, frozen seawater sample was melted at +4 °C. Then, we checked the presence/absence of ikaite crystals in the samples (Table 6.4). Ikaite crystals, if present, accumulated in the center of the container and could be detected by eye. When present, the ikaite crystals were sampled with a pipette and number and shape was measured with a stereomicroscope.

Table 6.4: Experimental conditions for ikaite precipitation experiments

Experiment	Temperature (°C)	Elapsed time (day)	Presence of crystals
Exp. 1	-80	1	No
Exp. 2	-25	1	No
Exp. 3	-25	7	Yes
Exp. 4	-25	21	Yes

Preliminary results

Table 6.5 summarizes the statistics on the measurements performed by our "Sea Ice Biogeochemistry" group during the AWECS cruise.

Table 6.5: Statistics on the measurements performed by the sea ice biogeochemistry group during the AWECS cruise

MEASUREMENT	NUMBER
Ice cores	240
Brine Holes	72
Snow	12
Temperature	300
Salinity	200
Chla	500
Thin sections	150
Nutrients, ¹⁸ O, CH ₄ , pH of sea water	180
DIC/TA	300
CO ₂ fluxes	1000
VOC and CH ₄	120
VOC fluxes	14

MEASUREMENT	NUMBER
GC runs	1988
DMS,P	1188
Ice crushing	120
Bacterial production	49
Bacterial strains isolation	61
Bacterial cell samples fixed	48
Cell enumeration samples	199
Bacteria, Algae and Protists DNA	66
Photosynthetic efficiency	44
Algae and Protists cultures	43
Bacteria cultures	15
Virus culture	1

Trace metals sample overview

- Pancake ice: stations 486, 488, 489
- Young ice: station 500
- Slush: station 500
- Frost flowers: station 503
- Sea ice: 17 ice cores at 11 stations
- Snow, brine, seawater: 49 TD-Me samples, 126 DMe samples, 134 PMe filters.
- CTD stations: stations 509-510-511-512-514-516-517, depths between 244 m and 2,475 m.

A total of 215 L was filtered on board.

Preliminary results from the first set of 9 stations, mainly sampled along the Greenwich meridian and the easternmost part of the Weddell Sea definitively breaks down the view of a biogeochemically "frozen" Antarctic Weddell sea ice during the Winter. This was already demonstrated for the Spring and Summer, but we now see that winter sea ice sustains considerable biological stocks and activities throughout, despite the reduced amount of available PAR radiation. Once again, building of the snow cover appears to play an essential role in triggering biogeochemical activity, both through warming from insulation and favouring brine transport, be it through potential convection, surface brine migration or flooding. This results in a "widening" of the internal autumnal layer and increase of the biological burden with age. As shown for the Spring in the Bellingshausen Sea, alternation of contrasted weather conditions at the small temporal scale of cyclonic activities also sustains the internal sea ice dynamics, switching the ice cover from partly impermeable to permeable status. The surface 10-15 cm of the ice however remains permeable mostly at all times, allowing CO₂ outgassing, that will need to be taken account in annual budgets as a "counterweight" to the generalized sink in Spring and Summer. Significant DMS,P levels were found in the ice, contrarily to Arctic sea ice in the winter, where these levels were recently described as very low (e.g. CFL IPY study, G. Carnat, pers. comm.). Regular changes in the thermal regime of the sea ice cover and potential changes in the microorganism communities (e.g. intrusion of phaeocystis colonies during the flooding events) result in large contrasts in DMSP and DMS concentration, with obvious losses of the latter to the atmosphere during permeable events.

Preliminary results from the second set of 3 stations in the western branch of the Weddell Sea Gyre has confirmed it is made of a mixture of older fast/second year ice floes with younger first-year ice floes. The older ice shows the highest Chl-a concentration of the whole cruise ($>200 \text{ mg l}^{-1}$), in a internal community that is enclosed in desalinated impermeable upper and lower layers. This potentially results in intense recycling of nutrients, adaptation to low light intensities, and sometimes anaerobic conditions, as witnessed by the peculiar smell of some of the ice cores drilled. The first-year ice differs from that in the eastern Weddell Sea as its texture is here dominated by columnar ice and algal communities are only bottom or surface ones (no internal maximum).

On the whole, Weddell Sea winter sea ice thus appears to be extremely dynamic, physically and bio-geochemically, and the snow cover seems to play a prominent role in this behaviour.

Specific contributions

Basic physical, chemical and biological parameters

Figures 6.5, 6.6 and 6.7 illustrate exemplary ice textures from all our AWECS biogeochemistry stations. All station cores but one in the western Weddell Sea, were below 1 meter in thickness, although thicker floes were observed along the cruise track. This reflects results from the sea ice bridge observations, with a mean icecover thickness of 68 cm. Conformingly with previous reports in the literature, frazil ice dominates at all sites in the Eastern Weddell Sea. Stations AW486 to 489 were sampled from the Mummy chair, while all others were full stations as described above.

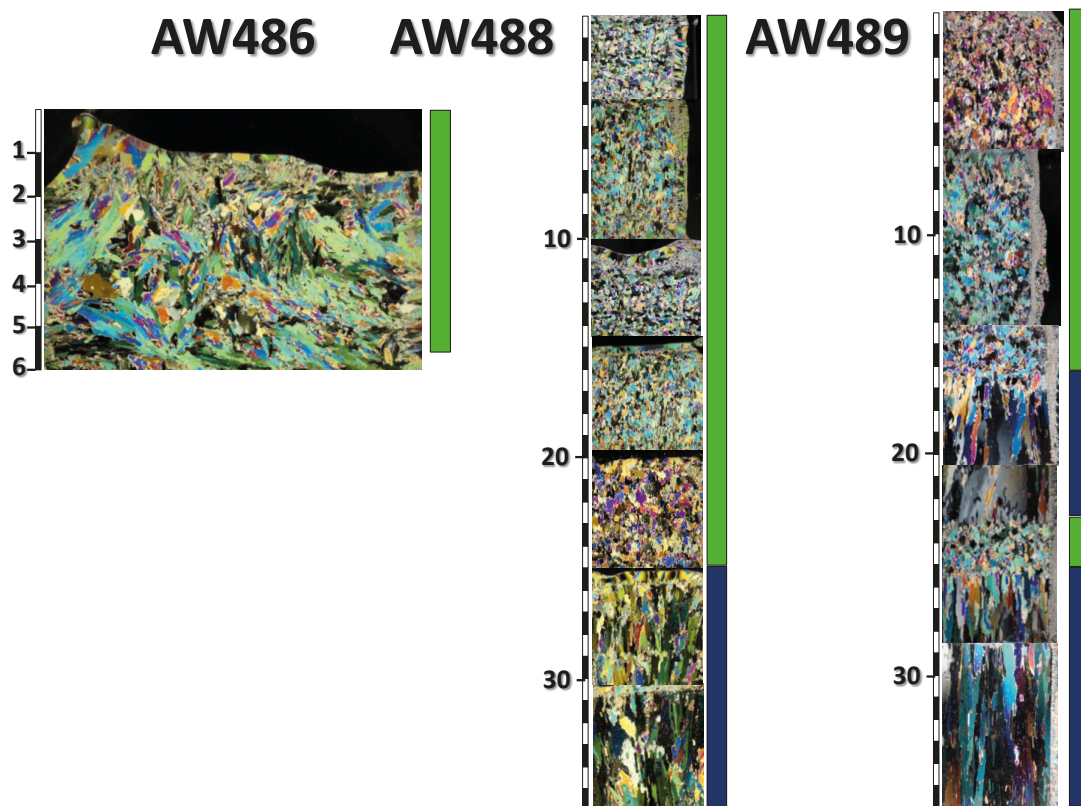


Fig. 6.5: Ice textures at Stations AW486 to AW489. Preliminary ice types: grey = snow ice; green = granular frazil ice; blue = columnar congelation ice.

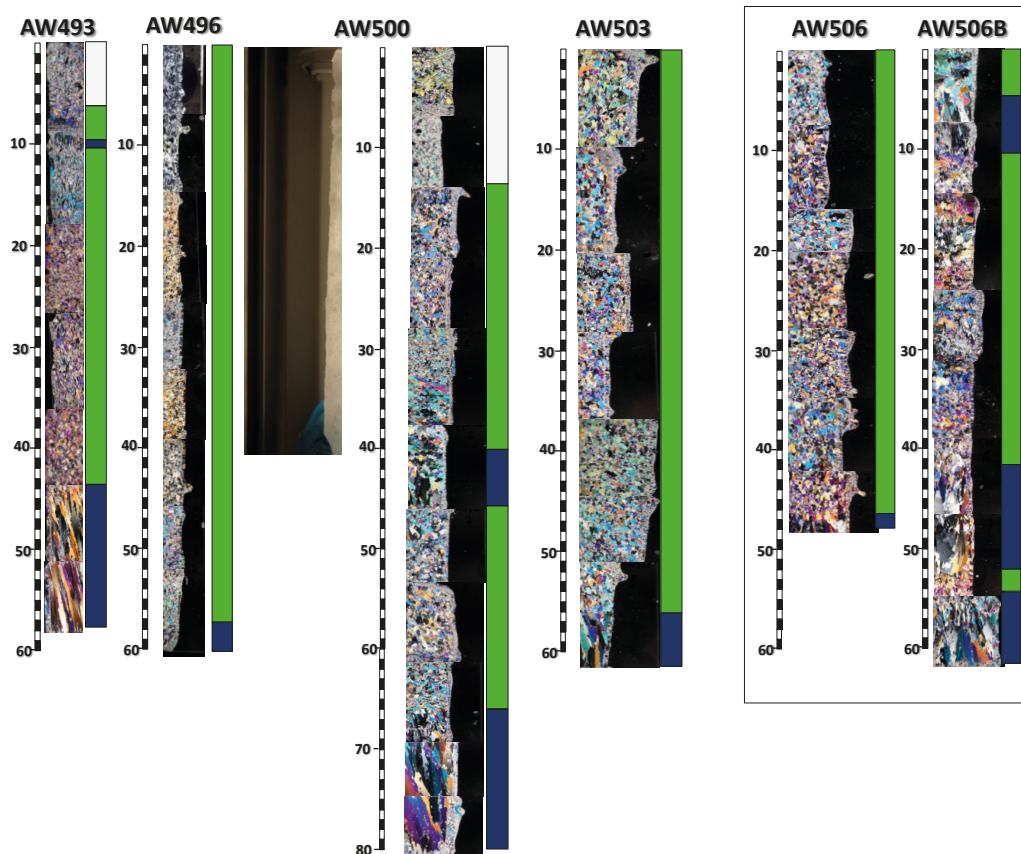


Fig. 6.6: Ice textures at Stations AW493 to AW506B. Ice types as in Fig. 6.5

Surprisingly, the texture of the initial pancakes sampled at station AW486, does not resemble any of the later core textures, neither, to our knowledge, to anything described in the literature. It is made of small acicular frazil ice crystals suggesting unbroken individual discs rapidly formed in supercooled waters, floating up and aggregating quickly, without much time to be reduced into the 'classical' granular frazil size and shape by further turbulence. Alternatively, maybe that frazil did not form with snow grains as a seed, therefore developing its peculiar acicular shape.

Stations AW488 and 489 show typical pancake structures, with only the start of columnar growth at the bottom. Repetition of the sequence in the latter suggests "rafting" of individual pancakes, a common feature in this very dynamical environment. This is also the signature of the following stations along the Greenwich meridian, floes getting generally thicker and more complex in structure. Often the snow cover increases further south, and flooding (negative freeboard) and snow ice are encountered (e.g. station AW 500). Fig. 6.8 summarizes the basic physical and biological characteristics of each station, with panels from left to right as: a) temperature profiles from air to snow to ice (also showing snow thickness); b) bulk ice salinity; brine salinity; brine volume (%) and Chl-a (dark green for organisms above 10 mm and light green for those between 10 and 0.8 mm). DMS and DMSP profiles are also shown in the last panel, but are discussed in the sulphur compounds section. It is clearly seen that, as the ice gets older (further south), it has more chance to show a thicker snow cover, which contributes in warming up the ice below, increasing brine volumes and therefore favouring potential

exchanges of nutrients and microbial communities through e.g. brine convection or even flooding in the most extreme cases (snow thickness above 25 cm, for this type of ice thickness).

Under equivalent snow thicknesses (e.g. stations 493 vs. 496), short term warming episodes of the ice appear to result from the regular transit of cyclonic events, therefore sustaining a very dynamic environment (possibly throughout the winter), in a similar way as observed e.g. in the Bellingshausen Sea (SIMBA cruise, 2007, Lewis et al., 2011) in the Spring. Frequently, we observed in the upper 30 cm of the ice cover the formation of vertical linear brine tubes (different from brine channels - e.g. AW500, Fig. 6.6) transferring downwards (in the "warmer" ice below) the highly concentrated brine forming closer to the surface under the cooling cycles (colder air masses from the Antarctic continent). Associated to these warming cycles under the snow cover, considerable primary production occurs, developing the Chl-a levels, both in intensity and spatial distribution. The moderate (few mg l⁻¹, AW 486, 488, 489) initial internal Chl-a maximum (probably inherited from the autumnal growth) indeed grows in amplitude (tens of mg l⁻¹) and extends across the whole ice thickness, once a significant snow thickness is developed (e.g. AW493, 496, 500, 506B). Comparing 506 (cold, partly impermeable) to 506B (warm and permeable, sampled on the same floe, ten meters apart, three days later) suggest that the microbial community might respond very fast to these cold-warm cycles (as also attested by PI curves and clear adaptation to low light environments, see sections below), although spatial variability might have also played a role in explaining the observed contrasting Chl-a burdens. Frequent observation from the bridge of "tipping over" of visually brown floes, all along the crossing, however witness the overall spatial extent and validity of these station observations.

Note also, that newer ice formed more recently in leads further South (AW503, 506), resemble those encountered further North, with low snow cover, partly disconnected brine network and limited amounts of embedded Chl-a.

The three stations from the Western Weddell Sea gave us a different picture. As also reported previously, this outflow of the Weddell Sea gyre is made of composite floes, mixing fast/second year/multiyear ice with younger first sea ice "welding" those together. Fast/second year ice was sampled at one station (515) and gave us a very peculiar signature: the ice cover combines snow ice, frazil ice, platelet ice and maybe granular "marine ice", indicating a landfast origin with potential contribution from ice shelf supercooled waters (Fig. 6.7). Bulk ice salinity is quite low (a hint for second year ice) and results in the ice being below the 5 % permeability threshold nearly at all depths. It is also there that we have found the strongest Chl-a maximum of the cruise (ca. 120 mg l⁻¹), as a double maximum, sandwiched between the impermeable upper and lower layers (Fig. 6.8), partly within the platelet ice layer. Because of these peculiar "closed system" conditions at depth, the microbial community must have developed specific properties such as low light adaptability, higher levels of degradation pigments (phaeophytin) or partially anaerobic conditions (e.g. H₂S smelly ice).

The first year sea ice growing between the older ice floes differs from the one described in the eastern Weddell Sea, at least for the limited number of cores that we were able to collect. It is indeed principally made of columnar ice, rather than frazil, and rafting signatures have not been observed within the cores. As a result, the internal Chl-a maximum is absent and only weak bottom and surface communities are encountered (517, 517B - Fig. 6.7 and 6.8).

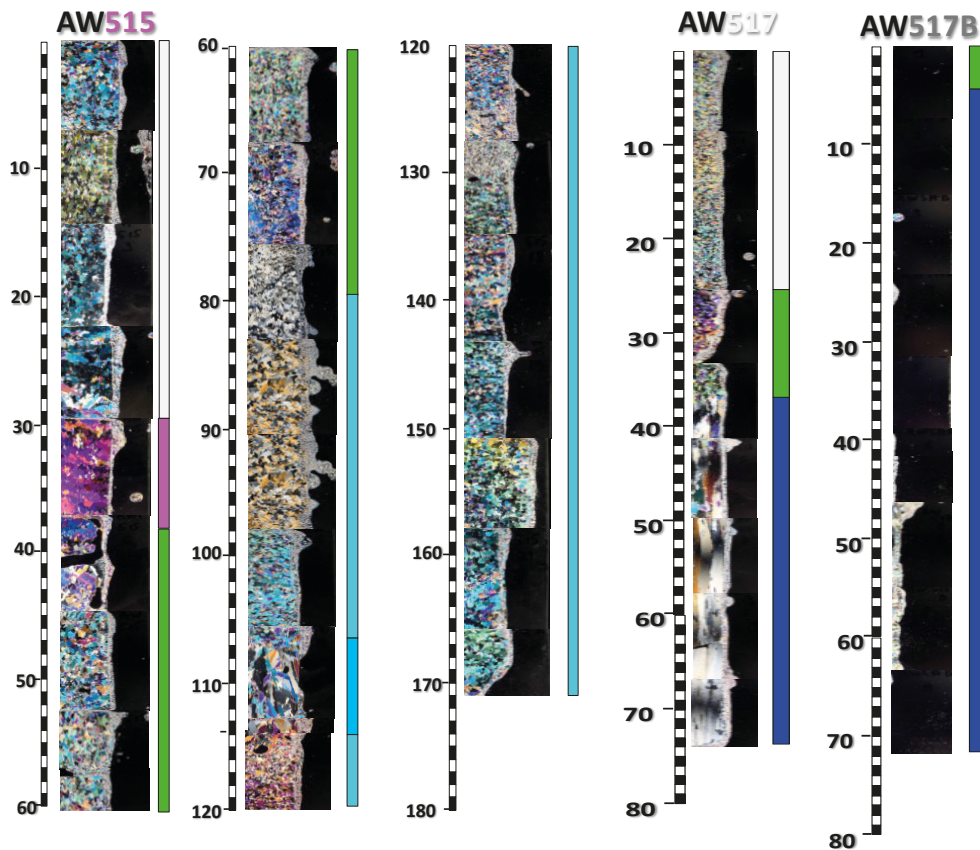


Fig. 6.7: Ice textures at Stations 515 to 517B. Ice types as in Fig. 6.5, pink and light blue representing potential different types of platelet and marine ice.

Brine $p\text{CO}_2$ and CO_2 fluxes

We carried out first measurements of $p\text{CO}_2$ in Antarctic winter pack ice. $p\text{CO}_2$ in winter appears to be significantly higher than $p\text{CO}_2$ measured in spring in Western Antarctica (Aurora Australis 2003 V1, September and October 2003), in the Weddell Sea (ISPOL, December 2005) and in the Bellingshausen Sea (SIMBA, October 2007). High $p\text{CO}_2$ in brines observed during AW ECS is not surprising since brines have been freshly formed from surface seawater whose $p\text{CO}_2$ ranged from 420 (station 506B) up to 450 μatm (station 517). The increase of $p\text{CO}_2$ with decreasing ice temperature observed in Fig. 6.9 corresponds to the concentration of brines during ice formation, and related increase in dissolved inorganic carbon of brines. This leads to the increase of $p\text{CO}_2$ with the decrease of sea ice temperature up to 637 μatm (Station 515).

Difference in $p\text{CO}_2$ between winter and spring/summer raises the question of the processes that lead to the decrease of $p\text{CO}_2$ from winter to summer. There are several candidates: (i) CO_2 expulsion at the ice surface driven by the equilibration of brines and the atmosphere, or transport of bubbles (ii) expulsion of CO_2 together with brines to the underlying water (iii) uptake by sympagic microalgae (iv) precipitation of calcium carbonate. It will be possible to decipher the influence of these processes using samples collected during the cruise. However, of particular interest is the rejection of CO_2 at the sea ice interface as this source of CO_2 for the atmosphere has been poorly documented.

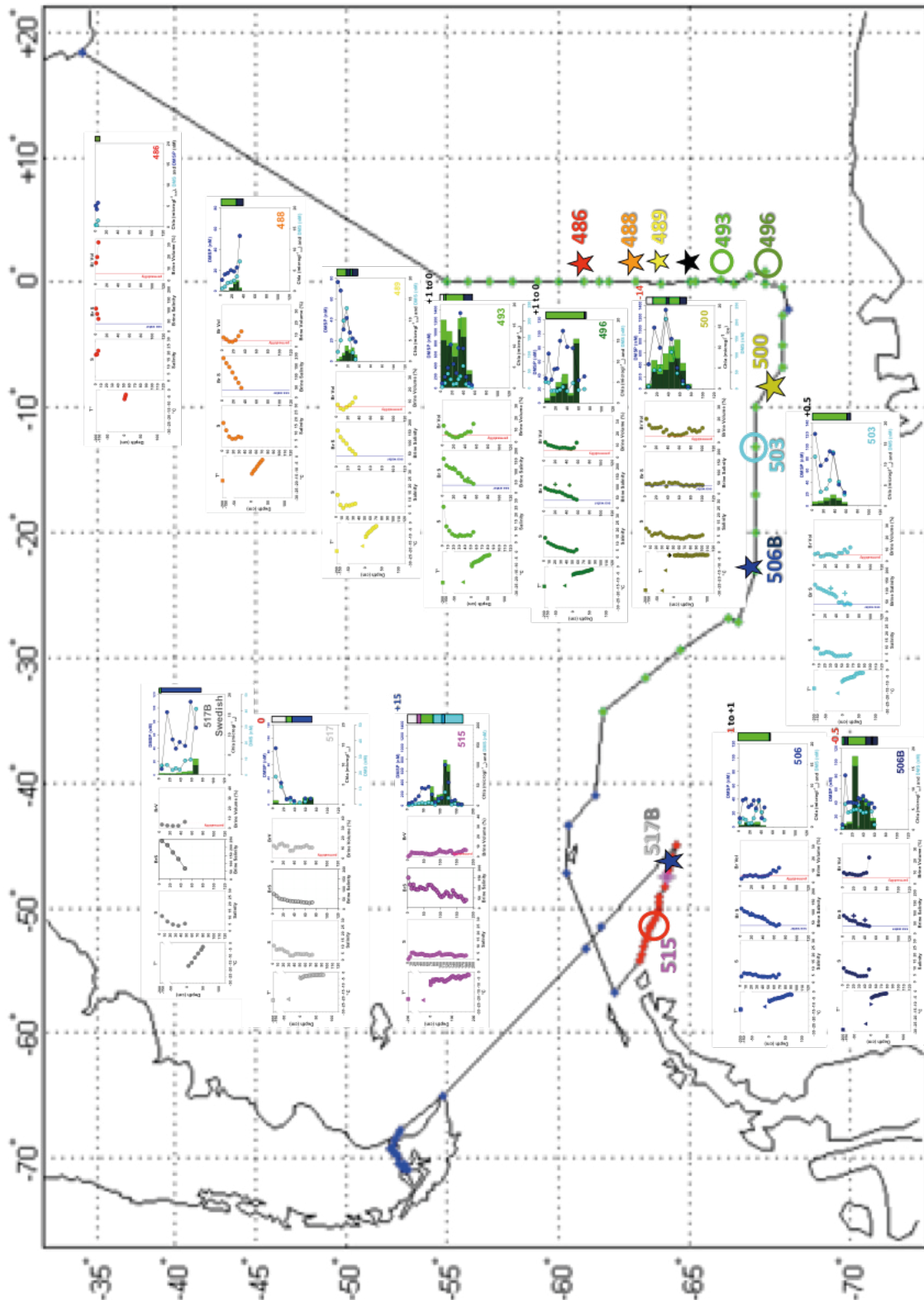


Fig. 6.8: Synthesis diagram of basic physical and biological parameters at AWACS biogeochemical ice stations. For each station, from left to right: Temperature in air, snow and ice (including snow thickness), salinity, brine salinity, brine volume (following Eicken and Petrich in Thomas and Dieckmann, 2010) and Chl-a (dark green >10 μm ; 10 μm >light green >0.8 μm), DMS (light blue) and DMSP (dark blue). Texture is shown to the extreme right (codes as in Fig. 6.5), with freeboard when available.

We carried out first measurements of air-snow and air-ice CO_2 fluxes over Antarctic pack ice with automated chambers (Figures 6.3, 6.10 and 6.11). Fig. 6.10 shows the result of our inter-comparison exercise between chamber types. The very good agreement lends support to the quality of the data obtained. Surprisingly (s) we observed repeatedly fluxes over the snow, so that Antarctic pack ice appears to act as a source of CO_2 for the atmosphere during winter. The fluxes are small but the significance of these fluxes should be assessed taking into account the surface covered by sea ice. Previous measurements over Arctic land fast sea ice (Geilfus et al., 2013) and in laboratory (Nomura et al., 2006) suggest that this release is likely to be a common feature for sea ice, so that these fluxes can potentially be up scaled taking into account the overall surface of Antarctic sea ice. Then this winter release fluxes can potentially be significant for the Southern Ocean.

Fig. 6.12 presents air-snow and air-ice CO_2 fluxes versus ice temperature, brine volumes and salinity for the top 5 cm of the ice. While air-ice CO_2 fluxes does not exhibit obvious trends, surface brine volume (and then sea ice permeability) appears to control air-snow fluxes. However, measurements carried out during the 4 days 506 station. Comparison with snow properties description from sea ice physics group can certainly help us to distinguish key parameters that affect CO_2 fluxes through the snow cover.

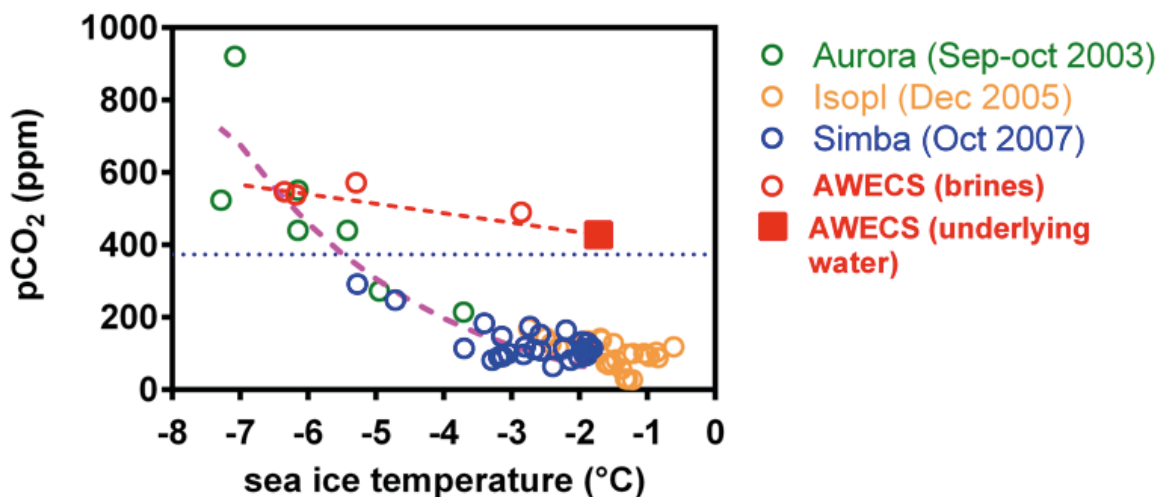


Fig. 6.9: Comparison of $p\text{CO}_2$ of brines measured during AWECS cruise and previous cruises carried out in spring and early summer in Antarctic pack ice. Note that Isopl cruise was carried out in the Weddell Sea.

Fig. 6.10: Comparisons of the CO₂ flux data from each chamber. Solid line indicates the 1:1

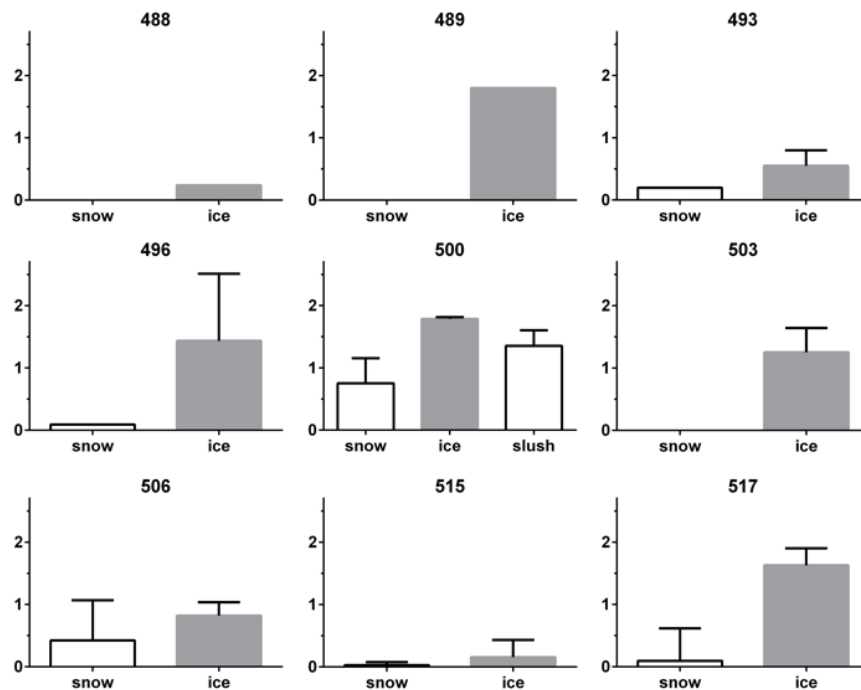
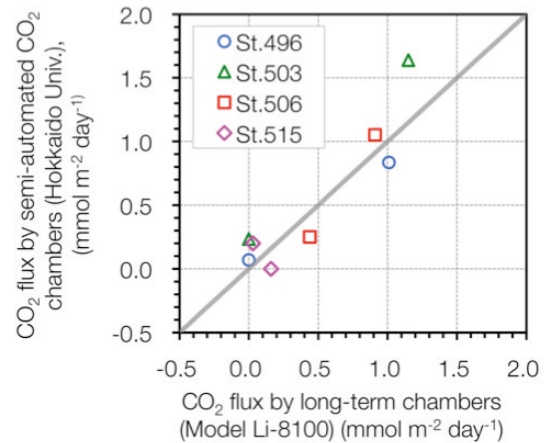


Fig. 6.11: Air-snow and air-ice CO₂ fluxes measured during AWACS

Ikaite precipitation experiments

For Exp. 1 and 2, there were no crystals (Table 6.4). On the other hand, crystals were found at Exp. 3 and 4. The number of ikaite crystals increased with elapsed time (Fig. 6.13), and the number of ikaite crystals reached up to 4,000 crystals for Exp. 4. In addition, the crystal size increased from Exp. 3 and Exp. 4, as can be seen on the crystals size frequency distribution of Fig. 6.14. These results suggested that the time (exposure time to the cold temperature) is one of the important factors controlling the amount and size of the ikaite crystals.

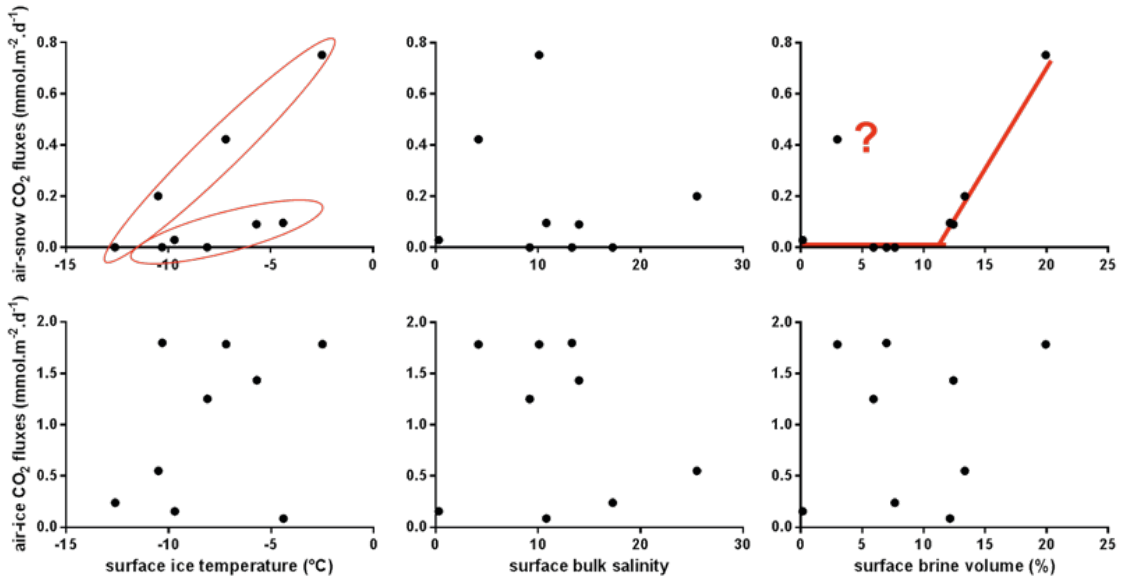


Fig. 6.12: Air-snow (top) and air-ice (bottom) CO₂ fluxes measured during AWECS against surface ice temperature (left), surface bulk salinity (middle) and surface brine salinity (right)

Fig. 6.13: Time revolution of the number of ikaite crystals for each experiment.

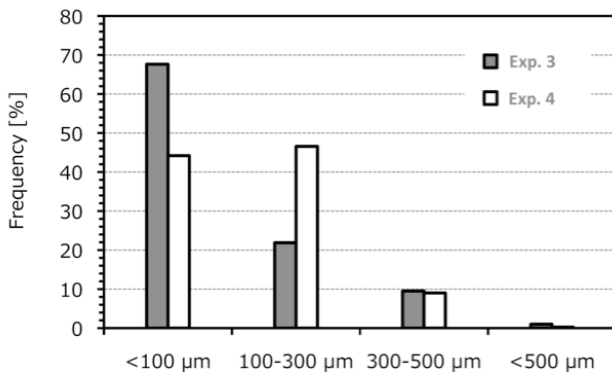
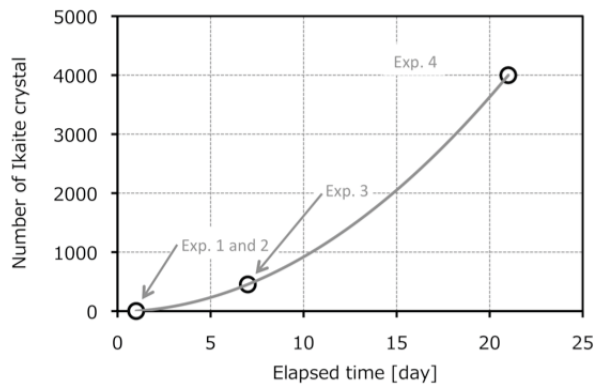


Fig. 6.14: Size distribution of the ikaite crystals for Exp. 3 and 4

Taxonomy

Both the Chl-a and highest diversity were found in the inner parts of the AW ECS winter Antarctic sea ice. Bottom communities were rarely observed (only in two occasions for the whole voyage).

The encountered organisms were identified only into general genus or even class level based on their gross morphology that was visible and species names used were only referential as most of the morphological characteristics are simply not visible i.e. without cleaning of the diatom frustules or cell stains, such as calcofluor white for dinoflagellates or without post-fixation and shadow casting of the coccoid cells (*cf. Phaeocystis*). Results gained are merely "present" vs "not present" or "present only as dead cells" (Fig. 6.15).

Primary production

According to Henley (1993), our short-term laboratory measurements are suitable for measuring physiological responses, but they cannot be accurately extrapolated to daily *in-situ* primary production ($\mu\text{g C l}^{-1} \text{ day}^{-1}$). Yet field incubations could not be carried out based on the gained information about the light spectra of the ships light was measured by Mario Hoppmann (scientist in the sea ice physics group) and the gained evidence was convincing enough that any field measurements would be error prone. Thus, these values gained from laboratory incubations values were normalized to chlorophyll-a [$P_{\text{max}} = \mu\text{g C } (\mu\text{g Chl-a}^{-1} \text{ h}^{-1})$, a and $b = \mu\text{g C } (\mu\text{g Chl-a}^{-1} \text{ h}^{-1}) (\mu\text{E m}^{-2} \text{ s}^{-1})^{-1}$, $E_k = \mu\text{E m}^{-2} \text{ s}^{-1}$] (Fig. 6.16). Later once the "*in-situ*" light conditions are known it is possible to use these to calculate an estimate which is closer to the natural case.

Bacterial production

Activity of the bacterial production samples have been measured onboard and thymidine incorporation rates ($\text{nmol TdR l}^{-1} \text{ h}^{-1}$) are presented on Fig. 6.17. Bacterial activity was low in most of the stations. The highest activity was found from the station 515 with visible brown layers in ice core. Activity was usually the highest in the middle parts of the cores.

Bacterial isolation

So far 61 bacterial strains have been isolated. These will be purified later and also more strains will be isolated. All purified bacterial strains will be used to screen viruses from the virus samples later.

		α^b	P_m^b	E_k	R^2
St. 486	pancake ice	Curve could not be fitted			
St. 488	Top	Curve could not be fitted			
	Middle	Curve could not be fitted			
	Bottom	Curve could not be fitted			
St. 489	Top	Curve could not be fitted			
	Middle	0,0196	0,28	14	0,30
	Bottom	0,0012	0,26	215	0,72
St. 493	Top	Curve could not be fitted			
	Middle	0,0108	1,05	97	0,96
	Bottom	0,0064	0,26	40	0,66
St. 496	Top	0,0036	0,20	56	0,43
	Middle	0,0038	0,48	126	0,67
	Bottom	0,0052	0,75	144	0,76
St. 500	Slush	Curve could not be fitted			
	Top	0,0132	0,66	50	0,42
	Upper Intermediate	0,0066	1,13	171	0,90
	Middle	0,0095	0,87	92	0,90
	Lower Intermediate	0,0084	0,94	112	0,81
	Bottom	0,0138	1,89	137	0,94
St. 503	Top	0,0011	0,15	140	0,35
	Upper Intermediate	0,0016	0,24	150	0,58
	Middle	0,0042	0,31	73	0,49
	Lower Intermediate	0,0015	0,29	196	0,49
	Bottom	0,0023	0,16	69	0,70
St. 506_1	Top	0,0040	0,23	57	0,11
	Middle	0,0013	0,36	278	0,88
	Bottom	0,0046	0,53	115	0,82
St. 506_2	Top	0,0032	0,41	128	0,59
	Upper Intermediate	Curve could not be fitted			
	Middle	0,0177	2,05	116	0,87
	Lower Intermediate	0,0241	2,66	110	0,69
	Bottom	0,0157	1,55	99	0,93
St. 515	Top	0,0119	0,98	82	0,52
	Upper Upper Interme	0,0044	0,34	77	0,19
	Upper Intermediate	0,0046	0,55	119	0,48
	Middle	0,0555	1,58	28	0,72
	Lower Intermediate	0,0494	4,53	92	0,94
	Lower Lower Interme	0,0841	5,77	69	0,76
	Bottom	Curve could not be fitted			
St. 517	Top	Curve could not be fitted			
	Upper Intermediate	0,0013	0,19	149	0,45
	Middle	Curve could not be fitted			
	Lower Intermediate	Curve could not be fitted			
	Bottom	Curve could not be fitted			

Fig. 6.16: The photosynthetic efficiency (a), maximum photosynthetic capacity (P_{max}), photoinhibition (b) and light saturation index ($E_k = P_{max}/a$) of the sympagic communities sampled during the expedition

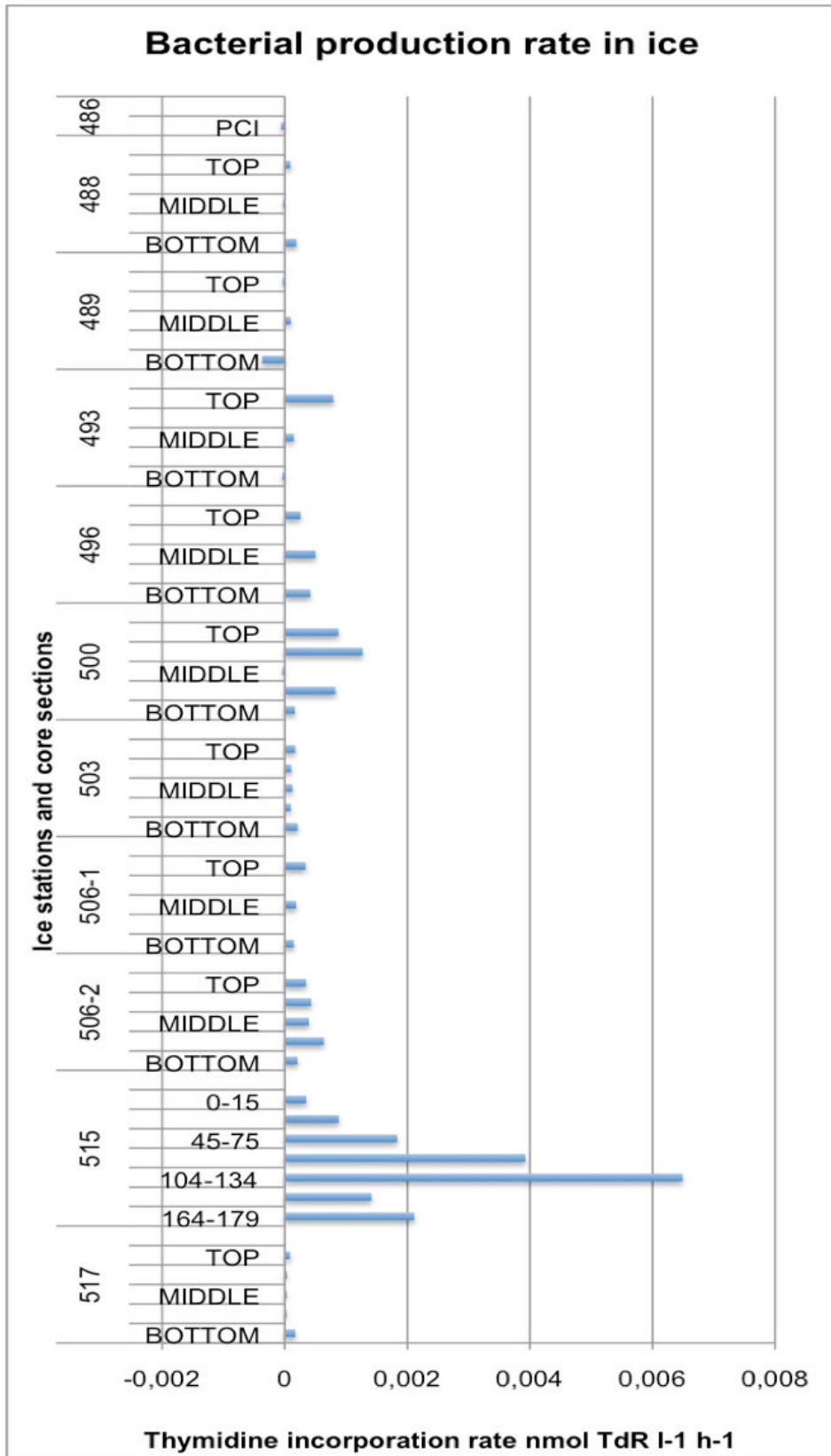


Fig. 6.17: Thymidine incorporation rates of bacteria in ice in all the measured stations.

The sulphur compounds (DMS,P,O)

DMSP and DMS profiles are compared to Chl-a concentrations at each AWECS station in Fig. 6.8, and some representative stations are shown in Fig. 6.18. Antarctic winter DMS,P concentration are far from negligible, in strong contrast with the Arctic (e.g. recent year-round CFL-IPY cruise in the Circumpolar Flaw Lead Polynya, G. Carnat, pers. comm.). Several reasons can be invoked to explain that contrast, e.g.: a) the essential role of the snow cover (extremely limited in the Arctic) in maintaining a very dynamic brine system sustaining a lively algal community, despite its expected inhibiting role with regards to light availability; b) the absence of an internal microbial community in the Arctic, where the sea ice cover is mainly formed of columnar ice (see also first year ice in the western Weddel Sea) and c) The higher Arctic latitudes, limiting the light input during the winter.

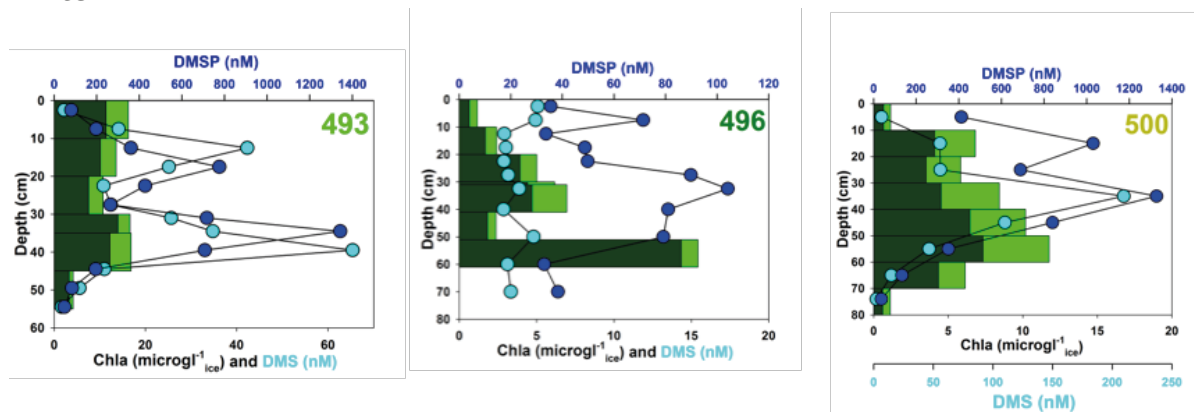


Fig. 6.18: Exemplative AWECS profiles of DMSP (dark blue) and DMS (light blue) compared to Chl-a profiles (dark green is $>10 \mu\text{g l}^{-1}$ and light green is between 10 and $0.8 \mu\text{g l}^{-1}$). Note the different scales.

DMS follows DMSP where the ice is impermeable (e.g. 493), but the correlation is lost in permeable ice (e.g. whole 496, top 500), because most of the DMS has escaped towards the atmosphere, a process commonly observed in the upper layers of spring and summer sea ice (Tison et al., 2010).

DMSP concentration profiles show a global synergy with the Chl-a content, although the details are complex. This most probably reflects the fact that different species show different DMSP/Chl-a ratios. As an example, diatoms, which dominate in the cold station 493 (see below), show low values of that ratio which is well expressed in the DMSP vs. Chl-a plot of Fig. 6.19 (light green dots). On the contrary, Station 500, which was flooded, shows high abundance of coccoids that might be diagnosed as *Phaeocystis sp.*, renowned for being efficient DMSP producers per individual. This shows up as a higher trend in Fig. 6.19 (olive dots). It also explains why the literature is somewhat contradictory as far as DMSP/Chl-a relationships in sea ice are concerned, a given core representing a combination of different algal species in the microbial assemblage. Our data set is, in that sense, rather unique since it will provide, once the species are correctly identified, the first "in-situ" specific DMSP/Chl-a ratio. Otherwise, the modelling literature relies until now on "in vitro" values of these ratios, obtained from sea water incubations (e.g. review of Stefels et al., 2007). It is clear from Fig. 6.19 that our values for the DMSP/Chl-a ratio at station 493 is up to two order of magnitudes higher than those reported for diatoms in sea water (ca. $4 \text{ nmoles DMSP mg}^{-1} \text{ Chl-a}$).

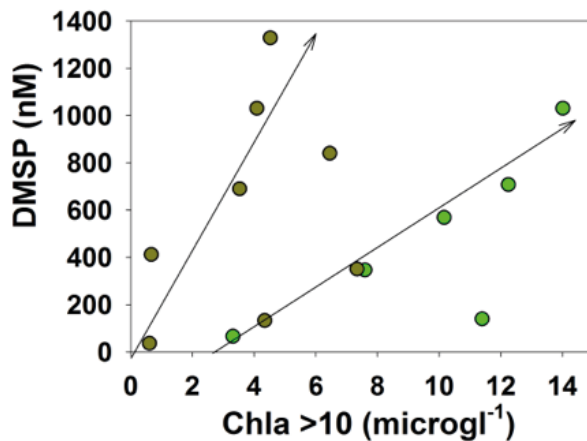


Fig. 6.19: DMSP/Chla relationships in samples from stations 493 (light green dots) and 500 (olive dots)

Incubation experiments on DMSP conversion to DMS and possibly methane

The first experiment with ice from station PS81/486 showed very low DMSP levels DMS could not be detected. In the second experiment (PS81/488) DMS could only be detected after spiking the experimental bottles with DMSP. The third and fourth (PS81/500 and Heli20130720) experiment both showed an increase in the DMS and a decrease in the DMSP concentration either with or without the external supply of DMSP. Nevertheless, no clear differences between the light and dark treatments in experiment 3, as well as treatments with nutrient additions in experiment 4 could be seen. Methane concentrations in the headspace were equal to air concentrations.

The complete dataset will be correlated with respect to the physical and biogeochemical parameters as well as species information from bacteria and microalgae determined from the sea ice in close vicinity from the same stations.

Methane concentrations determined directly from the headspace of melted ice core sections were in the range of air concentrations.

Foraminifera in sea ice

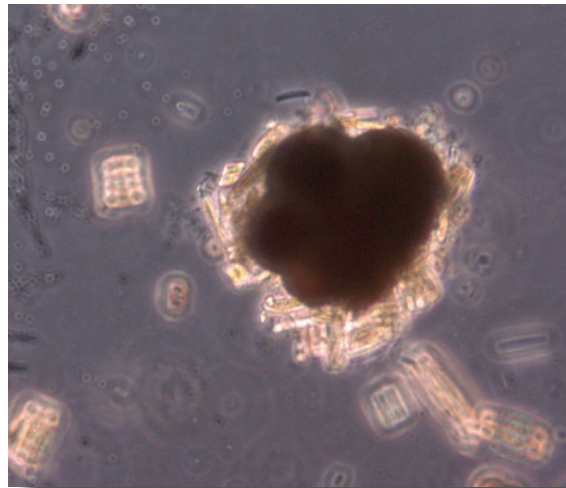
Neogloboquadrina pachyderma was found at basically all stations (Fig. 6.20 and 6.21) and a large part of the assembly was alive. Further onshore studies will provide information on distribution pattern and abundances of *N. pachyderma* within the cores. Geochemical analyses of the foraminifer tests will indicate, if anomalies in oxygen isotope or Mg/Ca element ratios suggest formation of chambers within the sea ice.

The individuals of the culture experiments will be further investigated onshore in the laboratory. The staining agent added to the culture medium will reveal if chambers have formed during the culture experiments, and thus indicating if formation of new chambers is possible under conditions similar to those in sea ice.



Fig. 6.20 : *Neogloboquadrina pachyderma* (sin.) from Site PS 81/489

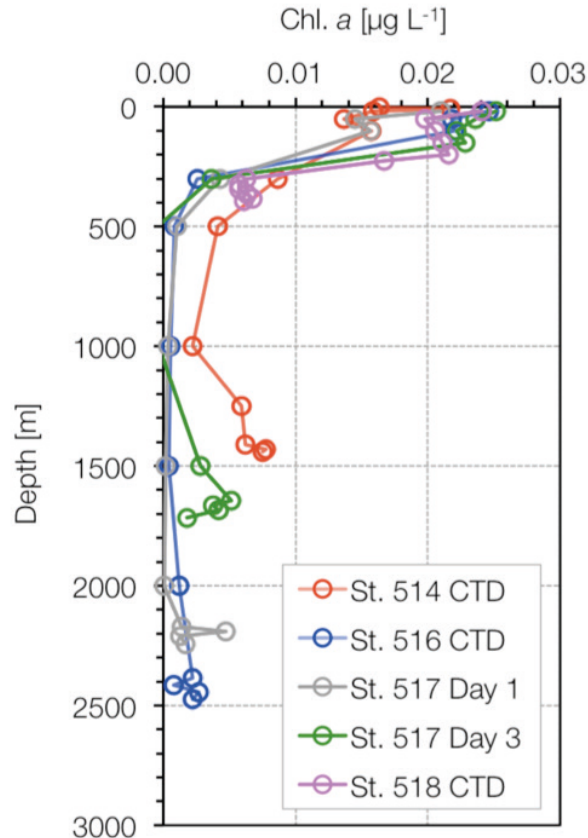
Fig. 6.21: *Neogloboquadrina pachyderma* (sin.) from Site PS 81/506 surrounded by ice algae



Chl a profiles from the Hydrocasts

Fig. 6.22 show the Chl-a in selected hydrocast profiles. Although Chl-a concentrations were basically very low throughout the water column, we observed an increase of the Chl-a concentration in the bottom part of the water column. These increases could either reflect transport of Chl-a-rich surface waters during bottom water formation or resuspension of the sediment at the sea floor surface. Chemical properties (dissolved inorganic carbon, nutrients, oxygen isotopic ratio) will be measured in the home laboratory. It will help us understanding better the relationships between bottom water formation processes and biogeochemical cycles in the Weddell Sea in the winter time.

Fig. 22: Vertical profiles of chl-a concentration at Sts. 514, 516, 517 and 518



Data management

Preliminary results will be available to the cruise participants and external users after request to Christiane Uhlig. Processed data will be published in PANGAEA after processing.

References

- Becquevort S, Dumont I, Tison JL, Lannuzel D, Sauvée ML, Chou L, Schoemann V. (2009) Biogeochemistry and microbial community composition in sea ice and underlying seawater off East Antarctica during early spring. *Polar Biol* 32, 879–895.
- Damm E, Helmke E, Thoms S, Schauer U, Nöthig E, Bakker K, Kiene RP (2010) Methane production in aerobic oligotrophic surface water in the central Arctic Ocean, *Biogeosciences*, 7, (3), 1099–1108.
- de Jong J, Schoemann V, Lannuzel D, Croot P, de Baar H, Tison JL (2012) Natural iron fertilization of the Atlantic Southern Ocean by continental shelf sources of the Antarctic Peninsula. *J Geophys Res*; 117, G01029, doi:10.1029/2011JG001679.
- de Jong J, Schoemann V, Tison J-L, Becquevort S, Masson F, Lannuzel D, Petit J, Chou L, Weis D, Mattielli N (2007) Precise measurement of Fe isotopes in marine samples by multi-collector inductively coupled plasma mass spectrometry (MC-ICP-MS). *Anal Chim Acta*; 589, 105–119.
- Dieckmann GS, Spindler M, Lange MA, Ackley S. F. & Eicken H. (1991) Antarctic sea ice: a habitat for the foraminifer *Neogloboquadrina pachyderma*, *J. of Foraminiferal Res.*, 21, p. 182-189.

- Fuhrman JA, Azam F (1980) Bacterioplankton secondary production estimates for coastal waters of British Columbia, Antarctica, and California. *Appl Environ Microbiol* 39, 1085–1095.
- Fuhrman JA, Azam F (1982) Thymidine incorporation as a measure of heterotrophic bacterioplankton production in marine surface waters: Evaluation and field results. *Mar Biol* 66, 109–120.
- Garrison R, Buck KR (1986) Organism losses during ice melting: a serious bias in sea-ice community studies. *Polar Biol* 6, 237–239.
- Geilfus NX, Carnat G, Dieckmann GS, Halden N, Nehrke G, Papakyriakou T, Tison J-L, Delille B. (2013), First estimates of the contribution of CaCO₃ precipitation to the release of CO₂ to the atmosphere during young sea ice growth. *Journal of geophysical Research - Oceans*, 118(1-12), doi:10.1029/2012JC007980.
- Hassler CS, Schoemann V, Mancuso Nichols C, Butler ECV, Boyd PW. Saccharides enhance iron bioavailability to Southern Ocean phytoplankton. *Proc Natl Acad Sci USA* 2011; 108, 1076-1081.
- Henley WJ (1993) Measurement and interpretation of photosynthetic and diel changes. *J Phycol* 29, 729–739.
- Kiene R. P. and Linn LJ, Distribution and turnover of dissolved DMSP and its relationship with bacterial production and dimethylsulfide in the Gulf of Mexico, *Limnology and Oceanography*, 45, (4), 849–861, 2000.
- Kottmeier ST Sullivan CW (1988) Sea-ice microbial communities 9. Effects of temperature and salinity on rates of metabolism and growth of autotrophs and heterotrophs. *Polar Biol* 8, 293–304.
- Lannuzel D, de Jong J, Schoemann V, Trevena A, Tison JL, Chou L (2006) Development of a sampling and flow injection analysis technique for iron determination in the sea ice environment. *Anal Chim Acta*; 556, 476–483.
- Lannuzel D, Schoemann V, de Jong J, Chou L, Delille B, Becquevort S, Tison, JL (2008) Iron study during a time series in the western Weddell pack ice. *Mar Chem*; 108, 85–95.
- Lannuzel D, Schoemann V, de Jong J, Tison JL, Chou L (2007) Distribution and biogeochemical behaviour of iron in the East Antarctic sea ice. *Mar Chem*; 106, 18–32.
- Löscher BM, de Baar HJW, de Jong JTM, Veth C, Dehairs F (1997) The distribution of Fe in the Antarctic Circumpolar Current. *Deep-Sea Res II*; 44, 143–187.
- Martin JH (1990) Glacial-interglacial CO₂ change: The iron hypothesis. *Paleoceanography*; 5, 1–13.
- Measures CI, Vink S. Dissolved Fe in upper waters of the Pacific sector of the Southern Ocean. *Deep-Sea Res II* 2001; 48: 3913–3941.
- Moran JJ, Beal EJ, Vrentas JM, Orphan VJ, Freeman KH, House CH (2008) Methyl sulfides as intermediates in the anaerobic oxidation of methane, *Environmental Microbiology*, 10, (1), 162–173.
- Nomura D, Yoshikawa-Inoue H, Toyota T (2006), The effect of sea-ice growth on air-sea CO₂ flux in a tank experiment. *Tellus Series B*, 58(5), 418–426, doi:10.1111/j.1600-0889.2006.00204.x.
- Platt T, Gallegos CL, Harrison WG (1980) Photoinhibition of photosynthesis in natural assemblages of marine phytoplankton. *J Mar Res* 38:687–701.

- Rysgaard S, Bendtsen J, DeLille B, Dieckmann GS, Glud RN, Kennedy H, Mortensen J, Papadimitriou S, Thomas DN, Tison J-L (2011) Sea ice contribution to the air-sea CO₂ exchange in the Arctic and Southern Oceans. *Tellus* 63B, 823–830.
- Sohrin Y, Urushihara S, Nakatsuka S, Kono T, Higo E, Minami T, Norisuye K, Umetani S (2008) Multielemental determination of GEOTRACES key trace metals in seawater by ICP-MS after preconcentration using an ethylenediaminetriacetic acid chelating resin. *Anal Chem*; 80, 6267-6273.
- Spindler M & Dieckmann GS (1986): Distribution and abundance of the planktic foraminifer *Neogloboquadrina pachyderma* in sea ice of the Weddell Sea, (Antarctica). *Polar Biol.*, 5, p. 185-191.
- Stefels J, Steinke M, Turner S, Malin G, and Belviso S (2007) Environmental constraints on the production and removal of the climatically active gas dimethylsulphide (DMS) and implications for ecosystem modeling, *Biogeochemistry*, 83, 245-275, DOI 10.1007/s10533-007-9091-5.
- Thomas C (1997) *Identifying Marine Phytoplankton*. Academic Press, Elsevier, California 858p.
- Tison J-L, Brabant F, Dumont I, and Stefels J (2010) High-resolution dimethyl sulfide and dimethylsulfoniopropionate time series profiles in decaying summer first-year sea ice at Ice Station Polarstern, western Weddell Sea, Antarctica, *Journal of Geophysical Research*, 115, doi: 10.1029/2010JG001427.
- Trevena AJ and Jones GB. Dimethylsulphide and dimethylsulphonio propionate in Antarctic sea ice and their release during sea ice melting, *Marine Chemistry*, 98, 210 – 222, 2006.
- Zhou J, Tison JL, Brabant F and Delille B. Gas concentrations in Barrow landfast sea ice: the winter/spring contrasts, *Solas News*, 13, 22–23, 2011.

7. OCEANOGRAPHY

7.1 Modification of water masses

Matthias Krüger¹, Friedrich Richter¹,
Johannes Sutter¹
Gerd Rohardt¹ (not on board)

¹AWI

Overall objectives

The densest bottom waters of the global oceans originate in the Southern Ocean. Production and export of these dense waters constitute an important component of the global climate system. The formation of dense water in polar areas is controlled by the balance between supply of fresh water through precipitation, and melt of continental and sea ice and the extraction of freshwater by sea ice formation and evaporation. As deep and bottom waters, they represent the deepest layer of the global overturning circulation. The influence of Southern Ocean waters can be traced into the Northern Hemisphere, far north of the Antarctic Circumpolar Current (ACC). The ACC is the world's most powerful current system, transporting about 140 Sv ($10^6 \text{ m}^3 \text{ s}^{-1}$) of water at all depths. It connects the Pacific, Atlantic and Indian Ocean and forms a ring around the Antarctic continent. South of the ACC, in the subpolar region, warm and salty water masses are carried in the subpolar gyres to the continental margins of Antarctica. The most prominent are the Weddell and Ross Gyres. In the subpolar gyres, water mass modification occurs through ocean-ice-atmosphere interactions and mixing with adjacent water masses. The ACC is dynamically linked to meridional circulation cells, formed by southward ascending flow at intermediate depth and feeding into northward flow above and below. In the deep cell, water sinking near the continental water spreads to the adjacent ocean basins whereas in the shallow cell, the northward flow occurs in the surface layers. Dense waters are produced at several sites near the continental margins of Antarctica. Quantitatively the most important region for dense water formation may well be the Weddell Sea, however other areas provide significant contributions as well.

The basic mechanism of dense water generation involves upwelling of Circumpolar Deep Water, which is relatively warm and salty, into the surface layer where it comes into contact with the atmosphere and sea ice. The newly formed bottom water is significantly colder and slightly fresher than the initial Circumpolar Deep Water, which indicates heat loss and the addition of freshwater. Since freshwater input in the upper oceanic layers would impede sinking due to increasing stratification of the water column, it has to be compensated by salt gain through fresh water extraction. The upwelled water is freshened by precipitation and melting of glacial and sea ice. Freshwater of glacial origin is supplied from the ice shelves or melting icebergs. Ice shelves melt at their fronts and bases in response to the oceanic circulation in the cavity. Iceberg melting depends highly on the iceberg drift and can supply freshwater to areas distant from the shelves as the Antarctic

7.1 Modification of water masses

frontal system. Due to the spatial separation of major sea-ice freezing and melting areas, cooling and salt release during sea-ice formation also help compensating the freshwater gain. Significant parts of salt accumulation occur on the Antarctic shelves in coastal polynyas. With extreme heat losses occurring only over ice free water areas, the polynyas are areas of intense sea ice formation. Offshore winds compress the newly formed sea ice and keep an open sea surface in the polynyas.

The cold and saline water accumulated on the shelves can descend the continental slope and mix with water masses near the shelf edge or it circulates under the vast ice shelves, where it is cooled further, below the surface freezing point, and freshened by melt water from the ice shelf. The resulting Ice Shelf Water spills over the continental slope and mixes with ambient waters to form deep and bottom water. For both mechanisms, relatively small scale processes at the shelf front, topographic features and the nonlinearity of the equation of state of sea water at low temperatures is of particular importance to induce and maintain the sinking motion. The various processes, topographic settings and the atmospheric forcing conditions lead to variable spatial characteristics of the resulting deep and bottom water masses which then spread along a variety of pathways to feed into the global oceanic circulation. Climate models suggest that dense water formation is sensitive to climate change. However, since the relatively small scale formation processes are poorly represented in the models, further improvement is needed.

The properties and volume of the newly formed bottom water underlies significant variability on a wide range of time scales, which are only scarcely explored due to the large efforts needed to obtain measurements in ice covered ocean areas. Seasonal variations of the upper ocean layers are only partially known and normally exceed other scales of variability in intensity. Impacts of longer term variations of the atmosphere-ice-ocean system, such as the Southern Hemispheric Annular Mode and the Antarctic Dipole, are only poorly observed and understood. Their influence on or interaction with oceanic conditions are merely guessed on the basis of models which are only superficially validated due to lack of appropriate measurements.

The extreme regional and temporal variability represents a large source of uncertainty when data sets of different origin are combined. Therefore circumpolar data sets of sufficient spatial and temporal coverage are needed. At present, such data sets can only be acquired by satellite remote sensing. However, to penetrate into the ocean interior and to validate the remotely sensed data, an ocean observing system is required, which combines remotely sensed data of sea ice and surface properties with *in-situ* measurements of atmospheric, sea ice and the ocean interior.

Significant progress towards this goal already occurred in the development of appropriate technology and logistics. The *Hybrid Antarctic Float Observing System* (HAFOS), which was installed during the expedition ANT-XXIX/2, aims to capitalize on these advances to investigate the ocean interior in the Atlantic Sector of the Southern Ocean. Around 50 NEMO floats have been deployed during that cruise extending the international *Argo* programme into the Weddell Sea and making an important step towards a *Southern Ocean Observing System* (SOOS). HAFOS is the extension of the frequently measured CTD-transect along the Greenwich Meridian from 50°S towards 69.5°S. Between 1992 and 2012 nine sections were obtained and long-term modifications of water masses could be studied. Seasonal sea ice formation and melt increased respectively decreased the salinity in the

surface water on top of the Warm Deep Water (WDW). Up to now one section was obtained during a winter cruise only (ANT-X/4; 1992), which can be taken to verify the correction method. A winter section is needed to get an additional comparison between the measured and adjusted surface salinity. Due to the sea ice the floats can measure a fraction of the winter surface layer only.

Another CTD section was frequently obtained at the tip of the Antarctic Peninsula, where a relatively thin layer of Weddell Sea Bottom Water (WSBW) flows northward. Its core with minimum potential temperature leaned against the continental slope in a depth of 2,400 m. A series of ten sections between 1989 and 2012 showed a slightly decreasing temperature. Moored CTD-recorders provide time series of seasonal variations in the WSBW layer. These moorings were recovered and re-deployed during ANT-XXIX/2. But the spatial distribution of the WSBW core was based on the CTD-section measured in summer or spring but not in winter.

7.1.2 CTD observations

Matthias Krüger¹, Friedrich Richter¹,
Johannes Sutter¹, Gerd Rohardt^{1,2}

¹AWI

²Not on board

Objectives

To continue the spatially highly resolved repeat CTD section along the Greenwich meridian and to collect temperature and salinity data at mooring positions for estimation of drifts of the sensors moored, a set of deep CTD casts was planned. However, time constraints did not allow to repeat deep CTDs every 30nm as during previous expeditions. Therefore deep CTDs were cast only every 60nm. Along the route CTD/water sampler was deployed to provide hydrographic properties and water samples e.g. at Multi-Net stations (see Station List). Another highly resolved repeat of a CTD section was carried out at the tip of the Antarctic Peninsula.

Work at sea

Hydrographic profiles

During this expedition, data from 36 full ocean depth CTD profiles were collected (Table 7.1). Locations of casts are depicted as red dots in Fig. 7.1, with labels given in the format "station number - cast number".

Tab. 7.1: List of CTD profiles taken during ANT-XXIX/6

File name	Date / time	Latitude	Longitude	Water depth [m]	max pres. [dbar]	Air Temp. [°C]	Wind Speed [m s ⁻¹]
478-1	12-Jun-2013 13:51:00	46 56.170 S	7 48.800 E	1665	1669	1.6	7.4
479-1	14-Jun-2013 18:09:00	55 0.042 S	0 0.228 E	1748	1716	0.6	7.8
480-1	15-Jun-2013 04:16:00	56 0.000 S	0 0.090 E	3854	3814	0.0	9.2
481-1	15-Jun-2013 12:28:00	57 0.228 S	0 0.018 E	3625	3613	-0.6	4.5

7.1 Modification of water masses

File name	Date / time	Latitude	Longitude	Water depth [m]	max pres. [dbar]	Air Temp. [°C]	Wind Speed [m s ⁻¹]
482-1	15-Jun-2013 23:39:00	58 0.000 S	0 0.048 E	4542	4566	-0.7	14.3
483-1	16-Jun-2013 08:50:00	59 0.078 S	0 0.300 E	4593	4637	-1.6	10.0
484-1	16-Jun-2013 20:10:00	60 0.228 S	0 0.720 E	5376	5448	-4.5	7.5
485-1	17-Jun-2013 05:28:00	60 59.982 S	0 0.348 E	5391	5469	-11.2	13.8
487-2	17-Jun-2013 20:53:00	61 58.590 S	0 1.632 E	5379	5438	-19.7	12.6
488-1	18-Jun-2013 09:38:00	62 58.932 S	0 0.630 E	5313	5386	-19.3	14.2
489-1	19-Jun-2013 07:07:00	63 56.982 S	0 1.440 E	5209	5278	-22.0	9.9
490-1	20-Jun-2013 03:22:00	64 59.538 S	0 0.072 E	3729	3737	-18.9	10.4
492-1	21-Jun-2013 00:41:00	65 58.572 S	0 10.878 E	3527	3518	-18.5	12.6
493-1	21-Jun-2013 12:13:00	66 28.182 S	0 2.292 E	4477	4515	-19.4	10.1
494-1	22-Jun-2013 15:34:00	66 59.778 S	0 35.658 E	4672	4718	-20.3	4.7
495-1	23-Jun-2013 07:17:00	67 30.570 S	0 50.688 E	4638	4681	-13.8	9.2
498-1	30-Jun-2013 01:27:00	68 0.810 S	2 42.858 W	3980	3994	-21.7	2.7
499-1	01-Jul-2013 00:43:00	67 41.880 S	4 40.542 W	4669	4718	-13.3	11.2
500-3	02-Jul-2013 17:12:00	68 1.620 S	6 40.482 W	4785	4835	-20.0	8.2
501-1	07-Jul-2013 16:44:00	67 12.360 S	10 0.882 W	4952	5007	-22.5	9.1

File name	Date / time	Latitude	Longitude	Water depth [m]	max pres. [dbar]	Air Temp. [°C]	Wind Speed [m s ⁻¹]
503-3	09-Jul-2013 03:26:00	67 12.270 S	13 16.398 W	4983	5046	-15.1	6.0
504-1	09-Jul-2013 21:11:00	67 10.980 S	16 59.970 W	4966	5024	-6.5	8.8
505-2	10-Jul-2013 15:29:00	67 11.958 S	19 59.298 W	4951	5006	-12.7	1.0
506-2	15-Jul-2013 16:37:00	67 21.888 S	23 10.632 W	4895	4950	-2.9	14.1
507-2	16-Jul-2013 23:31:00	66 34.440 S	27 2.682 W	4879	4932	-23.9	10.2
509-1	24-Jul-2013 12:56:00	63 8.910 S	54 10.428 W	267	247	-1.4	12.4
510-1	24-Jul-2013 15:59:00	63 13.200 S	53 42.432 W	309	290	-1.9	9.7
511-1	24-Jul-2013 21:22:00	63 19.368 S	53 3.648 W	468	440	-1.5	9.6
512-1	25-Jul-2013 03:41:00	63 25.578 S	52 30.978 W	545	518	0.7	16.1
513-1	25-Jul-2013 07:58:00	63 29.262 S	52 8.682 W	930	899	0.1	12.9
514-1	25-Jul-2013 16:46:00	63 31.992 S	51 44.310 W	1493	1461	-14.7	13.2
515-2	26-Jul-2013 19:49:00	63 24.300 S	51 13.692 W	2082	2047	-19.0	13.8
516-1	28-Jul-2013 20:13:00	63 41.958 S	50 51.462 W	2541	2514	-17.1	8.5
517-1	29-Jul-2013 08:47:00	63 37.638 S	51 12.570 W	2308	2277	-18.0	7.9
517-2	01-Aug-2013 07:46:00	63 21.252 S	51 10.278 W	1762	1740	-23.8	11.1
518-2	04-Aug-2013 22:54:00	62 57.390 S	53 24.630 W	422	398	-7.8	9.4

7.1 Modification of water masses

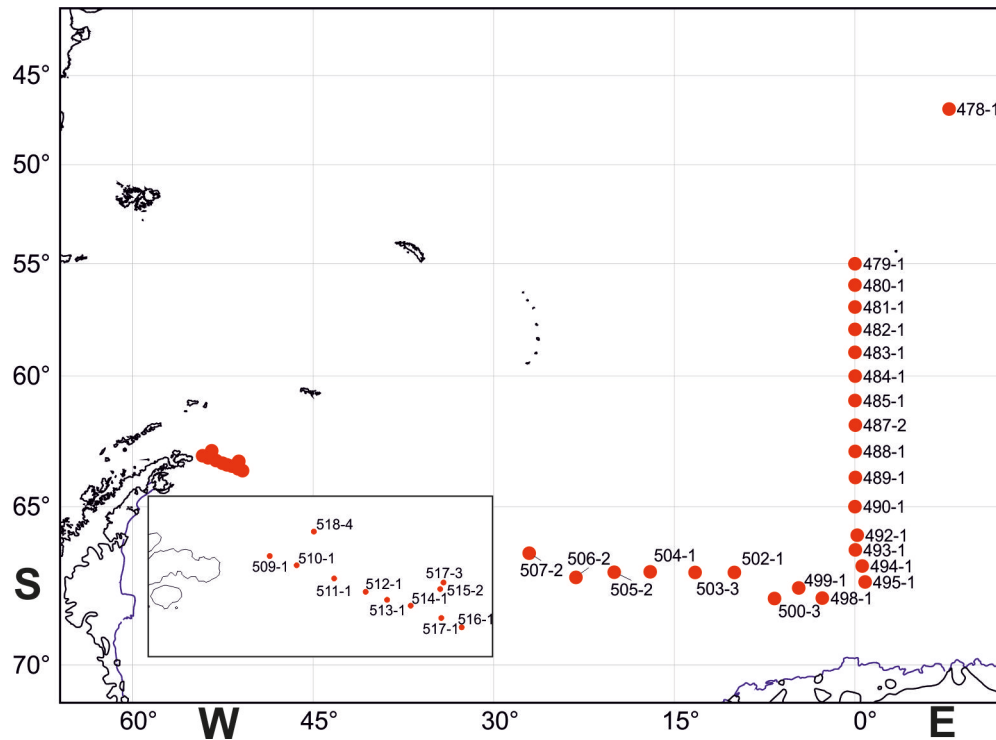


Fig. 7.1: Map of locations of CTD stations. Labels indicate station and cast numbers as given in the station list. Labels of the stations at the tip of Antarctic Peninsula are shown in the enlarged box.

CTD handling under cold conditions

The cold air temperature combined with strong wind causes freezing inside the conductivity cell when the CTD/water sampler goes into the water. Therefore air temperature and wind speed was also shown in Table 7.1. and underplayed in light blue when air temperature is below -10°C and wind speed above 10 m s^{-1} . Filling the conductivity cell with salt water taken from a sampler of the previous cast is the best precaution against freezing inside the conductivity cell. For this purpose 100 ml plastic shots were used as shown in Fig. 7.2. The shots and tubes were removed in the very last moment before the instrument goes overboard into the water. This procedure was undertaken every time when the air temperature was below -5°C . Nevertheless under extreme cold conditions freezing could not prevented completely. Seabird's SeaSaveV7 data acquisition software was used. Users can setup their individual layouts. To verify none frozen conductivity sensors a plot display was added to display the conductivity difference between the primary and secondary conductivity sensor. As soon as the pumps have been automatically switched on the difference should become approximately zero. But the difference will remain some orders larger as long as the sensors contained parts of frozen water. Therefore the CTD/water sampler was stopped in about 20 m depth until the conductivity difference switched to expected values.



Fig. 7.2: CTD/water sampler. The CTD with the pair of temperature/conductivity sensors are behind the samplers. The arrows indicated the shots and silicon tubes which were attached to the intake at each sensor pair. From the shots salt water was filled into the conductivity cell to prevent freezing. The shots were removed just before the CTD/water sampler goes overboard.

In Fig. 7.3 is a jump at cast 10 (station 485) in the salinity correction for the primary sensor pair based on salinometer measurements. Afterwards the corrections for the primary sensor pair increased steadily. Station 485 was the first extreme cold station before the cells were filled with salt water. Likely that the primary conductivity cell was broken due to freezing. But the cells could be kept in good condition by the procedure described above.

Instrument and data handling

The water sampler assembly comprises a SBE 911plus CTD system, combined with a carousel type SBE32 for Niskin water samplers of 12 liter volume, with 24 samplers installed. Additionally, the assembly was equipped with a transmissometer type Wetlabs C-Star (wave length 650 nm; path length 25 cm), a fluorometer type Wetlabs ECO-AFL/FL, an oxygen sensor type SBE43 and a Benthos/DataSonics altimeter type PSA 916D.

CTD data was logged with Seabird's *SeaSaveV7* data acquisition software to a local PC in raw format. *ManageCTD*, a Matlab™ based script developed at AWI, was employed to execute Seabird's *SBEDataProcessing* software, producing CTD profiles adjusted to 1-dbar intervals. *ManageCTD* further embedded metadata (header) information extracted from the DShip-Electronic Station Book before conducting a preliminary de-spiking and data validation of the profile data.

Preprocessed data were saved in OceanDataView compatible format, to provide near real-time visualization of e.g. potential temperature and salinity, particularly

7.1 Modification of water masses

to provide *enroute* (i.e. during the expedition) visualization of the unfolding hydrographic section.

The CTD was equipped with double sensors for temperature (SBE3plus) and conductivity (SBE4C). These sensors were calibrated prior to the expedition. *Enroute* comparison of the calibrated sensors nevertheless revealed differences of about of 0.0001°C in temperature and 0.005 mS·cm⁻¹ in conductivity for *insitu* measurements between the sensors.

Enroute comparisons between *in-situ* CTD data and salinometer based salinity measurements of water samples indicated that the conductivity sensors (SBE4C #5027 and #3585) used in the secondary sensor pair (Table 7.2, Fig. 7.3) featured the higher accuracies (see section *Salinometer* for more details). In addition, their drifts were smaller than that of the primary sensor for the duration of the expedition.

A definitive determination of sensors' drifts however requires post-expedition lab calibrations, for which the sensors will be returned to Seabird Electronics after leg ANT-XXIX/7. Hence all results reported hereinafter must be considered preliminary.

Tab. 7.2: CTD-Sensor configuration

	#1 (primary)	#2 (secondary)
Temperature (SBE3plus)	2929	5027
Conductivity (SBE4c)	2470	3885

Salinometer measurements

To monitor the accuracy and precision of the CTD's conductivity sensors, salinity/ conductivity of selected water samples was determined using an Optimare Precision Salinometer (OPS) for 22 CTD stations (Tab. 7.3) between 12.06.2013 and 28.07.2013. Duplicate water samples (bottles) were drawn from Niskin water samplers closed in homogeneous water layers at full ocean depth and in shallow depth which allows identifying possible pressure dependencies of the sensors' accuracy. Water probes were measured in reference to Standard Water batch no. P154; K15 = 0.9999, valid until date: 2014-10-20.

Tab. 7.3: Salinity samples taken

Colored cells indicated where the difference between the duplicates is more than 0.0005 g kg⁻¹.

Sample Number	Station	Cast	Niskin Nr.	Sample Depth (m)	Salinity Primary Sensor	Salinity Secondary Sensor	OPS Sample	OPS Duplicate
1	479	1	5	1610	34,6907	34,6902	34,6907	34,6904
2	479	1	8	1000	34,7142	34,7140	34,7137	34,7135
3	479	1	10	500	34,6700	34,6703	34,6697	34,6695
4	481	1	5	3480	34,6567	34,6549	34,6530	34,6528
5	481	1	6	3000	34,6597	34,6581	34,6563	34,6559
6	481	1	10	500	34,6914	34,6912	34,6897	34,6894
7	484	1	2	5310	34,6490	34,6465	34,6448	34,6447
8	484	1	10	500	34,6868	34,6869	34,6834	34,6854
9	485	1	4	5307	34,6491	34,6467	34,6460	34,6460
10	485	1	8	3000	34,6595	34,6583	34,6570	34,6569
11	485	1	11	500	34,6863	34,6863	34,6860	34,6860
12	492	1	1	3453	34,6534	34,6566	34,6559	34,6559
13	492	1	8	1000	34,6839	34,6882	34,6878	34,6880
14	492	1	20	40	34,6856	34,6907	34,3559	34,3538
15	493	1	1	4423	34,6472	34,6520	34,6507	34,6504
16	493	1	9	1000	34,6835	34,6899	34,6897	34,6896
17	494	1	1	4620	34,6445	34,6503	34,6502	34,6496
18	494	1	8	2000	34,6647	34,6715	34,6711	34,6711
19	494	1	19	50	34,3427	34,3524	34,3492	34,3493
20	495	1	1	4583	34,6437	34,6501	34,6494	34,6490
21	495	1	21	30	34,3263	34,3358	34,3367	34,3366
22	498	1	1	3917	34,6478	34,6544	34,6530	34,6530
23	498	1	6	3000	34,6524	34,6594	34,6572	34,6566
24	498	1	8	1000	34,6808	34,6885	34,6869	34,6865
25	498	1	10	500	34,6881	34,6964	34,6937	34,6928
26	499	1	2	4590	34,6406	34,6471	34,6464	34,6464
27	499	1	6	4000	34,6482	34,6549	34,6537	34,6534
28	499	1	8	2000	34,6623	34,6697	34,6688	34,6688
29	499	1	11	300	34,6902	34,6988	34,6978	34,6978
30	499	1	23	10	34,2556	34,2649	34,2653	34,2651
31	500	3	1	4733	34,6401	34,6469	34,6469	34,6466
32	500	3	7	3000	34,6528	34,6603	34,6591	34,6581
33	500	3	10	500	34,6879	34,6965	34,6948	34,6946
34	500	3	17	70	34,2704	34,2814	34,2802	34,2834
35	500	3	21	30	34,2658	34,2747	34,2735	34,2752
36	501	1	6	4000	34,6468	34,6540	34,6538	34,6539

7.1 Modification of water masses

Sample Number	Station	Cast	Niskin Nr.	Sample Depth (m)	Salinity Primary Sensor	Salinity Secondary Sensor	OPS Sample	OPS Duplicate
37	501	1	7	3000	34,6514	34,6590	34,6587	34,6591
38	501	1	9	1000	34,6743	34,6827	34,6835	34,6835
39	503	3	6	4550	34,6427	34,6495	34,6495	34,6495
40	503	3	8	2000	34,6588	34,6666	34,6673	34,6671
41	503	3	23	10	34,3222	34,3313	34,3334	34,3336
42	504	1	1	4916	34,6387	34,6459	34,6460	34,6459
43	504	1	8	2000	34,6574	34,6656	34,6659	34,6659
44	504	1	10	500	34,6796	34,6882	34,6892	34,6891
45	506	2	1	4843	34,6375	34,6446	34,6451	34,6452
46	506	2	7	3000	34,6499	34,6580	34,6578	34,6576
47	506	2	17	70	34,3596	34,3693	34,3711	34,3709
48	506	2	19	50	34,3596	34,3692	34,3707	34,3707
49	506	2	21	30	34,3598	34,3691	34,3711	34,3714
50	507	2	1	4827	34,6353	34,6425	34,6430	34,6434
51	509	1	1	244	34,5887	34,5992	34,5964	34,5966
52	509	1	19	50	34,5139	34,5243	34,5252	34,5249
53	510	1	2	286	34,5016	34,5130	34,5133	34,5126
54	510	1	12	123	34,4986	34,5089	34,5089	34,5092
55	510	1	19	39	34,4965	34,5069	34,5069	34,5067
56	513	1	1	888	34,6029	34,6139	34,6153	34,6152
57	513	1	13	150	34,4545	34,4653	34,4670	34,4652
58	513	1	14	100	34,4515	34,4625	34,4611	34,4619
59	514	1	2	1430	34,6024	34,6121	34,6126	34,6124
60	514	1	9	750	34,6661	34,6763	34,6763	34,6761
61	515	2	2	1987	34,6051	34,6146	34,6291	34,6225
62	515	2	8	1000	34,6684	34,6786	34,6802	34,6797
63	515	2	18	60	34,4551	34,4662	34,4991	34,4949
64	516	1	1	2474	34,6189	34,6285	34,6287	34,6286
65	516	1	8	750	34,6721	34,6824	34,6830	34,6836

Preliminary results

Due to the low temperature water in the Niskin sampler freezes while salinity samples were taken. The difference between the duplicate OPS measurements were used to identify questionable results; see Table 7.3, column [OPS Sample] and [OPS Duplicate]. 15 of 65 measurements were rejected because the difference is more than 0.0005; see Table 7.3.

Fig. 7.3 shows the record of salinity correction for the primary and secondary sensor. During the first few CTD casts the salinity difference between the secondary and primary sensor pair is in the order of a few 1/1000. After station 485 (sample number 10) the difference changed with a jump. Afterwards the difference continuously

increased between June 17th and July 28th by about 0.005 g kg^{-1} . This reports to use the secondary sensor pair. Further on the salinity corrections were separated into a group of samples taken above 1,000 m depth (shallow) and another one taken below 1,000 m depth. The comparison of shallow and deep record in Fig. 7.3; blue and cyan curve, could not clearly identify a pressure dependencies of the sensors. The average of 26 "deep" samples resulted in a mean salinity correction of $-0.0005 \text{ g kg}^{-1}$. This temporary offset was applied to salinity data derived from the secondary sensor, and used for preliminary results as presented hereinafter.

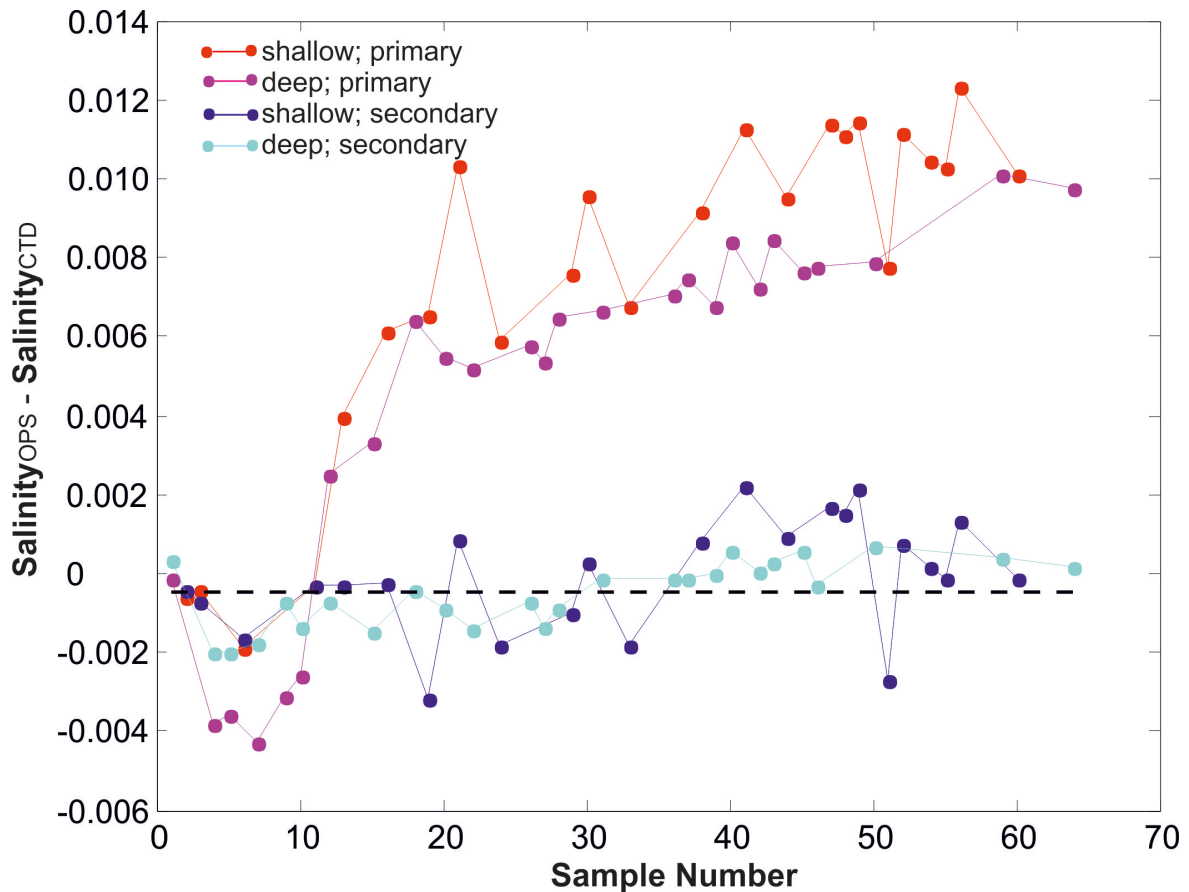


Fig. 7.3: Salinity deviations between OPS measurements and in-situ CTD measurements. The correction for the secondary sensor (black dashed line) is about $-0.0005 \text{ g kg}^{-1}$, and lacked any discernible pressure dependency.

First results (Figures 7.4 and 7.5) show an overall thermal structure resembling that of earlier cruises, but indicate a warming of the deep water masses, continuing the general trend as documented in this long term time series for some 20 plus years.

7.1 Modification of water masses

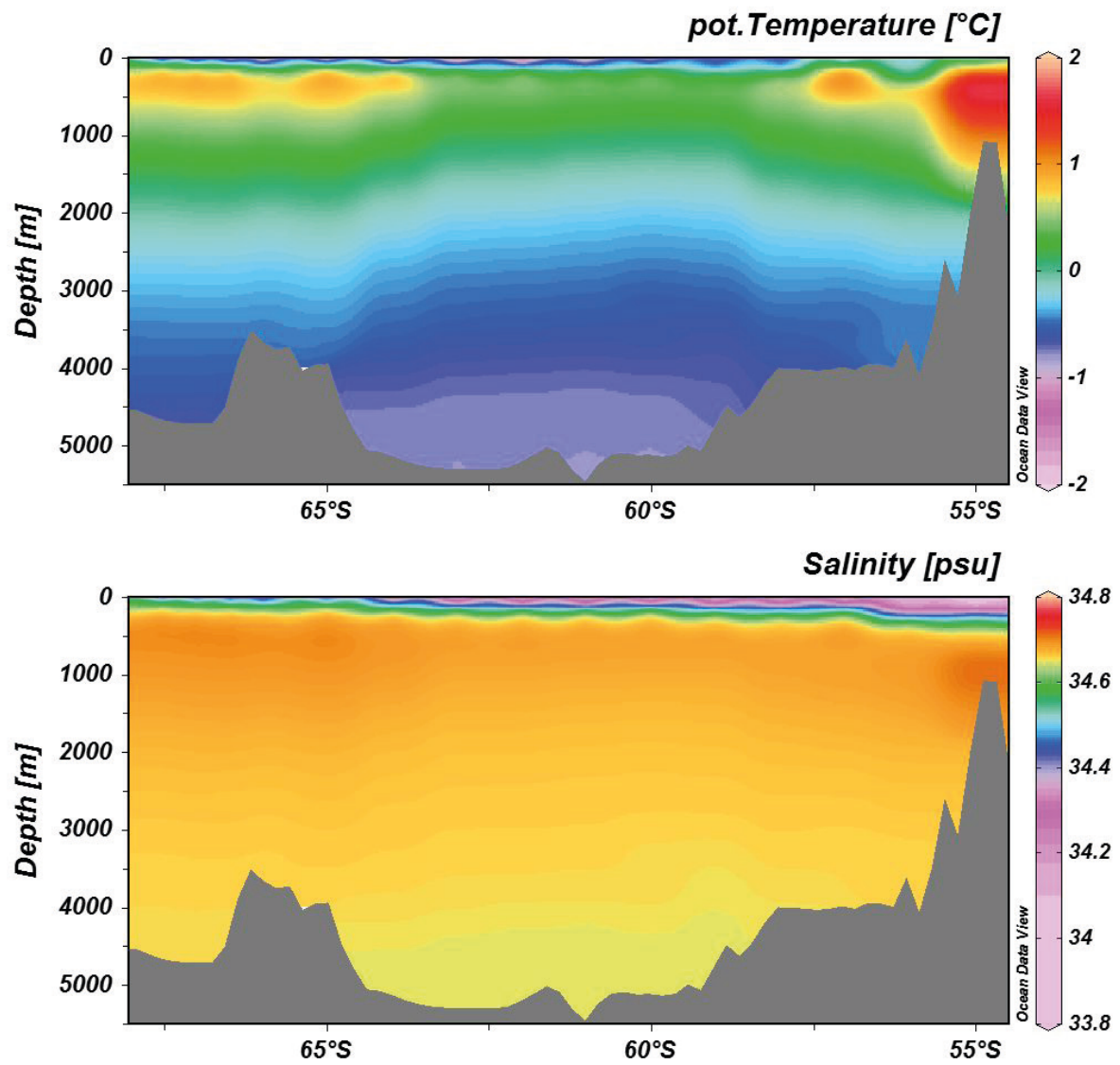


Fig. 7.4: Potential temperature (top) and salinity section (bottom) along the Greenwich Meridian

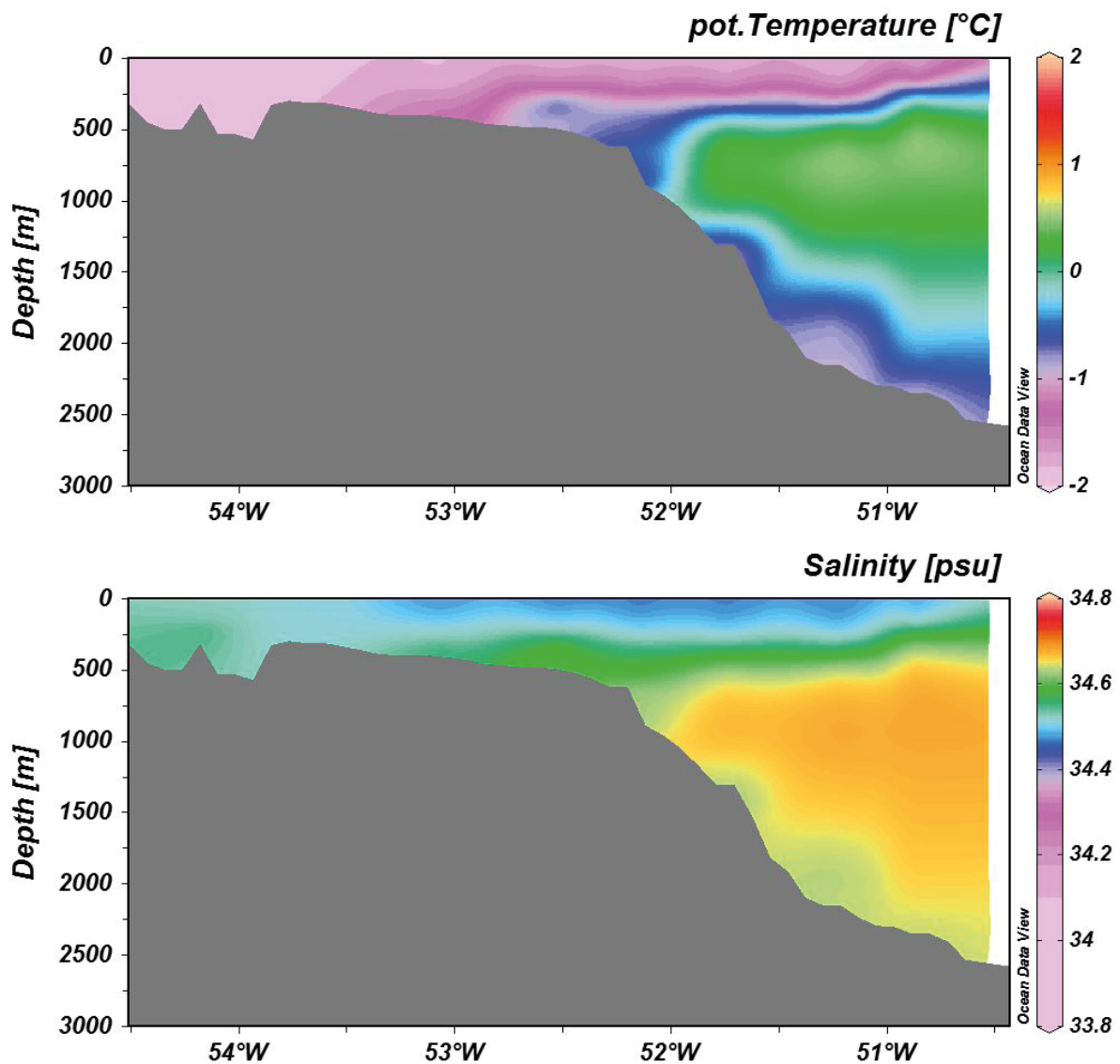


Fig. 7.5: Potential temperature (top) and salinity section (bottom) approaching the Antarctic Peninsula

Data management

The final processing of CTD-data will be conducted after post-expedition calibrations are finished. All data will be stored and available through the PANGAEA Data Publisher for Earth & Environmental Science. P.I.: Gerd Rohardt

<http://doi.pangaea.de/10.1594/PANGAEA.819714>

7.1.3 Thermosalinograph and vm-ADCP

Gerd Rohardt
not on board¹

¹AWI

Objectives

Please refer to overall objectives.

Work at sea

Enroute (starting on 9 Jun 2013 07:00:00 UTC at 35.6135° S 17.0199° E; ending on 11 Aug 2013 22:10:00 UTC at 52.6223° S 68.2704° W) surface temperature/salinity and near-surface current velocity profiles were acquired with the ship's thermosalinograph and the vessel mounted acoustic Doppler current profiler (vm-ADCP), respectively. The instrument was maintained throughout the expedition by FIELAX scientific data services. Data were stored directly in the DShip system.

Thermosalinograph

To minimize the risk of data loss due to blocking of the thermosalinograph's intake by ice particles, *Polarstern* features two SBE21 thermosalinographs (TSG) with intakes at 11 m (in the box keel) and at 5 m (in the bow-thruster tunnel) depth, respectively. Actually the intake in 5 m was jammed by sea ice as soon as *Polarstern* was operating in completely sea ice covered areas. Therefore the thermosalinograph in the bow-thruster tunnel was switched off from 17 Jun 2013 15:50 UTC until 19 Jul 2013 17:40 UTC.

Water samples were taken once daily from both bow and keel TSGs by FIELAX. Salinity of these samples was determined using the Optimare Precision Salinometer at least once every two weeks to determine the salinity correction and to identify possible sensor faults.

Tab. 7.4: Sensor specification for the SBE21 as given by Seabird Electronics www.seabird.com

	Temperature SBE38 remote	Temperature	Conductivity
Range	-5 to 35 °C	-5 to 35 °C	0 to 70 mS/cm
Accuracy	0.001 °C	0.01 °C	0.001 mS/cm
Resolution	0.0003 °C	0.001 °C	0.0001 mS/cm

vm-ADCP

The vessel mounted ADCP transducer (Table 7.5) is installed in the box keel at 11 m depth. An acoustic window protects the transducer against damage when *Polarstern* is operating in sea ice.

Tab. 7.5: Instrument specification given by RD Instruments for the 150 kHz Ocean Surveyor

Velocity range:	-5 to 9 m/s
Velocity accuracy:	$\pm 1.0\%$; 0.5 cm/s
Max. profile depth:	375 – 400 m
Max. altitude in bottom track:	600 m

Preliminary results

Fig. 7.6 depicts the *enroute* temperature from Cape Town to Punta Arenas as observed at 11 m depth (i.e. by the keel TSG).

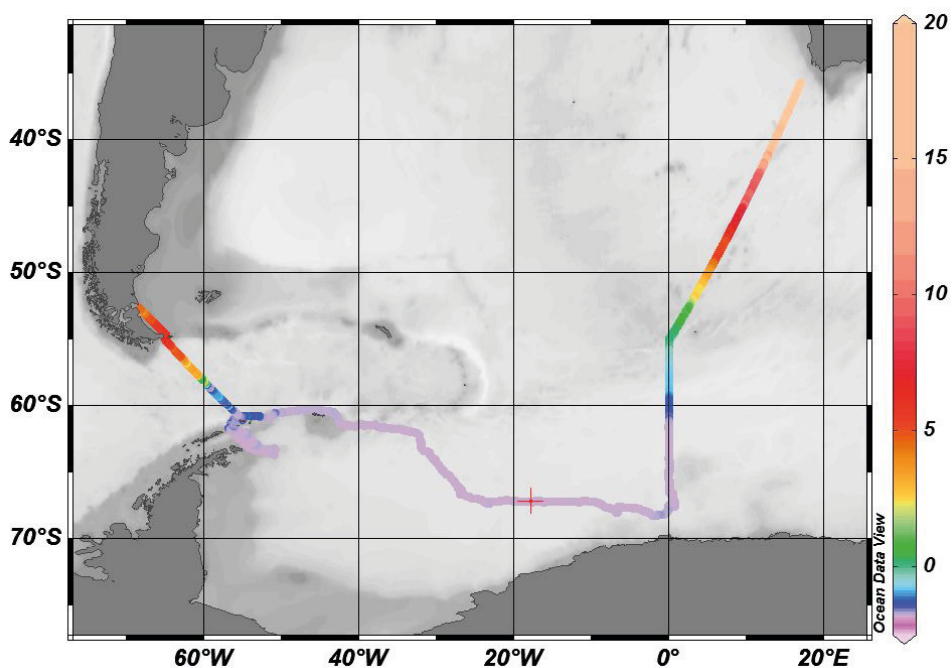


Fig. 7.6: Enroute temperature at 11 m depth retrieved from the PANGAEA Data Publisher for Earth & Environmental Science.

Data management

At the end of the expedition, the recorded data were directly transferred to AWI by the system manager. Final processing of TSG data occurred in Bremerhaven by FIELAX post expedition. TSG data is readily available via PANGAEA at:

<http://doi.pangaea.de/10.1594/PANGAEA.819831>

Please refer to this data set rather than data retrieved from the DShip data base directly. vm-ADCP data will be processed in Bremerhaven later in 2014.

P.I.: Gerd Rohardt

7.1 Modification of water masses

Appendix

Tab. 7.6: Water samples taken during ANT-XXIX/6 from the CTD/water sampler

	See Chapter	4	6	6	6	6	4
File name	Date /time	Hg G = gaseous H M = Methyl-HG T = Total	DOC Alkalinity Nutrients CH ₄ O ¹⁸ Chl _a	Fe Mn Al Co Ni Cu Zn Mo Cd Pb Ba	Micro-Bio.	Bio-Che.	Halo-carbons
478-1	12-Jun-2013 13:51:00						x
479-1	14-Jun-2013 18:09:00		X			X	x
480-1	15-Jun-2013 04:16:00						x
481-1	15-Jun-2013 12:28:00					X	x
482-1	15-Jun-2013 23:39:00						x
483-1	16-Jun-2013 08:50:00		X			X	x
484-1	16-Jun-2013 20:10:00				X		x
485-1	17-Jun-2013 05:28:00					X	x
487-2	17-Jun-2013 20:53:00						x
488-1	18-Jun-2013 09:38:00		X			X	x
489-1	19-Jun-2013 07:07:00						x
490-1	20-Jun-2013 03:22:00						x
492-1	21-Jun-2013 00:41:00					X	x
493-1	21-Jun-2013 12:13:00	G,M,T	X		X		x
494-1	22-Jun-2013 15:34:00	G					x
495-1	23-Jun-2013 07:17:00						x
498-1	30-Jun-2013 01:27:00	G,M,T				X	x
499-1	01-Jul-2013 00:43:00						x
500-3	02-Jul-2013 17:12:00	G,M,T	X		X		x
501-1	07-Jul-2013 16:44:00	G	X				x
503-3	09-Jul-2013 03:26:00	G,M,T					x
504-1	09-Jul-2013 21:11:00		X				x
505-2	10-Jul-2013 15:29:00						x
506-2	15-Jul-2013 16:37:00		X		X		x
507-2	16-Jul-2013 23:31:00						x
509-1	24-Jul-2013 12:56:00	G	X	X		X	x
510-1	24-Jul-2013 15:59:00			X			x
511-1	24-Jul-2013 21:22:00	G	X	X			x
512-1	25-Jul-2013 03:41:00			X			x
513-1	25-Jul-2013 07:58:00						x

7. Oceanography

File name	Date /time	Hg G = gaseous H M = Methyl-HG T = Total	DOC Alkalinity Nutrients CH ₄ O ¹⁸ Chl _a	Fe Mn Al Co Ni Cu Zn Mo Cd Pb Ba	Micro-Bio.	Bio-Che.	Halo-carbons
514-1	25-Jul-2013 16:46:00	G,M,T	X	X			x
515-2	26-Jul-2013 19:49:00	G,M,T					x
516-1	28-Jul-2013 20:13:00		X	X		X	x
517-1	29-Jul-2013 08:47:00		X	X			x
517-2	01-Aug-2013 07:46:00						x
518-2	04-Aug-2013 22:54:00						

8. OVERWINTERING STRATEGIES OF ANTARCTIC COPEPODS: PHYSIOLOGICAL MECHANISMS AND BUOYANCY REGULATION BY AMMONIUM

Sabine Schründer², Franz Josef Sartoris¹, Holger Auel² (not on board), Sigfried Schiel¹ (not on board)

¹AWI

²BreMarE

Objectives

Ontogenetic seasonal migration associated with a diapause is known as an adaptation to escape temporarily from an unfavourable environment in several calanoid copepod species in Polar Seas. Diapausing copepods reside for several months in greater depths where they are presumably neutrally buoyant without or with reduced swimming activities. In the Southern Ocean the mesozooplankton community is strongly dominated by only a few endemic copepod species. Within the calanoids, the epipelagic species *Calanoides acutus* and *Calanus propinquus* contribute substantially to the total mesozooplankton biomass (10 - 52 %). Most of the *C. propinquus* population remains active during winter in the upper and mid water layers and switches to a more omnivorous diet, whereas *C. acutus* is known to conduct extensive seasonal vertical migrations associated with a resting stage (diapause) at greater depths (≥ 500 m).

Previous studies dealing with life cycle strategies of Antarctic copepods have generally focused on the copepod population structure, the abundance, distribution and stage composition and its variety between seasons and regions. Only recent approaches concentrated on buoyancy regulation mechanisms of vertical migrations and on the termination of overwintering.

Our preliminary studies on *Polarstern* cruises ANT-XXIII/7 (September – October 2006), ANT-XXVII/3 (February – April 2011) and ANT-XXVIII/2 (December 2011 – January 2012) showed that only copepod species known to enter diapause contain highly elevated concentrations of ammonia (NH_4^+) in their haemolymph. The finding that high levels of ammonia are only found in species which undergo vertical ontogenetic migration is evidence that ontogenetic migration is related to and/or relies on ammonia aided buoyancy. Dependent on the pH, ammonia exists in solutions as both, NH_3 and NH_4^+ . NH_3 is more toxic than NH_4^+ and in contrast to NH_4^+ it easily penetrates cell membranes. Due to the toxicity and the higher diffusibility of NH_3 , we predicted a low haemolymph pH in diapausing copepods to favour the formation of ammonium (NH_4^+).

During ANT-XXVII/3 (February – April 2011) and ANT-XXVIII/2 (December 2011 – January 2012) we measured the extracellular pH values in the haemolymph of diapausing copepods with high levels of ammonia and found acidic values (about pH 6.0) low enough to prevent the formation of toxic NH_3 .

Our studies during ANT-XXIX/6 aim to test the hypotheses on the role of ammonia and pH for triggering metabolic depression and regulating buoyancy during the diapause of polar calanoid copepods. Still there are many open questions concerning buoyancy regulation in copepods.

The key questions of our studies were:

To test the hypotheses on the role of ammonia and pH for triggering metabolic depression and regulating buoyancy during the diapause of polar calanoid copepods in winter.

Are diapausing copepods neutral buoyant or do they have to swim to stay in the water column at a certain depth?

How do pH and NH_4^+ and lipid content change during moult when seawater is incorporated to increase the size of the copepod?

Work at sea

As standard devices for the quantitative collection of the zooplankton two multiple opening and closing nets (multinet, 0.25 m² and 0,5 m² mouth opening) equipped with 5 and 9 nets, respectively, of 100 µm were used. The multinetts were towed vertically, sampling standard layers between 2,000-1,000 m and the surface, at the shelf between sea floor and surface. At three stations a bongo-net was used (300 m depth) to collect a sufficient amount of *Calanus propinquus* for experiments.

Copepods have been eventually sorted on board ship from the different depth layers by species, sex and developmental stage. Deep-frozen (-80°C) samples of the different copepod species have been collected for biochemical analyses in the home lab, whereas live intact specimens have been kept in jars with filtered seawater in temperature-controlled refrigerators at *in-situ* temperatures for haemolymph extraction and experiments. The remaining zooplankton from each sample has been fixed in 4 % borax-buffered formaldehyde seawater solution for post-cruise studies on abundance, population structure, and vertical distribution.

In addition freshly moulted copepods (*Calanoides acutus* CIV-CV) were selected from the samples to measure pH and cation content.

Haemolymph extraction and cation analysis

Under a dissecting microscope, haemolymph was extracted manually using borosilicate glass capillaries. Each haemolymph sample was diluted in deionized water and kept in a deep-freezer at -80°C until measurement. The cation composition such as NH_4^+ , Na^+ , Mg^{++} , K^+ , and Ca^+ for all samples has been analysed on board by ion chromatography with a DIONEX ICS 2000.

pH_e-measurements

At least 500 nL of each haemolymph sample was needed to measure extracellular pH directly on board using a NanoDrop 3300 fluorometer (Thermo Fischer) and HPTS (8-Hydroxypyrene-1,3,6-trisulfonic acid trisodium salt) as a pH indicator. To avoid inaccuracies due to temperature induced changes, pH measurements have been carried out in temperature-controlled laboratory at *in-situ* temperatures.

Respiration

Respiration rates have been determined under simulated *in-situ* conditions in temperature-controlled laboratories on board the ship as a measure of metabolic

activity. Depending on the size, several individuals were incubated in gas-tight bottles filled with filtered and oxygenated seawater for 8 - 12 hours. Oxygen consumption was measured by oxygen micro-optodes using a 10- Channel Fiber-Optic Oxygen Meter (OXY-10, PreSens, Precision Sensing GmbH). At the end of the experiments, individuals were kept in the deep-freezer at -80°C for post-cruise measurements of dry weight and respiration rates.

Experiments

Long term incubations (up to 6 weeks) with diapausing copepods *Calanoides acutus* CV/CIV have been carried out at *in-situ* temperatures in natural seawater under different environmental conditions (with or without food, in the dark/with light). At regular intervals (once a week) the extracellular pH, NH_4^+ and metabolic activity has been measured.

To test whether diapausing *Calanoides acutus* are neutral buoyant, individuals were placed in measuring cylinders and the swimming activity was recorded with and without anaesthetising (MS222, 3-aminobenzoic acid ethyl ester, Sigma) them. As comparison these experiments were repeated with the active *Calanus propinquus*.

Preliminary (expected) results

Cat ion and pH measurement

In almost all individuals of *Calanoides acutus* and *Rhincalanus gigas* we found elevated haemolymph ammonia levels and low pH values ranging between pH 5.00 and 6.5 independent from state or depth whereas in the non diapausing *Calanus propinquus* pH was above 7.5 and ammonium levels were below detection limits. However, in some of the *Calanoides acutus* CV ammonium was low despite acidic pH and in general the standard deviation was highest in the *Calanoides acutus* CV. Since we found also low ammonium levels in freshly moulted CV this could indicate that the accumulation of ammonium takes a certain time after moulting. Since the low pH was preserved in freshly moulted copepods we found no differences in pH between CIV and CV. A low ammonium concentration in freshly moulted copepods would increase the density of the haemolymph and thus influence buoyancy. This could be compensated by an increase in lipid content. To examine the relative buoyancies of each compartment lipid content and C/N ratios will be measured.

Respiration rates

To determine respiration rates the dry weight of the animals is needed which will be measured at the home lab.

Experiments

The different environmental conditions of the incubations did not affect the response of the diapausing copepods in terms of pH and NH_4^+ . In the first 2-3 weeks extracellular pH rises significantly from ≈ 5.5 to about 6.5 and remained more or less stable for the rest of the incubation time. The impression of an increase in activity has to be validated by the respiration data.

Our experiments clearly show that diapausing *Calanoides acutus* are neutral buoyant since they stay motionless in the water column even if anaesthetised. In contrary anaesthetised *Calanus propinquus* sunk to the bottom. When anaesthesia was terminated they awake and start swimming again.

Data management

Parts of the collected data will be published within the framework of a PhD thesis (in progress, Sabine Schröder 2011-2013). If georeferenced data will be collected, they will be free available in the PANGAEA Open Access library within the next two years.

9. ACOUSTIC ECOLOGY OF ANTARCTIC MINKE WHALES

Lars Kindermann¹, Ariel Cabreira²

¹AWI

²INIDEP

Objectives

The largest inhabitant of the winterly pack ice is the Antarctic Minke whale, *Balaenoptera bonaerensis*. Up to 10 meters long and weighing 10 tons it is a rather small member of the baleen whale family. While its larger relatives like blue, fin, and humpback whales mostly leave Antarctica during winter for their subtropical mating grounds, this species has adapted for a permanent life in the ice. Little is known about this most frequent of all great whale species, population estimates differ between 360,000 to 1,000,000 individuals and there are contradicting opinions whether the stock is growing or shrinking. To the public it became famous as the main target of the controversially discussed contemporary whaling. Marine mammals can often be more easily detected and recognized by their songs than by visual observation. They spend most of their time submerged and often only their blow is visible for a short time. Hence, especially during polar night the study of these animals is extremely difficult. However, the calls of certain whales can be heard under water several hundred kilometres away. Therefore many of the oceanographic moorings in the Weddell Sea and the PALAOA observatory at Neumayer Base are equipped with long term acoustic recorders which continuously record the soundscape of the ocean for several years. Using this data the spatio-temporal distribution of many seal and whale species can be determined from their acoustic presence. But to assign a specific call unambiguously to a certain species, it is necessary at least for one time to see the animal and listen to it at the same time. This has not yet succeeded for the Antarctic minke whale so far. On the other hand, the underwater recorders have picked up many sounds which have not been attributed to any species yet. Some of them are present in Antarctic winter only. Especially a rhythmic sound called 'bioduck' which is prevailing in the Southern Ocean during Austral winter is suspected to be produced by minke whales. The main goal of the bioacoustic work on board is to test this hypothesis.

Work at sea

The polar night makes it impossible to observe whales for most of the time of the day. Therefore we employed a First-Navy 360° thermal imager along with the Tashtego software for automatic whale blow detection. The system was operational on 31 days of the cruise for a total of 712.5 hours, then it broke down for unknown reasons. During its uptime every 10 seconds a snapshot was taken, 256,000 images in total. 40 hours (6TB) of full 5Hz video footage were collected on demand i.e. during whale sightings the system allowed geo referenced localisation of the animals.

During the short daylight hours and on few occasions, when whales were seen in the ships searchlights, all visual sightings were logged from the bridge into the WaLog computer system.

9. Acoustic Ecology of Antarctic Minke Whales

As the ship is too loud to use hydrophones in close vicinity, we relied on sonobuoys to record underwater sound in a distance where the engines and propellers would not mask the much fainter calls of animals. 33 AN-SSQ 53D(3) Sonobuoys manufactured by Ultra-Electronics, Canada were deployed from ship (23) or helicopter (10). Operation time was set to 8 hours and depth to 300 m. Radio channels for transmission were individually selected to lowest background interference as determined using the receivers scanner option. Two Winradio G39WSB sonobuoy receivers were attached via a 3 dB splitter to a Winradio sonobuoy antenna, mounted at 53 m height on the backside of the ships chimney. If only one buoy was transmitting, just one receiver was connected directly to the antenna to avoid the 3dB loss. The demodulated signal was fed via soundcard into a workstation running the SpectrumLab software which performed life spectrogram display and file storage. Audio was saved as one minute wave files with filenames formatted like "yyyymmdd-HHMM AWECS Sonobuoy.wav". The full DIFAR signal was recorded with a sample rate of 48kHz to allow for later acoustic localisation of the sound sources. Additionally one minute spectrograms were saved for fast offline browsing and accordingly named "yyyymmdd-HHMM AWECS Sonobuoy.jpg". Additionally one hour spectrograms were created by a second instance of SpectrumLab for an overview.

Tab. 9.1: Sonobuoy deployments from ship (PS) or during helicopter flight (Hx)

Buoy Nr		Date		Position	
SON01	PS	2013-06-15	16:08	57°59.910'S	000°01.050'W
SON02	PS	2013-06-17	17:31	61°09.980'S	000°00.100'W
SON03	H1	2013-06-29	11:53	68°58.300'S	002°58.910'W
SON04	PS	2013-07-02	11:38	67°02.370'S	006°06.380'W
SON05	PS	2013-07-02	13:55	68°58.490'S	006°16.990'W
SON06	PS	2013-07-06	11:19	67°22.950'S	008°28.540'W
SON07	PS	2013-07-07	13:13	67°47.940'S	009°23.720'W
SON08	PS	2013-07-08	10:44	67°50.410'S	013°47.350'W
SON09	PS	2013-07-10	12:33	67°50.940'S	019°11.920'W
SON10	H2	2013-07-13	14:15	67°49.203'S	023°44.359'W
SON11	H2	2013-07-13	14:24	67°49.212'S	023°44.366'W
SON12	PS	2013-07-16	15:27	66°21.300'S	026°33.555'W
SON13	PS	2013-07-17	11:03	66°45.382'S	026°06.517'W
SON14	PS	2013-07-20	12:28	61°14.101'S	034°01.001'W
SON15	H3	2013-07-20	14:35	61°17.520'S	035°43.010'W
SON16	H3	2013-07-20	15:25	61°20.090'S	036°52.660'W
SON17	H4	2013-07-21	14:05	61°42.180'S	041°06.380'W
SON18	H5	2013-07-26	14:26	63°38.400'S	051°43.490'W
SON19	H6	2013-07-31	12:16	63°40.570'S	051°56.980'W
SON20	H6	2013-07-31	12:22	63°40.130'S	051°49.850'W

Buoy Nr		Date		Position	
SON21	H7	2013-08-02	16:40	63°44.900'S	051°21.950'W
SON22	PS	2013-08-02	23:06	63°45.472'S	051°24.027'W
SON23	PS	2013-08-08	06:15	60°07.711'S	054°00.071'W
SON24	PS	2013-08-08	21:24	59°00.343'S	056°10.424'W
SON25	PS	2013-08-09	01:08	59°29.926'S	057°18.890'W
SON26	PS	2013-08-09	05:12	58°00.003'S	058°27.244'W
SON27	PS	2013-08-09	05:29	58°01.910'S	058°23.531'W
SON28	PS	2013-08-09	09:07	58°30.032'S	059°36.512'W
SON29	PS	2013-08-09	09:07	58°30.032'S	059°36.512'W
SON30	PS	2013-08-09	13:18	57°00.041'S	060°46.283'W
SON31	PS	2013-08-09	13:38	57°01.890'S	060°42.794'W
SON32	PS	2013-08-09	16:08	57°19.804'S	060°13.747'W
SON33	PS	2013-08-09	16:12	57°20.190'S	060°13.026'W

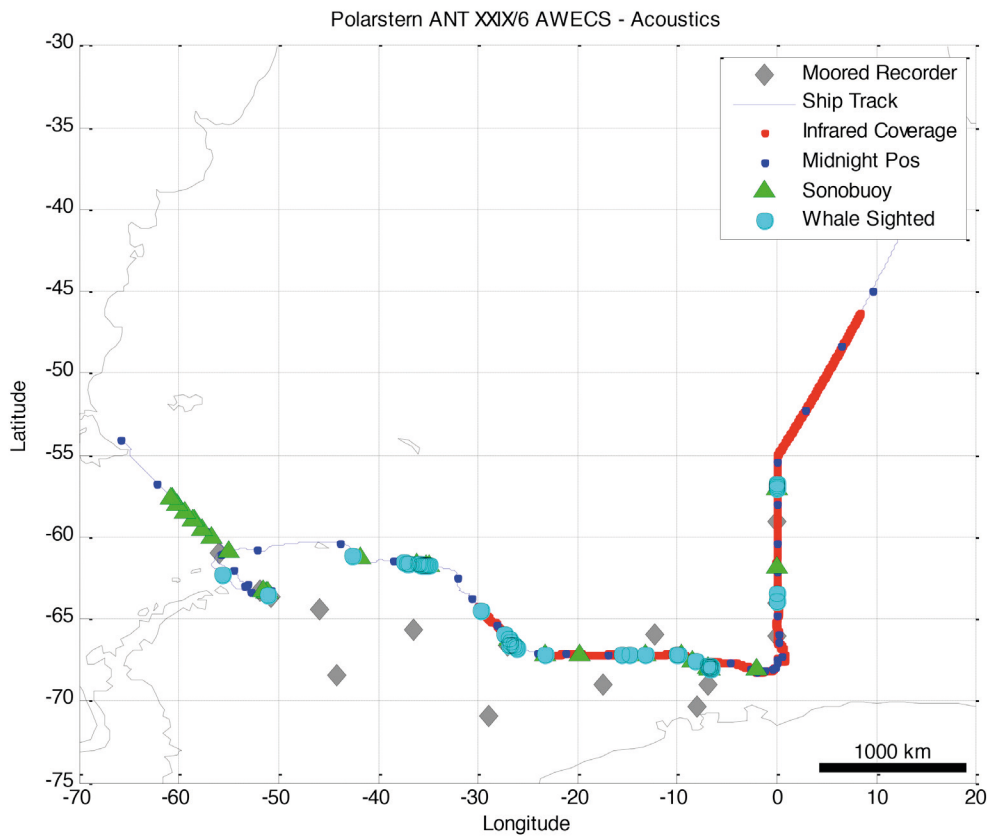


Fig. 9.1: Map of the cruise track showing operation of the FIRST/Navy in red, sonobuoy deployments in green and whale sightings in light blue. Moored long term audio recorders and the PALAOA observatory are shown as grey diamonds.

Preliminary and expected results

108 Antarctic minke whales, 12 humpback whales, 6 fin whales and 9 unrecognized whales were observed during the cruise and occasionally we could pick up the *bioduck* and other signals with the sonobuoys at the same time. Offline acoustic localisation using the DIFAR signal of the buoys will show, whether the signal can be affirmably attributed to the minkes. Additionally, humpback and blue whale vocalisations were also found in the recordings.

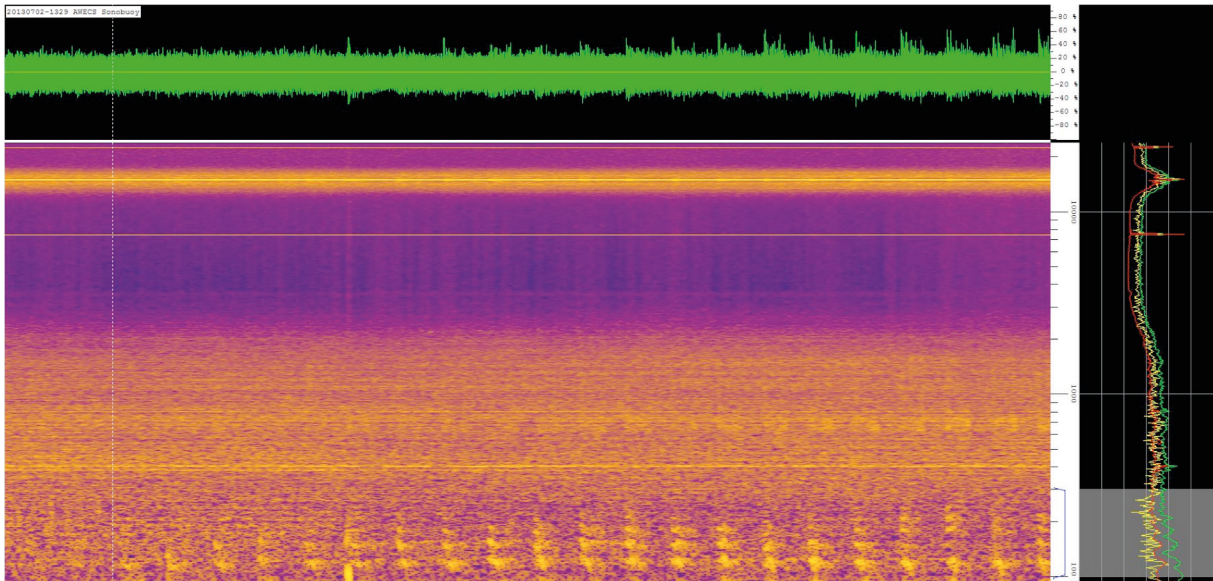


Fig. 9.2: Spectrogram of overlapping bioduck and downsweep signals



Fig. 9.3: Minke whale breaking through the ice

Data management

Recorded data will be made available via the PANGAEA Data Publisher for Earth & Environmental Science within one year or will be provided on request by the responsible PI: Lars Kindermann@awi.de

A.1 TEILNEHMENDE INSTITUTE / PARTICIPATING INSTITUTIONS

	Address
AAD	Australian Antarctic Division Channel Highway Kingston Tasmania 7050 / Australia
AWI	Alfred-Wegener-Institut Helmholtz-Zentrum für Polar- und Meeresforschung Postfach 120161 27515 Bremerhaven / Germany
BAS	British Antarctic Survey High Cross, Madingley Road CAMBRIDGE CB3 0ET / United Kingdom
Chalmers	Chalmers University of Technology SE-412 96 Gothenburg / Sweden
CIRES	Cooperative Institute for Research in Environmental Science University of Colorado at Boulder, 216 UCB Boulder, CO 80309-0216 / U.S.A.
DWD	Deutscher Wetterdienst Geschäftsbereich Wettervorhersage Seeschiffahrtsberatung Bernhard Nocht Str. 76 20359 Hamburg / Germany
FMI	Finnish Meteorological Institute Erik Palménin aukio 1, P.O.Box 503, FI-00101 Helsinki / Finland
GU	University of Gothenburg PO Box 100, SE-405 30 Gothenburg / Sweden
HELISERVICE	HeliService international GmbH Am Luneort 15 27572 Bremerhave / Germany
HU	Institute of Low Temperature Science, Hokkaido University, Sapporo 060-0819 / Japan

	Address
INIDEP	Instituto Nacional de Investigación y Desarrollo Pesquero Paseo Victoria Ocampo N°1 Escollera Norte B7602HSA Mar del Plata / Argentina
LGGE	Laboratoire de Glaciologie et Géophysique de l'Environnement 54 rue Molière 38402 - Saint Martin d'Hères cedex / France
LIPhy	Laboratoire interdisciplinaire de Physique: 140 Av. de la physique, BP 87 - 38402 Saint Martin d'Hères / France
Reederei Laeisz	Reederei F. Laeisz GmbH Brückenstr. 25 D-27568 Bremerhaven / Germany
TUBS	Institute of Aerospace Systems TU Braunschweig Hermann-Blenk-Str. 23 38108 Braunschweig / Germany
UH	University of Helsinki P.O. Box 33 (Fabianinkatu 18) FI-00014 University of Helsinki / Finland
UHB	Universität Bremen BreMarE – Bremen Marine Ecology Centre for Research & Education (FB 2) P.O. Box 330 440 D-28334 Bremen / Germany
UHD	Universität Heidelberg Grabengasse 1 69117 Heidelberg / Germany
ULB	Université libre de Bruxelles Avenue Franklin Roosevelt 50 1050 Bruxelles / Belgium
ULG	University of Liege Allée du 6 Août, 17 4000 Liège / Belgium

A.1 Teilnehmende Institute / Participating Institutions

	Address
UNAVACO	UNAVCO 6350 Nautilus Drive Boulder, CO 80301-5394 / USA
UTR	Universität Trier D-54286 Trier / Germany
WSL/SLF	WSL Institute for Snow and Avalanche Research Flüelastrasse 11 CH-7260 Davos Dorf / Schweiz
WWU	Westfälische Wilhelms-Universität Schlossplatz 2 D-48149 Münster / Germany

A.2 FAHRTTEILNEHMER / CRUISE PARTICIPANTS

Name/ Last name	Vorname/ First name	Institut/ Institute	Beruf/ Profession
Abrahamsson	Katarina	GU	Chemist
Ahnoff	Martin	GU	Chemist
Altstädter	Barbara	TUBS	Meteorologist
Arndt	Stefanie	AWI	Student, Meteorology
Buxmann	Joelle	UHD	Physicist
Cabreira	Ariel	INIDEP	PhD-Student, Hydroacoustics
De Jong	Jeroen	ULB	Engineer
Delille	Bruno	ULG	Biogeochemist
Dieckmann	Gerhard	AWI	Biologist
Frey	Markus	BAS	Atmospheric chemist
Gardfeldt	Katarina	Chalmers	Chemist
Granfors	Anna	GU	Chemist
Gussone	Nikolaus	WWU	Mineralogist
Hauer	Caroline	UHB	Biologist
Hendricks	Stefan	AWI	Physicist
Hoppmann	Mario	AWI	PhD-Student, Physics
Hunkeler	Prisca	AWI	Physicist
Janssens	Julie	AAD	PhD-Student, Biogeochemistry
Jonassen	Marius	FMI	Meteorologist
Jones	David	BAS	Engineer
Jourdain	Bruno	LGGE	Chemist
Kindermann	Lars	AWI	Physicist
Krüger	Matthias	AWI	Student
Lemke	Peter	AWI	Physicist
Leonard	Katherine	WSL/SLF, CIRES	Geologist
Luhtanen	Anne-Marie	UH	Microbiologist
Méjean	Guillaume	LIPhy	Physicist
Möllendorf	Carsten	HeliService	Heli. Technician
Müller	Thomas	HeliService	Heli. Technician
Nerentorp	Michelle	Chalmers	PhD-Student, Chemist
Nomura	Daiki	HU	Biogeochemist
Paul	Stephan	UTR	PhD-Student, Environ. Meteorol.

A.2 Fahrtteilnehmer / Cruise Participants

Name/ Last name	Vorname/ First name	Institut/ Institute	Beruf/ Profession
Rentsch	Harald	DWD	Meteorologist
Richter	Friedrich	AWI	Student, Meteorology
Rintala	Janne-Markus	UH	Microbiologist
Sartoris	Franz Josef	AWI	Biologist
Schwabe	Sascha	HeliService	Pilot
Scholtz	Andreas	TUBS	PhD Student, engineer
Schründer	Sabine	UHB	PhD-Student Biology
Schwegmann	Sandra	AWI	Physicist
Sonnabend	Hartmut	DWD	Met. Technician
Sutter	Johannes	AWI	PhD-Student, Physics
Tisler	Priit	FMI	Meteorologist
Tison	Jean-Louis	ULB	Biogeochemist/Glaciologist
Uhlig	Christiane	AWI	Biologist
von Neuhoff	Stephanie	AWI	Journalist
Wever	Nander	WSL/SLF	PhD-Student, Env. Engineering
White	Seth	UNAVCO	Engineer
Vaupel	Lars	HeliService	Pilot

A.3 SCHIFFSBESATZUNG / SHIP'S CREW

No.	Name	Rank
1	Pahl, Uwe	Master
2	Spielke, Steffen	1. Offc.
3	Ziemann, OIaf	Ch. Eng.
4	Hering, Igor	2. Offc.
5	Lauber, Felix	2. Offc.
6	Rackete, Carola	3. Offc.
7	Spilok, Norbert	Doctor
8	Koch, Georg	R. Offc.
9	Kotnik, Herbert	2. Eng.
10	Schnürch, Helmut	2. Eng.
11	Westphal, Henning	2. Eng.
12	Brehme, Andreas	Elec. Eng.
13	Dimmler, Werner	ELO
14	Feiertag, Thomas	ELO
15	Fröb, Martin	ELO
16	Winter, Andreas	ELO
17	Schröter, Renè	Boatsw.
18	Neisner, Winfried	Carpenter
19	Buzan, Gerd-Ekkeh.	A.B.
20	Clasen, Nils	A.B.
21	Hartwig-Lab.,Andreas	A.B.
22	Kreis, Reinhard	A.B.
23	Kretzschmar, Uwe	A.B.
24	Moser, Siegfried	A.B.
25	Schröder, Norbert	A.B.
26	Sedlak, Andreas	A.B.
27	Seibel, Sebastian	A.B.
28	Beth, Detlef	Storek.
29	Dinse, Horst	Mot-man
30	Fritz, Günter	Mot-man
31	Krösche, Eckard	Mot-man
32	Plehn, Markus	Mot-man
33	Watzel, Bernhard	Mot-man

A.3 Schiffsbesatzung / Ship's Crew

No.	Name	Rank
34	Fischer, Matthias	Cook
35	Tupy, Mario	Cooksmate
36	Völske, Thomas	Cooksmate
37	Dinse, Petra	1. Stwdess
38	Hennig, Christina	Stwdess/N.
39	Chen, Quan Lun	2. Steward
40	Hischke, Peggy	2. Stwdess
41	Hu, Guo Yong	2. Steward
42	Streit, Christina	2. Stwdess
43	Wartenberg, Irina	2. Stwdess
44	Ruan, Hui Guang	Laundrym.

A.4 STATIONSLISTE / STATION LIST PS81

Station	Date	Time	Gear	Action	Position Lat	Position Lon	Water depth [m]	Comment
PS81/478-1	12.6.2013	13:01	CTD/RO	in the water	46° 55.99' S	7° 48.59' E	1620.0	Teststation, SE32.1
PS81/478-1	12.6.2013	13:51	CTD/RO	on ground/ max depth	46° 56.17' S	7° 48.80' E	3374.5	SL=1676m
PS81/478-1	12.6.2013	13:51	CTD/RO	hoisting	46° 56.17' S	7° 48.80' E	3374.5	
PS81/478-1	12.6.2013	14:32	CTD/RO	on deck	46° 56.22' S	7° 49.05' E	1729.7	
PS81/479-1	14.6.2013	17:25	CTD/RO	in the water	55° 0.11' S	0° 0.14' W	1742.2	
PS81/479-1	14.6.2013	18:09	CTD/RO	on ground/ max depth	55° 0.04' S	0° 0.23' W	1747.5	SE32.1 1722m ausgesteckt
PS81/479-1	14.6.2013	18:54	CTD/RO	on deck	55° 0.02' S	0° 0.28' W	1754.2	
PS81/479-2	14.6.2013	19:02	MN	in the water	55° 0.04' S	0° 0.27' W	1755.2	
PS81/479-2	14.6.2013	19:45	MN	on ground/ max depth	54° 60.00' S	0° 0.47' W	1772.0	1492 m, EL 30
PS81/479-2	14.6.2013	20:33	MN	on deck	55° 0.10' S	0° 0.53' W	1719.7	
PS81/479-3	14.6.2013	20:44	BONGO	in the water	55° 0.12' S	0° 0.47' W	1720.0	
PS81/479-3	14.6.2013	21:06	BONGO	on ground/ max depth	55° 0.14' S	0° 0.61' W	1693.2	500m, 32.2
PS81/479-3	14.6.2013	21:27	BONGO	on deck	55° 0.18' S	0° 0.82' W	1692.0	
PS81/480-1	15.6.2013	3:00	CTD/RO	in the water	55° 59.99' S	0° 0.03' E	3746.2	SE32.1
PS81/480-1	15.6.2013	4:16	CTD/RO	on ground/ max depth	56° 0.00' S	0° 0.09' W	3853.7	3814 m, SE 32.1
PS81/480-1	15.6.2013	5:29	CTD/RO	on deck	55° 59.99' S	0° 0.08' W	3803.7	
PS81/481-1	15.6.2013	11:15	CTD/RO	in the water	57° 0.03' S	0° 0.05' E	3684.7	
PS81/481-1	15.6.2013	12:28	CTD/RO	on ground/ max depth	57° 0.23' S	0° 0.02' E	3624.5	SL=3614m
PS81/481-1	15.6.2013	12:28	CTD/RO	hoisting	57° 0.23' S	0° 0.02' E	3624.5	
PS81/481-1	15.6.2013	13:42	CTD/RO	on deck	57° 0.19' S	0° 0.11' E	3620.5	
PS81/481-2	15.6.2013	13:54	MN	in the water	57° 0.22' S	0° 0.14' E	3620.2	EL30
PS81/481-2	15.6.2013	14:59	MN	on ground/ max depth	57° 0.26' S	0° 0.48' E	3706.5	SL=1994m
PS81/481-2	15.6.2013	14:59	MN	hoisting	57° 0.26' S	0° 0.48' E	3706.5	
PS81/481-2	15.6.2013	15:59	MN	on deck	57° 0.14' S	0° 1.24' E	3699.0	
PS81/481-3	15.6.2013	16:09	SON	in the water	57° 0.09' S	0° 1.05' E	3707.5	
PS81/481-3	15.6.2013	16:09	SON	on ground/ max depth	57° 0.09' S	0° 1.05' E	3707.5	
PS81/482-1	15.6.2013	22:03	CTD/RO	in the water	57° 59.89' S	0° 0.05' W	4550.0	
PS81/482-1	15.6.2013	23:39	CTD/RO	on ground/ max depth	57° 60.00' S	0° 0.05' W	4541.5	4559m, 32.1
PS81/482-1	15.6.2013	23:39	CTD/RO	hoisting	57° 60.00' S	0° 0.05' W	4541.5	

A.4 Stationsliste / Station List PS81

Station	Date	Time	Gear	Action	Position Lat	Position Lon	Water depth [m]	Comment
PS81/482-1	16.6.2013	1:04	CTD/RO	on deck	57° 59.82' S	0° 0.78' E	4513.5	
PS81/483-1	16.6.2013	7:19	CTD/RO	in the water	59° 0.11' S	0° 0.08' E	4608.2	
PS81/483-1	16.6.2013	8:50	CTD/RO	on ground/ max depth	59° 0.08' S	0° 0.30' E	4593.0	4625m, 32.1
PS81/483-1	16.6.2013	8:51	CTD/RO	hoisting	59° 0.08' S	0° 0.30' E	4601.2	
PS81/483-1	16.6.2013	10:19	CTD/RO	on deck	59° 0.13' S	0° 0.07' E	4608.5	
PS81/483-2	16.6.2013	10:30	MN	in the water	59° 0.16' S	0° 0.10' W	4616.5	
PS81/483-2	16.6.2013	11:33	MN	on ground/ max depth	59° 0.19' S	0° 0.36' E	4601.5	2000m, 30
PS81/483-2	16.6.2013	11:34	MN	hoisting	59° 0.19' S	0° 0.36' E	4602.0	
PS81/483-2	16.6.2013	12:32	MN	on deck	59° 0.20' S	0° 0.60' E	4594.2	
PS81/484-1	16.6.2013	18:24	CTD/RO	in the water	59° 59.99' S	0° 0.01' E	5364.5	
PS81/484-1	16.6.2013	20:10	CTD/RO	on ground/ max depth	60° 0.23' S	0° 0.72' E	5376.2	5439m, 32.1
PS81/484-1	16.6.2013	21:44	CTD/RO	on deck	60° 0.24' S	0° 0.18' E	5364.5	
PS81/485-1	17.6.2013	3:40	CTD/RO	in the water	60° 59.92' S	0° 0.07' W	5397.7	SE32.1
PS81/485-1	17.6.2013	5:28	CTD/RO	on ground/ max depth	60° 59.98' S	0° 0.35' W	5390.7	5447 m, SE 32.1
PS81/485-1	17.6.2013	6:56	CTD/RO	on deck	60° 59.95' S	0° 0.19' W	5390.5	
PS81/485-2	17.6.2013	7:06	MN	in the water	60° 59.89' S	0° 0.21' W	5390.7	
PS81/485-2	17.6.2013	8:10	MN	on ground/ max depth	60° 59.95' S	0° 0.24' W	5390.2	1983m, 30
PS81/485-2	17.6.2013	9:11	MN	on deck	60° 59.95' S	0° 0.29' W	5391.0	
PS81/486-1	17.6.2013	13:44	ICE	in the water	61° 31.70' S	0° 7.17' W	5084.7	Schlauch- boot
PS81/486-1	17.6.2013	13:46	ICE	on deck	61° 31.68' S	0° 7.23' W	5080.2	Schlauch- boot
PS81/486-1	17.6.2013	13:52	ICE	in the water	61° 31.66' S	0° 7.42' W	5061.2	Schlauch- boot
PS81/486-1	17.6.2013	13:54	ICE	on deck	61° 31.67' S	0° 7.47' W	5058.2	
PS81/486-1	17.6.2013	14:00	ICE	in the water	61° 31.68' S	0° 7.64' W	5046.2	Schlauch- boot
PS81/486-1	17.6.2013	14:05	ICE	on deck	61° 31.68' S	0° 7.77' W	5018.0	Schlauch- boot
PS81/486-1	17.6.2013	14:05	ICE	at surface	61° 31.68' S	0° 7.77' W	5018.0	Mummy-chair
PS81/486-1	17.6.2013	14:37	ICE	on deck	61° 31.45' S	0° 9.05' W	4998.0	Mummy chair
PS81/486-1	17.6.2013	14:44	ICE	in the water	61° 31.43' S	0° 9.24' W	5015.5	Eiskorb
PS81/486-1	17.6.2013	14:45	ICE	on ground/ max depth	61° 31.42' S	0° 9.27' W	5015.0	
PS81/486-1	17.6.2013	14:47	ICE	on deck	61° 31.41' S	0° 9.32' W	5019.7	Eiskorb
PS81/486-1	17.6.2013	14:52	ICE	in the water	61° 31.39' S	0° 9.46' W	5032.5	Eiskorb

Station	Date	Time	Gear	Action	Position Lat	Position Lon	Water depth [m]	Comment
PS81/486-1	17.6.2013	14:54	ICE	on ground/ max depth	61° 31.38' S	0° 9.52' W	5038.2	
PS81/486-1	17.6.2013	14:56	ICE	on deck	61° 31.37' S	0° 9.58' W	5045.0	Eiskorb
PS81/486-1	17.6.2013	15:07	ICE	in the water	61° 31.31' S	0° 9.88' W	5106.7	
PS81/486-1	17.6.2013	15:11	ICE	on deck	61° 31.29' S	0° 9.98' W	5114.7	Eiskorb
PS81/487-1	17.6.2013	17:30	SON	in the water	61° 50.02' S	0° 0.10' E	5367.5	
PS81/487-1	17.6.2013	17:30	SON	on ground/ max depth	61° 50.02' S	0° 0.10' E	5367.5	
PS81/487-2	17.6.2013	19:05	CTD/RO	in the water	61° 59.74' S	0° 0.03' E	5371.5	
PS81/487-2	17.6.2013	20:53	CTD/RO	on ground/ max depth	61° 58.59' S	0° 1.63' W	5378.7	5580m, 32.1
PS81/487-2	17.6.2013	22:21	CTD/RO	on deck	61° 57.58' S	0° 2.81' W	5372.2	
PS81/488-1	18.6.2013	7:50	CTD/RO	in the water	63° 0.23' S	0° 0.78' E	5312.5	
PS81/488-1	18.6.2013	9:38	CTD/RO	on ground/ max depth	62° 58.93' S	0° 0.63' E	5313.0	5581m, 32.1
PS81/488-1	18.6.2013	11:18	CTD/RO	on deck	62° 57.55' S	0° 0.32' E	5319.5	
PS81/488-2	18.6.2013	11:36	ICE	action	62° 57.53' S	0° 0.16' E	5319.2	Mummy-chair wird über Eis bewegt
PS81/488-2	18.6.2013	13:36	ICE	on deck	62° 55.97' S	0° 0.28' W	5317.0	Mummy-chair
PS81/488-2	18.6.2013	13:40	ICE	in the water	62° 55.92' S	0° 0.29' W	5316.5	Mummy-chair
PS81/488-2	18.6.2013	14:06	ICE	on deck	62° 55.59' S	0° 0.38' W	5318.2	Mummy-chair
PS81/488-2	18.6.2013	14:12	ICE	in the water	62° 55.52' S	0° 0.40' W	5317.2	Mummy-chair
PS81/488-2	18.6.2013	15:16	ICE	on deck	62° 54.76' S	0° 0.57' W	5319.5	Mummy-chair
PS81/488-2	18.6.2013	15:19	ICE	action	62° 54.72' S	0° 0.58' W	5318.7	Mummy-chair on ice
PS81/488-2	18.6.2013	15:27	ICE	on ground/ max depth	62° 54.64' S	0° 0.60' W	5319.5	Messboje auf dem Eis
PS81/488-2	18.6.2013	15:30	ICE	on deck	62° 54.60' S	0° 0.60' W	5319.2	Mummy-chair
PS81/488-2	18.6.2013	15:40	ICE	action	62° 54.50' S	0° 0.62' W	5319.2	Mummy-chair on ice
PS81/488-2	18.6.2013	16:04	ICE	on deck	62° 54.24' S	0° 0.65' W	5319.0	
PS81/488-2	18.6.2013	16:18	ICE	action	62° 54.05' S	0° 0.55' W	5319.5	Mummy chair on ice
PS81/488-2	18.6.2013	16:50	ICE	on deck	62° 53.73' S	0° 0.55' W	5320.0	
PS81/488-3	18.6.2013	17:12	MN	in the water	62° 53.49' S	0° 0.20' W	5320.2	
PS81/488-3	18.6.2013	18:23	MN	on ground/ max depth	62° 52.80' S	0° 0.04' E	5322.7	EL30 2078m ausgesteckt
PS81/488-3	18.6.2013	19:28	MN	on deck	62° 52.14' S	0° 0.36' E	5324.0	
PS81/489-1	19.6.2013	5:16	CTD/RO	in the water	63° 57.80' S	0° 1.35' W	5206.0	
PS81/489-1	19.6.2013	7:07	CTD/RO	on ground/ max depth	63° 56.98' S	0° 1.44' W	5208.5	5281 m, SE 32.1

A.4 Stationsliste / Station List PS81

Station	Date	Time	Gear	Action	Position Lat	Position Lon	Water depth [m]	Comment
PS81/489-1	19.6.2013	8:44	CTD/RO	on deck	63° 56.18' S	0° 1.41' W	5210.2	
PS81/489-2	19.6.2013	9:12	ICE	action	63° 56.09' S	0° 1.53' W	5209.7	Mummy-chair auf Eis abgesetzt
PS81/489-2	19.6.2013	9:56	ICE	on deck	63° 55.70' S	0° 1.52' W	5210.5	
PS81/489-2	19.6.2013	10:03	ICE	action	63° 55.64' S	0° 1.52' W	5211.0	Mummy-chair auf dem Eis
PS81/489-2	19.6.2013	11:02	ICE	on deck	63° 55.11' S	0° 1.55' W	5213.0	
PS81/489-2	19.6.2013	11:17	ICE	action	63° 54.97' S	0° 1.58' W	5213.0	Mummy-chair auf Eis
PS81/489-2	19.6.2013	12:36	ICE	on deck	63° 54.25' S	0° 1.78' W	5213.5	Mummy-chair
PS81/489-2	19.6.2013	12:45	ICE	in the water	63° 54.18' S	0° 1.81' W	5214.0	Mummy-chair
PS81/489-2	19.6.2013	13:33	ICE	on deck	63° 53.79' S	0° 1.93' W	5214.7	Mummy-chair
PS81/489-2	19.6.2013	13:39	ICE	action	63° 53.74' S	0° 1.95' W	5214.7	Mummy-chair on ice
PS81/489-2	19.6.2013	14:01	ICE	on deck	63° 53.58' S	0° 2.07' W	5215.5	Mummy-chair
PS81/489-2	19.6.2013	14:08	ICE	action	63° 53.52' S	0° 2.11' W	5215.2	Mummy-chair on ice
PS81/489-2	19.6.2013	15:24	ICE	on ground/ max depth	63° 53.07' S	0° 2.75' W	5215.5	
PS81/489-2	19.6.2013	15:24	ICE	on deck	63° 53.07' S	0° 2.75' W	5215.5	
PS81/490-1	20.6.2013	2:07	CTD/RO	in the water	64° 59.96' S	0° 0.05' E	3737.2	SE32.1
PS81/490-1	20.6.2013	3:22	CTD/RO	on ground/ max depth	64° 59.54' S	0° 0.07' W	3729.2	SL=3757m
PS81/490-1	20.6.2013	3:22	CTD/RO	hoisting	64° 59.54' S	0° 0.07' W	3729.2	
PS81/490-1	20.6.2013	4:30	CTD/RO	on deck	64° 59.05' S	0° 0.34' W	3727.5	
PS81/490-2	20.6.2013	4:43	MN	in the water	64° 58.85' S	0° 0.32' W	3726.5	
PS81/490-2	20.6.2013	5:45	MN	on ground/ max depth	64° 58.62' S	0° 0.16' W	3722.7	1986 m, EL 30
PS81/490-2	20.6.2013	6:43	MN	on deck	64° 58.27' S	0° 0.04' E	3718.0	
PS81/491-1	20.6.2013	9:42	ICE	action	65° 10.79' S	0° 2.99' W	4074.0	Mummy-chair auf Eis
PS81/491-1	20.6.2013	10:50	ICE	on deck	65° 10.31' S	0° 3.29' W	4071.5	
PS81/491-1	20.6.2013	11:04	ICE	action	65° 10.21' S	0° 3.36' W	4070.5	Mummy-chair auf Eis
PS81/491-1	20.6.2013	12:12	ICE	on ground/ max depth	65° 9.71' S	0° 3.73' W	4037.7	alles an Deck
PS81/492-1	20.6.2013	23:29	CTD/RO	in the water	65° 59.47' S	0° 10.65' E	3504.0	
PS81/492-1	21.6.2013	0:41	CTD/RO	on ground/ max depth	65° 58.57' S	0° 10.88' E	3527.0	SL=3593m
PS81/492-1	21.6.2013	0:42	CTD/RO	hoisting	65° 58.56' S	0° 10.89' E	3527.0	
PS81/492-1	21.6.2013	1:48	CTD/RO	on deck	65° 57.78' S	0° 10.95' E	3561.7	

Station	Date	Time	Gear	Action	Position Lat	Position Lon	Water depth [m]	Comment
PS81/492-2	21.6.2013	2:02	ICE	action	65° 57.62' S	0° 11.10' E	3562.0	Mummy-chair on ice
PS81/492-2	21.6.2013	2:16	ICE	in the water	65° 57.47' S	0° 11.09' E	3564.0	Buoy
PS81/492-2	21.6.2013	2:16	ICE	on ground/ max depth	65° 57.47' S	0° 11.09' E	3564.0	Boje
PS81/492-2	21.6.2013	2:19	ICE	on deck	65° 57.44' S	0° 11.09' E	3563.2	Mummy-chair
PS81/493-1	21.6.2013	10:10	CTD/RO	in the water	66° 28.91' S	0° 1.54' E	4478.7	
PS81/493-1	21.6.2013	10:13	CTD/RO	on deck	66° 28.89' S	0° 1.52' E	4479.0	Maschine unklar
PS81/493-1	21.6.2013	10:36	CTD/RO	in the water	66° 28.77' S	0° 1.69' E	4483.5	
PS81/493-1	21.6.2013	12:13	CTD/RO	on ground/ max depth	66° 28.18' S	0° 2.29' E	4476.7	SL4518m
PS81/493-1	21.6.2013	12:14	CTD/RO	hoisting	66° 28.17' S	0° 2.29' E	4476.7	
PS81/493-1	21.6.2013	13:35	CTD/RO	on deck	66° 27.68' S	0° 2.67' E	4494.2	
PS81/493-2	21.6.2013	14:23	ICE	in the water	66° 27.85' S	0° 5.73' E	4403.2	stations- beginn
PS81/493-2	22.6.2013	0:29	ICE	on ground/ max depth	66° 25.96' S	0° 8.72' E	4195.7	
PS81/493-2	22.6.2013	0:29	ICE	on deck	66° 25.96' S	0° 8.72' E	4195.7	Ende der Station
PS81/493-3	22.6.2013	0:43	MN	in the water	66° 25.92' S	0° 8.86' E	4192.7	EL30
PS81/493-3	22.6.2013	1:41	MN	on ground/ max depth	66° 25.89' S	0° 9.41' E	4190.5	SL=1983m
PS81/493-3	22.6.2013	1:41	MN	hoisting	66° 25.89' S	0° 9.41' E	4190.5	
PS81/493-3	22.6.2013	2:41	MN	on deck	66° 25.85' S	0° 9.79' E	4191.7	
PS81/494-1	22.6.2013	14:00	CTD/RO	in the water	66° 59.79' S	0° 35.95' E	4672.0	SE32.1
PS81/494-1	22.6.2013	15:34	CTD/RO	on ground/ max depth	66° 59.78' S	0° 35.66' E	4672.0	SL=4707m
PS81/494-1	22.6.2013	15:34	CTD/RO	hoisting	66° 59.78' S	0° 35.66' E	4672.0	
PS81/494-1	22.6.2013	16:51	CTD/RO	on deck	66° 59.82' S	0° 35.43' E	4672.7	
PS81/495-1	23.6.2013	5:40	CTD/RO	in the water	67° 30.07' S	0° 51.03' E	4639.5	
PS81/495-1	23.6.2013	7:17	CTD/RO	on ground/ max depth	67° 30.57' S	0° 50.69' E	4637.5	4681 m, SE 32.1
PS81/495-1	23.6.2013	7:18	CTD/RO	hoisting	67° 30.57' S	0° 50.69' E	4637.5	
PS81/495-1	23.6.2013	8:35	CTD/RO	on deck	67° 31.01' S	0° 50.39' E	4635.5	
PS81/495-2	23.6.2013	8:46	MN	in the water	67° 31.07' S	0° 50.35' E	4638.0	
PS81/495-2	23.6.2013	9:48	MN	on ground/ max depth	67° 31.43' S	0° 50.17' E	4635.2	1993m, 30
PS81/495-2	23.6.2013	9:49	MN	hoisting	67° 31.44' S	0° 50.16' E	4635.5	
PS81/495-2	23.6.2013	10:46	MN	on deck	67° 31.76' S	0° 50.05' E	4634.2	
PS81/495-3	23.6.2013	11:04	ICE	action	67° 32.29' S	0° 49.85' E	4633.7	Mummy- chair auf Eis abgesetzt

A.4 Stationsliste / Station List PS81

Station	Date	Time	Gear	Action	Position Lat	Position Lon	Water depth [m]	Comment
PS81/495-3	23.6.2013	11:22	ICE	on ground/ max depth	67° 32.39' S	0° 49.82' E	4632.0	Boje ausgesetzt
PS81/495-3	23.6.2013	11:25	ICE	on deck	67° 32.41' S	0° 49.82' E	4631.7	Mummy-chair
PS81/496-1	24.6.2013	8:23	ICE	action	67° 26.76' S	0° 1.95' E	4643.0	Eisgangway ausgebracht
PS81/496-1	24.6.2013	8:35	ICE	on ground/ max depth	67° 26.80' S	0° 1.81' E	4642.7	Wissen- schaffler auf Eis
PS81/496-1	24.6.2013	18:18	ICE	action	67° 30.32' S	0° 7.17' W	4650.2	Stations- ende
PS81/496-1	24.6.2013	18:36	ICE	on deck	67° 30.54' S	0° 8.55' W	4650.5	Gangway an Deck
PS81/497-1	26.6.2013	11:20	ICE	action	68° 2.37' S	0° 20.22' W	4457.2	Eisgangway ausgebracht
PS81/497-1	26.6.2013	14:20	ICE	in the water	68° 3.58' S	0° 20.31' W	4457.2	
PS81/497-1	26.6.2013	14:20	ICE	on ground/ max depth	68° 3.58' S	0° 20.31' W	4457.2	
PS81/497-1	26.6.2013	14:20	ICE	on deck	68° 3.58' S	0° 20.31' W	4457.2	Ende der Eis- station, Alle Wissen- schaffler und Besatzungs- mitglieder an Bord
PS81/498-1	30.6.2013	0:06	CTD/RO	in the water	68° 0.82' S	2° 42.53' W	3976.7	SE32.1
PS81/498-1	30.6.2013	1:27	CTD/RO	on ground/ max depth	68° 0.81' S	2° 42.86' W	3979.5	SL=3991m
PS81/498-1	30.6.2013	1:29	CTD/RO	hoisting	68° 0.81' S	2° 42.87' W	3979.7	
PS81/498-1	30.6.2013	2:33	CTD/RO	on deck	68° 0.79' S	2° 43.14' W	3982.7	
PS81/498-2	30.6.2013	2:40	MN	in the water	68° 0.79' S	2° 43.17' W	3983.0	EL30
PS81/498-2	30.6.2013	3:11	MN	on ground/ max depth	68° 0.78' S	2° 43.31' W	3984.5	SL=1000m
PS81/498-2	30.6.2013	3:11	MN	hoisting	68° 0.78' S	2° 43.31' W	3984.5	
PS81/498-2	30.6.2013	3:39	MN	on deck	68° 0.78' S	2° 43.44' W	3985.7	
PS81/498-3	30.6.2013	3:43	MN	in the water	68° 0.78' S	2° 43.47' W	3986.0	EL30
PS81/498-3	30.6.2013	4:42	MN	on ground/ max depth	68° 0.79' S	2° 43.75' W	3987.7	2000 m, EL 30
PS81/498-3	30.6.2013	4:43	MN	hoisting	68° 0.79' S	2° 43.76' W	3987.5	
PS81/498-3	30.6.2013	5:36	MN	on deck	68° 0.81' S	2° 44.05' W	3992.5	
PS81/499-1	30.6.2013	23:09	CTD/RO	in the water	67° 42.03' S	4° 38.97' W	4666.2	
PS81/499-1	1.7.2013	0:43	CTD/RO	on ground/ max depth	67° 41.88' S	4° 40.54' W	4669.2	SL=4718m
PS81/499-1	1.7.2013	0:44	CTD/RO	hoisting	67° 41.87' S	4° 40.56' W	4669.5	
PS81/499-1	1.7.2013	2:02	CTD/RO	on deck	67° 41.64' S	4° 41.49' W	4659.5	
PS81/499-2	1.7.2013	2:16	MN	in the water	67° 41.59' S	4° 41.61' W	4660.5	EL30

Station	Date	Time	Gear	Action	Position Lat	Position Lon	Water depth [m]	Comment
PS81/499-2	1.7.2013	2:21	MN	on deck	67° 41.58' S	4° 41.66' W	4660.2	
PS81/499-2	1.7.2013	2:27	MN	in the water	67° 41.55' S	4° 41.73' W	4661.0	
PS81/499-2	1.7.2013	3:25	MN	on ground/ max depth	67° 41.34' S	4° 42.22' W	4668.0	SL=1989m
PS81/499-2	1.7.2013	3:25	MN	hoisting	67° 41.34' S	4° 42.22' W	4668.0	
PS81/499-2	1.7.2013	4:23	MN	on deck	67° 41.15' S	4° 42.59' W	4672.5	
PS81/500-1	2.7.2013	11:38	BUOY	in the water	67° 57.63' S	6° 53.62' W	4802.7	
PS81/500-1	2.7.2013	11:38	BUOY	on ground/ max depth	67° 57.63' S	6° 53.62' W	4802.7	
PS81/500-2	2.7.2013	13:55	BUOY	in the water	68° 1.51' S	6° 43.01' W	4790.7	
PS81/500-2	2.7.2013	13:55	BUOY	on ground/ max depth	68° 1.51' S	6° 43.01' W	4790.7	
PS81/500-3	2.7.2013	15:36	CTD/RO	in the water	68° 1.86' S	6° 40.32' W	4783.7	EL32.1
PS81/500-3	2.7.2013	17:12	CTD/RO	on ground/ max depth	68° 1.62' S	6° 40.48' W	4784.7	4824 m, SE 32.1
PS81/500-3	2.7.2013	17:13	CTD/RO	hoisting	68° 1.62' S	6° 40.49' W	4785.0	
PS81/500-3	2.7.2013	18:36	CTD/RO	on deck	68° 1.31' S	6° 40.52' W	4792.5	
PS81/500-4	2.7.2013	18:50	MN	in the water	68° 1.24' S	6° 40.50' W	4796.0	
PS81/500-4	2.7.2013	18:54	MN	hoisting	68° 1.22' S	6° 40.50' W	4795.5	
PS81/500-4	2.7.2013	18:58	MN	on deck	68° 1.20' S	6° 40.49' W	4796.5	
PS81/500-4	2.7.2013	19:12	MN	in the water	68° 1.13' S	6° 40.47' W	4798.2	
PS81/500-4	2.7.2013	20:12	MN	on ground/ max depth	68° 0.84' S	6° 40.42' W	4799.2	1987m, 30
PS81/500-4	2.7.2013	20:12	MN	hoisting	68° 0.84' S	6° 40.42' W	4799.2	
PS81/500-4	2.7.2013	21:13	MN	on deck	68° 0.55' S	6° 40.38' W	4798.0	
PS81/500-5	3.7.2013	8:00	ICE	action	67° 58.12' S	6° 39.40' W	4804.5	Schiff in Scholle gestoppt
PS81/500-5	3.7.2013	8:32	ICE	action	67° 58.01' S	6° 39.33' W	4804.2	Landgang hergestellt
PS81/500-5	4.7.2013	13:52	ICE	action	67° 55.19' S	6° 44.35' W	4813.0	Risse in der Scholle zwischen Schiff und Stationen, Teil- evakuierung angeordnet
PS81/500-5	5.7.2013	20:52	ICE	on ground/ max depth	67° 48.94' S	7° 0.55' W	4832.0	
PS81/500-5	5.7.2013	20:52	ICE	on deck	67° 48.94' S	7° 0.55' W	4832.0	Alle Geräte an Deck
PS81/501-1	6.7.2013	11:19	BUOY	in the water	67° 37.05' S	8° 13.46' W	4875.7	Walakkustik

A.4 Stationsliste / Station List PS81

Station	Date	Time	Gear	Action	Position Lat	Position Lon	Water depth [m]	Comment
PS81/501-1	6.7.2013	11:19	BUOY	on ground/ max depth	67° 37.05' S	8° 13.46' W	4875.7	
PS81/501-2	7.7.2013	13:14	BUOY	in the water	67° 12.06' S	9° 36.28' W	4914.7	
PS81/501-2	7.7.2013	13:14	BUOY	on ground/ max depth	67° 12.06' S	9° 36.28' W	4914.7	
PS81/502-1	7.7.2013	15:06	CTD/RO	in the water	67° 12.73' S	10° 0.75' W	4952.0	SE32.1
PS81/502-1	7.7.2013	16:44	CTD/RO	on ground/ max depth	67° 12.36' S	10° 0.88' W	4951.5	5000 m, SE 32.1
PS81/502-1	7.7.2013	18:10	CTD/RO	on deck	67° 12.17' S	10° 1.00' W	4948.7	
PS81/502-2	7.7.2013	18:23	MN	in the water	67° 12.15' S	10° 1.01' W	4948.5	
PS81/502-2	7.7.2013	19:25	MN	on ground/ max depth	67° 12.11' S	10° 0.99' W	4948.2	1983 m, EL 30
PS81/502-2	7.7.2013	19:25	MN	hoisting	67° 12.11' S	10° 0.99' W	4948.2	
PS81/502-2	7.7.2013	20:22	MN	on deck	67° 12.11' S	10° 0.80' W	4948.2	
PS81/502-3	7.7.2013	20:41	BONGO	in the water	67° 12.12' S	10° 0.71' W	4948.5	
PS81/502-3	7.7.2013	21:04	BONGO	on ground/ max depth	67° 12.13' S	10° 0.58' W	4948.5	500m, 32.2
PS81/502-3	7.7.2013	21:25	BONGO	on deck	67° 12.15' S	10° 0.43' W	4948.7	
PS81/502-4	7.7.2013	22:00	BUOY	action	67° 11.96' S	10° 1.54' W	4945.7	Mummy-chair auf Eis
PS81/502-4	7.7.2013	22:11	BUOY	on ground/ max depth	67° 11.97' S	10° 1.41' W	4946.2	Boje abgesetzt
PS81/502-4	7.7.2013	22:14	BUOY	on deck	67° 11.97' S	10° 1.37' W	4946.2	
PS81/503-1	8.7.2013	10:44	SON	in the water	67° 9.59' S	13° 12.65' W	4983.0	
PS81/503-1	8.7.2013	10:44	SON	on ground/ max depth	67° 9.59' S	13° 12.65' W	4983.0	
PS81/503-2	8.7.2013	11:50	ICE	action	67° 11.21' S	13° 13.49' W	4984.0	Landgang hergestellt
PS81/503-2	8.7.2013	23:39	ICE	on ground/ max depth	67° 11.87' S	13° 14.86' W	4983.5	Alle a. B.
PS81/503-2	8.7.2013	23:45	ICE	on deck	67° 11.88' S	13° 14.87' W	4983.5	Gangway
PS81/503-3	9.7.2013	1:45	CTD/RO	in the water	67° 12.07' S	13° 16.25' W	4983.0	SE32.1
PS81/503-3	9.7.2013	3:26	CTD/RO	on ground/ max depth	67° 12.27' S	13° 16.40' W	4982.5	SL=5033m
PS81/503-3	9.7.2013	3:27	CTD/RO	hoisting	67° 12.27' S	13° 16.40' W	4984.7	
PS81/503-3	9.7.2013	5:03	CTD/RO	on deck	67° 12.50' S	13° 16.85' W	4981.2	
PS81/503-4	9.7.2013	5:09	MN	in the water	67° 12.52' S	13° 16.89' W	4981.2	
PS81/503-4	9.7.2013	6:06	MN	on ground/ max depth	67° 12.69' S	13° 17.37' W	4981.0	2000 m, EL 30
PS81/503-4	9.7.2013	6:07	MN	hoisting	67° 12.69' S	13° 17.37' W	4981.0	
PS81/503-4	9.7.2013	6:57	MN	on deck	67° 12.86' S	13° 17.91' W	4981.5	
PS81/503-5	9.7.2013	7:03	BONGO	in the water	67° 12.88' S	13° 17.97' W	4981.7	

Station	Date	Time	Gear	Action	Position Lat	Position Lon	Water depth [m]	Comment
PS81/503-5	9.7.2013	7:23	BONGO	on ground/ max depth	67° 12.95' S	13° 18.22' W	4981.7	500 m, SE 32.2
PS81/503-5	9.7.2013	7:23	BONGO	hoisting	67° 12.95' S	13° 18.22' W	4981.7	
PS81/503-5	9.7.2013	7:42	BONGO	on deck	67° 13.03' S	13° 18.46' W	4982.0	
PS81/504-1	9.7.2013	19:39	CTD/RO	in the water	67° 10.85' S	16° 58.86' W	4981.2	
PS81/504-1	9.7.2013	21:11	CTD/RO	on ground/ max depth	67° 10.98' S	16° 59.97' W	4966.2	5015m, 30.1
PS81/504-1	9.7.2013	21:11	CTD/RO	hoisting	67° 10.98' S	16° 59.97' W	4966.2	
PS81/504-1	9.7.2013	22:37	CTD/RO	on deck	67° 11.10' S	17° 0.86' W	4966.0	
PS81/504-2	9.7.2013	22:43	MN	in the water	67° 11.10' S	17° 0.91' W	4966.2	
PS81/504-2	9.7.2013	23:50	MN	on ground/ max depth	67° 11.22' S	17° 1.49' W	4967.0	2000m, 30
PS81/504-2	9.7.2013	23:50	MN	hoisting	67° 11.22' S	17° 1.49' W	4967.0	
PS81/504-2	10.7.2013	0:51	MN	on deck	67° 11.33' S	17° 1.89' W	4966.7	
PS81/504-3	10.7.2013	1:12	BUOY	in the water	67° 11.36' S	17° 2.35' W	4966.5	Mummy-chair
PS81/504-3	10.7.2013	1:23	BUOY	on ground/ max depth	67° 11.38' S	17° 2.40' W	4966.5	Boje im eis
PS81/504-3	10.7.2013	1:27	BUOY	on deck	67° 11.39' S	17° 2.42' W	4966.5	Mummy-chair
PS81/505-1	10.7.2013	12:33	SON	in the water	67° 9.06' S	19° 48.08' W	4954.5	
PS81/505-1	10.7.2013	12:34	SON	on ground/ max depth	67° 9.06' S	19° 48.10' W	4954.2	
PS81/505-2	10.7.2013	13:47	CTD/RO	in the water	67° 12.01' S	19° 59.00' W	4949.7	SE32.1
PS81/505-2	10.7.2013	15:29	CTD/RO	on ground/ max depth	67° 11.96' S	19° 59.30' W	4951.0	SL=4992m
PS81/505-2	10.7.2013	15:30	CTD/RO	hoisting	67° 11.96' S	19° 59.31' W	4950.7	
PS81/505-2	10.7.2013	16:57	CTD/RO	on deck	67° 11.93' S	19° 59.51' W	4951.2	
PS81/505-3	10.7.2013	17:03	MN	in the water	67° 11.93' S	19° 59.53' W	4950.5	
PS81/505-3	10.7.2013	18:04	MN	on ground/ max depth	67° 11.90' S	19° 59.66' W	4951.5	EL30 1983m ausgesteckt
PS81/505-3	10.7.2013	18:05	MN	hoisting	67° 11.90' S	19° 59.67' W	4952.2	
PS81/505-3	10.7.2013	19:02	MN	on deck	67° 11.86' S	19° 59.82' W	4951.5	
PS81/506-1	11.7.2013	9:30	ICE	action	67° 11.88' S	23° 3.38' W	4908.2	Gangway über
PS81/506-1	11.7.2013	9:38	ICE	action	67° 11.85' S	23° 3.34' W	4909.2	Wissen- schaffler auf dem Eis
PS81/506-1	15.7.2013	12:41	ICE	on ground/ max depth	67° 21.33' S	23° 16.07' W	4892.0	Alle Wissen- schaffler an Bord

A.4 Stationsliste / Station List PS81

Station	Date	Time	Gear	Action	Position Lat	Position Lon	Water depth [m]	Comment
PS81/506-1	15.7.2013	12:48	ICE	on deck	67° 21.35' S	23° 15.96' W	4891.7	Gangway
PS81/506-2	15.7.2013	15:00	CTD/RO	in the water	67° 21.70' S	23° 13.09' W	4893.5	SE32.1
PS81/506-2	15.7.2013	16:37	CTD/RO	on ground/ max depth	67° 21.89' S	23° 10.63' W	4895.2	SL=4993m
PS81/506-2	15.7.2013	16:38	CTD/RO	hoisting	67° 21.90' S	23° 10.61' W	4895.5	
PS81/506-2	15.7.2013	18:01	CTD/RO	on deck	67° 22.04' S	23° 8.36' W	4896.7	
PS81/507-1	16.7.2013	15:28	SON	in the water	66° 38.71' S	26° 26.52' W	4879.5	
PS81/507-1	16.7.2013	15:28	SON	on ground/ max depth	66° 38.71' S	26° 26.52' W	4879.5	
PS81/507-2	16.7.2013	21:51	CTD/RO	in the water	66° 34.98' S	27° 2.65' W	4877.7	
PS81/507-2	16.7.2013	23:31	CTD/RO	on ground/ max depth	66° 34.44' S	27° 2.68' W	4879.2	4927m, 32.1
PS81/507-2	17.7.2013	0:58	CTD/RO	on deck	66° 34.03' S	27° 2.60' W	4879.7	
PS81/507-3	17.7.2013	1:09	MN	in the water	66° 33.98' S	27° 2.58' W	4879.7	
PS81/507-3	17.7.2013	1:13	MN	on deck	66° 33.97' S	27° 2.58' W	4879.7	Sensorfehler
PS81/507-3	17.7.2013	1:32	MN	in the water	66° 33.89' S	27° 2.53' W	4880.0	
PS81/507-3	17.7.2013	2:33	MN	on ground/ max depth	66° 33.66' S	27° 2.35' W	4880.5	SL=1987m
PS81/507-3	17.7.2013	2:33	MN	hoisting	66° 33.66' S	27° 2.35' W	4880.5	
PS81/507-3	17.7.2013	3:34	MN	on deck	66° 33.48' S	27° 2.08' W	4881.0	
PS81/507-4	17.7.2013	4:14	ICE	in the water	66° 33.22' S	27° 2.57' W	4881.2	Mummy-chair
PS81/507-4	17.7.2013	4:50	ICE	on ground/ max depth	66° 33.13' S	27° 2.35' W	4881.5	Boje
PS81/507-4	17.7.2013	5:30	ICE	on deck	66° 33.03' S	27° 2.05' W	4881.7	Mummy-chair
PS81/508-1	17.7.2013	11:03	SON	in the water	66° 14.62' S	26° 53.48' W	4847.7	
PS81/508-1	17.7.2013	11:03	SON	on ground/ max depth	66° 14.62' S	26° 53.48' W	4847.7	
PS81/508-2	20.7.2013	12:28	SON	in the water	61° 45.90' S	34° 59.00' W	3848.0	
PS81/508-2	20.7.2013	12:28	SON	on ground/ max depth	61° 45.90' S	34° 59.00' W	3848.0	
PS81/509-1	24.7.2013	12:44	CTD/RO	in the water	63° 8.90' S	54° 10.43' W	267.0	
PS81/509-1	24.7.2013	12:56	CTD/RO	on ground/ max depth	63° 8.91' S	54° 10.43' W	266.7	248m, 32.1
PS81/509-1	24.7.2013	12:57	CTD/RO	hoisting	63° 8.91' S	54° 10.43' W	268.0	
PS81/509-1	24.7.2013	13:13	CTD/RO	on deck	63° 8.92' S	54° 10.45' W	266.7	
PS81/510-1	24.7.2013	15:48	CTD/RO	in the water	63° 13.15' S	53° 42.37' W	307.2	SE32.1
PS81/510-1	24.7.2013	15:59	CTD/RO	on ground/ max depth	63° 13.20' S	53° 42.43' W	308.5	SL=291m
PS81/510-1	24.7.2013	15:59	CTD/RO	hoisting	63° 13.20' S	53° 42.43' W	308.5	
PS81/510-1	24.7.2013	16:15	CTD/RO	on deck	63° 13.30' S	53° 42.52' W	306.5	
PS81/511-1	24.7.2013	21:09	CTD/RO	in the water	63° 19.25' S	53° 3.75' W	470.0	

Station	Date	Time	Gear	Action	Position Lat	Position Lon	Water depth [m]	Comment
PS81/511-1	24.7.2013	21:22	CTD/RO	on ground/ max depth	63° 19.37' S	53° 3.65' W	468.2	444 m, SE 32.1
PS81/511-1	24.7.2013	21:23	CTD/RO	hoisting	63° 19.38' S	53° 3.65' W	467.2	
PS81/511-1	24.7.2013	21:41	CTD/RO	on deck	63° 19.58' S	53° 3.54' W	468.5	
PS81/511-2	24.7.2013	21:45	MN	in the water	63° 19.62' S	53° 3.51' W	470.2	
PS81/511-2	24.7.2013	22:01	MN	on ground/ max depth	63° 19.77' S	53° 3.38' W	470.7	450m, 30
PS81/511-2	24.7.2013	22:15	MN	on deck	63° 19.92' S	53° 3.27' W	470.7	
PS81/512-1	25.7.2013	3:26	CTD/RO	in the water	63° 25.53' S	52° 31.48' W	540.5	SE32.1
PS81/512-1	25.7.2013	3:41	CTD/RO	on ground/ max depth	63° 25.58' S	52° 30.98' W	544.5	SL=522m
PS81/512-1	25.7.2013	3:41	CTD/RO	hoisting	63° 25.58' S	52° 30.98' W	544.5	
PS81/512-1	25.7.2013	4:05	CTD/RO	on deck	63° 25.68' S	52° 30.07' W	549.2	
PS81/513-1	25.7.2013	7:36	CTD/RO	in the water	63° 29.24' S	52° 8.97' W	924.7	
PS81/513-1	25.7.2013	7:58	CTD/RO	on ground/ max depth	63° 29.26' S	52° 8.68' W	929.7	904 m, SE 32.1
PS81/513-1	25.7.2013	7:59	CTD/RO	hoisting	63° 29.26' S	52° 8.66' W	930.0	
PS81/513-1	25.7.2013	8:26	CTD/RO	on deck	63° 29.37' S	52° 8.39' W	937.5	
PS81/513-2	25.7.2013	8:33	MN	in the water	63° 29.33' S	52° 8.32' W	937.7	
PS81/513-2	25.7.2013	9:01	MN	on ground/ max depth	63° 29.36' S	52° 7.93' W	945.2	895 m, EL 30
PS81/513-2	25.7.2013	9:02	MN	hoisting	63° 29.36' S	52° 7.92' W	945.2	
PS81/513-2	25.7.2013	9:28	MN	on deck	63° 29.31' S	52° 7.69' W	948.0	
PS81/514-1	25.7.2013	16:15	CTD/RO	in the water	63° 32.32' S	51° 44.39' W	1503.2	SE32.1
PS81/514-1	25.7.2013	16:46	CTD/RO	on ground/ max depth	63° 31.99' S	51° 44.31' W	1493.0	SL=1470m
PS81/514-1	25.7.2013	16:47	CTD/RO	hoisting	63° 31.98' S	51° 44.31' W	1492.7	
PS81/514-1	25.7.2013	17:23	CTD/RO	on deck	63° 31.59' S	51° 44.20' W	1483.0	
PS81/515-1	26.7.2013	11:30	ICE	action	63° 27.66' S	51° 18.74' W	2146.0	Landgang hergestellt
PS81/515-1	26.7.2013	23:56	ICE	on ground/ max depth	63° 22.12' S	51° 8.19' W	1828.0	
PS81/515-1	27.7.2013	0:00	ICE	on deck	63° 22.07' S	51° 8.10' W	1815.5	
PS81/515-2	26.7.2013	18:55	CTD/RO	in the water	63° 24.52' S	51° 14.61' W	2074.2	
PS81/515-2	26.7.2013	19:49	CTD/RO	on ground/ max depth	63° 24.30' S	51° 13.69' W	2082.2	2059 m, SE 32.1
PS81/515-2	26.7.2013	19:50	CTD/RO	hoisting	63° 24.29' S	51° 13.67' W	2083.2	
PS81/515-2	26.7.2013	20:38	CTD/RO	on deck	63° 24.04' S	51° 12.74' W	2070.7	
PS81/516-1	28.7.2013	19:20	CTD/RO	in the water	63° 42.24' S	50° 51.53' W	2542.0	
PS81/516-1	28.7.2013	20:13	CTD/RO	on ground/ max depth	63° 41.96' S	50° 51.46' W	2541.0	2529 m, SE 32.1
PS81/516-1	28.7.2013	20:14	CTD/RO	hoisting	63° 41.96' S	50° 51.46' W	2542.0	

A.4 Stationsliste / Station List PS81

Station	Date	Time	Gear	Action	Position Lat	Position Lon	Water depth [m]	Comment
PS81/516-1	28.7.2013	21:08	CTD/RO	on deck	63° 41.72' S	50° 51.48' W	2541.7	
PS81/516-2	28.7.2013	21:26	MN	in the water	63° 41.66' S	50° 51.50' W	2541.2	
PS81/516-2	28.7.2013	22:29	MN	on ground/ max depth	63° 41.44' S	50° 51.60' W	2539.5	1991 m, EL 30
PS81/516-2	28.7.2013	22:30	MN	hoisting	63° 41.44' S	50° 51.60' W	2539.2	
PS81/516-2	28.7.2013	23:28	MN	on deck	63° 41.27' S	50° 51.66' W	2537.7	
PS81/516-3	28.7.2013	23:31	MN	in the water	63° 41.26' S	50° 51.66' W	2539.0	
PS81/516-3	29.7.2013	0:03	MN	on ground/ max depth	63° 41.17' S	50° 51.65' W	2540.2	993m, 30
PS81/516-3	29.7.2013	0:32	MN	on deck	63° 41.09' S	50° 51.60' W	2539.0	
PS81/516-4	29.7.2013	0:48	BUOY	action	63° 40.99' S	50° 51.66' W	2539.5	Mummy-chair
PS81/516-4	29.7.2013	1:03	BUOY	on ground/ max depth	63° 40.94' S	50° 51.63' W	2540.0	Boje ausgebracht
PS81/516-4	29.7.2013	1:06	BUOY	on deck	63° 40.93' S	50° 51.62' W	2540.0	Mummy-chair
PS81/517-1	29.7.2013	7:57	CTD/RO	in the water	63° 37.97' S	51° 12.54' W	2310.5	
PS81/517-1	29.7.2013	8:47	CTD/RO	on ground/ max depth	63° 37.64' S	51° 12.57' W	2307.5	2288 m, SE 32.1
PS81/517-1	29.7.2013	8:47	CTD/RO	hoisting	63° 37.64' S	51° 12.57' W	2307.5	
PS81/517-1	29.7.2013	9:33	CTD/RO	on deck	63° 37.33' S	51° 12.63' W	2305.5	
PS81/517-2	29.7.2013	12:35	ICE	action	63° 36.16' S	51° 12.91' W	2292.7	Landgang hergestellt
PS81/517-2	2.8.2013	20:24	ICE	on ground/ max depth	63° 15.47' S	51° 13.38' W	662.7	Alle am Bord
PS81/517-2	2.8.2013	20:40	ICE	on deck	63° 15.44' S	51° 13.29' W	678.2	Gangway am Bord und sicher
PS81/517-3	1.8.2013	7:09	CTD/RO	in the water	63° 21.58' S	51° 9.95' W	1806.5	
PS81/517-3	1.8.2013	7:46	CTD/RO	on ground/ max depth	63° 21.25' S	51° 10.28' W	1762.0	1770 m , SE 32.1
PS81/517-3	1.8.2013	7:47	CTD/RO	hoisting	63° 21.24' S	51° 10.29' W	1758.7	
PS81/517-3	1.8.2013	8:23	CTD/RO	on deck	63° 20.94' S	51° 10.63' W	1718.5	
PS81/518-1	2.8.2013	23:06	SON	in the water	63° 14.53' S	51° 35.97' W	1053.5	
PS81/518-1	2.8.2013	23:06	SON	on ground/ max depth	63° 14.53' S	51° 35.97' W	1053.5	
PS81/518-2	3.8.2013	14:15	BUOY	action	63° 10.14' S	52° 55.75' W	470.5	Mummy-chair auf Eis
PS81/518-2	3.8.2013	14:40	BUOY	on ground/ max depth	63° 10.18' S	52° 55.64' W	469.7	Boje ausgelegt
PS81/518-2	3.8.2013	14:41	BUOY	on deck	63° 10.17' S	52° 55.64' W	470.2	Mummy-chair
PS81/518-3	4.8.2013	13:02	ICE	action	62° 57.21' S	53° 17.37' W	436.5	Gangway am Kran
PS81/518-3	4.8.2013	13:44	ICE	action	62° 56.83' S	53° 18.12' W	436.0	Landgang hergestellt

Station	Date	Time	Gear	Action	Position Lat	Position Lon	Water depth [m]	Comment
PS81/518-3	5.8.2013	20:18	ICE	on ground/ max depth	62° 52.60' S	53° 14.13' W	520.2	Alle an Bord
PS81/518-3	5.8.2013	20:36	ICE	on deck	62° 52.72' S	53° 14.11' W	514.5	Gangway
PS81/518-4	4.8.2013	22:37	CTD/RO	in the water	62° 57.22' S	53° 24.88' W	425.5	
PS81/518-4	4.8.2013	22:54	CTD/RO	on ground/ max depth	62° 57.39' S	53° 24.63' W	421.7	399 m, SE 32.1
PS81/518-4	4.8.2013	23:11	CTD/RO	on deck	62° 57.48' S	53° 24.28' W	425.0	

Die "**Berichte zur Polar- und Meeresforschung**" (ISSN 1866-3192) werden beginnend mit dem Heft Nr. 569 (2008) als Open-Access-Publikation herausgegeben. Ein Verzeichnis aller Hefte einschließlich der Druckausgaben (Heft 377-568) sowie der früheren "**Berichte zur Polarforschung**" (Heft 1-376, von 1981 bis 2000) befindet sich im open access institutional repository for publications and presentations (**ePIC**) des AWI unter der URL <http://epic.awi.de>. Durch Auswahl "Reports on Polar- and Marine Research" (via "browse"/"type") wird eine Liste der Publikationen sortiert nach Heftnummer innerhalb der absteigenden chronologischen Reihenfolge der Jahrgänge erzeugt.

To generate a list of all Reports past issues, use the following URL: <http://epic.awi.de> and select "browse"/"type" to browse "Reports on Polar and Marine Research". A chronological list in declining order, issues chronological, will be produced, and pdf-icons shown for open access download.

Verzeichnis der zuletzt erschienenen Hefte:

Heft-Nr. 666/2013 — "The Expedition of the Research Vessel 'Polarstern' to the Antarctic in 2013 (ANT-XXIX/5)", edited by Wilfried Jokat

Heft-Nr. 667/2013 — "The Sea Ice Thickness in the Atlantic Sector of the Southern Ocean", by Axel Behrendt

Heft-Nr. 668/2013 — "The Expedition of the Research Vessel 'Polarstern' to the Antarctic in 2013 (ANT-XXIX/4)", edited by Gerhard Bohrmann

Heft-Nr. 669/2013 — "Processes in the Southern Ocean carbon cycle: Dissolution of carbonate sediments and inter-annual variability of carbon fluxes", by Judith Hauck

Heft-Nr. 670/2013 — "The Expedition of the Research Vessel 'Polarstern' to the Antarctic in 2012 (ANT-XXIX/1)", edited by Holger Auel

Heft-Nr. 671/2013 — "The Expedition of the Research Vessel 'Polarstern' to the Antarctic in 2012/2013 (ANT-XXIX/2)", edited by Olaf Boebel

Heft-Nr. 672/2014 — "The Expedition of the Research Vessel 'Polarstern' to the Antarctic in 2013 (ANT-XXIX/8)", edited by Vera Schlindwein

Heft-Nr. 673/2014 — "Airborne Measurements of Methane Fluxes in Alaskan and Canadian Tundra with the Research Aircraft 'Polar 5'", by Katrin Kohnert, Andrei Serafimovich, Jörg Hartmann, and Torsten Sachs

Heft-Nr. 674/2014 — "The Expedition of the Research Vessel 'Polarstern' to the Antarctic in 2013 (ANT-XXIX/7)", edited by Bettina Meyer and Lutz Auerswald

Heft-Nr. 675/2014 — "Polarforschung und Wissenschaftsutopien: Dargestellt und kommentiert am Beispiel von zehn Romanen aus der Zeit von 1831 bis 1934", by Reinhard A. Krause

Heft-Nr. 676/2014 — "The Expedition of the Research Vessel "Sonne" to the Mozambique Basin in 2014 (SO230)", edited by Wilfried Jokat

Heft-Nr. 677/2014 — "The Expedition of the Research Vessel "Sonne" to the Mozambique Ridge in 2014 (SO232)", edited by Gabriele Uenzelmann-Neben

Heft-Nr. 678/2014 — "Effects of cold glacier ice crystal anisotropy on seismic data", by Anja Diez

Heft-Nr. 679/2014 — "The Expedition of the Research Vessel 'Polarstern' to the Antarctic in 2013 (ANT-XXIX/6)", edited by Peter Lemke